





## A Specialist Periodical Report

# Photochemistry

## Volume 45

### Editors

**Angelo Albini**, University of Pavia, Italy  
**Elisa Fasani**, University of Pavia, Italy  
**Stefano Protti**, University of Pavia, Italy

### Authors

**Yutaka Amao**, Osaka City University, Japan  
**Valeria Amendola**, University of Pavia, Italy  
**Greta Bergamaschi**, University of Pavia, Italy  
**Rui Fausto**, University of Coimbra, Portugal  
**Andrea Gómez-Zavaglia**, University of Coimbra, Portugal  
**Jingzhi Lu**, University of Nebraska-Lincoln, USA  
**Timur Nikitin**, University of Coimbra, Portugal  
**J. Sérgio Seixas de Melo**, University of Coimbra, Portugal  
**Tomáš Slanina**, Goethe University Frankfurt, Germany  
**Jian Zhang**, University of Nebraska-Lincoln, USA



ISBN: 978-1-78801-006-1  
PDF ISBN: 978-1-78801-069-6  
EPUB ISBN: 978-1-78801-319-2  
ISSN: 0556-3860  
DOI: 10.1039/9781788010696-FP001

A catalogue record for this book is available from the British Library

© The Royal Society of Chemistry 2018

*All rights reserved*

*Apart from fair dealing for the purposes of research for non-commercial purposes or for private study, criticism or review, as permitted under the Copyright, Designs and Patents Act 1988 and the Copyright and Related Rights Regulations 2003, this publication may not be reproduced, stored or transmitted, in any form or by any means, without the prior permission in writing of The Royal Society of Chemistry or the copyright owner, or in the case of reproduction in accordance with the terms of licences issued by the Copyright Licensing Agency in the UK, or in accordance with the terms of the licences issued by the appropriate Reproduction Rights Organization outside the UK. Enquiries concerning reproduction outside the terms stated here should be sent to The Royal Society of Chemistry at the address printed on this page.*

*Whilst this material has been produced with all due care, The Royal Society of Chemistry cannot be held responsible or liable for its accuracy and completeness, nor for any consequences arising from any errors or the use of the information contained in this publication. The publication of advertisements does not constitute any endorsement by The Royal Society of Chemistry or Authors of any products advertised. The views and opinions advanced by contributors do not necessarily reflect those of The Royal Society of Chemistry which shall not be liable for any resulting loss or damage arising as a result of reliance upon this material.*

The Royal Society of Chemistry is a charity, registered in England and Wales, Number 207890, and a company incorporated in England by Royal Charter (Registered No. RC000524), registered office: Burlington House, Piccadilly, London W1J 0BA, UK, Telephone: +44 (0) 207 4378 6556.

For further information see our web site at [www.rsc.org](http://www.rsc.org)

Printed in the United Kingdom by CPI Group (UK) Ltd, Croydon, CR0 4YY, UK

---

## Preface

DOI: 10.1039/9781788010696-FP005

Volume 45 follows the pattern of previous issues from vol. 39 on, which combines a review on the latest advancements in photochemistry (every other year on a part of this discipline) and highlights on some topics. A planned report on solar energy conversion did not materialize.

We thank the reviewers, who maintained their thorough work once again, as well as the contributors of highlights. It has been, as usual, quite a tough job to complete all the contributions (almost) within the planned deadlines. We must admit that, hard work as it may have been, having the opportunity of seeing such a large wealth of photochemical experience has been a really nice experience.

We thank the staff of Specialist Periodical Reports at the Royal Society of Chemistry and our colleagues of the Photochemical Group at the University of Pavia, who made photochemistry such an entertaining experience every day.

Angelo Albini, Elisa Fasani and Stefano Protti

---

# Author biographies

DOI: 10.1039/9781788010696-FP006



**Angelo Albini** (b. 1946) is currently retired Professor of Organic Chemistry at the University of Pavia, Italy, where he spent much of his career, after a stay in Turin and postdoctoring in Germany, Canada, Denmark. Active in organic photochemistry, from synthetic to medicinal applications, he is the (co)author of several books, reviews and research articles on such topics.



**Yutaka Amao** was born in Kanagawa (1968). He received doctor degree of Engineering in 1997 in Tokyo Institute of Technology in Japan. He worked as a Researcher at Kanagawa Academy of Science and Technology from 1997 to 1998 and worked as a Researcher at National Aerospace Laboratory from 1998 to 2001. He started to work as an Associate Professor in the Department of Applied Chemistry of Oita University. He also started to work as a Precursory Research for Embryonic Science and Technology researcher of Japan Science and Technology

Agency (JST) from 2011 to 2015. In 2013, he was appointed as a full Professor of Osaka City University. Now he also was appointed as a Director of Research Center for Artificial Photosynthesis (ReCAP) in Osaka City University. His current research interests include green chemistry, photochemistry, biocatalytic chemistry, the development of solar to fuel conversion system, and CO<sub>2</sub> conversion to organic molecules based on the photoredox system with biocatalyst.



**Valeria Amendola** was born in Milano in 1974. She studied chemistry in Pavia, where she graduated summa cum laude in 1997. She obtained her PhD degree in 2000 under the supervision of Prof. Luigi Fabbrizzi, defending the thesis “Transition metal ions in supramolecular chemistry”. In 2005 she was appointed as Assistant Professor at the Department of Chemistry of the University of Pavia, where ten years later she took her current position as Associate Professor. She spent some time as a visiting scientist in the laboratory of Prof. F.-P. Schmidtchen at the

Department of Chemistry of the Technical University of Munich, in 2010 and 2011, and in the laboratory of Prof. R. Alberto at the Department of Chemistry of the University of Zurich, in 2012 and 2013. Dr Amendola’s research activity is principally aimed to the study of multi-component systems, capable to perform controlled specific functions, *e.g.* for the development of nano-containers and nano-reactors, chemo-sensors and molecular machines. At the moment, she is author or co-author of more than 70 publications on international scientific journals and books.



**Greta Bergamaschi** was born in Milano in 1983. She studied chemistry in Pavia, where in 2014 obtained her PhD degree under the supervision of Prof. Valeria Amendola, with a doctoral thesis titled “Anion recognition and sensing with urea-based receptors and azacryptands.” She spent research periods in Germany (Department of Chemistry, TUM, Munich) and Switzerland (EPFL, Lausanne and UZH, Zurich). Since November 2016 she has been a postdoctoral researcher at the Politecnico of Milano. She received the Fernando Pulidori Award 2013 (6th edition)

conferred by The European Group of Thermodynamics of Metal Complex (ISMEC 2013) to a young researcher author of an original paper. Her research interests are focused on supramolecular chemistry and molecular recognition.



**Elisa Fasani**, graduated in Chemistry and Pharmaceutical Technologies at the University of Pavia, in 1981 became research assistant in the Photochemical Unit of the Department of Organic Chemistry at the University of Pavia and was promoted Associated Professor in Chemistry in 1998. Her research activity centers on various aspects of photochemistry, mechanistic, preparative and applied. She has extensively studied the photochemistry of some classes of compounds of applicative interest such as dyes, pollutants and drugs. She is co-editor

of Specialist Periodical Reports: Photochemistry, as well as coauthor of several research papers on international journals.



**Rui Fausto**, Professor of Chemistry and Director of the Laboratory for Molecular Cryospectroscopy and Biospectroscopy and of the Coimbra Chemistry Research Centre at the University of Coimbra, Portugal. His research interests range from spectroscopy and solid-state photochemistry to chemical imaging, theoretical and computational chemistry and hot-vibrational chemistry. He has published more than 350 scientific articles in peer-reviewed journals and he is Editor of several books, either dedicated to the general public or to professional chemists and physicists.

He has been Editor of the Journal of Molecular Structure since 2009. Along his career, he has occupied many different positions in the administration and scientific boards of the University of Coimbra, including the presidency of the Academic Council and the vice-presidency of the Scientific and Directive boards of the Sciences Faculty, and the presidency of the Institute for Interdisciplinary Research and of the Chemistry Department. Prof. Rui Fausto has served as University of Coimbra Senator and as President of the Physicochemical Division of the Portuguese Chemical Society. In 2004 and 2005 he was awarded the “*Stimulus to the Excellence in Science Prize*” of the Portuguese Science Foundation. He is member of the European Academy of Arts, Sciences and Humanities (Paris), of several international scientific societies, member of the Honor Committee of the Portugal-Latvia Association, and coordinator of the Education Committee of the International Observatory of Human Rights.



**Andrea Gómez-Zavaglia** is a member of the Research Career from the Argentinean National Research Council (CONICET) and Head of the Center for Research and Development in Food Cryotechnology (CIDCA, CONICET). Her research interests are focused on using vibrational spectroscopic techniques both at a fundamental and applied level, aiming at solving different biologically relevant problems. She has published more than 120 papers in peer reviewed journals and 5 patents. She is Associated Editor of *Frontiers in Microbiology* (impact factor 4.0) since 2015 and has edited 2 books. She has been visiting Professor at the University of Vigo (2009), the Autonomous University of Madrid (since 2010), University Paris Diderot (since 2014) and University Paris Descartes (since 2016). She has well-established collaborations with research groups and enterprises from more than 15 different countries in Europe and America. She has been invited speaker in more than 25 academic institutions and enterprises in the European Union and in Argentina. She is member of the Advisory Council of the International Society for Clinical Spectroscopy (London). She has led more than 30 R + D + i projects, including three multilateral networks, joining more than 30 research groups and 21 enterprises. She has acted as peer reviewer for more than 30 international journals, and as jury of PhD theses and research projects in Argentina, Chile, France, Spain and Portugal. She has organized or co-organized more than 15 international conferences, being member of the International Advisory Board in several occasions. She has received the Mercosur Prize for Science and Technology in 2009.



**Jingzhi Lu** obtained his BS degree in 2012 from Nanjing University where he worked on semiconductor nanocrystals in Prof. Jin Zhu's group. He is currently a PhD graduate student at the University of Nebraska-Lincoln under the supervision of Prof. Jian Zhang. His research focuses on synthesis and application of nanoporous materials and organic photoredox catalysts.



**Timur Nikitin** graduated from Saint-Petersburg State University, Russia in 1999. He obtained his PhD degree in Chemistry from the University of Helsinki, Finland, where he studied optical and structural properties of different nanomaterials, including silicon nanocrystals embedded in silica, and carbon nanotubes, by Raman spectroscopy and other optical methods. After his PhD, he was involved in the investigation of optical and pyroelectric properties of self-assembled diphenylalanine microtubes at the University of Aveiro,

Portugal and at Ural Federal University, Russia. He is an author of 22 scientific articles in peer-reviewed journals. His current scientific activity is in the field of matrix isolation technique. He is working in a project, which aims at obtaining energetic crystals by generating high-energy rare conformers prepared by selective vibrational excitation using narrowband near-infrared light.



**J. Sérgio Seixas de Melo**, PhD in Physical-Chemistry (IST-UL, 1996) and aggregation in chemistry, University of Coimbra (UC) in 2012 is currently Associate Professor in the Department of Chemistry of the UC. He was General Secretary of the Portuguese Chemical Society (2013–2016) and is presently sub-director of FCTUC (since 2010). His research activities have been centred on photochemistry and photophysics, ranging from the excited state characterization of polymers and oligomers to, more recently, Chemistry & Art. He published more than 150 ISI

papers (h-index: 35), several book chapters, including Specialist Periodic Reports in Photochemistry (Royal Society of Chemistry) in 2009/2011/2013/2016. He supervised more than 10 Masters, PhD and Post-doc students. His current group includes three PhD students, four Post-docs and two Masters students.



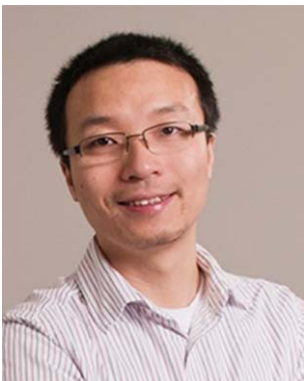
**Stefano Protti** (b. 1979) completed his PhD from the University of Pavia in 2006. He was post-doctoral fellow at the LASIR laboratory (Lille, France), at the iBitTec-S Laboratory (CEA Saclay, France), and at the PhotoGreen Lab (University of Pavia). Since December 2015, he is senior researcher at the same University. His research work is mainly focused on the photogeneration of high energy intermediates and the optimization of photochemical arylations procedures under metal free conditions. He is currently a co-author of more than 75 research articles

and reviews, besides 9 contributed chapters in multi-authored books and the book ‘Paradigms in Green Chemistry and Technology’, Springer UK (with Angelo Albini).



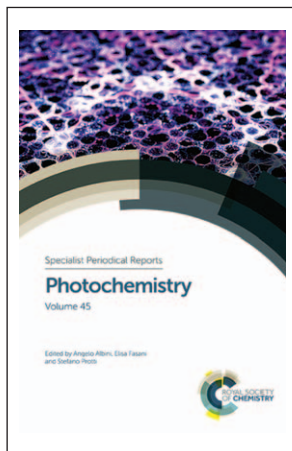
**Tomáš Slanina** was born in Brno, Czech Republic. He received his Bachelor and Master degree from the Masaryk University in Brno. He obtained a PhD degree in 2015 in a joint program between Masaryk University and University in Regensburg, Germany under the supervision of Prof. Petr Klán and Prof. Burkhard König. His PhD dissertation and other research activities were awarded by Experientia Fellowship in 2016, Award of J.-M. Lehn for Chemistry in 2015 and European Photochemistry Association Prize for the best PhD Thesis in

Photochemistry in 2014–2015. He is currently a post-doctoral researcher at Goethe University in Frankfurt am Main, Germany in the research group of prof. Alexander Heckel. His research focuses on organic molecules activatable by visible light, organic synthesis, photochemistry, photocatalysis, steady-state and transient spectroscopy, electrochemistry and reaction mechanisms.



**Jian Zhang** obtained his PhD in 2008 from University of Pittsburgh under the supervision of Stéphane Petoud. After the post-doctoral training at Northwestern with Chad A. Mirkin, he joined the faculty of University of Nebraska-Lincoln in 2011 and was promoted to Associate Professor in 2017. He received the NSF CAREER Award in 2016. His research focuses on the synthesis of nanoporous frameworks including MOFs and POFs for chemical catalysis and photochemical applications.

## CONTENTS



### Cover

A quote from a century ago (back cover) showing that the peculiarity of photochemical reactions is that only a few molecules absorb and react in a way that would otherwise require temperatures >1000 °C.

E. Warburg, *Naturwissenschaft.*, 1917, **30**, 489–494.

Front cover image courtesy of Sakkmesterke/Shutterstock.

### Preface

v

*Angelo Albini, Elisa Fasani and Stefano Protti*

### Author biographies

vi

## Periodical Reports: Physical and Inorganic Aspects

### Introduction and review of the year 2016

3

*Elisa Fasani, Stefano Protti and Angelo Albini*

1 Introduction	3
2 The sentence of the year, 1917	4
3 Awards and medals	5
4 Reviews of the year 2016	7
5 Highlights in volumes 37 to 45	17
References	18

### Light induced reactions in cryogenic matrices (highlights 2015–2016)

22

*Rui Fausto, Timur Nikitin and Andrea Gómez-Zavaglia*

1 Introduction	22
2 Light induced conformational isomerizations in cryomatrices	24

---

3 Tautomerizations and other structural isomerizations	38
4 Fragmentation reactions, unstable intermediates, and formation of complexes or weakly bound species	42
5 Noble gas chemistry	61
Acknowledgements	62
References	63

---

**The molecules of colour** 68

*J. Sérgio Seixas de Melo*

1 Introduction	68
2 The origin of electronic transitions: absorption and transmission of light	69
3 Electronic transitions in molecules	69
4 Processes occurring upon electronic excitation: photophysics and photochemistry	70
5 The chemistry of colour: the molecular origin	72
6 On the track of Maya Blue	88
7 Reds	90
8 Mauveine: colour and stability	93
9 Conclusions	96
Acknowledgements	96
References	96

---

**Photochemical and photocatalytic properties of transition metal compounds** 101

*Valeria Amendola and Greta Bergamaschi*

1 Introduction	101
2 First-row transition metals	102
3 Second- and third-row transition metals	114
References	127

---

**Photophysics of transition metal complexes** 133

*Valeria Amendola*

1 Introduction	133
2 First-row transition metals	133
3 Second- and third-row transition metals	137
References	156

---

## Highlights in Photochemistry

<b>Photoredox systems for building C–C bonds from carbon dioxide</b>	<b>165</b>
<i>Yutaka Amao</i>	
1 Introduction	165
2 Biocatalysts for CO <sub>2</sub> reduction and fixation	166
3 Photoredox/biocatalytic systems for the formation of C–C bonds from CO <sub>2</sub>	168
4 Conclusions	173
Acknowledgements	173
References	173
 <hr/>	
<b>Pushing the limits of photoactivatable compounds</b>	<b>175</b>
<i>Tomáš Slanina</i>	
1 Introduction	175
2 Photoremovable protecting groups	175
3 Photoactivatable carbon monoxide-releasing molecules (photoCORMs): 1st generation	181
4 Second generation of photoCORMs	184
5 Summary	188
References	189
 <hr/>	
<b>Photocatalytic applications of conjugated microporous polymers</b>	<b>191</b>
<i>Jingzhi Lu and Jian Zhang</i>	
1 Introduction	191
2 Photocatalytic applications of CMPs	192
3 Conclusions and outlook	217
References	218



# **Periodical Reports: Physical and Inorganic Aspects**



# Introduction and review of the year 2016

Elisa Fasani, Stefano Protti and Angelo Albini\*

DOI: 10.1039/9781788010696-00003

Important advancement in photochemistry in the year 2016 are illustrated by presenting awards, including the Nobel Prize in Chemistry, some historical perspective and some representative examples of photochemical research published in 2016.

## 1 Introduction

The present volume, no. 45 in the series “Photochemistry” of the Specialist Periodical Reports published by the Royal Society of Chemistry follows the format of previous issues from Volume 39 onwards. Accordingly, the first section consists of a series of reviews on the advancements in inorganic, physical and solar photochemistry reported in the biennium 2014–2015. The second part of the issue consists of highlights on recent topics, with the aim to provide the reader with a flavor of advanced research that may be a pleasant reading for practitioners.

In the attempt to better serve our readers, the introduction chapter includes, along with reviews, thematic issues and papers published in 2016, as well as a section on awards and prizes assigned to researchers operating in the different sectors of photochemistry and a presentation of the quote of the series “one hundred years ago” printed on the back cover.

This year we are glad to be in the lucky position of congratulating with colleagues and friends working in one of the key topics of photochemistry, the design and the operation of ‘machines’ at the molecular scale. Indeed, they exploited the incommensurable advantage of light to be not only useful to synthesize molecules with mechanical properties but also to play the role of trigger by furnishing the energy required to make molecular machine able to perform a movement.

Thus, a specific energy quantum allows to all chemists that built a ship in a bottle, to follow an invitation to “take to the sea and travel!”. Similarly, we aim to consider these yearly books as a boat that adjusts a bit the route every year for better serving the photochemical community.

Accordingly, this volume consists of two parts. The reviews section is devoted to the photochemical and the photophysical properties of transition metal complexes, the properties of organic dyes, the application of solar photochemistry and to spectroscopical studies. On the other hand, the highlights section includes reports on the application of photocatalytic reduction of CO<sub>2</sub> in synthesis, the photoisomerization of Azobenzene derivatives and on photoredox catalysis by acridine and xanthene dyes.

## 2 The sentence of the year, 1917

By the outbreak of the World War some key outlines of photochemistry had been established. The scientists had defined the field of application of photochemistry, that is photochemistry refers to reactions caused by light or other electromagnetic radiations different from light, thus excluding e.g. electron emission to give ions.

The most important photochemical reactions in nature was photosynthesis. Photography was the only artificial application extensively developed, but farther there was possibly no chemical substance that was not decomposed by irradiation by the suited wavelength. In photolysis, just as in electrolysis, primary and secondary reactions (that led to the actually isolable products) were to be distinguished. There were two limitations in studying quantitatively a photochemical reaction. One of these was theoretical: only rays absorbed had a chemical effect, as first recognized by Grotthuss.<sup>1</sup> The independence of photochemical reactions on temperature was difficult to accept, in particular due to the success kinetic studies were having during those decades, however. As an example, if a  $\lambda = 0.2 \mu$  was considered, the medium translation energy of a molecule at 20 °C was only the 163rd part of the energy of a quantum of this wavelength, and it became equal to it only at 47 370 °C. The absorption of such a wavelength thus had a peculiar strength that made it able to cleave a chemical bond. Noteworthy, already in 1810, Gay-Lussac and Thenard had stated that ‘in order to explain all of the chemical effects of light it is sufficient to accept the hypothesis by Count Rutherford that light makes nothing more than strongly enhancing the temperature of the particles on which it acted, while it enhanced minimally the temperature of the whole mass’.<sup>2</sup> Introducing the quantum hypothesis involved a complete change of approach, as E. Warburg suggested in 1917:

*According to the old approach, it could be assumed that all of the molecules encountered participated in the same way to the absorption, as it is the case, e.g. for the water particles that are all moved in the same way when hit by a wave. With the new approach, it is impossible to understand how it may happen that a very weak irradiation causes an effect that might be obtained otherwise only by using high temperatures. Things were different when the quantum hypothesis was introduced, according to which the effect was concentrated on a relatively small number of molecules, as only as many molecules participate into the absorption as are the quanta absorbed,<sup>3</sup> provided that, of course, the quantum  $h\nu$  was larger than the work required for causing the observed chemical change,  $2c/\lambda > q$ . Einstein had considered that all of the absorbing molecules were cleaved and had formulated what he had called the equivalence law, where the primary cleavage actually had  $S = \lambda/2c$ .<sup>4</sup> Such a case was well represented by the photolysis of HBr at 0.309  $\mu$ , which had a unitary quantum yield, provided that secondary processes were taken into account.*

Other examples included the photolysis of ammonia to give the elements and the cleavage of ozone. On the other hand, the catalytic effect was strong e.g. with H<sub>2</sub>/Cl<sub>2</sub> mixtures (Chlorknallgas), where most of the experiments had been done under conditions, where it was

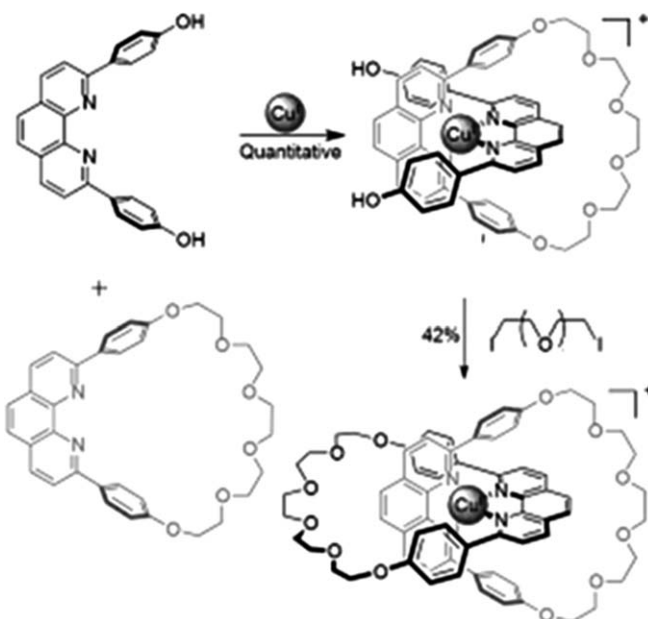
difficult to be sure that only a negligible amount of water vapor was present. These were difficulties of the experiments and had led to a number of conflicting reports (*e.g.* Dux and Bodenstein had washed their instruments with the reagent gas mixture for one month before beginning their experiments),<sup>5</sup> and nevertheless, Bunsen and Roscoe began a paper by them on that reaction with this sentence: ‘*Photochemical measurements that claim to be more than an estimate, are bound to such relevant troubles, that up to now any attempt to investigate into the laws of the photochemical reactions has been forcedly abandoned.*’<sup>6</sup> Such reactions, where secondary processes were so large and fully drew out primary processes were unsuitable for fundamental experiments.

Furthermore, as for the energetic aspects, Warburg distinguished true and false equilibria (the latter to those that involved a farther push to reach the actual equilibrium position) and further whether these increased or decreased (first and second type) the free energy of the system that is whether this displaced the system toward the equilibrium position of farther from it. An example of an effect of primary reaction is the ozonization of oxygen, where the primary reaction involves the fragmentation of an oxygen molecule into two atoms, and then the secondary step, the addition of each oxygen atom to an oxygen molecule.<sup>7</sup>

### 3 Awards and medals

The *Nobel Prize in Chemistry* 2016 was awarded jointly to Professors **Jean-Pierre Sauvage**, (University of Strasburg), Sir **J. Fraser Stoddart**, (North-Western University of Evanston, USA) and **Bernard L. Feringa** (University of Groningen), “*for the design and synthesis of molecular machines*”. According to the Royal Swedish Academy of Sciences,<sup>8</sup> a molecular-level machine can be defined as “*an assembly of a distinct number of molecular components that are designed to perform machinelike movements (output) as a result of an appropriate external stimulation (input)*”. As reported by S. Erbas-Cakmak *et al.* in 2015, “*the widespread use of molecular machines in biology has long suggested that great rewards could come from bridging the gap between synthetic molecular systems and the machines of the macroscopic world.*”<sup>9</sup> Leigh, in an excellent recent review from 2016,<sup>10a</sup> pointed out that one of the main progresses in molecular machinery is the development of efficient and selective synthetic approach to interlocked molecules such as catenanes (which are based on two interlocked rings)<sup>10b</sup> and rotaxanes (consisting of a ring threaded over an axle with stoppers at each end) that have been made available in large amounts through a template synthesis firstly proposed by Sauvage in 1983 (an example in Scheme 1).<sup>11</sup>

Thus, starting from the seminal work of Stoddard,<sup>12</sup> a series of so-defined *molecular shuttles* based on rotaxanes and catenanes able to shift from one position to another following a chemical, electrochemical or photochemical<sup>13</sup> trigger was then designed and prepared in early 90’s. A third decisive contribution was afforded by Ben Feringa some years ago, that addressed his efforts on the unidirectionality issue of molecular motors and published the synthesis of the first rotary molecular motor, based on both photo-and thermo-isomerisable overcrowded alkene.<sup>14</sup>



**Scheme 1** Sauvage's synthesis of [2]-catenanes. Adapted with permissions from ref. 10b, G. Gil-Ramírez, D. A. Leigh, and A. J. Stephens, *Angewandte Chemie International Edition*, John Wiley and Sons. © 2015 The Authors. Published by Wiley-VCH Verlag GmbH & Co. KGaA.

The report by the Nobel Committee can be found in ref. 15.

More recently, several applications of molecular machines have been proposed, including the preparation of molecular electronic devices<sup>16</sup> and nanocontainer-release systems<sup>17</sup> and the use of such machines able to make mechanical work or to act as catalyst. It should be noticed that other researchers obtained significant results in this fields, including Prof. Vincenzo Balzani (University of Bologna)<sup>18</sup> and Prof. Masahiro Irie (Kyushu University).<sup>19</sup>

Another field where supramolecular photochemistry has reached an excellent target, based not on molecules substituting tools but on nano-shaping materials, is photochemical machinery, the advantage of which has been recently demonstrated by Saraf and Sadaiah in the preparation of a novel cardiovascular stent.<sup>20</sup>

In 2016 **Ben L. Feringa** was also awarded with the Tetrahedron Prize for Creativity in Organic Chemistry, since “*his contributions to molecular nanotechnology, including molecular switches and rotors, have played a major role in shaping the field of nanomachines*” and “*his discoveries in catalysis, particularly of enantioselective transformations, have had a profound influence in synthetic organic chemistry and its applications to natural product chemistry.*”<sup>21</sup>

The Porter Medal 2016 has gone to Professor **Frederick D. Lewis**, Northwestern University, and to Professor **James Barber**, Imperial College, London.<sup>22</sup> Lewis is well known for his excellent contributions to many aspects of photochemistry, and in recent years his activity has centered on the elucidation of the mechanism and dynamics of photoinduced electron

transfer in DNA, as well as on the investigation of the photoreactivity of DNA bases.<sup>23</sup>

On the other hand Barber focused most of his studies in the field of artificial and natural photosynthesis<sup>24</sup> and of photochemistry in restricted media.<sup>25</sup>

In 2016 Professor F. D. Lewis was also awarded by the Josef Michl ACS Award for his excellent contribution to photochemistry.<sup>26</sup>

Finally, during the 2016 edition of the Central European Conference on Photochemistry in Bad Hofgastein (Austria), **Tomáš Slanina** from the Masaryk University received the EPA PhD Prize for the Best PhD Thesis in Photochemistry for his work entitled “Photocatalysis by Visible Light Absorbing Xanthene and Acridine Dyes: Synthetic Applications and Mechanistic Investigations”.<sup>27</sup> In the same meeting, the paper “A triplet-triplet annihilation based up-conversion process investigated in homogeneous solutions and oil-in-water microemulsions of a surfactant” by **Fausto Ortica et al.** won the EPA-PPS Prize for the most highly cited paper published in PPS during the previous two calendar years.<sup>28</sup>

## 4 Reviews of the year 2016

### 4.1 Reviews and original papers

In the field of environmental photochemistry and energy storage, Nicola Armaroli and Vincenzo Balzani summarized the main issues in the energy transition from fossil to renewable fuels, with particular attention to the significant growth of solar electricity technologies. Different photovoltaic alternatives, such as copper/indium/gallium/selenide (CIGS) or CdTe, have been discussed and compared therein. In addition, the energy return on investment (EROI) and the limited availability of natural resources needed to manufacture energy converters and storage devices have been discussed in the book.<sup>29</sup> A review concerning the role of graphene in environmental photocatalysis, in particular in the photocatalytic degradation of organic pollutants, hydrogen production and CO<sub>2</sub> reduction was published by Li *et al.*<sup>30</sup> Analogously, the preparation, and applications of  $\gamma\text{-C}_3\text{N}_4/\text{TiO}_2$  heterojunction catalysts was discussed by Zhou *et al.*<sup>31</sup> In the same research field, Kaiving *et al.* summarized the recent advances in engineering titanium dioxide nanotubes for both photochemical and photoelectrochemical water splitting, with particular attention on the efforts recently devoted to optimize light absorption processes while minimizing, at the same time, charge recombination.<sup>32</sup>

The photoconversion of primary greenhouse gas CO<sub>2</sub> into useful products is one of the challenges in sustainable development. He *et al.* reviewed the use of metal organic frameworks as heterogeneous photocatalysts and their application in this field.<sup>33</sup> Another interesting report on the use of metal organic frameworks in photoredox catalyzed processes and fuel production has been published by Garcia and co-workers.<sup>34</sup> Artificial photosynthesis and CO<sub>2</sub> reduction were the subjects of a review authored by Frei and Coll. that focused on the use of oxo-bridged heterobinuclear based hierarchical inorganic assemblies as the photocatalysts.<sup>35</sup>

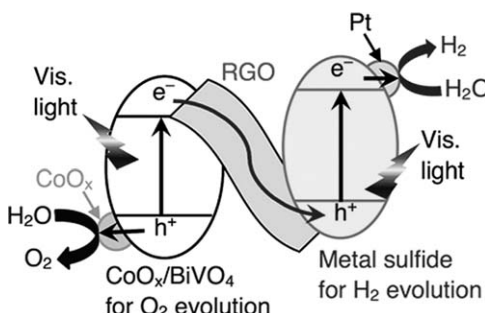


**Fig. 1** Z-scheme system for water splitting consisting of a Pt-loaded metal sulfide photocatalyst and a RGO-CoO<sub>x</sub>/BiVO<sub>4</sub> composite photocatalyst.<sup>36</sup> Reprinted with permission from A. Iwase, S. Yoshino, T. Takayama, Y. H. Ng, R. Amal and A. Kudo, *J. Am. Chem. Soc.*, 2016, **138**, 10260–10264. Copyright (2016) American Chemical Society.

As concerning original papers, a Z-scheme photocatalytic system (Fig. 1) consisting in a Pt loaded metal sulfide ( $\text{Pt}/\text{CuGaS}_2$ ) as the reduction site, a  $\text{CoO}_x/\text{BiVO}_4$  (as the oxygen evolving photocatalyst) and reduced graphene oxide (RGO) as the electron mediator was successfully employed in water splitting as well in  $\text{CO}_2$  reduction to  $\text{CO}$ .<sup>36</sup>

An oxychloride  $\text{Bi}_4\text{NbO}_8\text{Cl}$ , with a single layer Sillen–Aurivillius perovskite, that was demonstrated to act as a stable and efficient oxygen-evolving photocatalyst, was combined with a Rh-doped  $\text{SrTiO}_3$  to form a Z-scheme catalyst for water splitting in the presence of the  $\text{Fe}^{2+}/\text{Fe}^{3+}$  pair as the redox mediator.<sup>37</sup> Copper nanoparticles (Cu-NPs) loaded  $\text{TiO}_2$  was prepared by Kumar and coworkers and then exploited in the reduction of  $\text{CO}_2$  with water vapor under UV-C irradiation. Best results have been obtained with 1% Cu/TiO<sub>2</sub> with the production rate of CO and H<sub>2</sub> of 334 and 452  $\mu\text{mol g}^{-1}\text{ h}^{-1}$ , respectively.<sup>38</sup> Suib and coworkers reported a strategy that combined photocatalytic oxidation with reduction technology in the one-pot sunlight conversion of organic pollutants into valuable products by using 5% Graphene Quantum Dots (GQDs)/V-TiO<sub>2</sub> photocatalyst (Fig. 2). Investigations carried out in the presence of Methylene Blue (MB) as the model substrate revealed that the dye is initially mineralized to  $\text{CO}_2$ , which was subsequently photoreduced to methanol (13.24  $\mu\text{mol g}^{-1}\text{ h}^{-1}$ , Fig. 2a and b), ethanol (5.65  $\mu\text{mol g}^{-1}\text{ h}^{-1}$ ) and methane (0.445  $\mu\text{mol g}^{-1}\text{ h}^{-1}$ ) with an apparent quantum efficiency of 4.87% at 420 nm.<sup>39</sup>

A peculiar approach for carbon dioxide fixation was proposed by Jamison *et al.*, who reported the direct coupling of  $\text{CO}_2$  and amines *via* the single-electron reduction of the former to afford  $\alpha$ -amino acids under continuous flow conditions (see some examples in Scheme 2). By following this protocol, the selective, metal free  $\alpha$ -carboxylation of amines **1a,b** to **2a,b** was carried out in DMF and in the presence of *p*-terphenyl as the photoredox catalyst.<sup>40</sup>

As concerning pharmaceutical and medical applications of photochemistry, the emerging of photonanomedicine in oncology was remarked by Obaid *et al.*<sup>41</sup> The application of tetratriethyleneoxysulfonyl substituted zinc phthalocyanine (ZnPc, **3**, Fig. 3a) in the photodynamic

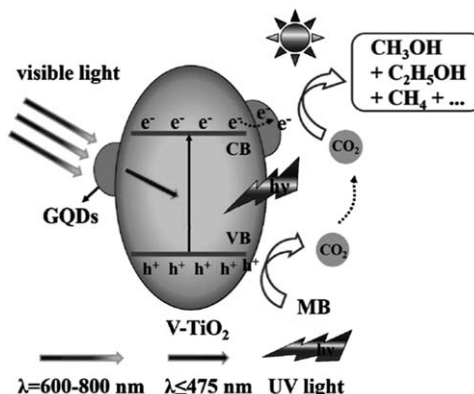
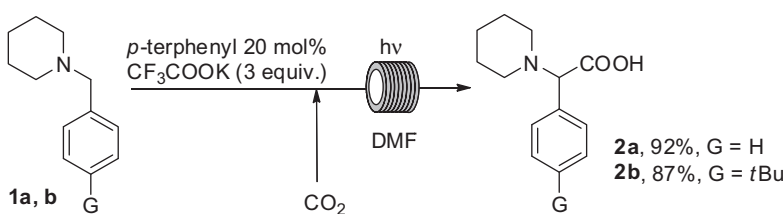


**Fig. 2** Proposed mechanism of the One-Pot Conversion of MB to Useful Organic Compounds over the 5% GQDs/V-TiO<sub>2</sub>.<sup>39</sup> Reprinted with permission from J.-P. Zou, D.-D. Wu, J. Luo, Q.-J. Xing, X.-B. Luo, W.-H. Dong, S.-L. Luo, H.-M. Du and S. L. Suib, ACS Catal., 2016, **6**, 6861–6867. Copyright (2016) American Chemical Society.



**Scheme 2** Photocatalytic synthesis of  $\alpha$ -aminoacids under continuous flow conditions.

cancer therapy was discussed in a review authored by Kuzyniak *et al.*<sup>42</sup> Recent advances in understanding the potentialities of quinones (such as the hypocrellin A, **4**, Fig. 3b) in PDT as well as the mechanisms involved in the generation of Reactive Oxygen Species (ROS) were summarized by M. Rajendran.<sup>43</sup>

Apart from reviews, new photosensitizers for PDT have been also proposed in the primary literature. As an example, Liu *et al.* described the self-assembly of simple dipeptides or amphiphilic aminoacids in the presence of photosensitiser Ce<sub>6</sub> (Chlorin e6) to form a nanodrugs with tunable size and high loading efficiency. Moreover, the release of Ce<sub>6</sub> is dependent on pH, as well as on enzyme stimuli, making cellular uptake and biodistribution selective. This system has been successfully applied *in vitro* and *in vivo*, with an almost complete tumor (MCF-7 breast cancer cell line) eradication in mice after only single drug dose and subsequent exposure to light (Fig. 4).<sup>44</sup>

The use of porphyrin-loaded nanoparticles in theranostics was also reviewed in this year.<sup>45</sup> The theranostic system **5** (Fig. 5) was synthesized by combining a two-photon-absorbing photosensitizer usually employed in PDT and a Gadolinium(III) complex for Magnetic Resonance Imaging (MRI) analysis and tested on cancer cellular systems (HeLa cells).<sup>46</sup>

The journal *Photodiagnosis and Photodynamic Therapy* dedicated in 2016 some reviews on applications of PDT in the treatment of health

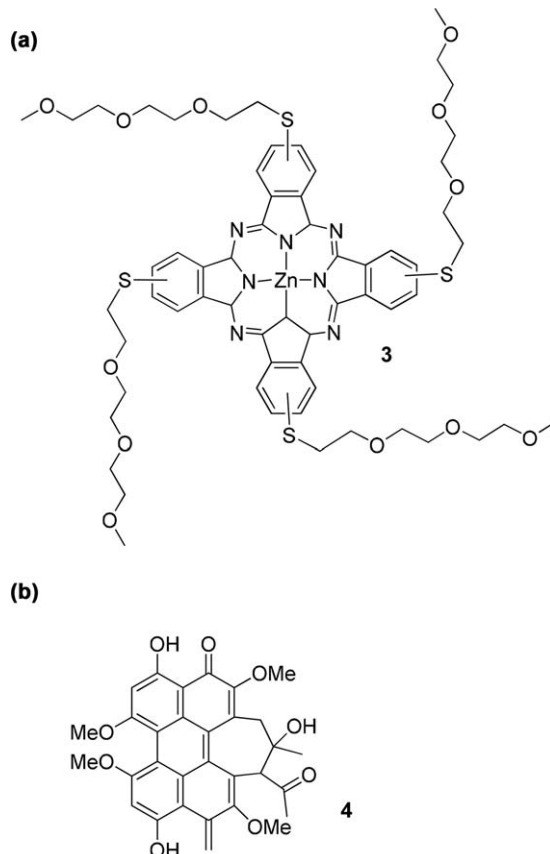


**Fig. 3** Tetratriethylenoysulfonyl substituted zinc phthalocyanine **3** and hypocrellin A (**4**) used in the photosensitised generation of Reactive Oxygen Species.

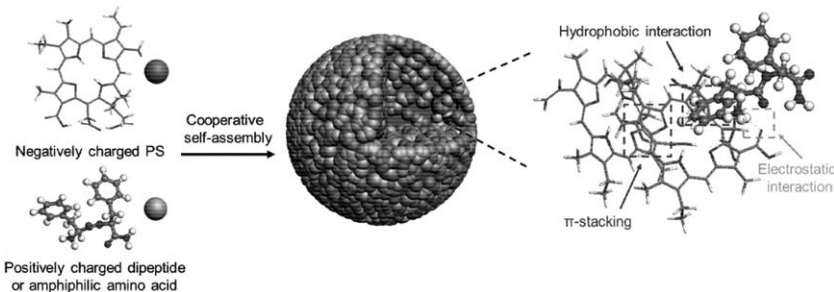


**Fig. 4** Fabrication of photosensitive nanoparticles by amphiphilic dipeptide- or amino-acid-tuned self-assembly. Reprinted with permission from ref. 44, K. Liu, R. Xing, Q. Zou, G. Ma, H. Mchwald and X. Yan, *Angewandte Chemie International Edition*, John Wiley and Sons. © 2016 Wiley-VCH Verlag GmbH & Co. KGaA, Weinheim.

disorders different from cancer diseases, such as aggressive periodontitis<sup>47</sup> and acne.<sup>48</sup>

The light triggered release of drugs from cyclodextrins with small guest molecules have been reported by Yuan *et al.*, and this approach has been compared to other controlled-release drug delivery systems.<sup>49</sup>

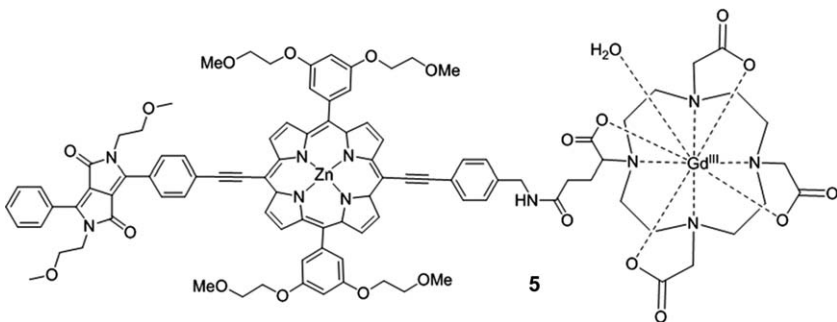


**Fig. 5** Theranostic system obtained by assembling a porphyrin based two-photon absorbing photosensitizer and a Gd<sup>III</sup> complex for MRI. See ref. 44 for further details.

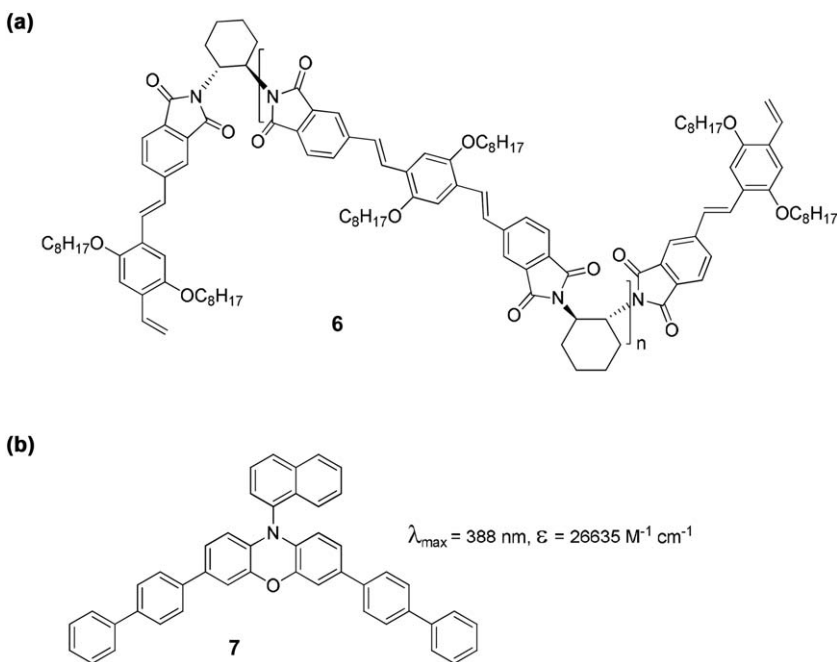


**Fig. 6** Photocatalysts recently tested in visible-light promoted polymerization processes (see ref. 53 and 54 for further details).

The role of time-resolved photochemistry in actually following the course of a reaction has been demonstrated and applied to the *in situ* high energy resolution off-resonant spectroscopy for a time-resolved study of single site Ta catalyst during oxidation.<sup>50</sup> Moreover Castellano published a survey of the emerging investigators on inorganic photochemistry and photophysics.<sup>51</sup>

A brief review of the photocatalysts used in polymerization reactions was furnished by Lalevée *et al.*<sup>52</sup> The same authors tested an oligomeric and copolymerizable photocatalyst currently used in organic light emitting diodes (OLEDs) in polymerization photoinitiating systems. Interestingly, the performances of such photocatalyst (**6**, Fig. 6a) are

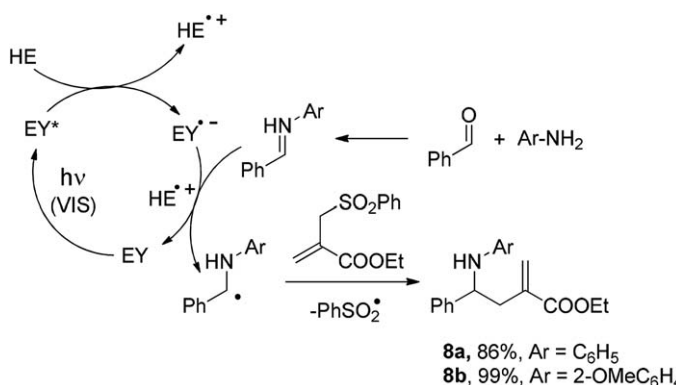
satisfactory in both free radical and cationic polymerization as well in the production of interpenetrating polymer networks (IPNs).<sup>53</sup>

A *N*-aryl phenoxazine has been employed as the visible light photoredox catalyst in metal free atom-transfer radical polymerization for the synthesis of polyacrylates. Polymers with targeted molecular weights were thus obtained by using this catalyst under white LEDs irradiation (7, Fig. 6b).<sup>54</sup>

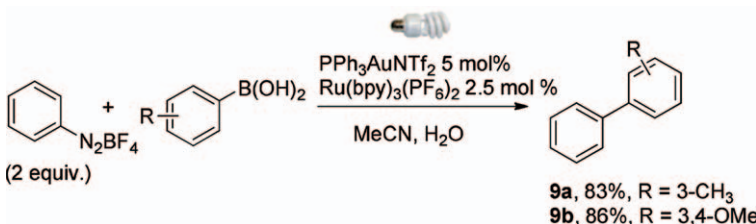
The development of light driven multicomponent processes has been recently noticed to open new and interesting scenarios in the field of organic synthesis.<sup>55</sup> The three component reductive coupling of aromatic amines, aldehydes and electron-poor olefins was performed under eosin Y photocatalysis, to afford a set of  $\gamma$ -amino acids. In the process a  $\alpha$ -amino radical was generated *via* photoinduced single electron reduction of an *in situ* generated aldimine and thus trapped by allylsulfone to afford the branched  $\alpha$ -functionalized amine (Scheme 3).<sup>56</sup>

A wide range of substituted oxazoles was produced *via* a three-component cyclization of 2*H*-azirines, alkynyl bromides, and molecular oxygen under 9-phenyl-*N*-methyl-acrydinium perchlorate photoredox catalysis.<sup>57</sup> A protocol for the diastereoselective preparation of a set of differently substituted hydrazide-containing chroman-2-ones and dihydroquinolin-2-ones was reported by Xiao *et al.* The protocol envisaged a photocatalytic  $\alpha$ -amino carbon radical-based cascade reaction taking place in arylhydrazones, in the presence of Ir(ppy)<sub>2</sub>(dtbbpy)PF<sub>6</sub> as the photocatalyst. Notably, natural sunlight has been successfully used as the light source.<sup>58</sup> The dual visible light photoredox/gold-catalysed C(sp<sup>2</sup>)–C(sp<sup>2</sup>) cross coupling for the synthesis of biaryls **9** from arenediazonium salts and arylboronic acids was developed by the groups of Lee<sup>59</sup> (Scheme 4) and employed the Ru(bpy)<sub>3</sub>(PF<sub>6</sub>)<sub>2</sub> complex as the photoredox catalyst.<sup>60</sup>

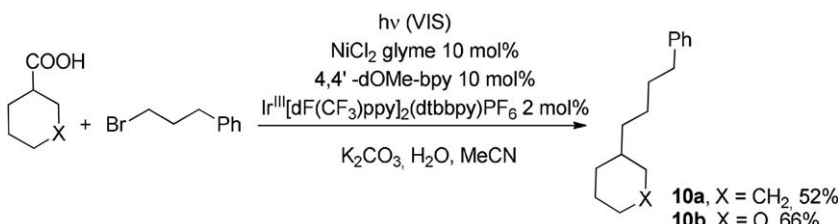
A synthetic protocol for the construction of carbon(sp<sup>2</sup>)–carbon(sp<sup>3</sup>) bonds *via* reductive cross-coupling of aryl bromides with alkyl bromides has been achieved under photoredox/nickel catalysis.<sup>61</sup> In the same year the research group of David MacMillan described the direct formation of



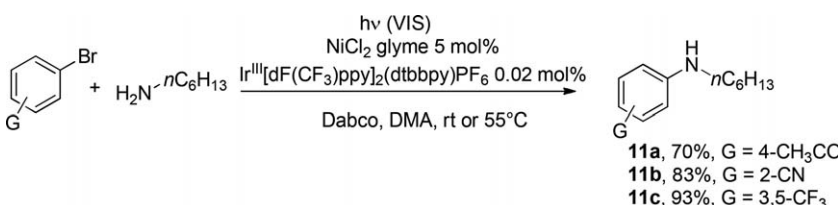
**Scheme 3** Three component synthesis of  $\gamma$ -amino acids **8** under visible light photoredox catalysis.



**Scheme 4** Synthesis of biaryls 9a,b under dual photoredox/gold catalysis.



**Scheme 5** Direct formation of C(sp<sup>3</sup>)–C(sp<sup>3</sup>) bonds under dual Nickel/photoredox conditions.



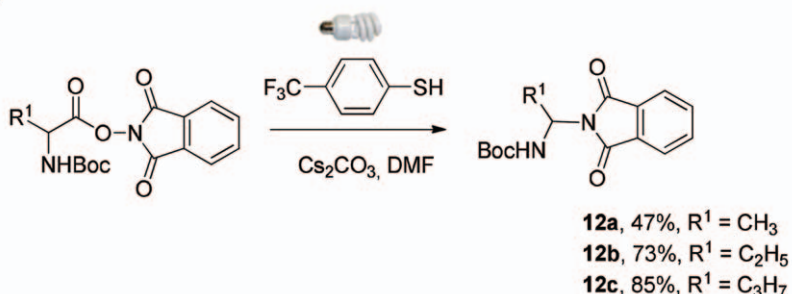
**Scheme 6** Ligand-free amination of aryl bromides under photoredox/nickel catalysis.

C(sp<sup>3</sup>)–C(sp<sup>3</sup>) bonds by starting from primary and secondary carboxylic acids and alkyl halides under metallaphotoredox catalysis, in the presence of Ni<sup>0</sup>Cl<sub>2</sub>·glyme and Ir<sup>III</sup>[dF(CF<sub>3</sub>)ppy]<sub>2</sub>(dtbbpy)PF<sub>6</sub> as the metal catalyst source and the photoredox catalyst, respectively (see a few examples in Scheme 5). The approach has been applied to the four-step synthesis of antiplatelet drug Tirofiban from commercially available starting materials.<sup>62</sup>

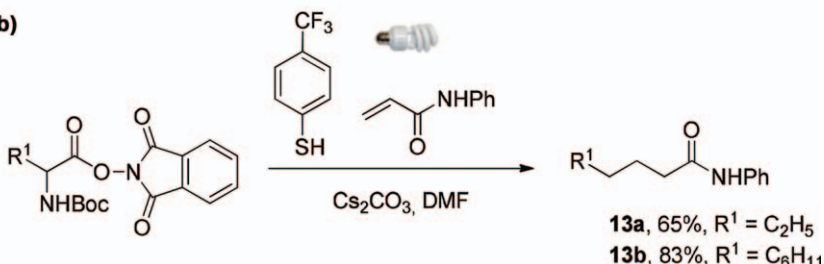
The same research group, in collaboration with that of Stephen L. Buchwald, described the highly efficient and versatile ligand-free amination of aryl bromides under photoredox/nickel catalysis. In this case, destabilization of a nickel-amido complex *via* photoredox catalysis to induce reductive elimination and release of the desired aniline 11 or aminopipridine has been exploited as alternative to the design of specialized ligands, which facilitate reductive elimination from the metal catalyst center (some example in Scheme 6).<sup>63</sup>

The adoption of photoorganocatalysts in the *mise au point* of metal-free synthetic protocols is currently a challenge in organic synthesis.<sup>64</sup> The visible-light decarboxylative generation of alkyl radicals from *N*-(acetoxymethyl)phthalimides in the presence of 4-(trifluoromethyl)thiophenol

(a)



(b)



**Scheme 7** Decarboxilative (a) C–N and (b) C–C bond formation under visible light organophotocatalysis.

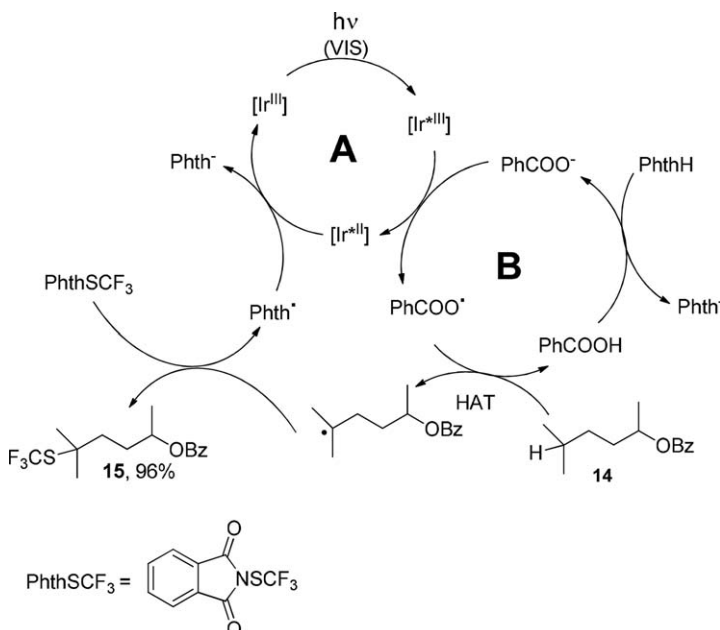
as the organic photocatalyst was described by Fu *et al.* and exploited in the formation of both C–N and C–C bonds (selected examples in Scheme 7).<sup>65</sup>

The long-time known catalyst 9,10-dicyanoanthracene (DCA) has been recently rediscovered and applied to the decarboxylative alkynylation of  $\alpha$ -amino acids,  $\alpha$ -oxo acids, and  $\alpha$ -keto acids under either blue LED or natural sunlight irradiation.<sup>66</sup>

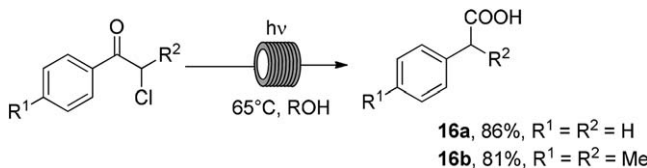
The chemoselective functionalization of complex molecules is another challenge of photocatalysis. A process combining a photoredox (A) and an organocatalytic (B) cycle and resulting in the selective trifluoromethylthiolation process of ubiquitous  $\text{C}(\text{sp}^3)\text{-H}$  bonds in the presence of an electrophilic trifluoromethylthiolating reagent (Phth-SF<sub>3</sub>) was proposed by Glorius *et al.* The methodology allowed for the functionalization of a wide range of substrates **14** under mild conditions. In this case the tetrabutylammonium benzoate salt was used as precursor of the benzoyloxy radical that act as the hydrogen atom transfer agent (Scheme 8).<sup>67</sup>

The advantages of flow photochemistry in terms of waste reduction have been recently summarized by Ciriminna *et al.*<sup>68</sup> As concerning this field, the continuous flow synthesis of nonsteroidal anti-inflammatory drug ibuprofen analogues **16** *via* a photo-Favorskii rearrangement has been optimized on a multigram scale by Bauman and Baxendale (Scheme 9).<sup>69</sup>

Finally, the advantages of investigating in depth the mechanism of photochemical reactions in terms of optimization of the reaction conditions as well as in the development of new photochemical reactors set-up have been reviewed by Hoffmann and Oelgemoeller.<sup>70</sup>



**Scheme 8** Selective trifluoromethylthiolation reaction under dual organo/photoredox catalysis.

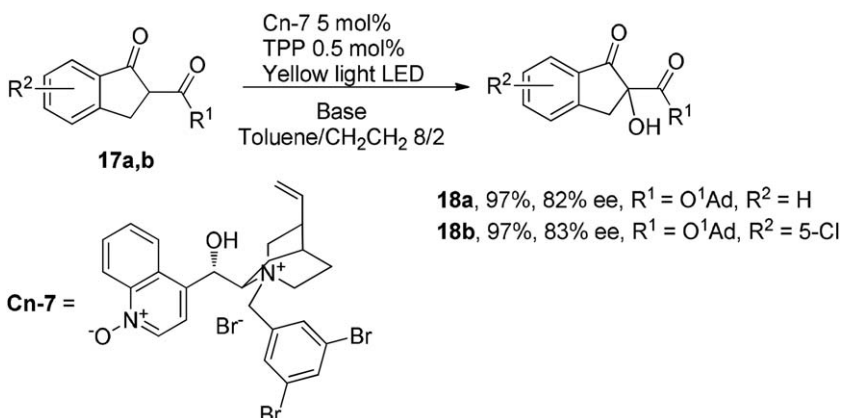


**Scheme 9** Photochemical synthesis of ibuprofen analogues **16** under flow conditions.

#### 4.2 Handbook and special issues

The volume *Photochemistry: Past, Present and Future* devoted to the history and applications of photochemistry has been published by one of the present Authors.<sup>71</sup> The first part focuses on the development of photochemistry, including early reports describing light-matter interaction, the discovery of photochemical reactions and photochemical mechanisms, and the second part outlines current applications in different fields including sustainable synthesis, diagnostics, medicine and nanotechnology. Giacomo Bergamini and Serena Silvi recently edited the multi-authored book *Applied Photochemistry: When Light Meets Molecules*,<sup>72</sup> which focused on different advances in photochemical techniques ranging from photodynamic therapy to the development of Light-Emitting Electrochemical Cells.

A special issue focused on photocatalysis was edited by Marisa Kozlowski and Tehshik Yoon on the *Journal of Organic Chemistry*. A range of synthetic strategies was represented to point out the potentiality of light in chemical transformations. A representative number of groups working in photocatalysis as well as in photoredox catalysis participated



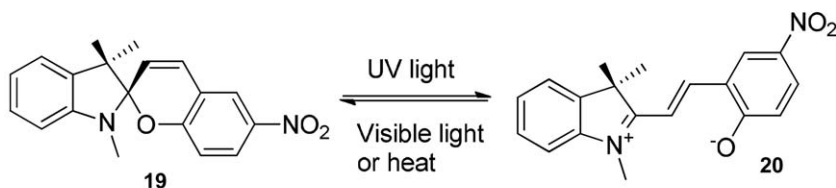
**Scheme 10** Enantioselective synthesis of  $\alpha$ -hydroxy- $\beta$ -keto esters **18** under PTC conditions.

with either original works or reviews/synopsys.<sup>73</sup> As an example, a set of  $\alpha$ -hydroxylated of  $\beta$ -keto esters and amides **18** (a structural motif that is present in a wide range of bioactive products) was synthesized in an enantioselective fashion from **17** under phase transfer catalysis (PTC) conditions in the presence of molecular oxygen as the oxidant, triphenylpyrilium (TPP) as the photosensitiser and cinchona-derived *N*-oxides (Cn-7 in Scheme 10) as asymmetric PTC catalysts. The desired products were obtained in excellent yields (up to 98%) and enantioselectivity. Furthermore, the catalysts could be recycled and reused six times without any loss in efficiency.<sup>74</sup>

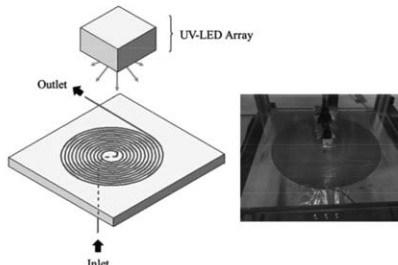
The new trends in photochemical engineering and technologies were the subject of a selection of papers published on *Chemical Engineering & Technology* (guest editors: Michael Oelgemöller and Karine Loubiere).<sup>75</sup> Notably, microreactor technology was applied for the first time to kinetic analysis of a photochemical reaction, the rearrangement of photochromic T-system **19** to **20** (Scheme 11a). Thus, kinetic parameters of a reaction, namely quantum yield and thermal back reaction have been determined in a spiral-shaped microreactor equipped with ultraviolet light emitting diode (LED) array (Scheme 11b).<sup>76</sup>

Tehshik Yoon and Corey Stephenson were the guest editors of an issue of the *Accounts of Chemical Research* devoted to the photoredox catalysis. The issue comprised more than twenty contributions of researchers leader in this field reviewing their work, including Frank Glorius,<sup>77</sup> David Nicewicz<sup>78</sup> and Oliver Reiser.<sup>79</sup> In September 2016 *Chemical Reviews* published a thematic issue entitled *Photochemistry in Organic Synthesis* with A. Beeler as the guest editor.<sup>80</sup> An almost exhaustive range of topics was described, including, among others, cyclobutane ring construction,<sup>81</sup> arene/alkene cycloadditions,<sup>82</sup> reactions forming new C–C bonds,<sup>83</sup> photooxidation,<sup>84</sup> photochemistry applied to the multistep synthesis of natural products,<sup>85</sup> flow chemistry,<sup>86</sup> dual catalysis,<sup>87</sup> and solar photochemistry.<sup>88</sup>

(a)



(b)



**Scheme 11** (a) Rearrangement of a photochromic T-system. (b) Spiral-shaped photochemical microreactor. Adapted with permission from ref. 76, T. Aillet, K. Loubière, O. Dechy-Cabaret and L. Prat, *Chemical Engineering & Technology*, John Wiley and Sons. Copyright © 2016 Wiley-VCH Verlag GmbH & Co. KGaA, Weinheim.

A theme issue dedicated to Professor Yoshihisa Inoue on the occasion of his retirement from Osaka University was published by the *Journal of Photochemistry and Photobiology A, Chemistry*, (Editors: T. Mori, G. Fukuhara and T. Wada) and included a detailed academic and scientific biography of prof. Inoue<sup>89</sup> and a collection of papers devoted to supramolecular chemistry and photochirogenesis. Among others, Fujiki reported the design of photoluminescent bis(*p*-*n*-butylphenyl)polysilanes (nBuPS) aggregates surrounded by organic media containing (*S*)-/ (*R*)-limonene, that led to a more efficient chirality generation during aggregation, as proven by circular dichroism (CD) and circularly polarized luminescence (CPL) spectral analysis.<sup>90</sup> Finally, *Coordination Chemistry Reviews* dedicated a volume to the 21st International Symposium on the Photophysics and Photochemistry of Coordination Compounds (guest editors: K. Szaciłowski and W. Macyk) with a collection of papers devoted to the research work presented in the 2015 edition of the meeting, in Kraków. Among others, the synthesis and the properties of ceramics of doped and undoped Lu<sub>2</sub>O<sub>3</sub> have been discussed in view of their application in energy storage.<sup>91</sup>

## 5 Highlights in volumes 37 to 45

Azobenzene photoisomerization, 2017, **44**, 294–321

Cultural heritage, and photochemistry. 2011, **39**, 256–284

Cyclodextrins, photoresponsive, 2016, **43**, 226–269

Exiton fission, 2016, **43**, 270–285

- Flow photochemistry, 2016, **43**, 173–190  
 Fluorescence Imaging, nanoscale, 2011, **39**, 191–210  
 Global artificial photosynthesis, 2017, **44**, 259–282.  
 History of photochemistry, APA, 2012, **40**, 230–244  
 History of photochemistry, EPA, **40**, 197–229  
 History of photochemistry, IAPS, 2013, **41**, 269–278  
 Human skin, photoprotection of, 2012, **40**, 245–273  
 Industrial applications, of photochemistry 2010, **38**, 344–368  
 Interfacial electronic processes, on the surface of nanostructured semiconductors, 2009, **37**, 362–392  
 Nitric oxide photorelease, 2013, **41**, 302–318  
 Nucleic acids, caged, 2013, **41**, 319–341  
 OLEDs, 2009, **37**, 393–406  
 Organic solid-state luminescence, 2016, **43**, 191–225  
 Photocatalysis for depollution, 2017, **44**, 346–361  
 Photocatalytic applications of conjugated microporous polymers, 2017, **45**, 191–220  
 Photochromic, nanoparticles, 2011, **39**, 211–227  
 Photo-induced water oxidation, 2012, **40**, 274–294  
 Photolithography materials, 2010, **38**, 369–387  
 Photoluminescence sensors, 2017, **44**, 322–345  
 Photon–molecule coupling fields, 2011, **39**, 228–255  
 Photo-oxygenation, 2010, **38**, 307–329  
 Photoredox systems for building C–C bonds from carbon dioxide, 2017, **45**, 165–174  
 Polymerization, 2015, **42**, 215–232  
 Prebiotic atmosphere, 2013, **41**, 342–359  
 Prebiotic photochemistry, 2010, **38**, 330–343  
 Proton transfer, in flavonols, 2012, **40**, 295–322  
 Pushing the limits of photoactivatable compounds, 2017, **45**, 175–190  
 Reactive oxygen species, 2013, **41**, 279–301  
 Singlet oxygen, in biological media, 2015, **42**, 233–278  
 Solar energy conversion, 2017, **44**, 283–293  
 Solid-state, photoreactions, 2016, **43**, 286–320 and 2016, **43**, 321–329  
 TiO<sub>2</sub> photoredox catalysis, 2017, **44**, 362–381  
 UV spectra, calculated, 2015, **42**, 197–214

## References

- 1 Grotthuss and T. Sitzber, *Gesell. Liter. Kunst.*, 1916, **1**, 119–189.
- 2 L. J. Gay-Lussac and L. J. Thénard, *Gilbert's Ann. Phys.*, 1810, **35**, 8.
- 3 E. Warburg, *Naturwissenschaften*, 1917, **5**, 490–494.
- 4 A. Einstein, *Ann. Phys.*, 1905, **17**, 132–148.
- 5 M. Bodenstein and W. Z. Dux, *Phys. Chem.*, 1913, **85**, 325.
- 6 R. Bunsen and H. E. Roscoe, *Poggendorff's Ann.*, 1855, **96**, 373.
- 7 E. Warburg, *Z. Elektrochem. Angew. Phys. Chem.*, 192, **27**, 133–142.
- 8 (a) Royal Swedish Academy of Arts, *Scientific background to the Nobel Prize in Chemistry*, 2016, Molecular Machines, RSAS, Stockholm, 2016; (b) B. L. Feringa, *Angew. Chem. Int. Ed.*, 2017, **56**, 11060–11078; (c) J. Fraser Stoddart, *Angew.*

- Chem. Int. Ed.*, 2017, **56**, 11094–11125; (d) J.-P. Sauvage, *Angew. Chem. Int. Ed.*, 2017, **56**, 11080–11093.
- 9 S. Erbas-Cakmak, D. A. Leigh, C. T. McTernan and A. L. Nussbaumer, *Chem. Rev.*, 2015, **115**, 10081–10206, see also E. R. Kay and D. A. Leigh, *Angew. Chem., Int. Ed.*, 2015, **54**, 10080–10088.
  - 10 (a) D. A. Leigh, *Angew. Chem., Int. Ed.*, 2016, **55**, 14506–14508; (b) G. Gil-Ramírez, D. A. Leigh and A. J. Stephens, *Angew. Chem., Int. Ed.*, 2015, **54**, 6110–6150.
  - 11 C. O. Dietrich-Buchecker, J.-P. Sauvage and J. P. Kintzinger, *Tetrahedron Lett.*, 1983, **24**, 5095–5098.
  - 12 P. R. Ashton, T. T. Goodnow, A. E. Kaifer, M. V. Reddington, A. M. Z. Slawin, N. Spencer, J. F. Stoddart, C. Vicent and D. J. Williams, *Angew. Chem., Int. Ed. Engl.*, 1989, **28**, 1396–1399.
  - 13 See for reviews; V. Balzani, A. Credi, F. Raymo and J. F. Stoddart, *Angew. Chem., Int. Ed.*, 2000, **39**, 3348–3391.
  - 14 N. Koumura, R. W. J. Zijlstra, R. A. van Delden, N. Harada and B. L. Feringa, *Nature*, 1999, **401**, 152–155.
  - 15 Olof Ramström, Scientific Background on the Nobel Prize in Chemistry, *Kungl Vetenskaps Acad*, 2016, [https://www.nobelprize.org/nobel\\_prizes/chemistry/laureates/2016/advanced-chemistry-prize2016.pdf](https://www.nobelprize.org/nobel_prizes/chemistry/laureates/2016/advanced-chemistry-prize2016.pdf).
  - 16 A. R. Hirst, B. Escuder, J. F. Miravet and D. K. Smith, *Angew. Chem., Int. Ed.*, 2008, **47**, 8002–8018.
  - 17 See for instance: X. J. Loh, J. del Barrio, P. P. C. Toh, T.-C. Lee, D. Jiao, U. Rauwald, E. A. Appel and O. A. Scherman, *Biomacromolecules*, 2012, **13**, 84–91
  - 18 V. Balzani, V. A. Credi and M. Venturi, *Molecular Devices and Machines: Concepts and Perspectives for the Nanoworld*, Wiley-VCH, 2008.
  - 19 M. Irie, T. Fukaminato, K. Matsuda and S. Kobatake, *Chem. Rev.*, 2014, **114**, 12174–12277.
  - 20 A. R. Saraf and M. Sadaiah, *Mater. Manuf. Processes*, 2016, DOI: 10.1080/10426914.2016.1198025.
  - 21 S. Martin, *Chairman of the Editorial Board of Tetrahedron Journals*, <https://www.elsevier.com/awards/global/tetrahedron-prize-for-creativity>.
  - 22 J. Pérez Prieto, *EPA Newslett.*, 2016, 123–124.
  - 23 R. M. Young, A. P. N. K. Singh, A. Thazhathveetil, V. Y. Cho, Y. Zhang, N. Renaud, F. C. Grozema, D. N. Beratan, M. A. Ratner, G. C. Schatz, Y. A. Berlin, F. D. Lewis and M. R. Wasielewski, *J. Am. Chem. Soc.*, 2015, **137**, 5113–5122; F. D. Lewis and Y. Wu, *J. Photochem. Photobiol. C: Photochem. Rev.*, 2001, **2**, 1–16.
  - 24 P. D. Tran, L. H. Wong, J. Barber and J. S. C. Loo, *Energy Environ. Sci.*, 2012, **5**, 5902–5918; J. Barber, *Inorg. Chem.*, 2008, **47**, 1700–1710.
  - 25 J. Barber and R. Malkin, in *Techniques and New Developments in Photosynthesis Research*, Springer, UK, 2012.
  - 26 <https://www.acs.org/content/acs/en/funding-and-awards/awards/national/bytopic/josef-michl-acs-award-in-photochemistry.html>.
  - 27 See for instance: L. A. P. Antony, T. Slanina, P. Šebej, T. Šolomek and P. Klán, *Org. Lett.*, 2013, **15**, 4552–4555; A. U. Meyer, T. Slanina, C.-J. Yao and B. König, *ACS Catal.*, 2016, **6**, 369–375.
  - 28 M. Penconi, P. L. Gentili, G. Massaro, F. Elisei and F. Ortica, *Photochem. Photobiol. Sci.*, 2014, **13**, 48–61.
  - 29 N. Armaroli and V. Balzani, *Chem. – Eur. J.*, 2016, **22**, 32–57.
  - 30 X. Li, J. Yu, S. Wageh, A. A. Al-Ghamdi and J. Xie, *Small*, 2016, **12**, 6640–6696.
  - 31 L. Zhou, W. Liang, Z. Lingzhi, L. Jinlong, L. Juying and Y. Liu, *Res. Chem. Intermed.*, 2016, DOI: 10.1007/s11164-016-2748-8.

- 32 Y. Zhao, N. Hoivik and K. Wang, *Nano Energy*, 2016, **30**, 728–744.
- 33 H. He, J. A. Perman, G. Zhu and S. Ma, *Small*, 2016, **12**, 6309–6324.
- 34 A. Dhakshinamoorthy, A. M. Asiri and H. García, *Angew. Chem., Int. Ed.*, 2016, **55**, 5414–5445.
- 35 W. Kim, E. Edri and H. Frei, *Acc. Chem. Res.*, 2016, **49**, 1634–1645.
- 36 A. Iwase, S. Yoshino, T. Takayama, Y. H. Ng, R. Amal and A. Kudo, *J. Am. Chem. Soc.*, 2016, **138**, 10260–10264.
- 37 H. Fujito, H. Kunioku, D. Kato, H. Suzuki, M. Higashi, H. Kageyam and R. Abe, *J. Am. Chem. Soc.*, 2016, **138**, 2082–2085.
- 38 N. Singhal, A. Ali, A. Vorontsov, C. Pendem and U. Kumar, *Appl. Catal., A*, 2016, **523**, 107–117.
- 39 J.-P. Zou, D.-D. Wu, J. Luo, Q.-J. Xing, X.-B. Luo, W.-H. Dong, S.-L. Luo, H.-M. Du and S. L. Suib, *ACS Catal.*, 2016, **6**, 6861–6867.
- 40 H. Seo, M. H. Katcher and T. F. Jamison, *Nat. Chem.*, 2016, DOI: 10.1038/nchem.2690.
- 41 G. Obaid, M. Broekgaarden, A.-L. Bulin, H. C. Huang, J. Kuriakose, J. Liu and T. Hasan, *Nanoscale*, 2016, **8**, 12471–12503.
- 42 W. Kuzyňiak, E. A. Ermilov, D. Atilla, A. G. Gürek, B. Nitzsche, K. Derkow, B. Hoffmann, G. Steinemann, V. Ahsen and M. Höpfner, *Photodiagn. Photodyn. Ther.*, 2016, **13**, 148–157.
- 43 M. Rajendran, *Photodiagn. Photodyn. Ther.*, 2016, **13**, 175–187.
- 44 K. Liu, R. Xing, Q. Zou, G. Ma, H. Mchwald and X. Yan, *Angew. Chem., Int. Ed.*, 2016, **55**, 3036–3039.
- 45 Y. Zhou, X. Liang and Z. Dai, *Nanoscale*, 2016, **8**, 12394–12405.
- 46 J. Schmitt, V. Heitz, A. Sour, F. Bolze, P. Kessler, L. Flamigni, B. Ventura, C. S. Bonnet and É. Tüth, *Chem. – Eur. J.*, 2016, **22**, 2775–2786.
- 47 F. Vohraa, Z. Akram, S. H. Safii, R. D. Vaithilingam, A. Ghanem, K. Sergis and F. Javed, *Photodiagn. Photodyn. Ther.*, 2016, **13**, 139–147.
- 48 U. Keyal, A. K. Bhatta and X. L. Wang, *Photodiagn. Photodyn. Ther.*, 2016, **14**, 191–199.
- 49 Z. Yuan and L. Zhang, *Curr. Org. Chem.*, 2016, **20**, 17–68–1785.
- 50 W. Blachucki, J. Szlachetko, Y. Kayser, J.-C. Dousse, J. Hoszowska, F. Zeeshan and J. Sa, *Nucl. Instrum. Methods Phys. Res., Sect. B*, 2016, DOI: 10.1016/j.nimb.2016.11.029.
- 51 F. N. Castellano, *Inorg. Chem.*, 2016, **55**, 12483–12487.
- 52 N. Zivic, M. Bouzrati-Zerelli, A. Kermagoret, F. Dumur, J.-P. Fouassier, D. Gigmes, J. Lalevée and Jacques, *ChemCatChem*, 2016, **8**, 1617–1631, see also F. Dumur, D. Gigmes, J.-P. Fouassier and J. Lalevée, *Acc. Chem. Res.*, 2016, **49**, 1980–1989.
- 53 E. Ay, Z. Raad, O. Dautel, F. Dumur, G. Wantz, D. Gigmes, J.-P. Fouassier and J. Lalevée, *Macromolecules*, 2016, **49**, 2124–2134.
- 54 R. M. Pearson, C.-H. Lim, B. G. McCarthy, C. B. Musgrave and G. M. Miyake, *J. Am. Chem. Soc.*, 2016, **138**, 11399–11407.
- 55 S. Garbarino, D. Ravelli, S. Protti and A. Basso, *Angew. Chem., Int. Ed.*, 2016, **55**, 15476–15484.
- 56 A. L. Fuentes de Arriba, F. Urbitsch and D. J. Dixon, *Chem. Commun.*, 2016, **52**, 14434–14437.
- 57 L. Chen, H. Li, P. Li and L. Wang, *Org. Lett.*, 2016, **18**, 3646–3649.
- 58 Y. Zhao, J.-R. Chen and W.-J. Xiao, *Org. Lett.*, 2016, **18**, 6304–6307.
- 59 V. Gauchot and A.-L. Lee, *Chem. Commun.*, 2016, **52**, 10163–10166.
- 60 A photocatalyst free variant of the process has been recently published by Fouquet and coworkers, see T. Cornilleau, P. Hermange and E. Fouquet, *Chem. Commun.*, 2016, **52**, 10040–10043

- 61 Z. Duan, W. Li and A. Lei, *Org. Lett.*, 2016, **18**, 4012–4015.
- 62 C. P. Johnston, R. T. Smith, S. Allmendinger and D. W. C. MacMillan, *Nature*, 2016, **536**, 322–325.
- 63 E. B. Corcoran, M. T. Pirnot, S. Lin, S. D. Dreher, D. A. DiRocco, I. W. Davies, S. L. Buchwald and D. W. C. MacMillan, *Science*, 2016, **353**, 279–283.
- 64 N. A. Romero and D. A. Nicewicz, *Chem. Rev.*, 2016, **116**, 10075–10166.
- 65 Y. Jin, H. Yang and H. Fu, *Org. Lett.*, 2016, **18**, 6400–6403.
- 66 C. Yang, J.-D. Yang, Y.-H. Li, X. Li and J.-P. Cheng, *J. Org. Chem.*, 2016, **81**, 12357–12363.
- 67 S. Mukherjee, B. Maji, A. Tlahuext-Aca and F. Glorius, *J. Am. Chem. Soc.*, 2016, **138**, 16200–16203.
- 68 R. Ciriminna, R. Delisi, Y.-J. Xu and M. Pagliaro, *Org. Process Res. Dev.*, 2016, **20**, 403–408.
- 69 M. Baumann and I. R. Baxendale, *React. Chem. Eng.*, 2016, **1**, 147–150.
- 70 M. Oelgemöller and N. Hoffmann, *Org. Biomol. Chem.*, 2016, **14**, 7392–7442.
- 71 A. Albini, *Photochemistry: Past, Present and Future*, Springer, UK, 2016.
- 72 *Applied Photochemistry. When Light Meets Molecules*, ed. S. Silvi and G. Pergamini, Springer, UK, 2016.
- 73 M. Kozlowski and T. Yoon, *J. Org. Chem.*, 2016, **81**, 6895–6897.
- 74 Y. Wang, H. Yin, X. Tang, Y. Wu, Q. Meng and Z. Gao, *J. Org. Chem.*, 2016, **81**, 7042–7050.
- 75 M. Oelgemöller and K. Loubiere, *Chem. Eng. Technol.*, 2016, **39**, 12.
- 76 T. Aillet, K. Loubière, O. Dechy-Cabaret and L. Prat, *Chem. Eng. Technol.*, 2016, **39**, 115–122.
- 77 M. N. Hopkinson, A. Tlahuext-Aca and F. Glorius, *Acc. Chem. Res.*, 2016, **49**, 2261–2272.
- 78 K. A. Margrey and D. A. Nicewicz, *Acc. Chem. Res.*, 2016, **49**, 1997–2006.
- 79 O. Reiser, *Acc. Chem. Res.*, 2016, **49**, 1990–1996.
- 80 A. Beeler, *Chem. Rev.*, 2016, **116**, 9629–9630.
- 81 S. Poplat, A. Tröster, Y.-Q. Zouand and T. Bach, *Chem. Rev.*, 2016, **116**, 9748–9815.
- 82 R. Remy and C. G. Bochet, *Chem. Rev.*, 2016, **116**, 9816–9849.
- 83 D. Ravelli, S. Protti and M. Fagnoni, *Chem. Rev.*, 2016, **116**, 9850–9913.
- 84 A. A. Ghogare and A. Greer, *Chem. Rev.*, 2016, **116**, 9994–10034.
- 85 M. D. Kärkäs, J. A. Porco Jr. and C. R. J. Stephenson, *Chem. Rev.*, 2016, **116**, 9683–9747.
- 86 D. Cambié, C. Bottecchia, N. J. W. Straathof, V. Hesseland and T. Noël, *Chem. Rev.*, 2016, **116**, 10276–10341.
- 87 K. L. Skubi, T. R. Blum and T. P. Yoon, *Chem. Rev.*, 2016, **116**, 10035–10074.
- 88 M. Oelgemöller, *Chem. Rev.*, 2016, **116**, 9664–9682.
- 89 T. Mori, G. Fukuhara and T. Wad, *J. Photochem. Photobiol. A*, 2016, **331**, 2–7.
- 90 M. Fujiki, K. Yoshida, N. Suzuki, N. Azur, A. Rahim and J. A. Jalil, *J. Photochem. Photobiol. A*, 2016, **331**, 120–129.
- 91 D. Kulesza, P. Bolek, A. J. J. Bos and E. Zych, *Coord. Chem. Rev.*, 2016, **325**, 29–40.

---

# Light induced reactions in cryogenic matrices (highlights 2015–2016)

Rui Fausto,\* Timur Nikitin and Andrea Gómez-Zavaglia

DOI: 10.1039/9781788010696-00022

This chapter reviews investigations on light induced reactions in cryogenic matrices that were reported in 2015 and 2016. Conformational isomerizations and tautomerizations as well as other types of structural isomerizations triggered by ultraviolet/visible or infrared irradiation of matrix-isolated organic compounds are discussed. Light-initiated fragmentation processes taking place in cryomatrices are also considered. The studies herein highlighted exemplify recent applications of the matrix isolation technique in these fields of research. Photochemical processes involving direct participation of noble gas atoms, leading to the formation of covalently bound noble gas compounds, are also addressed in short.

## 1 Introduction

Following previous reports published in volumes 37, 38, 39, 41 and 43 of this series,<sup>1–5</sup> where literature dealing with light induced reactions in cryogenic matrices published from July 2004 to December 2014 was reviewed, this chapter highlights relevant investigations on this topic appearing in the specialized literature during 2015 and 2016.

The present review focuses only on studies performed on organic compounds. Section 2 centers on conformational isomerization processes promoted either by ultraviolet/visible (UV/Vis) or infrared (IR) light. Section 3 addresses the general subject of photoinduced structural isomerizations, including tautomerizations. Section 4 refers to photo-fragmentation reactions, which in general involve the formation of reactive intermediates or weakly bound species. Finally, Section 5 considers in brief the processes where the matrix noble gas atoms participate directly, leading to the formation of covalently bound noble gas compounds.

For those that are less aware of the fundamental principles of matrix isolation and strategies of research usually applied in connection with this technique, the classic books by Meyer,<sup>6</sup> Andrews and Moskovits,<sup>7</sup> Barnes *et al.*,<sup>8</sup> Dunkin,<sup>9</sup> and Fausto<sup>10</sup> may be used as introductory textbooks to this chapter. More recent and specialized general publications on this subject are also available,<sup>11–21</sup> including the thematic special issue of the *Journal of Molecular Structure* edited by Fausto, Lapinski and Reva,<sup>19</sup> dedicated to the matrix isolation technique and its applications in the study of light induced reactions. Frija *et al.*<sup>22</sup> have recently reviewed the strategies for *in situ* preparation of rare molecules (e.g., antiaromatic diazirines, diaziridines, carbodiimides, nitriles, reactive isocyanates, azides, and tetrazetes) resulting from UV/Vis irradiation of matrix-isolated tetrazole precursors. Khlebnikov and Novikov<sup>23</sup> have presented an elegant review on the chemistry of 2*H*-azirines. The spectroscopy, dynamics,

---

Department of Chemistry, University of Coimbra, P-3004-535 Coimbra, Portugal.  
E-mail: rfausto@ci.uc.pt

reactivity, and electronic structure of iso-halocarbons have been reviewed by Reid.<sup>24</sup> Hama and Watanabe<sup>25</sup> and Zack and Maier<sup>26</sup> have focused on astrophysically relevant photochemical investigations based on the use of matrix isolation. Bahou *et al.*<sup>27</sup> presented an interesting synopsis on the use of *para*-hydrogen matrices in the investigation of free radicals. The book “*Physics and chemistry at low temperatures*”,<sup>28</sup> edited by Khriachtchev, covers a wide range of topics on low-temperature chemistry and physics and also gives particular emphasis to applications of the matrix isolation method. General information on light-induced noble gas chemistry in cryogenic matrices has been gathered in the reviews by Nemukhin *et al.*,<sup>29</sup> Khriachtchev, Räsänen and Gerber,<sup>30</sup> Gerber, Tsivion, Khriachtchev and Räsänen,<sup>31</sup> and Brock and Schrobilgen.<sup>32</sup> The last review presents a digest of the literature reported during 2012 about the noble gases, with emphasis given to the synthesis, isolation, and characterization of new noble gas compounds.

In the 2015–2016 period, the interesting review by Khriachtchev<sup>33</sup> describing new approaches to the study of non-covalent interactions in matrix-isolated systems, where the use of *in situ* photolysis techniques to this objective is addressed in detail, shall be highlighted here as well as that on radiation induced transformations of small molecules, by Feldman *et al.*,<sup>34</sup> where some interesting mechanistic insights on astrophysical and atmospheric relevant processes are presented.

Particularly sound studies on light induced reactions in cryogenic matrices reported during the period 2015–2016 must be pointed out: (i) the series of studies that share the feature of having demonstrated the remarkable possibility of occurrence of conformational isomerizations by vibrational excitation of a remote bond to the group undergoing the structural changes, which include the works of Halasa *et al.*<sup>35,36</sup> on 2-thiocytosine and kojic acid and that of Lopes Jesus *et al.*<sup>37</sup> on 6-methoxyindole; (ii) the interesting work of Lopes *et al.*,<sup>38</sup> in which rare dimers of acetic acid containing the higher energy *trans* conformer were produced and characterized structurally and vibrationally for the first time, taking advantage of the possibility of efficient *in situ* generation of *trans* acetic acid by vibrational excitation of the more stable *cis* conformer and of the different mobility in a N<sub>2</sub> matrix of the two conformers upon thermal mobilization; (iii) the investigation carried out by Ünsalan *et al.*<sup>39</sup> on matrix-isolated stilbene unimolecular photochemistry, leading to experimental detection of a metastable non-planar form of *E*-stilbene and its structural characterization by a combined chemometrics/spectroscopic approach; (iv) the two milestone studies of Nunes *et al.*,<sup>40,41</sup> where bond-shift isomers (allenic and propargylic) were discovered for phenylnitrile imine generated *in situ* by photolysis of 5-phenyltetrazole in Ar and Kr matrices,<sup>40</sup> and reporting the first observation of a tunneling reaction involving a nitrene;<sup>41</sup> (v) the report by Krupa, Kosendiak and Wierzejewska<sup>42</sup> of preparation and characterization of the first hydrogen-bonded molecular complex to atomic sulfur (<sup>3</sup>P) detected experimentally; (vi) the first production and characterization of a series of fluorinated cyanide and isocyanide krypton and xenon derivatives, by Zhu, Räsänen and Khriachtchev.<sup>43</sup>

## 2 Light induced conformational isomerizations in cryomatrices

In this section, relevant contributions reported in the period covered by this review on conformational isomerization processes induced by light and taking place for matrix-isolated molecules are summarized.

Wong *et al.*<sup>44</sup> investigated the conformational composition of  $\beta$ -alanine in *para*-hydrogen (*p*-H<sub>2</sub>) matrices and identified five out of the eleven lowest energy conformers of the compound, with the support of quantum chemical calculations performed at the B3LYP/aug-cc-pVTZ level of theory (Fig. 1). The authors highlighted the isolation, for the first time, of conformer **III**, which, contrarily to the two most stable conformers **I** and **II**, does not possess any intramolecular hydrogen bond. Identification of conformer **V**, the only low-energy conformer bearing an OH $\cdots$ N intramolecular hydrogen bond, was not successful. UV irradiation of the matrices resulted in the decrease of the populations of conformers **I**, **II** and **VII**, and an increase of those of the high-energy conformers **III** and **IV**, allowing for a clear spectroscopic characterization of all these species. The results were compared with those obtained for the compound trapped in argon matrices, and it was concluded that the high-energy conformers (*e.g.*, conformer **III**) could only be efficiently trapped in *p*-H<sub>2</sub> because of the specific properties of this type of matrix.<sup>44</sup>

This fact was considered an indication of the utility of investigating molecules with large conformational flexibility under these experimental conditions.

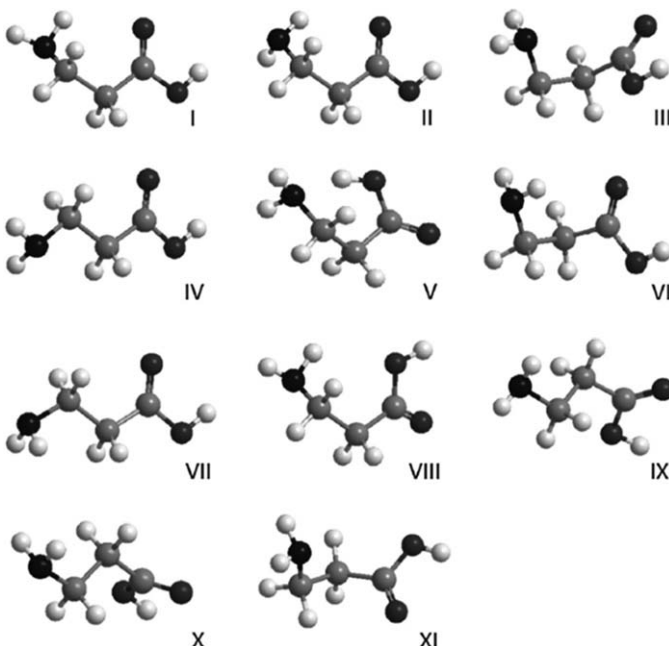


**Fig. 1** B3LYP/aug-cc-pVTZ predicted structures for the 11 lowest energy  $\beta$ -alanine conformers. Reprinted from *J. Mol. Spectrosc.*, 310, Y. T. A. Wong, S. Y. Toh, P. Djuricanin and T. Momose, 2015, Conformational composition and population analysis of  $\beta$ -alanine isolated in solid parahydrogen, 23–31. Copyright (2015), with permission from Elsevier.<sup>44</sup>

In a later work, Stepanian *et al.*<sup>45</sup> investigated  $\beta$ -alanine-d<sub>3</sub> to confirm the conformational composition of  $\beta$ -alanine in argon matrix, in particular, to re-evaluate the presence of conformer V in a freshly deposited argon matrix of this compound (Fig. 1). The observation in the spectra of a broad band at 2201 cm<sup>-1</sup>, ascribable to an OD stretching vibration involved in an intramolecular hydrogen bond, was considered as a direct evidence of conformer V (Fig. 2). The authors also confirmed the presence of conformers I, II, and IV in that matrix. As observed by Wong *et al.*,<sup>44</sup> for the non-substituted isotopomer, UV irradiation led to a decrease of the populations of conformers I and II (with an N–D···O intramolecular H-bond), together with an increase of the populations of conformers V and IV, bearing respectively an O–D···N H-bond and no intramolecular H-bonds. On the other hand, conformers III and VII, previously reported in the study of non-deuterated  $\beta$ -alanine,<sup>44</sup> were not identified in the matrix of the  $\beta$ -alanine-d<sub>3</sub> isotopomer. The observed photoisomerizations, together with calculated IR spectra for the various conformers of the molecule, assisted the assignment of the experimental bands to the different species.

Kócs *et al.*<sup>46</sup> investigated the structures of glycine·H<sub>2</sub>O complexes in low-temperature inert matrices. The matrices were irradiated with near-infrared (NIR) laser light to change the relative abundances of the complexes. Irradiations at the frequencies of the first overtone of the OH stretching mode of glycine and of the water molecule in the complex and at combinations of the OH stretching and the COH/HOH bending modes promote structural changes that enable the study of high-energy

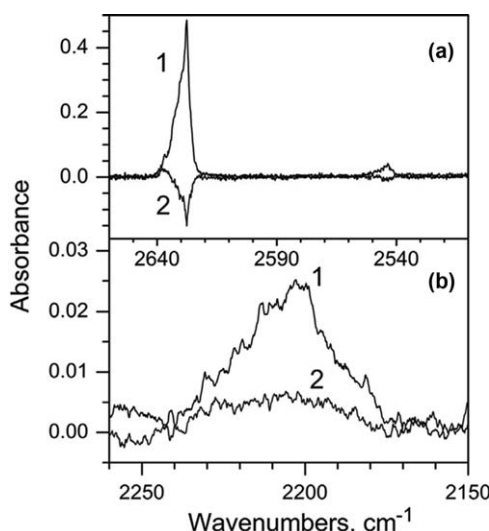


**Fig. 2** IR spectra of  $\beta$ -alanine-d<sub>3</sub> isolated in Ar matrix ( $T=6$  K): (a) region of OD and ND stretching vibrations; (b) region where the stretching vibration of H-bonded OD group of conformer V is observed. (1) Spectrum registered immediately after deposition of the matrix; (2) difference spectrum, UV irradiated matrix ( $t=40$  min) minus as-deposited matrix. Reprinted from *J. Mol. Spectrosc.*, 320, S. G. Stepanian, A. Y. Ivanov and L. Adamowicz, FTIR spectra and conformational structure of deuteron- $\beta$ -alanine isolated in Ar matrices, 13–24. Copyright (2016), with permission from Elsevier.<sup>45</sup>

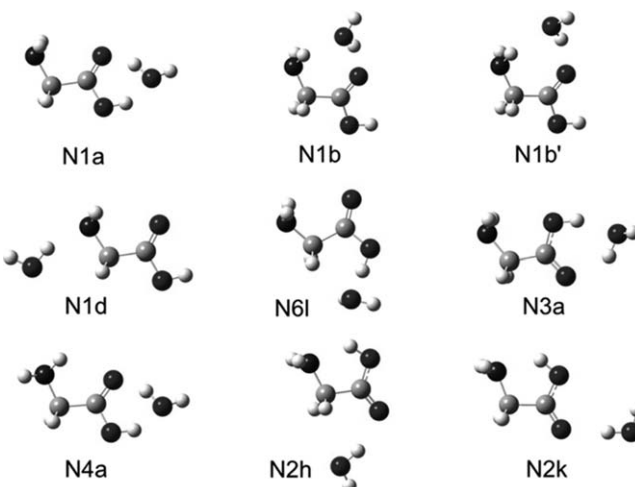


**Fig. 3** Structures of glycine·H<sub>2</sub>O complexes discussed in Kócs *et al.* Reprinted with permission from L. Kócs, E. E. Najbauer, G. Bazsó, G. Magyarfalvi and G. Tarczay, *J. Phys. Chem. A*, 2015, **119**, 2429–2437. Copyright (2015) American Chemical Society.<sup>46</sup>

complexes as well as characterization in deeper detail of the IR spectra of the formerly identified **N1a** species (Fig. 3). The authors identified complexes **N1b** and **N1d**, which as **N1a** have the glycine molecule in its most stable conformer 1 (although the latter with some uncertainty), but also complexes where the glycine unit exists as conformers 2 (**N2h** and **N2k**) or 6 (**N6l**). The population of conformer 2 of glycine can be significantly enriched in the matrices by NIR laser irradiation of conformer 1, and the annealing of water-containing argon matrices after this enrichment leads to the formation of the **N2h** and **N2k** complexes. In turn, 6 is a short-lived glycine conformer in low-temperature matrices that can also be prepared by irradiating the OH stretching overtone of conformer 1. Therefore, the NIR irradiation of conformer 1 in water-rich argon matrices followed by thermal mobilization was also found to lead to the formation of the **N6l** complex.

Coussan and Tarczay<sup>47</sup> have also investigated the conformational changes of matrix-isolated glycine and glycine·H<sub>2</sub>O complexes induced by IR light, but in this case, the fundamental OH and NH stretching vibrational modes were selected for irradiation (in the mid-IR region). Although mid-IR irradiations were found to be less efficient than NIR irradiations in promoting conformational changes, they were shown to efficiently promote the selective depletion of different glycine conformers and glycine·water complexes and formation of new forms. The simultaneous use of mid-IR and NIR irradiation to induce conformational changes can thus facilitate the conformational analysis in complicated cases. Nevertheless, the authors stressed that, while the analysis of the simpler difference spectra obtained after mid-IR irradiation can be a good starting point for the spectral scrutiny and discovery of novel conformers and new aggregated species based on rare conformers, the more effective NIR irradiations are important to obtain spectra with better signal-to-noise level and to access the conversion paths with larger barriers.

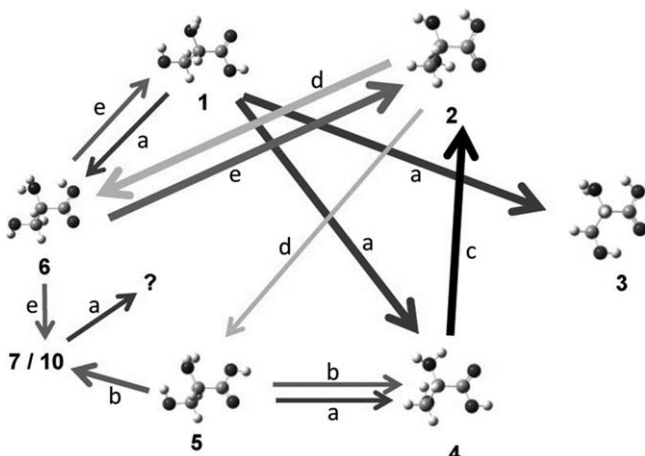


**Fig. 4** Scheme of conformational conversions promoted by NIR laser irradiations of serine in an Ar matrix at different frequencies. Irradiations in the region of the first overtone of the carboxylic OH-stretching:  $6941\text{ cm}^{-1}$  (a),  $6950\text{ cm}^{-1}$  (b), and  $6960\text{ cm}^{-1}$  (c), and in the region of the first overtone of the side-chain OH-stretching:  $7082\text{ cm}^{-1}$  (d) and  $7150\text{ cm}^{-1}$  (e). Reprinted with permission from E. E. Najbauer, G. Bazsó, R. Apóstolo, R. Fausto, M. Biczysko, V. Barone and G. Tarczay, *J. Phys. Chem. B*, 2015, **119**, 10496–10510. Copyright (2015) American Chemical Society.<sup>48</sup>

Najbauer *et al.*<sup>48</sup> focused their attention on another amino acid: serine. By using matrix isolation 2D IR spectroscopy to probe the results of NIR laser irradiation of the matrices, they unambiguously assigned the spectral lines to individual conformers. Comparison of the experimental data with IR spectra computed using high-level theoretical methods that included electron correlation and dispersion forces together with mechanical and electrical anharmonicities allowed the unequivocal identification of six conformers (**1–6** in Fig. 4) and revealed the presence of at least one additional conformer (**7** and/or **10**) in the matrices. Other low energy conformers that could in principle be expected to be observed (forms **8**, **9**, **11**) remained to be detected. These results were explained taking into account the low conformational isomerization barriers between these forms and low-energy conformers, which are small enough to allow conformational relaxation to take place even at the temperature of the matrix.

Besides the formerly observed stable conformers, the authors were also able to generate, for the first time by NIR irradiation, a rather unstable conformer that rapidly decays by H-atom tunneling to another conformer, even in a nitrogen matrix, and that could not be observed in the argon matrices. Although the exact side-chain conformation of this short-lived conformer could not be determined, its carboxylic group conformation was identified as being *trans*, and the absence of any intramolecular H-bond was also established.<sup>48</sup>

Very interestingly, it was found that the excitation of the stretching overtones of both the side-chain and the carboxylic OH groups can effectively promote conformational changes, but the two kinds of excitations induce different types of conversions.

Noble and Coussan<sup>49</sup> addressed the conformational equilibria and IR-induced isomerization processes of 1-propanol and some of its isotopomers ( $-\text{OD}$  and  $-\text{CD}_3$ ). The effects of deuteration were investigated. Upon selective IR irradiation of the isotopically substituted species in the  $\nu\text{OH}$  and  $\nu\text{OD}$  regions, several conformers that interconvert into each other were identified. The interpretation of the experimental results received support from data obtained using theoretical methods.

The authors found that alkyl chain isomerization in the studied molecules can be induced in both rare gas and nitrogen matrices by appropriate selective IR irradiation, and noticed that the competition between intramolecular vibrational energy relaxation and interaction with the matrix determines the torsional subspace dynamics of the vibrationally excited 1-propanol molecules. Mechanistic insights for intramolecular vibrational relaxation in the studied molecule were discussed in detail, and some interesting questions on this subject rose for future investigation.

Canneva *et al.*<sup>50</sup> studied the conformational composition of  $(\text{CH}_3)_3\text{CSNO}$  in several phases using different techniques. The gas phase composition was investigated by electron diffraction and gas phase and matrix isolation IR spectroscopies. Two conformers, *anti* and *syn* (Fig. 5), were identified in the vapor phase at room temperature in an 80 : 20 population ratio, in good agreement with the theoretical predictions obtained at the MP2(full)/cc-pVTZ level of approximation. Both conformers co-existed in the gas phase at room temperature and were successfully trapped in argon matrix. Broadband UV/Vis irradiation led to partial *anti* to *syn* isomerization, accompanied by photolysis of the compound.

2-Thiocytosine was isolated in Ne, Ar, and  $\text{N}_2$  matrices and the nature of the trapped forms was investigated by Halasa and co-workers.<sup>35</sup> Two trapped amino-thiol conformers, differing in the orientation of the SH group, were selectively excited to the 1st overtone (or combination mode) of the  $\text{NH}_2$  stretching vibrational states, using narrowband NIR light generated in a tunable diode laser (Fig. 6). The conformational transformations were monitored using IR spectroscopy, providing a clear evidence of the vibrational energy redistribution from the initially excited  $\text{NH}_2$  moiety to the remote SH group, which changes its orientation.

In a somewhat similar study, published almost simultaneously with that of Halasa *et al.* on 2-thiocytosine,<sup>35</sup> Lopes Jesus *et al.*<sup>37</sup> reported the reversible interconversion between the two conformers of 6-methoxyindole (Fig. 7), accomplished by selective vibrational excitation of a bond ( $\text{NH}$ ) remotely located in relation to the isomerizing fragment ( $\text{OCH}_3$ ).

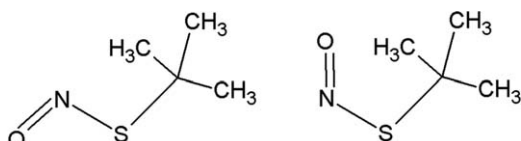


**Fig. 5** Molecular structures of *anti* (left) and *syn* (right) conformers of  $(\text{CH}_3)_3\text{CSNO}$ . Adapted with permission from ref. 50, A. Canneva, M. F. Erben, R. M. Romano, Y. V. Vishnevskiy, C. G. Reuter, N. W. Mitzel and C. O. della Védova, *Chem. - A Eur. J.*, John Wiley and Sons. © 2015 WILEY-VCH Verlag GmbH & Co. KGaA, Weinheim.

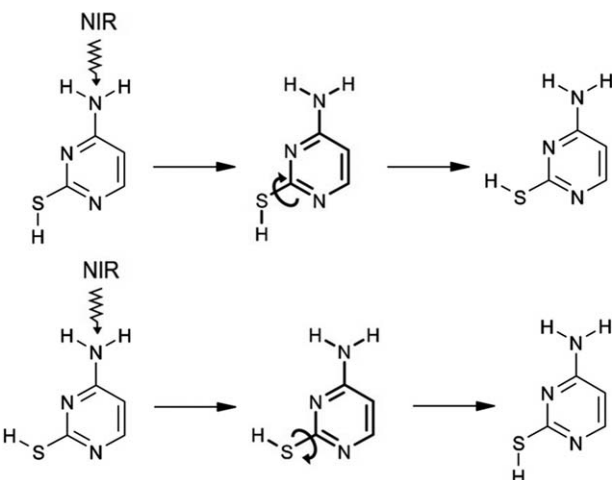


**Fig. 6** Long range conformational changes induced in isolated 2-thiocytosine monomers by narrowband, selective NIR excitations of  $2\nu_a\text{NH}_2$  or  $\nu_a\text{NH}_2 + \nu_s\text{NH}_2$  stretching vibrations. Reprinted with permission from A. Halasa, L. Lapinski, H. Rostkowska and M. J. Nowak, *J. Phys. Chem. A*, 2015, **119**, 9262–9271. Copyright (2015) American Chemical Society.<sup>35</sup>

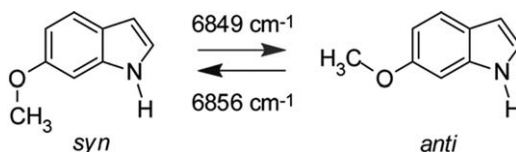


**Fig. 7** Conformers of 6-methoxyindole and effects of the narrow band NIR irradiations. The numbers next to the arrows correspond to the experiments performed in a xenon matrix. Reprinted with permission from A. J. Lopes Jesus, I. Reva, C. Araujo-Andrade and R. Fausto, *J. Am. Chem. Soc.*, 2015, **137**, 14240–14243. Copyright (2015) American Chemical Society.<sup>37</sup>

The excited NH stretching coordinate is separated by four bonds from the methoxy group that changes its orientation. The observed processes are nondestructive and take place in large scale, proving the efficiency of the intramolecular vibrational relaxation to carry the energy deposited in the distant NH stretching coordinate into the reactive C–O torsional mode.

In a subsequent study, Lopes Jesus *et al.*<sup>51</sup> investigated the conformational changes induced thermally or upon broadband IR excitation of matrix-isolated 6-methoxyindole. The results were found to be substantially different in argon and xenon matrices. In argon, the gas phase conformational equilibrium prior to matrix preparation could be efficiently trapped in the matrix: at 323 K, a *syn*:*anti* population ratio of about 2:1 was measured, matching well the theoretically predicted population ratio at that temperature. Due to the tight trapping cages in the argon solid lattice (compared with xenon), no conformational isomerization was observed when exposed to the unfiltered broadband IR radiation of the spectrometer beam. On the other hand, the conformational composition existing in xenon in the gas phase could only be efficiently trapped in the matrix when the high-energy IR light

( $>2200\text{ cm}^{-1}$ ) of the spectrometer beam was blocked during the experiments. Exposition of the sample to the unfiltered spectrometer IR beam led to IR-induced conformational interconversions even below the temperature at which the thermally induced *anti*  $\rightarrow$  *syn* conversion becomes accessible ( $\sim 35\text{ K}$ ). Prolonged exposition to the unfiltered spectrometer IR beam led to the attainment of a photo-stationary state with a population ratio of about 1:1, regardless of the initial conformational composition of 6-methoxyindole in the xenon matrix.

The effect of the unfiltered spectrometer IR beam on the 6-methoxyindole conformational mixture was also shown<sup>51</sup> to be the reason why it was found to be impossible to completely depopulate the high-energy *anti* conformer upon annealing (at 50 K) of the xenon matrix when the spectrometer IR beam was used during spectra collection. The different population ratio (about 1.5 : 1) measured immediately after deposition of the xenon matrix, compared to that observed in the case of both the argon matrix and xenon matrix kept protected from radiation with  $\lambda > 2200\text{ cm}^{-1}$ , results from a partial *anti*  $\rightarrow$  *syn* conversion, induced by the spectrometer light source.

Another interesting study, proving the efficiency of long-range vibrational energy redistribution, focused on kojic acid.<sup>36</sup> In this case, irradiation with narrowband NIR light tuned at frequencies corresponding to the overtone of the stretching vibrations of the OH bond of both hydroxymethyl and phenol substituents was found to lead to conversion between two conformers of the compound (Fig. 8). The result of excitation of the phenol moiety is another interesting case of efficient vibrational energy redistribution leading to conformational changes in a remotely located fragment of the molecule.

Vibrational excitation was also successfully used to generate a rare conformer of 2-furoic acid trapped in argon and neon matrices.<sup>52</sup> In the gas phase, the compound exists as a mixture of two *cis* conformers differing in the orientation of the carboxylic group relative to the furan ring (**I** and **II**; Fig. 9). Narrowband NIR excitation of the OH stretching overtone vibrations resulted in the transformation of one of the initially observed conformers (**I**) into a new form (**III**), which bears a *trans* carboxylic group. The hydrogen-bond-like O-H  $\cdots$  O interaction (between the O-H group of the carboxylic moiety and the oxygen atom of the furan ring) was shown to be rather weak in the photoproduced conformer but

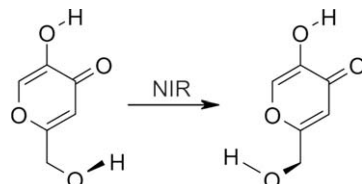


**Fig. 8** NIR-induced conformational conversion in kojic acid. The transformations were induced by excitation of the hydroxymethyl group (in the two directions) or the remotely located phenol group (in the direction indicated in the figure). Reprinted with permission from A. Halasa, I. Reva, L. Lapinski, H. Rostkowska, R. Fausto and M. J. Nowak, *J. Phys. Chem. A*, 2016, **120**, 2647–2656. Copyright (2016) American Chemical Society.<sup>36</sup>

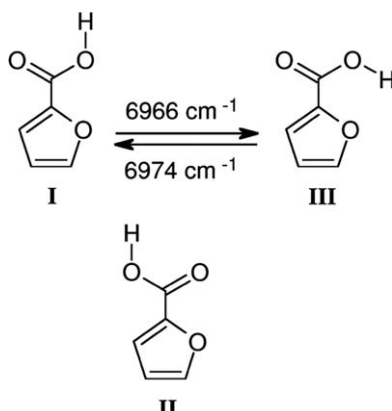


**Fig. 9** Observed conformers of 2-furoic acid and reversible conformational isomerization induced by selective *in situ* narrowband NIR irradiation (in the OH stretching region). The III → I isomerization was also found to take place in the dark, spontaneously, by tunneling on a time scale of hours (depending on the matrix material and temperature). Reprinted with permission from A. Halasa, L. Lapinski, I. Reva, H. Rostkowska, R. Fausto and M. J. Nowak, *J. Phys. Chem. A*, 2015, **119**, 1037–1047. Copyright (2015) American Chemical Society.<sup>52</sup>

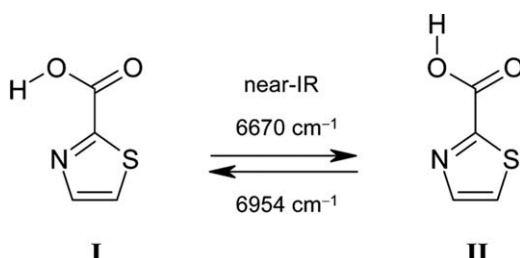


**Fig. 10** NIR induced conformational isomerizations in matrix-isolated thiazole-2-carboxylic acid (the wavenumbers 6670 and 6954 cm<sup>-1</sup> refer to excitations of the compound isolated in argon). UV excitations at different wavelengths (300 nm (I → II) and 305 nm (II → I)) also induce these conformational transformations. The II → I process can also take place spontaneously by tunneling. Reprinted with permission from A. Halasa, I. Reva, L. Lapinski, M. J. Nowak and R. Fausto, *J. Phys. Chem. A*, 2016, **120**, 2078–2088. Copyright (2016) American Chemical Society.<sup>53</sup>

yet able to stabilize its structure, so that it was still present in the matrix after several hours following its NIR-induced generation. The photo-generated form III was also found to spontaneously convert back into the more stable conformer I at a rate that is dependent on the temperature and the matrix material. The experimentally determined half-life times of this conformational conversion occurring in the dark are 1390 and 630 min in Ar matrices kept at 5.5 K and 15 K, respectively, and 240 min in a Ne matrix at 5.5 K.

Other similar investigations were performed on thiazole-2-carboxylic, 2-pyridinecarboxylic acid, oxamic, pyruvic, and gallic acids.<sup>53–57</sup>

In the case of thiazole-2-carboxylic acid,<sup>53</sup> the most stable conformer I (Fig. 10), with the carboxylic moiety assuming the *trans* orientation and with the hydrogen atom of the OH group directed towards the nitrogen atom of the ring, could be reversibly converted into conformer II

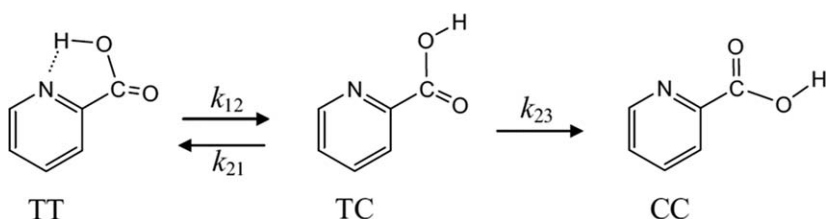


**Fig. 11** Observed conformational isomerization transformations induced by UV light in matrix-isolated 2-pyridinecarboxylic acid. Reprinted from *J. Mol. Struct.*, 1086, M. Miyagawa, N. Akai and M. Nakata, UV light induced conformational changes of 2-pyridinecarboxylic acid in low-temperature argon matrices, 1–7. Copyright (2015), with permission from Elsevier.<sup>54</sup>

(differing from **I** by 180° rotation of the OH group around the C–O bond) upon narrowband NIR νOH overtone excitation. The conformational isomerizations could also be achieved by narrowband UV excitations at 300 nm (**I**→**II**) and 305 nm (**II**→**I**). In addition, a slow spontaneous conversion of **II** into the most stable form **I** was also observed for the compound trapped in the N<sub>2</sub> matrix at 15 K and kept in the dark, on a time-scale larger than 50 h. Thiazole-2-carboxylic acid was also shown to partially decompose thermally at room temperature into CO<sub>2</sub> and thiazole.

2-Pyridinecarboxylic acid has some structural similarities with 2-thiazole-carboxylic acid. Miyagawa *et al.*<sup>54</sup> were able to isolate the lowest energy conformer (**TT**; Fig. 11) of that compound, which is stabilized by an intramolecular OH···N hydrogen bond, in argon matrix. Upon *in situ* irradiation with UV light provided by a super high-pressure mercury lamp, the hydrogen bond brakes leading to two less stable conformers (**TC** and **CC**). The second more stable conformer (**TC**), having a C=O···HC interaction, is produced during the early stages of the UV irradiation performed without any optical filter, while conformer **CC** is produced upon prolonged irradiation. The reverse transformation from **TC** to **TT** occurs upon irradiation at  $\lambda > 270$  nm. The authors identified the conformers by comparing the observed IR bands of the photo-produced species with results from DFT calculations and performing a kinetic analysis based on the changes of the IR intensities with the irradiation time. The relative similarity of the results obtained in the studies on 2-pyridinecarboxylic acid<sup>54</sup> and 2-thiazole-carboxylic acid<sup>53</sup> is interesting, since in the first case, broadband UV irradiation was applied, while in the second, narrowband IR light was used. The last procedure is considerably more selective, but the first one, when applicable, may lead to generation of conformers otherwise not accessible to experimentation.

For oxamic acid, the most stable conformer **I** (Fig. 12), with the *trans* orientation of both the O=COH and the O=CC=O moieties, was trapped from the gas phase into low-temperature matrices and irradiated with narrowband NIR light tuned at its OH stretching overtone (Ar: 6833<sup>-1</sup>; Ne: 6840 cm<sup>-1</sup>).<sup>55</sup> Upon such irradiations, a new conformer (**II**) was generated, with the *cis* orientation of the O=COH group and the *trans* orientation of the O=CC=O fragment. Subsequent irradiations of the matrices at 6940 (Ar) or 6991 cm<sup>-1</sup> (Ne), where the OH stretching

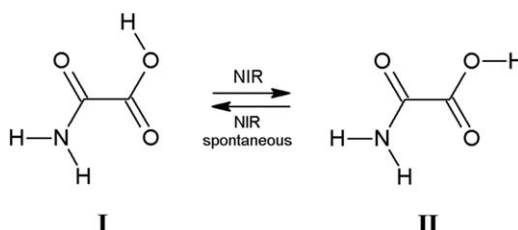


**Fig. 12** NIR-induced conformational transformations between forms I and II of oxamic acid. The II → I isomerization was also found to take place in the dark, spontaneously, by tunneling. Adapted with permission from A. Halasa, L. Lapinski, H. Rostkowska, I. Reva and M. J. Nowak, *J. Phys. Chem. A*, 2015, **119**, 2203–2210. Copyright (2015) American Chemical Society.<sup>55</sup>

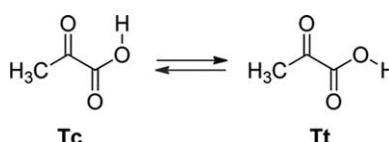


**Fig. 13** NIR-induced selective conformational isomerizations observed for matrix-isolated pyruvic acid. Reprinted with permission from I. Reva, C. M. Nunes, M. Biczysko and R. Fausto, *J. Phys. Chem. A*, 2015, **119**, 2614–2627. Copyright (2015) American Chemical Society.<sup>56</sup>

overtone of the photoproduced conformer is observed, led to the reverse conversion of this form into conformer **I**. The spontaneous **II** → **I** transformation (by tunneling) was also observed for samples kept in the dark.

In the case of pyruvic acid, the detailed structural and vibrational characterization of several conformers was performed by combining matrix isolation IR spectroscopy (in argon and nitrogen matrices) with fully anharmonic calculations of the fundamental modes, overtones, and combinations up to two quanta.<sup>56</sup> The initially dominating conformer in the matrices (**Tc**), with a *trans* CCOH arrangement and stabilized by a strong intramolecular H-bond (Fig. 13), was successfully converted in large amounts to the high-energy conformer **Tt** (with a *trans* CCOH arrangement) by selective NIR excitation of its first OH overtone ( $6630\text{ cm}^{-1}$  in Ar;  $6643\text{ cm}^{-1}$  in N<sub>2</sub>). The **Tt** conformer was then converted back to **Tc** using a similar strategy, through irradiation at  $6940\text{ cm}^{-1}$  (in Ar) or  $6894\text{ cm}^{-1}$  (in N<sub>2</sub>). It was found that in the N<sub>2</sub> matrix the **Tt** form is stabilized due to interaction between the OH group and the matrix molecules. This stabilization manifests itself in the absence of spontaneous **Tt** → **Tc** relaxation (as observed in the argon matrix) and in a considerable change of the vibrational **Tt** signature upon going from argon to nitrogen matrices. It was also demonstrated that in the presence of broadband NIR light the **Tt** → **Tc** relaxation taking place in argon matrix considerably increases its rate, and mechanistic details explaining this fact were provided.

For the structurally more complex gallic acid (3,4,5-trihydroxybenzoic acid; Fig. 14), Justino *et al.*<sup>57</sup> observed NIR-induced selective interconversions between its two most stable conformers (stabilized by two intramolecular OH · · · OH H-bond like interactions and exhibiting different

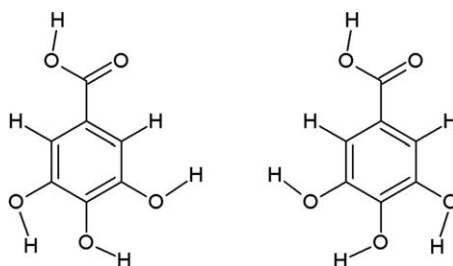


**Fig. 14** Most stable conformers of gallic acid. Adapted from L. L. G. Justino, I. Reva and R. Fausto, *J. Chem. Phys.*, 2016, **145**, 14304 with the permission of AIP Publishing.<sup>57</sup>

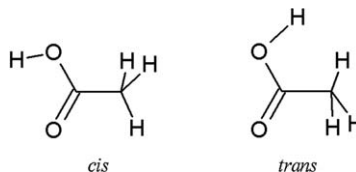


**Fig. 15** Conformers of trifluoroacetic acid. Reprinted from *J. Mol. Struct.*, **1125**, R. F. G. Apóstolo, G. Bazsó, R. R. F. Bento, G. Tarczay and R. Fausto, The first experimental observation of the high-energy trans conformer of trifluoroacetic acid, 288–295. Copyright (2016) with permission from Elsevier.<sup>59</sup>

orientation of the carboxylic acid group relatively to the trihydroxy-substituted aromatic ring), and extracted in depth mechanistic insights into the observed isomerization processes. The experimental studies were carried out for the compound isolated in nitrogen, xenon, and argon matrices and were complemented by a detailed theoretical analysis of the potential energy surface of the molecule, which provided important clues to the mechanistic interpretation of the experimental results.

Narrowband NIR vibrational excitation was also used to generate the high-energy *trans*-carboxylic conformer of trifluoroacetic and trichloroacetic acids.<sup>58,59</sup> For trifluoroacetic acid, the lowest energy *cis* conformer of the compound was isolated in argon, krypton, and nitrogen matrices, and the high-energy *trans* form generated upon pumping the OH stretching vibration of the *cis* conformer. Once generated, the *trans* conformer was found to spontaneously decay back to the *cis* form. It was noticed that, in contrast with the *cis* conformer, where the trifluoromethyl group eclipses the C=O bond of the carboxylic moiety, the *trans* conformer has an unusual orientation of this group, which is eclipsing the C–O bond. This unusual arrangement observed in the *trans* conformer was explained as resulting from the fact that the relative orientation of the CF<sub>3</sub> and COOH groups in that geometry facilitates the establishment of an intramolecular hydrogen-bond-like interaction between the OH group and the closely located in-plane fluorine atom of the CF<sub>3</sub> moiety (Fig. 15). The stability of the *trans* form was evaluated from the corresponding tunneling decay rates in the rare-gas matrices. It was found that the lifetime of *trans*-trifluoroacetic acid does not differ much from that of acetic acid and is shorter than that of formic acid trapped in the same matrices in identical experimental conditions.

This is consistent with the relative magnitude of the *trans*→*cis* energy barriers in these three molecules (32.2, 32.9, and 38.5 kJ mol<sup>-1</sup>, respectively). In N<sub>2</sub> matrices, the lifetime of *trans*-trifluoroacetic acid (90 min) is noticeably shorter than those of the *trans* forms of acetic and formic acids (5 and 7 h, respectively) because of the reduced accessibility of the OH group in the *trans* form to the matrix N<sub>2</sub> molecules resulting from the distinctive intramolecular OH/F interaction present in this molecule.

In the case of trichloroacetic acid, the compound was isolated in an N<sub>2</sub> matrix (15 K) and the high-energy *trans* conformer was generated *in situ* following a similar strategy to that used for trifluoroacetic acid.<sup>58,59</sup> The spontaneous decay, by tunneling, of the generated *trans* conformer into the *cis* form was evaluated. The much faster decay of the *trans* conformer of trichloroacetic acid compared to both formic and acetic acids (by ~35 and *ca.* 25 times, respectively) was found to correlate well with the lower energy barrier for the *trans*→*cis* isomerization in the studied compound. The experimental studies received support from quantum chemistry calculations undertaken at the DFT(B3LYP)/cc-pVDZ level of approximation, which allowed a detailed characterization of the potential energy surface of the molecule and the detailed assignment of the IR spectra of the two conformers.

Another interesting study dealing with conformational isomerizations induced by light was reported by Kwiatek and Mielke,<sup>60</sup> dealing with pyridoxal. Five minima stabilized by intramolecular OH···O bonds between the phenolic OH group and the carbonyl aldehyde group, and another thirteen conformers in which the OH and/or aldehyde groups are rotated by 180° around CO and/or CC bonds, were found on the studied potential energy surface of the molecule. The two most stable conformers, with intramolecular hydrogen bonds, were trapped in an argon matrix. UV irradiation ( $\lambda > 345$  nm) led to conformational change from the most stable form (**I**) to a high-energy conformer (**II**;  $\Delta E = 47.7$  kJ mol<sup>-1</sup>) without any intramolecular H-bond (Fig. 16).

Lopes *et al.*<sup>38</sup> investigated acetic acid dimers by IR spectroscopy in an N<sub>2</sub> matrix, and theoretically at the MP2/6-311++G(2d,2p) level of approximation. As a result, 9 *cis-cis*, 14 *cis-trans*, and 6 *trans-trans* dimers were theoretically predicted. Among them, 5 *cis-cis* and a number of *cis-trans* dimers were experimentally observed, with 4 *cis-cis* dimers and all

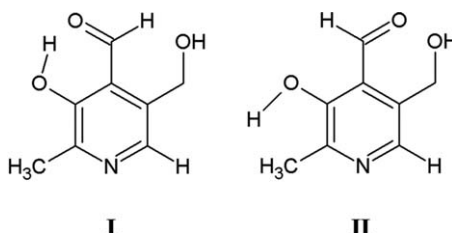


**Fig. 16** The DFT/B3LYP/6-311++G(2d,2p) optimized most stable conformer of pyridoxal (**I**), and the obtained high-energy conformer resulting from UV irradiation of the first conformer in argon matrix (**II**).<sup>60</sup>

detected *cis-trans* dimers being observed for the first time. Interestingly, no *trans-trans* dimers could be experimentally observed, which was explained assuming that the *trans* monomer has a reduced mobility (compared to the *cis* monomer) in the matrices.

Generation of dimers containing the high-energy *trans* conformer of acetic acid was achieved by two alternative procedures: (i) the high-energy *trans* monomer was first generated in the matrix by vibrational excitation of the more stable *cis* form and then thermally mobilized to produce the dimers; (ii) dimers containing only the more stable conformer were initially produced by annealing the matrix, at a temperature that allows for molecular diffusion of the acetic acid molecules, and then vibrationally excited to generate the dimers containing the *trans* unit. Some of the novel *cis-cis* dimers resulted from the relaxation of the high-energy *cis-trans* dimers taking place through the tunneling mechanism. Fig. 17 summarizes the obtained results.

In a later study, Lopes *et al.*<sup>61</sup> addressed the non-covalent interaction of acetic acid and water in a nitrogen matrix. The work was focused on the first preparation and characterization of complexes of the high-energy *trans* conformer of acetic acid with water and relies on the previously developed strategies of producing that conformer by vibrational excitation of the most stable *cis* form.

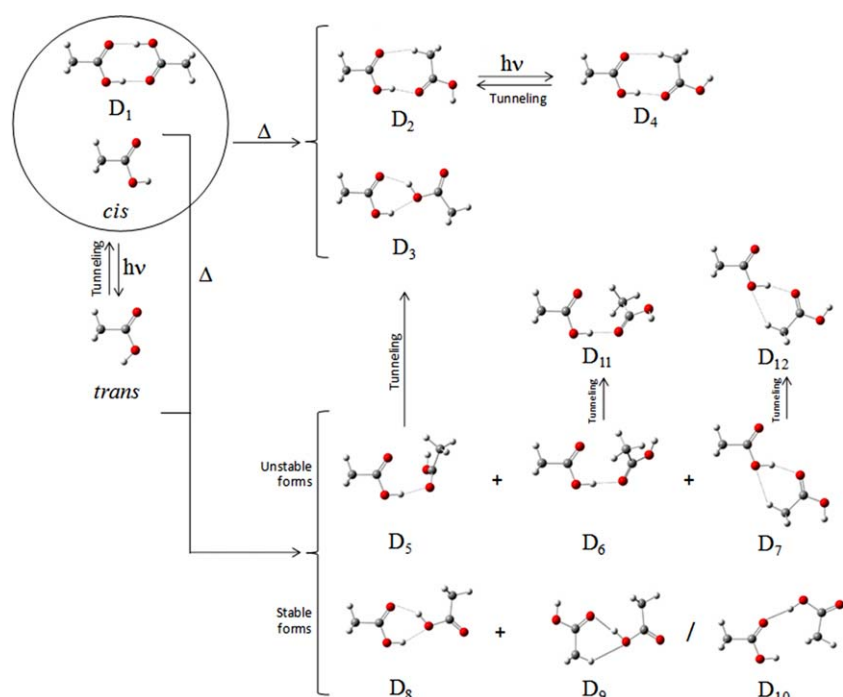


**Fig. 17** Summary of the experiments combining selective NIR irradiation, thermal mobilization, and tunneling decay yielding several rare dimers of acetic acid.<sup>38</sup> The deposited N<sub>2</sub> matrix contained essentially the *cis* monomer and dimer D<sub>1</sub>. On the whole, 11–12 different dimers were detected (D<sub>9</sub> and D<sub>10</sub> have very similar predicted IR spectra, and the experimental data is compatible with the presence of both forms in the matrix or just one of them) plus the two monomeric species.

Theoretical calculations at both the MP2 and coupled-cluster with single and double and perturbative triple excitations [CCSD(T)]/6-311++G(2d,2p) levels of theory predicted the existence of 3 acetic acid·H<sub>2</sub>O complexes for each conformer of acetic acid (Fig. 18).<sup>61</sup> The acetic acid·(H<sub>2</sub>O)<sub>2</sub> complexes were also calculated at the MP2/6-311++G(2d,2p) level of approximation. Experimentally, two *cis* acetic acid·H<sub>2</sub>O and two *trans* acetic acid·H<sub>2</sub>O complexes were identified and characterized structurally and spectroscopically. The two *trans* acetic acid·H<sub>2</sub>O complexes were obtained by annealing of a matrix containing water and *trans* acetic acid molecules prepared by selective vibrational excitation of the ground-state *cis* form. The less stable *cis* acetic acid·H<sub>2</sub>O complex was obtained by vibrational excitation of the less stable *trans* acetic acid·H<sub>2</sub>O complex. In addition, the most stable 1:2 complexes of *cis* and *trans* acetic acid conformers with water were experimentally identified (Fig. 19).

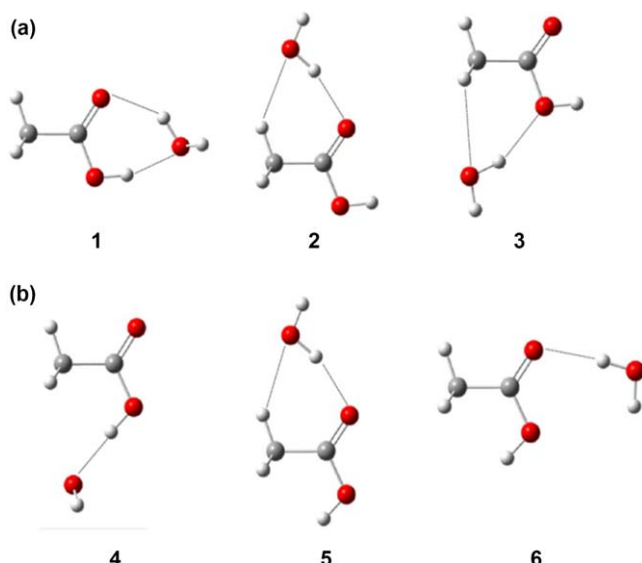


**Fig. 18** Calculated (a) *cis* acetic acid·H<sub>2</sub>O and (b) *trans* acetic acid·H<sub>2</sub>O complexes. Complexes 1, 2, 4, and 5 were observed experimentally. Adapted from S. Lopes, R. Fausto and L. Khriachtchev, *J. Chem. Phys.*, 2016, **144**, 84308 with the permission of AIP Publishing.<sup>61</sup>

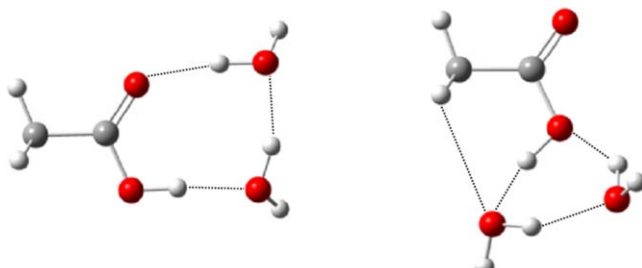


**Fig. 19** Most stable *cis* (left) and *trans* (right) acetic acid·(H<sub>2</sub>O)<sub>2</sub> complexes, which have been reported for the first time in ref. 61. Adapted from S. Lopes, R. Fausto and L. Khriachtchev, *J. Chem. Phys.*, 2016, **144**, 84308 with the permission of AIP Publishing.

Finally, Martínez *et al.*<sup>62</sup> prepared and characterized perfluoropropanoyl fluoride (PFPF) using vibrational spectroscopy in different phases. Matrix isolation coupled with IR spectroscopy allowed resolving the contributions of the *anti* and *gauche* conformers and, in addition, those of a dimeric species formed by *gauche* rotamers. While increasing the concentration of PFPF under matrix conditions and performing annealing experiments resulted in an increased concentration of the dimers, the irradiation of the matrix with UV/Vis light induced cleavage of the dimers into *gauche* monomers.

### 3 Tautomerizations and other structural isomerizations

During the period covered by this review, several relevant reports dealing with phototautomerizations and other types of structural isomerization processes induced by UV/Vis light were published, including an interesting study by Horta *et al.*<sup>63</sup> on the quinolone–hydroxyquinoline tautomerism in quinolone 3-esters, which pointed out relevant issues related to the action of this type of compounds against malaria. Most of the described studies focused on alkene-type compounds bearing aromatic substituents. Some of these reactions were observed alongside with conformational isomerization processes and have already been mentioned in the previous section.

Reva *et al.*<sup>64</sup> have investigated the UV-induced hydrogen atom transfer reactions in thiophenol isolated in solid argon, leading to photogeneration of two new thione isomers (Fig. 20). The transformations were induced by irradiation of the matrices with narrowband tunable UV light. Upon irradiation at 290–285 nm, the initial thiol form of thiophenol converted into its thione isomer, cyclohexa-2,4-diene-1-thione, by H-atom-transfer from the SH group to a carbon atom at the *ortho* position of the ring. Subsequent irradiation at longer wavelengths (300–427 nm) led to the reverse reaction. In addition, upon irradiation at 400–425 nm, the cyclohexa-2,4-diene-1-thione product converted into cyclohexa-2,5-diene-1-thione, which was also found to be photoreactive upon irradiation at 332 nm.

The obtained results clearly showed that H-atom-transfer isomerization reactions dominate the unimolecular photochemistry of thiophenol confined in a solid argon matrix. Noteworthy, the presence of phenylthiyl radical, which acts as an intermediate in the observed photoprocesses, was experimentally confirmed. Alongside the H-atom-transfer and H-atom-detachment processes, a ring-opening photoreaction was found to take place in cyclohexa-2,4-diene-1-thione, leading to an open-ring conjugated thioketene that adopts several isomeric forms differing by orientations around single and double bonds.

Ünsalan *et al.*<sup>39</sup> isolated monomers of *trans* and *cis* stilbene in argon and xenon matrices and investigated the effects of UV irradiation and thermal activation of the isolated species. *In situ* broadband UV irradiation of the *cis* form led to the formation of the transisomer, which appeared as both non-planar and planar structures (Fig. 21). Upon subsequent annealing of the matrices, the non-planar species converted into

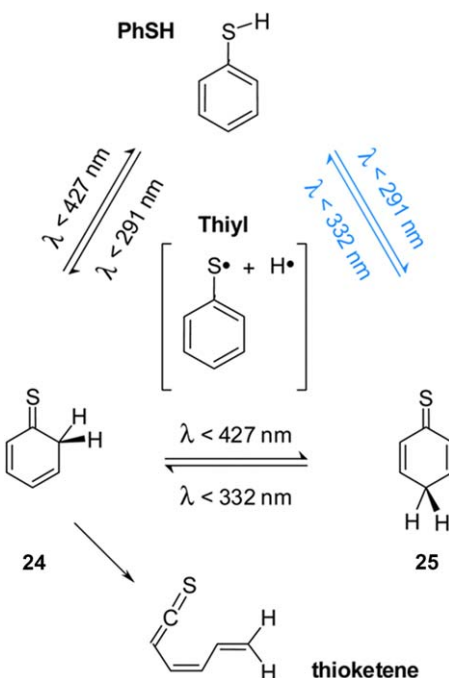


**Fig. 20** Photoinduced transformations of matrix-isolated thiophenol. Abbreviations: PhSH – thiol form of thiophenol; 24 – cyclohexa-2,4-diene-1-thione; 25 – cyclohexa-2,5-diene-1-thione; thiyl – phenylthiyl radical. The direct PhSH/25 photoisomerization (indicated in blue) could not be confirmed or discarded from the obtained results. Reproduced from ref. 64 with permission from the PCCP Owner Societies.

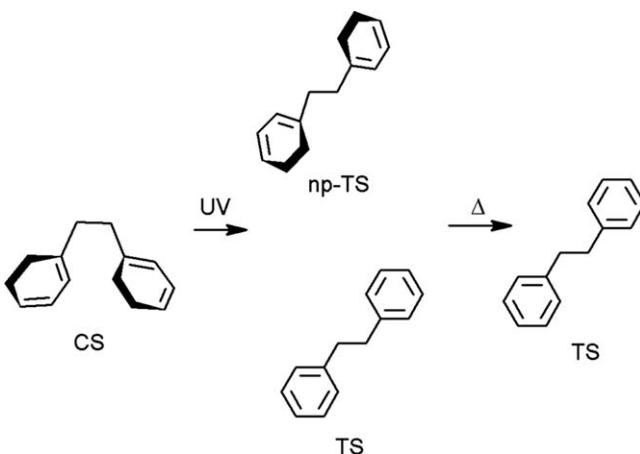


**Fig. 21** Structures of *cis* and *trans* stilbene (CS and TS). Adapted from *Spectrochim. Acta Part A Mol. Biomol. Spectrosc.*, 136, O. Ünsalan, N. Kuş, S. Jarmelo and R. Fausto, 2015, *Trans- and cis-stilbene isolated in cryogenic argon and xenon matrices*, 81–94. Copyright (2015), with permission from Elsevier.<sup>39</sup>

the more stable planar form. It was concluded that *in situ* photoisomerization of the cage confined *cis* form of stilbene isolated in inert matrices results in a particularly favorable strategy to populate the

non-planar metastable *trans* form. The authors successfully used chemometrics to assign the structure of the non-planar *trans* form.

The photoinduced reactions of a series of azobenzenes, 2,2'-dihydroxyazobenzene (DAB), 2,2'-azotoluene (AT), and azobenzene (AB), isolated in argon and xenon matrices were studied by Duarte and co-workers.<sup>65</sup> By combining IR spectroscopy and theoretical calculations, the authors were able to elucidate the structures of these compounds showing that they can adopt both the *E* and *Z* isomeric forms around the central CN=NC moiety. For DAB and AT, each structural isomer exists in different possible conformers.

A number of isomeric forms of DAB and AT were identified for the first time.<sup>65</sup> For DAB, the *E* azo-enol isomer, with two intramolecular six-membered rings formed *via* OH $\cdots$ N hydrogen bonds, was found after matrix deposition. Irradiation with UV light generated a different *E* azo-enol form, with two intramolecular H-bonded five-membered rings. The phototransformation was found to be reversible, with the forms being interconvertible by irradiation at different wavelengths. The observed isomerization constitutes a direct experimental observation of an *E*-*E* isomerization in azobenzene-type molecules. Further irradiations generated forms bearing both OH and NH groups. For AT, two *E* isomers with the CH<sub>3</sub> groups forming five-membered and five/six-membered rings with the azo group were observed in the as-deposited matrices. UV-irradiation led to a *Z* form that could then be converted back to the *E* form upon irradiation at different wavelengths. *E*-Azobenzene was deposited in a xenon matrix, and both *E* $\rightarrow$ *Z* and *Z* $\rightarrow$ *E* photo-transformations could be observed. The different photoisomerization channels observed for the studied compounds were discussed in terms of a small-amplitude pedal motion.

Miyazaki *et al.*<sup>66</sup> studied the photoisomerization of *p*-methoxy methylcinnamate in neon matrices (Fig. 22). A *trans* $\rightarrow$ *cis* conformational isomerization was found to take place in the S<sub>1</sub> state when the sample was irradiated at  $\lambda > 300$  nm. The formation of the *cis* photoproduct was probed by the characteristic lower-frequency shifts of the IR bands of the C=O stretch of the ester group, C-H bend of the aromatic ring, C=C stretch of the propenyl group, and C=O stretch. The authors also observed the reverse *cis* $\rightarrow$ *trans* photoisomerization upon irradiation at  $\lambda > 275$  nm thus demonstrating the reversibility of the process. Interestingly, the photoproducts were found to exhibit a preference in the population ratio of conformers indicating that the reactions are dynamically controlled on the potential energy surface rather than being statistically controlled.

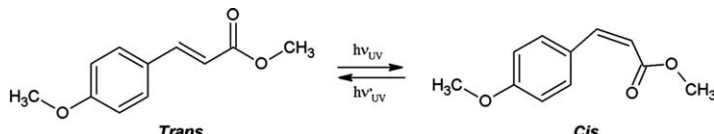


**Fig. 22** Observed photoisomerization reactions of Ne matrix-isolated *p*-methoxy methylcinnamate. Adapted with permission from Y. Miyazaki, Y. Inokuchi, N. Akai and T. Ebata, *J. Phys. Chem. Lett.*, 2015, **6**, 1134–1139. Copyright (2015) American Chemical Society.<sup>66</sup>

Avadanei *et al.*<sup>67</sup> investigated the structure and the photochemistry of *N*-salicylidene-*p*-carboxyaniline, a very interesting compound belonging to the *o*-hydroxyaryl Schiff bases family. IR matrix isolation spectroscopy and theoretical calculations were used to characterize the conformational space of the enol-imine and keto-amine tautomers of the compound in both their *E* and *Z* isomeric forms. Upon isolation of the compound in an argon matrix (15 K), only the most stable conformer of the *E*-enol isomer was observed. The *E*-enol isomeric form was then subjected to UV irradiation ( $\lambda = 335$ ; 345 nm, or  $\lambda > 235$  nm), and the photoinduced processes were probed by IR spectroscopy. Two nearly isoprobable and efficient photoreactions were observed, corresponding to *E*-enol  $\rightarrow$  *Z*-enol isomerization and *E*-enol  $\rightarrow$  *E*-keto tautomerization (see Fig. 23).

Identification of the photoproduced species of a *Z*-enol conformer differing from the reactant only by *E*-to-*Z* isomerization suggests the initial photoproduction of this conformer, which subsequently decays into the lowest energy *Z*-enol conformer (also identified experimentally). The *E*-enol  $\rightarrow$  *E*-keto tautomerization requires an excited state intramolecular proton transfer and twisting about the exocyclic CC bond, and it was suggested to take place as a sequential process, but the *Z*-keto isomer, which should act as intermediate in this sequence of processes, was not detected.

Among studies dealing with smaller non-aromatic molecules, one shall highlight the studies of Liu *et al.*<sup>68</sup> who have investigated the photoisomerization of allene and propyne cations in solid argon, and that of Tajti *et al.*,<sup>69</sup> who studied the reversible FCNS  $\rightarrow$  C(NS) photoisomerization, a process of crucial importance in finding a synthetic route to thiazirines.

Liu *et al.*<sup>68</sup> produced allene cations upon electron bombardment during matrix deposition of Ar containing a small proportion of allene. The intensities of the absorption features of the allene cation decreased after irradiation with UV light, whereas new bands attributed to propyne

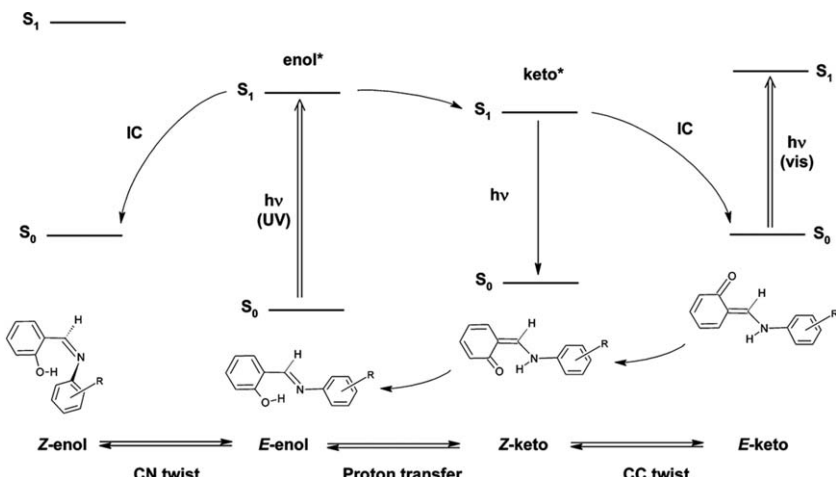


**Fig. 23** General scheme of the photochemistry of *N*-salicylidene anilines. Reprinted with permission from M. Avadanei, N. Kuş, V. Cozan and R. Fausto, *J. Phys. Chem. A*, 2015, **119**, 9121–9132. Copyright (2015) American Chemical Society.<sup>67</sup>

cations increased. The observed frequencies, relative intensities, and deuterium-substituted isotopic ratios of the isomers of  $C_3H_4^+$  were found to agree satisfactorily with those predicted by DFT.

In their study on the FCNS $\rightarrow$ C(NS) photoisomerization, Tajti and co-workers<sup>69</sup> undertook a series of UV spectroscopic measurements before the matrix isolation IR spectroscopic experiments in order to assist the interpretation of the investigated mechanisms of the ring closure and ring opening processes and also to verify the accuracy of the computations of the vertical excitation energies. The authors computed vertical excitation energies by the EOMEE-CCSD, MCSCF, and MR-CISD methods and searched for relevant conical intersections, locating three conical intersections along the reaction path FCNS $\rightarrow$ FC(NS): one conical intersection between the  $2A'$  and  $1A''$  states, one between the  $1A''$  and  $1A'$  states, and one where all three states intersect. Combining computational and experimental results, the authors concluded that upon 365-nm irradiation the ring closure FCNS $\rightarrow$ FC(NS) occurs under participation of all three conical intersections, while 254-nm irradiation causes ring opening FC(NS) $\rightarrow$ FCNS. Both processes, especially the ring opening, were found to be accompanied by fragmentation into FCN + S.

## 4 Fragmentation reactions, unstable intermediates, and formation of complexes or weakly bound species

This section deals with photofragmentation reactions, focusing on the formation of unstable intermediates. It is organized as follows: subsections 4.1 and 4.2 report reactions involving nitrenes, carbenes, 1,3-dipolar reactive species (4.1), or radicals (4.2). Subsection 4.3 addresses photoreactions involving ketenes as well as a representative collection of general fragmentation reactions of other types. Finally, subsection 4.4 highlights processes leading to the formation of complexes or weakly bound species together with their photoreactivity.

### 4.1 Nitrenes, carbenes, and 1,3-dipolar reactive species

Photolysis reactions involving the formation of carbenes, nitrenes, or 1,3-dipolar species were addressed mainly by the groups of Wentrup, Sanders, Ault, Fausto, Schreiner, Stanton, Willner, and Wierzejewska.

Nunes *et al.*<sup>40</sup> have found two bond-shift isomers of a 1,3-dipole, phenylnitrile imine (PhCNNH). Phenyl nitrile imine was generated by photolysis of 5-phenyltetrazole in Ar and Kr matrices, and both the allenic (**2A**; Fig. 24) and the propargylic (**2P**) bond-shift isomers were observed. They were identified by means of their experimental IR signatures and found to react photochemically, upon irradiation with monochromatic UV light in the 370–400 nm region, with different rates, both yielding *1H*-diazirine (**3**). The existence of two distinct energy minima of PhCNNH was confirmed by calculations up to the CASSCF(14,12) theory level. This study provides a new view on the structural nature of nitrile imines.

In another work, Nunes *et al.*<sup>70</sup> studied 5-aminotetrazole (sublimated at 330 K) isolated in argon matrix at 15 K by IR spectroscopy. They found

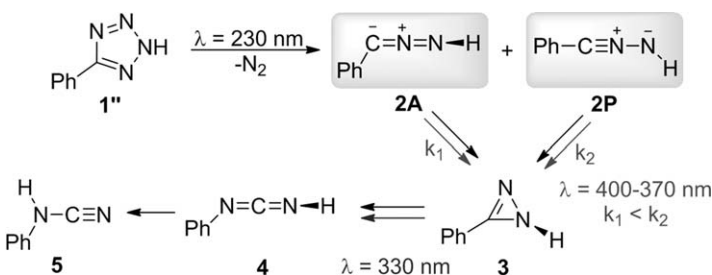


**Fig. 24** Allenic 2*A* and propargylic 2*P* phenylnitrile imines captured in the photochemistry of 5-phenyl-2*H*-tetrazole. Reproduced from ref. 40 with permission from The Royal Society of Chemistry.

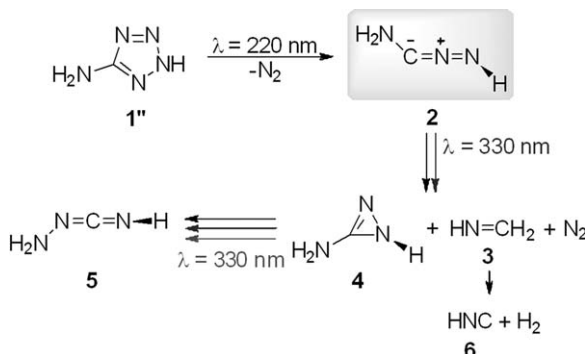


**Fig. 25** Summary of experimental observations on the UV-induced photochemistry of 5-amino-2*H*-tetrazole (1'') isolated in argon matrix. Adapted with permission from ref. 70, C. M. Nunes, I. Reva, M. T. S. Rosado and R. Fausto, *Eur. J. Org. Chem.*, John Wiley and Sons. Copyright © 2015 WILEY-VCH Verlag GmbH & Co. KGaA, Weinheim.

that under these experimental conditions only the 2*H*-tautomeric form 1'' (see Fig. 25) is present in the sample, in agreement with the theoretical predictions of the relative energies of isomers of 5-aminotetrazole. Photolysis of 1'' in argon matrix at  $\lambda = 220 \text{ nm}$  allowed the capture of *C*-amino nitrile imine 2 as the primary photoproduct.

The identification of 2 as *C*-amino nitrile imine was unequivocally confirmed by its IR spectrum, which was characterized in detail during subsequent photochemical experiments at  $\lambda = 330 \text{ nm}$ . These experiments also revealed two different pathways for the photochemistry of *C*-amino nitrile imine 2: (i) isomerization to the corresponding three-membered ring 1*H*-diazirine 4 (which rearranges to carbodiimide 5) and (ii) decomposition to methylenimine 3 (which gives hydrogen isocyanide 6). The observed isomerization route to 1*H*-diazirine 4 confirms the previous authors' findings on other nitrile imines,<sup>40</sup> whereas the decomposition route to methylenimine 3 was reported for the first time. The authors hypothesize that the carbenic character of 2 is crucial to open up the decomposition pathway to 3, because it can be expected to increase the negative charge at the C atom to which the hydrogen atom migrates in the first stage of the decomposition process.

Moreover, the authors noticed the low experimental frequency of the  $\nu_{\text{as}}(\text{CNN})$  mode of *C*-amino nitrile imine 2 at  $1998 \text{ cm}^{-1}$ , which indicates

that **2** should have considerable carbenic character. This was corroborated by the calculated optimized geometry of the molecule, particularly when compared with those of the parent nitrile imine and the *C*-methyl-substituted derivative. This conclusion was supported by the analysis of the electronic structure using natural resonance theory, which shows that **2** has a contribution of around 20% of the carbenic resonance hybrid contrasting with its absence in the parent nitrile imine and *C*-methyl nitrile imine, which can be described only by contributions of propargylic and allenic resonance hybrids. The p-electron-donating effect of the NH<sub>2</sub> group is most likely the key to the carbenic character of *C*-amino nitrile imine **2**.

Lopes, Reva and Fausto<sup>71</sup> presented a novel study of matrix-isolated methyl aziridine-2-carboxylate (MA2C) and its photochemistry. The theoretical calculations at the DFT(B3LYP)/6-311++G(d,p) level of theory predicted the existence of two low-energy MA2C conformers differing by the orientation of the O=C-C-N dihedral angle, which were also identified in the studied matrices. UV irradiation resulted in the formation of two conformers of methyl 2-(methylimino)-acetate (MMIA) and the *Z* isomer of methyl 3-iminopropanoate (M3IP). The production of one of the observed conformers of MMIA was interpreted as resulting from MA2C aziridine ring C-C bond cleavage *via* the corresponding ylide. Subsequent irradiation of that conformer at 290 nm led to the production of the second observed conformer *via* *E* → *Z* isomerization, which, in turn, could be reverted upon irradiation at 330 nm. Production of M3IP results from the cleavage of the weakest C-N bond of the MA2C aziridine ring. Surprisingly, the cleavage of the same bond does not lead to the formation of expected methyl 3-aminoacrylate (M3AA) photoproduct. The observation of M3IP and non-observation of M3AA seems to indicate that the H-atom migration to the vicinal carbon is a strongly preferred process. Another interesting observation was that no products resulting from the cleavage of the second C-N bond of the MA2C aziridine ring were observed. Several photofragmentation products of MA2C were also detected, including acetonitrile, methanol, methane, CO, and CO<sub>2</sub>, reflecting a complex photodecomposition pattern of the compound.

Sarkar *et al.*<sup>72</sup> studied the vinyl nitrene formed from the bicyclic 2-azido-1,4-naphthoquinone **1** (Fig. 26) through intramolecular triplet

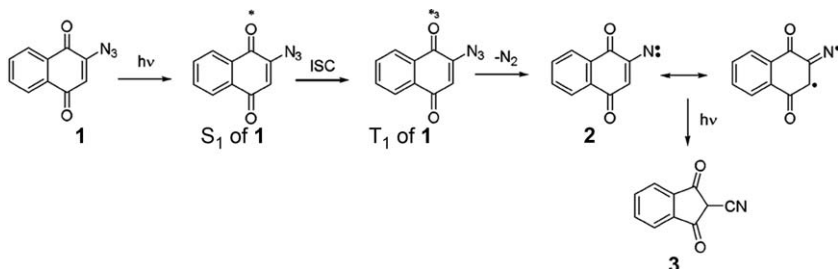


**Fig. 26** Mechanism of the formation of triplet vinyl nitrene <sup>3</sup>**2** and nitrile **3** from **1**. Adapted with permission from S. K. Sarkar, A. Sawai, K. Kanahara, C. Wentrup, M. Abe and A. D. Gudmundsdottir, *J. Am. Chem. Soc.*, 2015, **137**, 4207–4214. Copyright (2015) American Chemical Society.<sup>72</sup>

sensitization upon irradiation. The obtained triplet vinyl nitrene <sup>3</sup>**2** was detected directly in cryogenic matrices using IR and electron spin resonance spectroscopy, and it was stable up to at least 100 K. Under the used irradiation conditions in the Ar matrix at 8 K, the triplet nitrene <sup>3</sup>**2** was found to rearrange to the nitrile **3**.

Using the ESR spectroscopy the authors also demonstrated that triplet vinyl nitrene <sup>3</sup>**2** has a significant 1,3-biradical character. Because triplet vinyl nitrene <sup>3</sup>**2** is a part of a bicyclic ring system, it is rigid, which restricts the rotation around the vinylic C=C bond and renders it more stable than other vinyl nitrenes due to less facile intersystem crossing. It was then suggested that the unique reactivity of triplet vinyl nitrenes might be ascribed to their flexibility, which is a reflection of their significant 1,3-biradical character. Since triplet vinyl nitrenes can be stabilized by limiting the flexibility of the vinyl C=C bond, it appears to be possible to design various triplet vinylnitrenes as potential building blocks for high-spin assemblies. The DFT calculations also supported the characterization of vinylnitrene <sup>3</sup>**2** and the proposed mechanism for its formation.

In a later work, Sarkar *et al.*<sup>73</sup> investigated the photoreactivity of 3-azido-1-indenone (**1**; Fig. 27) using a light-emitting diode (LED,  $\lambda = 405$  nm) or mercury arc lamp as irradiation sources. The irradiation of the vinyl azide **1** resulted in the formation of a heterodimer through dimerization of triplet vinylnitrene <sup>3</sup>**2**. The vinyl nitrene intermediate was also characterized directly with IR and ESR spectroscopies in cryogenic matrices. The proposed mechanism for the formation and reactivity of triplet vinylnitrene <sup>3</sup>**2** was supported by DFT calculations. The ESR spectrum of vinylnitrene revealed that vinylnitrene <sup>3</sup>**2** had significant 1,3-biradical character, which was responsible for the observed trend for dimerization to a C–N bond. Thus, the authors showed that triplet

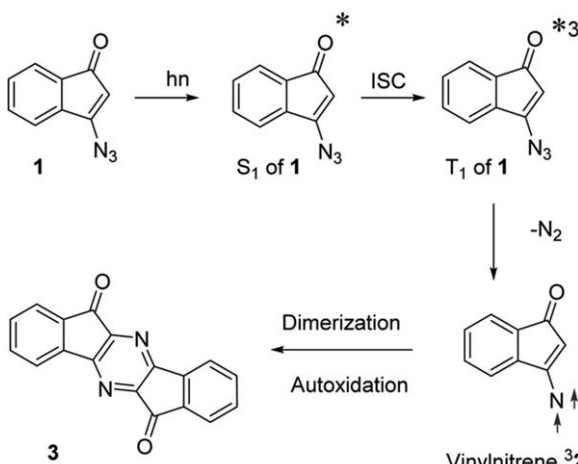


**Fig. 27** Proposed mechanism of formation of heterocyclic dimer **3** from vinyl azide **1**. Reprinted with permission from S. K. Sarkar, O. Osisioma, W. L. Karney, M. Abe and A. D. Gudmundsdottir, *J. Am. Chem. Soc.*, 2016, **138**, 14905–14914. Copyright (2016) American Chemical Society.<sup>73</sup>

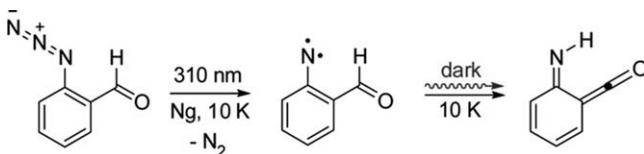


**Fig. 28** Generation and observed reactions of the triplet 2-formyl phenylnitrene. Adapted with permission from C. M. Nunes, S. N. Knezz, I. Reva, R. Fausto and R. J. McMahon, *J. Am. Chem. Soc.*, 2016, **138**, 15287–15290. Copyright (2016) American Chemical Society.<sup>41</sup>

vinylnitrenes could be selectively formed with visible light and used to form new C–N bonds in synthetic applications.

Nunes *et al.*<sup>41</sup> provided the first direct evidence of a tunneling reaction involving a nitrene. They investigated triplet 2-formyl phenylnitrene generated by photolysis of 2-formyl phenylazide isolated in Ar, Kr, and Xe matrices and characterized by IR, UV/Vis, and EPR spectroscopies. Upon generation at 10 K, the triplet nitrene spontaneously rearranged in the dark to singlet 6-imino-2,4-cyclohexadien-1-ketene on the time scale of several hours (Fig. 28). The intramolecular [1,4] H-atom shift from the nitrene to the imino ketene occurred by tunneling, on the triplet manifold, followed by intersystem crossing.

Ismael *et al.*<sup>74</sup> performed a combined matrix isolation IR and theoretical study of the molecular structure and photochemistry of 5-thio-saccharyl-1-methyltetrazole (TSMT). The conformational preferences of TSMT, in both the matrix-isolated situation and in the crystalline phase, were investigated. DFT calculations predicted two conformers of TSMT that differ in energy by more than 15 kJ mol<sup>-1</sup>. Only the most stable conformer was detected both in the cryomatrices (15 K) prepared from the vapor of the compound and in the studied crystal. The IR spectrum of matrix-isolated TSMT was fully assigned on the basis of the B3LYP/6-311++G(3df,3pd) spectra calculated for the most stable conformer. Upon irradiation of the matrix-isolated compound with UV light ( $\lambda = 265$  nm), two photodegradation pathways were observed, both arising from cleavage of the tetrazole ring. One pathway involved photoinduced cleavage of the N<sub>1</sub>–N<sub>2</sub> and N<sub>3</sub>–N<sub>4</sub> bonds of the tetrazole ring with extrusion of molecular nitrogen and led to the production of diazirine and thiocarbodiimide with no apparent sign of photodegradation. A nitrene type intermediate was postulated to be involved in this process, though it could not be experimentally observed. The second pathway involved photoinduced cleavage of the tetrazole C<sub>5</sub>–N<sub>1</sub> and N<sub>4</sub>–N<sub>3</sub> bonds leading to thiocyanate and methyl azide as primary photoproducts.

Nunes *et al.*<sup>75</sup> identified, for the first time, the spiro-2*H*-azirine **2** (Fig. 29) and ketenimine **3** as intermediates in the photoisomerization of 1,2-benzisoxazole (**1**) to 2-cyanophenol (**4**). These results constitute also an indirect evidence for the existence of vinylnitrene intermediates in the photochemistry of 1,2-benzisoxazoles. The authors concluded that **2** photoisomerizes to **4** via [1,4]-H-shift of vinylnitrene (1A'')-VN formed by C–N bond cleavage. For the photoisomerization of **3** to **4**, the authors postulated the occurrence of a concerted [1,5]-H-shift. Although the

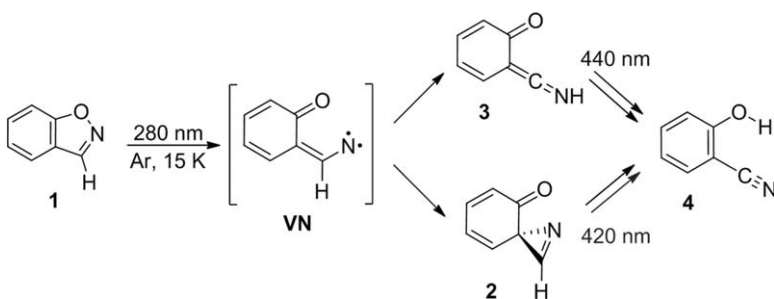


**Fig. 29** Summary of the experimental observations of the photochemistry of 1,2-benzisoxazole **1** isolated in argon matrix at 15 K. Reprinted with permission from ref. 75, C. M. Nunes, S. M. V Pinto, I. Reva and R. Fausto, *Eur. J. Org. Chem.*, John Wiley and Sons. © 2016 WILEY-VCH Verlag GmbH & Co. KGaA, Weinheim.

triplet vinylnitrene ( $3\text{A}''$ )-VN was not detected, the capture and characterization of elusive **2** and **3**, as intermediates in the photoisomerization of **1** to **4**, constitutes indirect evidence for the existence of vinylnitrenes in 1,2-benzisoxazole chemistry. Overall, the obtained experimental results corroborated the authors' general mechanistic proposal for isoxazole reactivity, wherein vinylnitrenes play a key role.

Deng *et al.*<sup>76</sup> reported a spectroscopic and structural characterization of methane-sulfonyl azide  $\text{CH}_3\text{SO}_2\text{N}_3$  in a neat form and also its photochemistry in noble gas matrices. In both gas and solid states, the azide adopts a single *gauche* conformation with the azido ligand being *syn*-periplanar to one of the  $\text{S}=\text{O}$  bonds, and the molecules in the solid state are interconnected through three-dimensional  $\text{O}\cdots\text{H}-\text{C}-\text{H}\cdots\text{O}$  hydrogen bonds. Upon laser irradiation at 193 nm, the matrix-isolated azide underwent stepwise pseudo-Curtius rearrangement *via* the key nitrene intermediate  $\text{CH}_3\text{SO}_2\text{N}$  directly observed by IR spectroscopy. Further photolysis of the nitrene with UV light (266 nm) caused its rearrangement into  $\text{CH}_3\text{NSO}_2$ . DFT calculations supported the identification of the intermediates detected by IR spectroscopy.

A Curtius-type rearrangement was also reported for matrix-isolated carbonyl azides  $\text{RC(O)N}_3$  subjected either to photolysis or thermolysis by Sun *et al.*<sup>77</sup> The reaction led to the production of isocyanates (RNCO) in almost quantitative yield. A thermally persistent triplet carbonyl nitrene  $\text{FC(O)N}$  was produced by flash pyrolysis of  $\text{FC(O)N}_3$  in 49% yield. The authors stated that the thermal persistence of triplet  $\text{FC(O)N}$  not only could contribute to the fundamental knowledge of the rich nitrene chemistry but would also enable future structural characterization of a carbonyl nitrene using gas-phase spectroscopy methods such as high-resolution IR or microwave spectroscopy.

Zeng *et al.*<sup>78</sup> investigated the complex stepwise photodecomposition of the matrix-isolated diazo transfer reagent (trifluoromethylsulfonyl) azide,  $\text{CF}_3\text{SO}_2\text{N}_3$ . The observations were discussed in terms of the photolysis products and quantum chemical calculations. Upon irradiation at 193 nm, the azide eliminates  $\text{N}_2$  and furnishes triplet [(trifluoromethyl)sulfonyl]-nitrene,  $\text{CF}_3\text{SO}_2\text{N}$ , whereas subsequent UV irradiation at 260–400 nm of the nitrene converts it to  $\text{CF}_3\text{N}=\text{SO}_2$  and  $\text{CF}_3\text{S(O)NO}$  through a Curtius-type

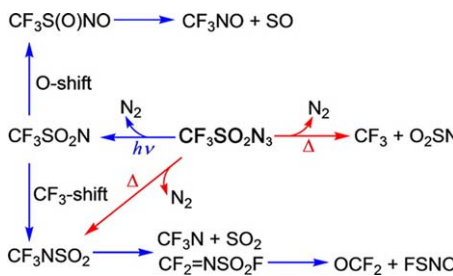


**Fig. 30** Photodecomposition and thermal decomposition pathways for  $\text{CF}_3\text{SO}_2\text{N}_3$ . Reprinted with permission from X. Zeng, H. Beckers, H. Willner, P. Neuhaus, D. Grote and W. Sander, *J. Phys. Chem. A*, 2015, **119**, 2281–2288. Copyright (2015) American Chemical Society.<sup>78</sup>

rearrangement. Further two new species,  $\text{CF}_2\text{N}=\text{SO}_2\text{F}$  and  $\text{FSNO}$ , were identified together with  $\text{CF}_2\text{NF}$ ,  $\text{SO}_2$ ,  $\text{F}_2\text{CO}$ ,  $\text{CF}_3\text{NO}$ , and  $\text{SO}$  as side products (see Fig. 30).

Li *et al.*<sup>79</sup> revisited the photolysis ( $\lambda = 193$  nm) of the two simplest carbamoyl azides,  $\text{H}_2\text{NC(O)N}_3$  and  $\text{Me}_2\text{NC(O)N}_3$ , in solid  $\text{N}_2$ , Ar, and Ne matrices, which led to stepwise decomposition of the initial compounds and formation of the corresponding carbamoylnitrenes,  $\text{H}_2\text{NC(O)N}$  and  $\text{Me}_2\text{NC(O)N}$ . Subsequent visible-light irradiations caused efficient rearrangement of these nitrenes into the respective aminoisocyanates. The directly observed photoproducts for the first time clearly supported a stepwise photochemical decomposition pathway for this type of reaction proposed initially by Curtius and Burkhardt in the 1890s.

Liu *et al.*<sup>80</sup> investigated the photolysis of diisocyanate  $\text{OC(NCO)}_2$ . The authors found that the compound exists as a mixture of two conformers (62% *syn-syn* and 38% *syn-anti*) in the gas phase at room temperature and determined, for the first time, their energy difference ( $\Delta H_{\text{exptl}} = 0.9(2)$  kcal mol<sup>-1</sup>). Upon ArF laser photolysis, both conformers split off CO and furnish a novel triplet nitrene intermediate  $\text{OCNC(O)N}$ , which was also generated in two conformations, *syn* and *anti*. The IR spectral identification of these nitrene forms was supported by *ab initio* calculations. Further irradiation of  $\text{OCNC(O)N}$  with visible light ( $\lambda > 395$  nm) led to a Curtius rearrangement into  $\text{OCNNCO}$ , which, in turn, produced an additional species,  $\text{NOCN}$ , upon ArF laser photolysis through a diazomethanone (NNCO) intermediate. The proposed photo-transformations were validated by considering photolysis of the closely related NNNNCO and *cyclo-N*<sub>2</sub>CO (Fig. 31).

Carbene intermediates have been addressed in a considerably less extension than nitrenes.

Costa *et al.*<sup>81</sup> studied the photochemistry of diphenylcarbene 5 (Fig. 32) in solid argon by UV/Vis, IR, and EPR spectroscopies. They observed that carbene 5 slowly rearranges to 1-phenyl-1,2,4,6-cycloheptatetraene 8 upon irradiation with a 445-nm diode laser. The absence of possible paramagnetic intermediates involved in the rearrangement of 5 was reliably verified by EPR spectroscopy. The authors also concluded that carbene 5 is stable towards UV photolysis. The observed formation of 8 supported the previously proposed carbene–carbene rearrangement as

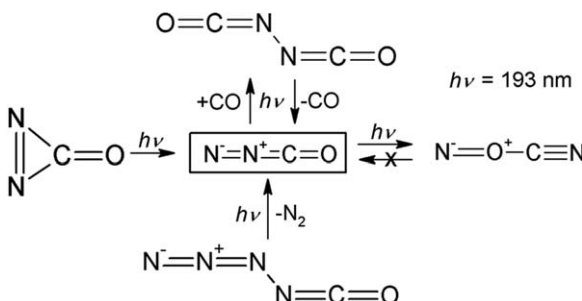


**Fig. 31** A schematic description of the experiments used for generation of NNCO. Adapted with permission from ref. 80, Q. Liu, H. Li, Z. Wu, D. Li, H. Beckers, G. Rauhut and X. Zeng, *Chem. - Asian J.*, John Wiley and Sons. © 2016 Wiley-VCH Verlag GmbH & Co. KGaA, Weinheim.<sup>80</sup>

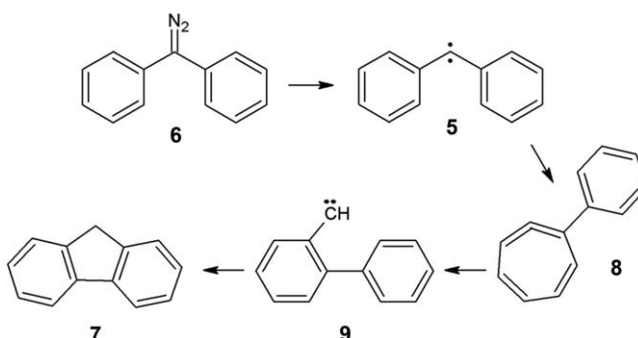


**Fig. 32** Formation of fluorene 7 via diphenylcarbene. Adapted with permission from ref. 81, P. Costa and W. Sander, *J. Phys. Org. Chem.*, John Wiley and Sons. Copyright © 2014 John Wiley & Sons, Ltd.

the preferred mechanism for the formation of fluorene 7, with **8** being the key intermediate.

In a later work, Costa *et al.*<sup>82</sup> investigated both thermal and photochemical interconversions between the singlet and triplet states of bis(*p*-methoxyphenyl)carbene by EPR, IR, and UV/Vis spectroscopies in solid argon, by EPR and ENDOR spectroscopies in 2-methyltetrahydrofuran, and by theoretical methods. It was demonstrated that the lowest energy singlet and triplet states of the investigated carbene co-exist. It was also predicted that this bi-stability of states of different spin multiplicity results from the near degeneracy of these states and, therefore, may be a general phenomenon in similar systems. In particular, the performed experiments clearly demonstrated that: (i) the singlet and triplet states of the carbene coexist in argon at 3 K and that there is no intersystem crossing within several hours; (ii) under the same conditions, a photostationary equilibrium between the two states is established by irradiation either into the strong UV absorption of the singlet species or into the weak visible absorption of the triplet. Thus, Vis-light irradiation (450 nm) shifts the equilibrium towards the singlet and UV irradiation (365 nm) towards the triplet; (iii) annealing at slightly higher temperatures (10–25 K) results in conversion to the singlet state carbene, which

allowed to conclude that this state is thermodynamically more stable than the triplet and that these states are separated by an activation barrier that prevents interconversion at 3 K. Importantly, the authors demonstrated that in a bi-stable carbene the magnetic properties of the system could be switched by irradiation with light of different color, and, thus, this property might be of general interest for applications such as information storage.

Knezz *et al.*<sup>83</sup> reported the spectroscopic characterization of triplet 1,3-dimethylpropynylidene ( $\text{MeC}_3\text{Me}$ ) in cryogenic matrices obtained as a result of photolysis ( $\lambda > 472$  nm) of 2-diazo-3-pentyne. Quantum chemical calculations (CCSD(T)/ANO1) predicted an unsymmetrical equilibrium structure for triplet  $\text{MeC}_3\text{Me}$  and a very shallow potential energy surface. The experimental IR spectrum of the compound was best interpreted in terms of a quasi linear, axially symmetric structure. The EPR spectra yielded zero field splitting parameters that are typical for triplet carbenes with axial symmetry, while theoretical analysis suggested that the methyl substituents confer significant spin polarization to the carbon chain. Upon irradiation into the near-UV electronic absorption ( $\lambda_{\text{max}} = 350$  nm), triplet  $\text{MeC}_3\text{Me}$  was found to undergo [1,2] H-migration to yield pent-1-en-3-yne in a photochemical reaction that is typical of carbenes bearing a methyl substituent.

Finally, Richter, Mendez-Vega and Sander<sup>84</sup> described the formation of hydrogen-bonded complexes between chlorophenylcarbene or fluorophenylcarbene and water or methanol in argon matrices. To obtain the carbenes, the authors used *in situ* photolysis of the corresponding diazirines isolated in water or methanol-doped matrices. The hydrogen-bonded complexes were formed when diffusion of  $\text{H}_2\text{O}$  or methanol was induced by annealing of the matrices at temperatures above 20 K. The authors stressed the fact that none of the studied carbenes formed ylides with HOR *via* interaction of the lone pairs at oxygen with the vacant p-orbital at the carbene center. In fact, hydrogen bonding was found to be strongly preferred, at least under the conditions of matrix isolation.

## 4.2 Radicals

A variety of studies dealing with the photoproduction or photochemistry of radicals were published during the period covered by this review. Low temperature together with the inert nature or small diamagnetic character of the matrices stabilizes radicals, making matrix isolation a powerful method for the study of these usually highly reactive species. Studies of radicals in *p*-H<sub>2</sub> matrices have also become more and more popular, as the diminished cage effect of these matrices is particularly useful for the production of radicals either *via* photofragmentation *in situ* or as a result of bimolecular reactions promoted by irradiation.

Butscher *et al.*<sup>85</sup> studied, theoretically and experimentally, the formation mechanism of two of the largest detected molecules in the interstellar medium: glycolaldehyde (GA; HOCH<sub>2</sub>CHO) and ethylene glycol (EG; HOCH<sub>2</sub>CH<sub>2</sub>O). To strengthen the characterization of intermediate species, DFT calculations were performed using the popular

B3LYP functional. The authors were able to produce  $\text{HCO}^{\bullet}$  radicals by vacuum-UV photolysis of formaldehyde in noble gas matrices. Subsequent annealing of the photolyzed matrices led to formation of intermediate  $\cdot\text{CH}_2\text{OH}$  radicals from hydrogenation of  $\text{H}_2\text{CO}$  within the matrix. After sublimation of the matrix, they observed the formation of GA and EG by radical recombination. Thus, the authors proposed a likely scenario to explain the formation of GA and EG in the interstellar medium: first,  $\text{HCO}^{\bullet}$  and  $\cdot\text{CH}_2\text{OH}$  radicals are formed by successive hydrogenation of CO on the interstellar grains, then these radicals react to form EG and GA.

Krupa and Wierzejewska<sup>86</sup> reported on the UV-tunable laser-induced decomposition reactions of anisole isolated in a low-temperature argon matrix. The observed photoproducts, the phenoxy and methyl radicals, recombined to form two isomers of methylcyclohexadienone. The *ortho* isomer readily decomposes producing different isomers of long-chain ketene and bicyclohexenone molecules. Decarbonylation was also detected in the studied systems. Interpretation of the experimental observations was supported by DFT(B3LYP)/6-311++G(2d,2p) calculations.

Lee *et al.*<sup>87</sup> photolyzed a  $\text{CH}_3\text{ONO}/p\text{-H}_2$  (or  $\text{CD}_3\text{ONO}/p\text{-H}_2$ ) matrix and observed fundamental, overtone, and combination lines of  $\text{CH}_3\text{O}^{\bullet}$  (or  $\text{CD}_3\text{O}^{\bullet}$ ) radical; nearly all Jahn-Teller components were characterized. The assignments were based on the photolytic behavior and comparisons of observed vibrational wavenumbers and IR intensities with those predicted with a fitted CCSD(T)/cc-pVTZ force field. The authors also found that  $\text{CH}_3\text{O}^{\bullet}$  ( $\text{CD}_3\text{O}^{\bullet}$ ) reacts with *p*-H<sub>2</sub> rapidly to form CH<sub>2</sub>OH (CD<sub>2</sub>OH) within 5 min after UV irradiation. A tunneling reaction of  $\text{CH}_3\text{O}^{\bullet}$  with *p*-H<sub>2</sub> was proposed.

In a somewhat similar work, Yu-Fang Lee and Yuan-Pern Lee<sup>88</sup> investigated irradiation of a *p*-H<sub>2</sub> matrix containing diiodomethane ( $\text{CH}_2\text{I}_2$ ) and O<sub>2</sub> at 3.2 K with light with  $\lambda = 280 \pm 20$  nm, followed by annealing of the matrix at 4.0 K, which yielded formation of *syn*-iodomethylperoxy radical (*syn*-ICH<sub>2</sub>OO<sup>•</sup>). Further irradiation of the matrix at 365 nm diminished the IR absorption of the photoproduct. Experiments with CH<sub>2</sub>I<sub>2</sub> and <sup>18</sup>O<sub>2</sub> yielded production of *syn*-ICH<sub>2</sub><sup>18</sup>O<sup>18</sup>O<sup>•</sup>. The assignments of IR absorption bands were done based on the simulated spectra computationally obtained at the B3LYP/aug-cc-pVTZ-pp level of theory. The proposed mechanism involves photolysis of CH<sub>2</sub>I<sub>2</sub> at 280 nm, resulting in formation of CH<sub>2</sub>I<sup>•</sup>, which subsequently reacts with O<sub>2</sub> to yield *syn*-ICH<sub>2</sub>OO<sup>•</sup>.

Mutunga and Anderson<sup>89</sup> spectroscopically characterized the products of the 193-nm photodecomposition of methylamine (MA,  $\text{CH}_3\text{NH}_2$ ) isolated in *p*-H<sub>2</sub>matrices at 1.8 K and measured the photo-kinetics to determine the reaction branching ratios. The  $\cdot\text{CH}_3$  and  $\cdot\text{NH}_2$  intermediates were detected in the production of CH<sub>4</sub> and NH<sub>3</sub> in the 193-nm *in situ* photolysis of MA. A single exponential decay of the MA precursor upon irradiation was observed, and the quantum yield for MA photodissociation was measured to be  $\Phi = 0.26(2)$ . By comparing the obtained data with the gas phase results, the authors showed that *in situ* photolysis results in the larger production of molecular products (CH<sub>2</sub>=NH + H<sub>2</sub>) compared to radical products (CH<sub>3</sub>NH<sup>•</sup> + H<sup>•</sup>), consistent

with the idea of partial caging of the H atom photofragments. The authors also concluded that, although quantum effects are more important in solid *p*-H<sub>2</sub>, the *in situ* photodissociation of a molecule at high excess energies can likely be accurately modeled using classical molecular dynamics simulations that could be used to test if the concept of partial caging is relevant.

Reisenauer *et al.*<sup>90</sup> observed that the atmospherically highly-relevant methylsulfinyl radical (CH<sub>3</sub>(O)S<sup>•</sup>) readily reacts with molecular triplet oxygen in cryogenic argon matrices containing small amounts of <sup>3</sup>O<sub>2</sub>. Comparison of experimental and computed IR and UV/Vis spectra, including isotope exchange, showed that the initially formed <sup>3</sup>O<sub>2</sub> adduct has the structure of a peroxy radical (CH<sub>3</sub>(O)SOO<sup>•</sup>), which, upon irradiation with UV light, isomerizes to the methylsulfonyl radical (CH<sub>3</sub>SO<sub>3</sub><sup>•</sup>). The latter transforms into the methansulfonic acid radical (<sup>•</sup>CH<sub>2</sub>SO<sub>3</sub>H) by irradiation with visible light. During the matrix photolysis, small amounts of SO<sub>3</sub> and the methyl radical were detected indicating competitive direct photodissociation. The authors stressed that the results underscored earlier postulates regarding the existence of a reactive oxygen adduct of the methylsulfinyl radical and demonstrated the importance of photochemical transformations in atmospheric oxidation processes of volatile organic sulfur compounds.

Toh *et al.*<sup>91</sup> investigated the UV photochemistry of benzene induced by 193 and 253.7-nm excitations using matrix isolation IR spectroscopy in *p*-H<sub>2</sub> matrix. In addition to the formation of benzvalene, fulvene, and Dewar benzene as photoproducts of the UV photolysis of benzene, they confirmed the production of cyclohexadienyl radical (c-C<sub>6</sub>H<sub>7</sub>) in *p*-H<sub>2</sub> as an intermediate species for a ring-opening reaction to 1,3,5-hexatriene (Fig. 33). The cyclohexadienyl radical subsequently underwent a ring-opening reaction to produce 1,3,5-hexatriene after prolonged 193-nm UV irradiation. 1,3-hexadien-5-yne and *o*-benzyne were identified as minor products of the photochemical reaction.

Zhu *et al.*<sup>92</sup> studied methylsulfonyloxy radical <sup>•</sup>CH<sub>3</sub>SO<sub>3</sub>, one of the key intermediates in the atmospheric oxidation of dimethylsulfide, generated by flash pyrolysis of CH<sub>3</sub>SO<sub>2</sub>OOSO<sub>2</sub>CH<sub>3</sub> and subsequently isolated in solid noble gas matrices. The radical was characterized by UV/Vis and IR

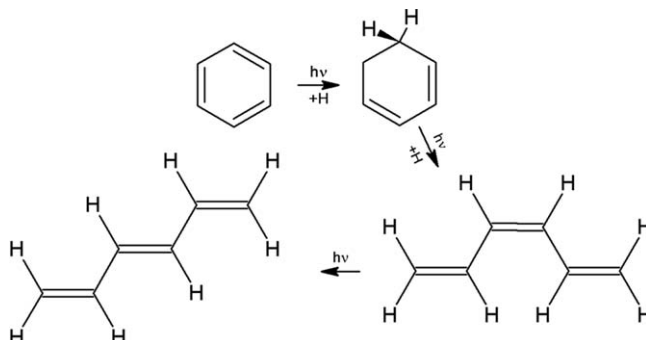


**Fig. 33** Photochemical reactions of matrix-isolated benzene upon 193 and 253.7 nm excitations.<sup>91</sup>

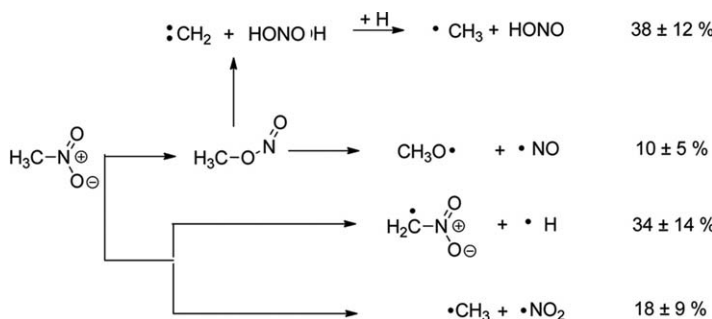


**Fig. 34** Isomerization and decomposition mechanisms of nitromethane ( $\text{CH}_3\text{NO}_2$ ) along with overall branching ratios of the four pathways identified. Reprinted with permission from Y. A. Tsegaw, W. Sander and R. I. Kaiser, *J. Phys. Chem. A*, 2016, **120**, 1577–1587. Copyright (2016) American Chemical Society.<sup>93</sup>

spectroscopies and its tautomerization to  $\cdot\text{CH}_2\text{SO}_3\text{H}$  radical observed upon irradiation with light of  $\lambda \geq 360$  nm. The authors highlighted the possible important role of this radical in the atmosphere. In addition to the formation of acid rain in the form of  $\text{CH}_3\text{SO}_3\text{H}$ , it can photo-rearrange to the reactive isomeric radicals  $\cdot\text{CH}_2\text{SO}_3\text{H}$  and  $\cdot\text{CH}_3\text{OSO}_2$ . The later sulfur-centered radical, in turn, can readily dissociate into  $\text{SO}_2$  and the atmospherically important  $\text{CH}_3\text{O}^\bullet$  radical.

Tsegaw, Sander, and Kaiser<sup>93</sup> reported on the UV photolysis of nitromethane ( $\text{CH}_3\text{NO}_2$ ) ices. Their studies identified a comprehensive suite of radicals formed in these processes with the corresponding branching ratios (Fig. 34): two carbon-centered radicals [methyl ( $\cdot\text{CH}_3$ ), nitromethyl ( $\cdot\text{CH}_2\text{NO}_2$ )], one oxygen-centered radical[methoxy ( $\text{CH}_3\text{O}^\bullet$ )], two nitrogen-centered radicals [nitrogen monoxide ( $\cdot\text{NO}$ ), nitrogen dioxide ( $\cdot\text{NO}_2$ )], as well as atomic hydrogen ( $\cdot\text{H}$ ). These studies provide valuable insights into the underlying reaction mechanisms in the decomposition of nitromethane as a model compound to forecast the aging behavior, performance, and sensitivity to heat and shock of energetic materials.

Zhu, Duarte, and Khriachtchev<sup>94</sup> prepared two new radicals,  $\text{H}_2\text{CCl}^\bullet$  and  $\text{H}_2\text{CCBr}^\bullet$ , in low-temperature noble gas matrices and characterized them using IR spectroscopy. These radicals were made by UV photolysis of  $\text{HCCl}$  and  $\text{HCCBr}$  and subsequent thermal annealing to mobilize hydrogen atoms in the matrices and promote their reaction with the residual precursor molecules. The assignments were supported by quantum chemical calculations at the B3LYP and CCSD(T) levels of theory with the def2-TZVPPD basis set.

Ryazantsev and Feldman<sup>95</sup> compared the effect of radiolysis and photolysis on matrix-isolated formic acid ( $\text{HCOOH}$ ). The formation of  $\text{HOOC}^\bullet$  radicals represents a primary dissociation channel for formic acid, which was not reported previously under UV photolysis in solids. The contribution of this channel was found to be strongly dependent on the matrix material and, in the case of krypton, its yield is comparable to that of CO. In addition, it was demonstrated that the  $\text{CO}_2/\text{CO}$  production ratio under radiolysis was much higher than that reported for the 193-nm photolysis. The authors explained their results by the

involvement of the recombination-induced excited states, which are not populated in photolysis. They also stressed that their results provide a new insight into the effects of high-energy impact on the simplest carboxylic acid with possible implications for astrochemical problems, in particular the prebiotic evolution in the interstellar medium.

Mieres-Pérez *et al.*<sup>96</sup> obtained a new sextet ground state molecule, the 2,4,6-trichloro-1,3-dinitrenophenoxy radical, upon UV photolysis of the corresponding diazido precursor in argon at 5 K. The sextet molecule is formed stepwise with the triplet nitrene, the quartet nitreno radical, and the quintet dinitrene as intermediates, which were detected by EPR spectroscopy. IR and UV/Vis measurements only allowed observation of the main product, the quintet dinitrene.

Finally, in a very recent study, Cluysts *et al.*<sup>97</sup> studied the photochemistry of 4-pyridinecarboxaldehyde by matrix isolation IR spectroscopy and quantum chemical calculations undertaken at different levels of approximation. The molecule was found to have a planar structure ( $C_s$  point group), with a MP2/6-311++G(d,p) predicted internal rotation barrier of 26.6 kJ mol<sup>-1</sup>. Upon *in situ* UV irradiation of the matrix-isolated compound, prompt decarbonylation was observed leading to the formation of pyridine. The authors proposed a mechanism for this photoreaction where, after excitation to  $S_2$ , inter system crossing to the triplet manifold leads to the cleavage of the C–H aldehyde bond. The formed radical then releases CO and recombines with the hydrogen atom within the matrix cage leading to the observed photoproducts.

#### 4.3 Ketenes and other species

A few studies involving generation or investigation of the photoreactivity of ketenes were reported in the period covered by this review. This section also presents data for other types of molecules not belonging to any of the families of compounds already considered in this chapter.

Gómez Castaño *et al.*<sup>98</sup> prepared the hitherto unknown diacetyl diselenide [ $\text{CH}_3\text{C}(\text{O})\text{Se}]_2$  by oxidation of selenoacetic acid,  $\text{CH}_3\text{C}(\text{O})\text{SeH}$ . Gas phase composition of diacetyl diselenide at room temperature was found to be an equilibrium mixture between two conformers, **a**( $C_2$ ) and **b**( $C_1$ ) (Fig. 35). According to B3LYP/6-311++G(3df,3pd) or MP2/aug-cc-pvdz calculations, conformer **a** is more stable than conformer **b** by 0.18 or 0.42 kcal mol<sup>-1</sup>, respectively. Exposure of [ $\text{CH}_3\text{C}(\text{O})\text{Se}]_2$  isolated in argon to a broadband radiation ( $200 \leq \lambda \leq 800$  nm) led to a rapid photolysis of the compound to bring about ketene,  $\text{H}_2\text{C}=\text{C=O}$ , together with  $\text{CH}_3\text{SeH}$  and OCSe.

As reported by Justino *et al.*,<sup>57</sup> the UV-induced photochemistry of the matrix-isolated monomeric gallic acid follows the general patterns exhibited by phenol-type compounds, leading to the 2,4-cyclohexadienone derivative (2,4-CHD), which results from cleavage of the free OH bond of gallic acid followed by recombination of the hydrogen atom with the formed phenoxy radical analogue at the *ortho*-position. Other photofragmentation products, including acetylene,  $\text{CO}_2$ , ketene, and ethynediol, were also produced upon matrix UV irradiation of the compound (Fig. 36).

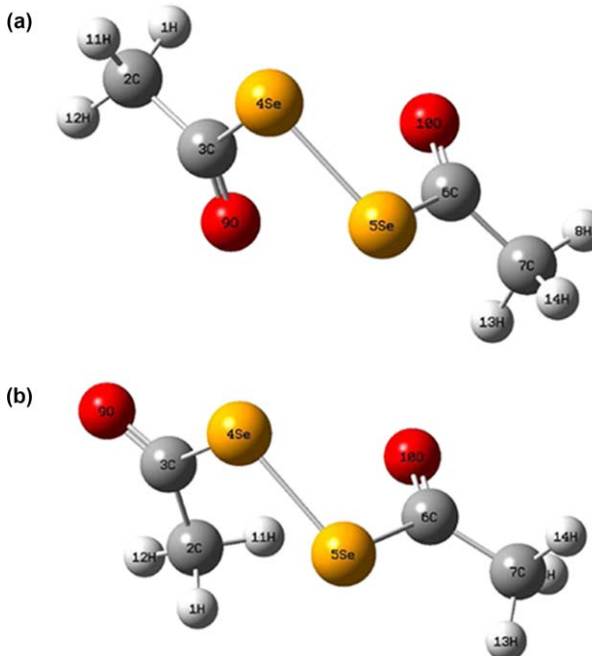


**Fig. 35** Molecular models of two stable conformers of  $[\text{CH}_3\text{C}(\text{O})\text{Se}]_2$ . Adapted with permission from ref. 98, J. A. Gómez Castaño, R. M. Romano, A. R. Salamanca, G. Amésquita, H. Beckers, H. Willner and C. O. della Védova, *J. Phys. Org. Chem.*, John Wiley and Sons. Copyright © 2016 John Wiley & Sons, Ltd.

Juncal *et al.*<sup>99</sup> obtained  $\text{ROC}(\text{S})\text{SC}(\text{O})\text{OCH}_2\text{CH}_3$  [ $\text{R}=\text{CH}_3-$ ,  $(\text{CH}_3)_2\text{CH}-$  and  $\text{CH}_3(\text{CH}_2)_2-$ ] from potassium xanthate salts  $[\text{ROC}(\text{S})\text{SK}]$  and ethyl chloroformate  $[\text{ClC}(\text{O})\text{OCH}_2\text{CH}_3]$ . First, the liquid compounds were identified and characterized by  $^1\text{H}$  and  $^{13}\text{C}$  NMR and mass spectrometry, and conformational isomers determined using DFT calculations. Six conformers were theoretically predicted for  $\text{R}=\text{CH}_3-$  and  $(\text{CH}_3)_2\text{CH}-$ . Because of the conformational flexibility of the *n*-propyl substituent, 21 conformers were found for  $\text{R}=\text{CH}_3(\text{CH}_2)_2-$ . The authors clustered the conformers in three groups. The most stable forms were the AS forms, with the C=S group *anti* (A) with respect to the C-S single bond and the S-C single bond *syn* (S) with respect to the C=O, followed by AA and SS conformers. The vibrational spectra were interpreted in terms of the predicted conformational equilibrium, the  $\nu\text{C}=\text{O}$  spectral region showing signals of the three groups of conformers.

A moderated pre-resonance Raman enhancement of the  $\nu\text{C}=\text{S}$  vibrational mode of  $\text{CH}_3(\text{CH}_2)_2-\text{OC}(\text{S})\text{SC}(\text{O})\text{OCH}_2\text{CH}_3$  was detected when the excitation radiation approached the energy of a  $\pi\rightarrow\pi''$  electronic transition associated with the C=S chromophore.<sup>99</sup> The UV/Vis spectra in different solvents were measured and interpreted in terms of TD-DFT calculations. The unknown molecule  $\text{CH}_3\text{CH}_2\text{OC}(\text{O})\text{SH}$  was produced by UV/Vis photolysis of  $\text{CH}_3\text{OC}(\text{S})\text{SC}(\text{O})\text{OCH}_2\text{CH}_3$  isolated in Ar matrix, and also obtained as a side-product of the reaction between potassium xanthate salts,  $\text{ROC}(\text{S})\text{SK}$ , and ethyl chloroformate,  $\text{ClC}(\text{O})\text{OCH}_2\text{CH}_3$ .

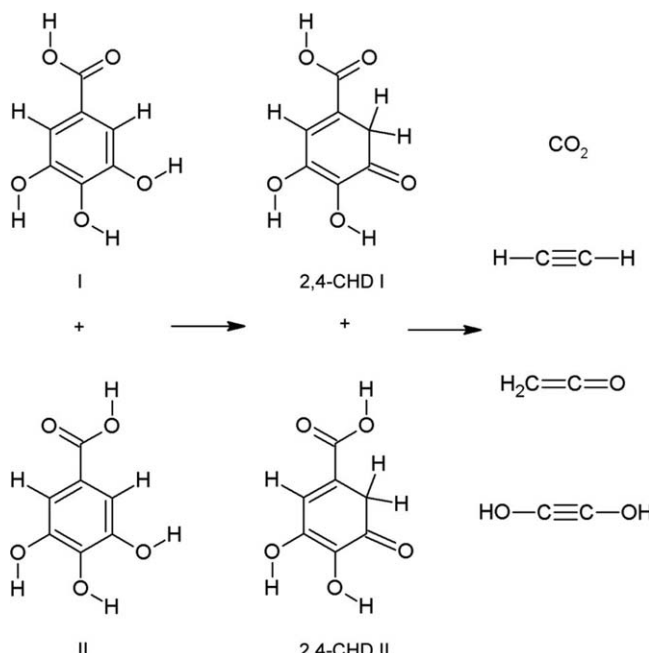


**Fig. 36** Photochemical processes observed upon UV irradiation of gallic acid monomers isolated in cryogenic matrices. Among other products, ketene was observed. Reprinted from L. L. G. Justino, I. Reva and R. Fausto, *J. Chem. Phys.*, 2016, **145**, 14304 with the permission of AIP Publishing LLC.<sup>57</sup>

Voros *et al.*<sup>100</sup> studied the equilibrium structures and relative energies of nine-nine (seven open-chain and two cyclic) isomers of the [2C, 2N, X] systems (X = O, S, Se). To this aim, they prepared and investigated NCSCN and NCSeCN in low-temperature Ar and Kr matrices. Photolysis of the matrices at 254 nm led to the formation of other isomers, namely, the novel NCSNC, NCSeNC, and NCNCSe species. The isomerization process was more efficient in Kr matrices than in Ar ones probably because of the larger sites in Kr matrices and the larger space requirement of the NCXCN  $\rightarrow$  NCNCX isomerization reaction compared to the NCXCN  $\rightarrow$  NCXNC isomerization. All the generated compounds were experimentally identified and spectroscopically characterized.

Kuş, Sagdinc, and Fausto<sup>101</sup> concluded on the existence of two conformers (*trans* and *cis*) of 5-hydroxyquinoline (5HQ; 1 in Fig. 37) based on DFT(B3LYP)/6-311++G(d,p) calculations, the *trans* conformer being more stable than the *cis* form by  $\sim 8.8 \text{ kJ mol}^{-1}$ . Isolation of the compound in solid nitrogen allowed observation of the most stable *trans* conformer. Broadband *in situ* UV irradiations ( $\lambda \geq 288 \text{ nm}$  and  $\lambda \geq 235 \text{ nm}$ ) led to several chemical transformations. In particular, initial irradiation of 5HQ at  $\lambda \geq 288 \text{ nm}$  led to observation of quinolin-5(6*H*)-one (3, major product) and quinolin-5(8*H*)-one (4, minor product) *via* the quinolinyl radical 2. Subsequent irradiation at  $\lambda \geq 235 \text{ nm}$  resulted in the major production of 4, together with generation of isomeric open-ring ketene forms (5), and fragmentation products (mainly CO and allene).

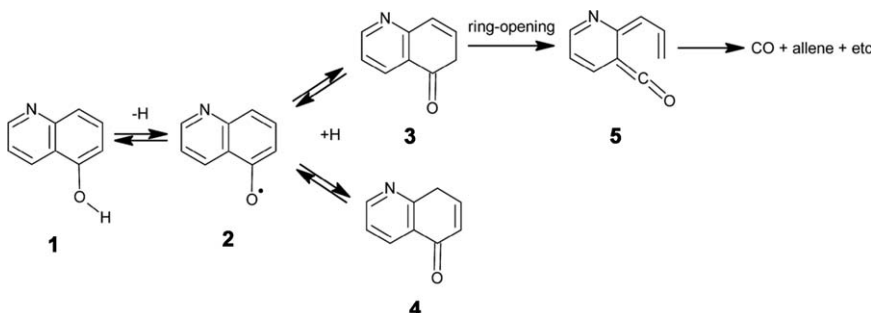


**Fig. 37** Photochemical reactions resulting from UV irradiation of 5HQ (1) isolated in  $\text{N}_2$  matrix. Reprinted with permission from N. Kuş, S. Sagdinc and R. Fausto, *J. Phys. Chem. A*, 2015, **119**, 6296–6308. Copyright (2015) American Chemical Society.<sup>101</sup>

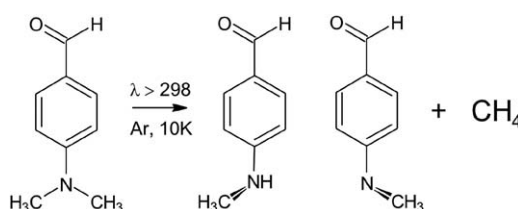


**Fig. 38** UV-induced major photoprocess observed for matrix-isolated DMABA. Adapted from *Tetrahedron*, 72, N. Kuş, A. Sharma and R. Fausto, First observation of methane photochemical generation from an *N,N*-dimethylamino-substituted arene: the case of 4-(*N,N*-dimethylamino)benzaldehyde (DMABA), 5914–5922. Copyright (2016) with permission from Elsevier.<sup>102</sup>

In another study, broadband UV irradiation ( $\lambda > 298$  nm) of 4-(*N,N*-dimethylamino)benzaldehyde (DMABA) isolated in argon matrix (10 K) was undertaken by Kuş, Sharma, and Fausto.<sup>102</sup> The photolysis led to major unimolecular fragmentation of the compound to methane and 4-(methylideneamino)benzaldehyde (4MAB) (Fig. 38). The authors proposed the following mechanism for the observed photochemical reaction: first, DMABA is photo-excited to the  $S_2$  state, then intersystem crossing to the triplet manifold takes place, followed by cleavage of the N-CH<sub>3</sub> bond and formation of the final products, methane and 4MAB, presumably *via* the corresponding radicals. The last step of the reaction was tentatively described as resulting from hydrogen atom abstraction from the methyl group of the 4MAB radical by the methyl radical initially formed in the same matrix cage. Interestingly, the observed photo-fragmentation reaction channel was found to be strongly preferred over the photochemical decarbonylation. The experimentally obtained results were supported by an extensive set of quantum chemical calculations undertaken using both *ab initio* (MP2) and DFT methods.

Kugel and Ault<sup>103</sup> studied the reactions of ozone with three bicyclic alkenes,  $\alpha$ -pinene, norbornene, and norbornadiene, in argon matrix (14 K) by IR spectroscopy. Redlight ( $\lambda \geq 600$  nm) irradiation of the argon matrices containing  $\alpha$ -pinene and ozone produced  $\alpha$ -pinene oxide and one or two isomeric ketones, which could have resulted from initial ozone photolysis followed by subsequent reaction of O(<sup>3</sup>P) oxygen atoms

with matrix-isolated  $\alpha$ -pinene molecules. Norbornene and norbornadiene were both found to react with ozone in the gas phase during twin-jet or merged-jet deposition of these mixtures with argon. New peaks observed in the IR spectra were assigned to the primary ozonides, Criegee intermediates, and secondary ozonides of norbornene and norbornadiene indicating that the bulk of these reactions proceeded *via* the “classic” Criegee mechanism for ozonolysis of alkenes. Peak assignments were made by comparing the experimental spectra and  $^{18}\text{O}$  isotopic shifts with those calculated for intermediate and product molecules using DFT(B3LYP)/6-311G++(d,2p) calculations. UV irradiation of these mixtures resulted in complete decomposition of the early intermediates and the formation of acids, aldehydes, alcohols, carbon dioxide, and carbon monoxide.

McMahon *et al.*<sup>104</sup> investigated the photophysics and photochemistry of  $[(\text{CO})_5\text{MC}(\text{OMe})\text{Me}]$  using picosecond time-resolved IR spectroscopy ( $\text{M} = \text{Cr}$  or  $\text{W}$ ), low-temperature matrix isolation techniques ( $\text{M} = \text{Cr}$ ), and time-dependent density functional calculations ( $\text{M} = \text{Cr}$  or  $\text{W}$ ). These studies provided unambiguous evidence for the photochemical formation of a long-lived 18-electron metallaketene species capable of acting as a synthetically useful intermediate.

Toumi, Piétri and Couturier-Tamburelli<sup>105</sup> carried out a low-temperature Ar matrix isolation investigation of ethylcyanide ( $\text{CH}_3\text{CH}_2\text{CN}$ ), a molecule present in the atmosphere of Titan. The  $\lambda > 120$  nm and  $\lambda > 230$  nm photolysis wavelengths have been used to reproduce the radiation reaching the various parts of the atmosphere. Several photoproducts have been identified during photolysis, such as, vinyl cyanide ( $\text{CH}_2=\text{CHCN}$ ), cyanoacetylene ( $\text{HC}_3\text{N}$ ), ethylene/hydrogen cyanide ( $\text{C}_2\text{H}_4/\text{HCN}$ ), ethylene/hydrogenisocyanide ( $\text{C}_2\text{H}_4/\text{HNC}$ ), acetylene/hydrogen cyanide ( $\text{C}_2\text{H}_2/\text{HCN}$ ), acetylene/hydrogen isocyanide ( $\text{C}_2\text{H}_2/\text{HNC}$ ), and acetylene/methylenimine ( $\text{C}_2\text{H}_2/\text{HNCH}_2$ ) complexes. Ethyl isocyanide and aketenimine form ( $\text{CH}_3\text{CH}=\text{C}=\text{NH}$ ) have been identified as well. Photoproducts identification and spectral assignments were done using data reported in previous studies and DFT calculations with the B3LYP/cc-pVTZ basis set.

Broadband irradiation of 3,5-diphenyloxazole (**1** in Fig. 39) isolated in argon matrix, resulting in the formation of azirine **3**, was investigated by

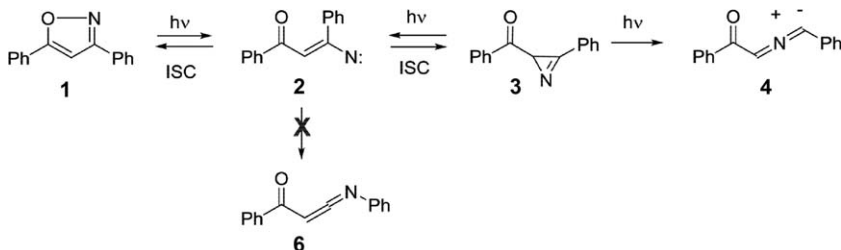


**Fig. 39** Proposed reaction mechanism for photoreactivity of isoxazole **1** in matrices. Adapted with permission from ref. 106, H. D. M. Sriyaratne, S. K. Sarkar, S. Hatano, M. Abe and A. D. Gudmundsdottir, *J. Phys. Org. Chem.*, John Wiley and Sons, Copyright © 2016 John Wiley & Sons, Ltd.

Sriyaratne *et al.*<sup>106</sup> Further irradiation of the matrix reduces the amount of azirine 3 with concurrent formation of the ylide 4. The authors theorized that the conversion of isoxazole 1 to azirine 3 goes through a triplet vinylnitrene 2 that shows no intersystem crossing to ketenimine 6. The  $\alpha$ -phenyl substituent in 2 is thought to lower the rotational barrier and to facilitate intersystem crossing to azirine 3 rather than ketenimine 6. DFT calculations supported this conclusion. The authors emphasized that a better understanding of the reactivity of vinylnitrene intermediates would make it possible to use them as building blocks for high-spin assemblies.

Borba *et al.*<sup>107</sup> investigated 5-phenoxy-1-phenyltetrazole (5PPT) isolated in Ar and N<sub>2</sub> cryogenic matrices and its molecular structure, conformational landscape, vibrational signature, and photochemistry by IR spectroscopy and theoretical calculations DFT(B3LYP)/6-311++G(d,p). Two different minima were located on the potential energy surface of the molecule, both being eightfold degenerate by symmetry and belonging to the C<sub>1</sub> symmetry point group. However, consideration of zero-point vibrational energy allowed concluding that the higher energy minimum shall relax barrierlessly to the lower energy form so that in the gas phase the compound exists in a single conformer. These theoretical predictions were confirmed by the experimental results, with only one conformer of 5PPT contributing to the IR spectra of the compound isolated in Ar and N<sub>2</sub> matrices. UV laser irradiation ( $\lambda = 250$  nm) of matrix-isolated 5PPT was found to lead to photolysis of the compound to the corresponding carbodiimide accompanied by N<sub>2</sub> release. Relevant characteristics of the experimental spectrum of the observed photoproduct, specifically the intensity smearing noticed in the  $\nu$ N–O and  $\nu$ C–O spectral regions, were interpreted based on the effect of the low-frequency, large-amplitude  $\tau$ N–O mode in this compound.

Pinelo, Kugel, and Ault<sup>108</sup> reported the formation of charge transfer complexes of O<sub>3</sub> with ferrocene (cp<sub>2</sub>Fe) and with *n*-butylferrocene (*n*-butyl cp<sub>2</sub>Fe) showing a broad absorption near 800 nm resulting from a n → π\* transition on the ozone subunit. The combined results of both the IR and UV/Vis studies provided strong evidence that the formation of these charge-transfer complexes affects how readily O<sub>3</sub> undergoes photodissociation when irradiated with red light ( $\lambda \geq 600$  nm). The identification of the charge-transfer complexes and photochemical products were supported by TD-DFT calculations at the B3LYP/6-311G++(d,2p) level of theory (Fig. 40). The results of this work support and enhance previous IR studies on the mechanism of the photooxidation of ferrocene by ozone.

In a later work, Pinelo and Ault<sup>109</sup> revisited the photochemical reaction of matrix-isolated ozone and *n*-butyl cp<sub>2</sub>Fe. Initial dark deposition of O<sub>3</sub> with *n*-butyl cp<sub>2</sub>Fe resulted in the formation of a *n*-butyl cp<sub>2</sub>Fe–O<sub>3</sub> charge-transfer complex. Irradiation of the complexed ozone with red light ( $\lambda \geq 600$  nm) led to the photodissociation and production of an oxygen atom O(<sup>3</sup>P) and a dioxygen molecule O<sub>2</sub>(<sup>3</sup>Σ). The O(<sup>3</sup>P) then reacted with *n*-butylferrocene to form products consisting of an iron atom with a coordinated *n*-butylcyclopentadienyl or cyclopentadienyl ring and either: (1) a pyran, (2) an aldehyde, or (3) a bidentate cyclic aldehyde with a

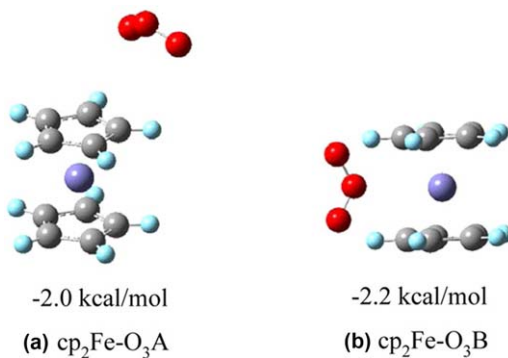


**Fig. 40** Calculated structures and the ground-state energy relative to the ground-state parent species of two charge-transfer complexes of  $\text{O}_3$  with  $\text{cp}_2\text{Fe}$  (a and b). Reprinted with permission from L. F. Pinelo, R. W. Kugel and B. S. Ault, *J. Phys. Chem. A*, 2015, **119**, 10272–10278. Copyright (2015) American Chemical Society.<sup>108</sup>

seven-membered ring including the iron atom. The authors assumed the presence of multiple regioisomers of each product in the matrix; however, they were unable to assign them due to similarities in the calculated spectra.  $^{18}\text{O}$ -labeled  $\text{O}_3$  experiments and DFT(B3LYP)/6-311++G(d,2p) calculations supported the interpretation of the observed data.

Other studies describing photochemical reactions with  $\text{O}_3$  during the described period included works by Sriyaratne *et al.*<sup>110</sup> and by Kugel, Pinelo, and Ault.<sup>111</sup>

The photolysis of  $\text{C}_2\text{H}_4$  in solid nitrogen at 10 K was studied by Chen *et al.*<sup>112</sup> The photoproducts of irradiation of the matrix samples with 121.6-nm light included  $\text{C}_2\text{H}_2$ , CN, and isomers of  $\text{C}_2\text{N}_2$ , as well as HCN and HNC. The results of this study provided insights into the formation of HNC and HCN, as well as nitriles in  $\text{N}_2$ -rich ice samples containing a small proportion of  $\text{C}_2\text{H}_4$ .

Another study from the same laboratory described UV irradiation of  $\text{C}_2\text{H}_4^+$  trapped in solid Ar.<sup>113</sup>  $\text{C}_2\text{H}_4^+$  were obtained through electron bombardment of a mixture of ethylene and Ar during matrix deposition. Upon UV radiation, IR lines of  $\text{C}_2\text{H}_4$ ,  $\text{C}_2\text{H}_2$ , and  $\text{C}_2\text{H}_3$  were detected indicating simultaneous photodissociation and photoassisted neutralization of  $\text{C}_2\text{H}_4^+$  in the matrix.

#### 4.4 Complexes and weakly bound species

Formation of complexes and weakly bound species is a rather probable event after photolysis of matrix-isolated compounds, considering that under these experimental conditions the reactions are cage-confined and molecular diffusion is very limited. A few studies focusing on the formation or photoreactivity of these species have been reported during the period covered by this review, some of them having already been briefly described in the previous sections of this chapter because the formation of the complexes or weakly bound species appears concomitantly with other (major) processes. In here, one wants to highlight the interesting investigation of Krupa, Kosendiak, and Wierzejewska<sup>42</sup> dealing with

phototransformations of isothiocyanic acid (HNCS) induced by tunable UV laser. Concomitantly with the formation of two isomers of the precursor HNCS molecule, thiocyanic acid (HSCN) and isothiofulminic acid (HSNC), a complex between hydrogen cyanide and a ground state ( ${}^3P$ ) sulfur atom appears at irradiation with a wavelength  $\lambda < 290$  nm. The authors noted that the  $S({}^3P)\cdots HCN$  species was the first hydrogen-bonded molecular complex to the atomic sulfur ( ${}^3P$ ) detected experimentally. Among three theoretical methods used in this work, the best reproduction of the experimental wavenumber shifts of the complex vibrations was obtained using the UB2PLYP(D3) method, which takes into account the contribution of the dispersion forces to the hydrogen bond interaction. The formation of  $S\cdots HCN$  was found to be twice more efficient in Ar than in N<sub>2</sub> indicating enhancement of cage exit of sulfur atoms in nitrogen matrix.

## 5 Noble gas chemistry

Following the trends noticed in the previous reviews of this series,<sup>4,5</sup> the studies on noble gas chemistry appearing in the scientific literature during the period 2015–2016 focused mainly on noble gas hydrides.

Willmann *et al.*<sup>114</sup> reported a matrix isolation and computational study of the HKrCCH···HCCH complex, which was successfully identified in Kr matrix by its characteristic H–Kr stretching bands at 1316.5 and 1305 cm<sup>-1</sup>. Upon complexation, the H–Kr stretching mode shifts up by about +60 cm<sup>-1</sup>, significantly more than the shift reported previously for the HXeCCH···HCCH complex in Xe matrix (about +25 cm<sup>-1</sup>).<sup>115</sup> The HKrCCH···HCCH complex was produced in Kr matrix at ~40 K *via* the attachment of mobile acetylene molecules to the HKrCCH monomers formed at somewhat lower annealing temperatures upon thermally-induced mobility of H atoms (~30 K). A similar mechanism describing the formation of the HXeCCH···HCCH complex in Xe matrix was proposed previously. The comparative results for the HKrCCH···HCCH and HXeCCH···HCCH complexes confirmed that the complexation effects are more relevant for less stable noble gas hydrides.

Zhu, Räsänen, and Khriachtchev<sup>116</sup> characterized a series of Kr and Xe hydrides containing the C≡C moiety, as well as several fluorinated cyanide and isocyanide derivatives.<sup>43</sup> The HKrCCl and HXeCCl molecules were prepared in low-temperature Kr and Xe matrices by UV *in situ* photolysis of HCCl and subsequent annealing.<sup>116</sup> The HCCl precursor was produced by microwave discharge of a mixture of the matrix gas with trichloroethylene (HClC=CCl<sub>2</sub>). The assignments of the new noble gas molecules were supported by deuteration experiments and quantum chemical calculations. Interestingly, no evidence of formation of ClXeCCH, which was predicted to be a stable species, was found in the experiments. The ClKrCCH and the Ar compounds, HArCCl and ClArCCH, were not observed either, in agreement with the calculations predicting those species to be rather unstable.

The new noble gas molecules, FKrCN, FXeCN, and FXeNC, were prepared in Kr and Xe matrices by UV photolysis of FCN and subsequent

annealing.<sup>43</sup> The FCN precursor was produced by deposition of the matrix gas containing (FCN)<sub>3</sub> through a microwave discharge. The new molecules were assigned with the help of quantum chemical calculations. Failed attempts to produce similar Ar compounds (FArCN and FArNC) as well as FKrNC were reported, in agreement with their calculated energetic data.

Zhu *et al.*<sup>117</sup> focused on HXeI and HXeH molecules in Ar, Kr, and Xe matrices. They characterized these species spectroscopically and investigated the effects of media on their spectral properties, concluding that the matrix effects are stronger for less stable molecules. Interestingly, they found that HXeI appears as a special case, regarding the frequency order of the H-Xe stretching mode in Ar and Kr matrices, compared to all previous results on noble gas hydrides. For previously studied HXeCl, HXeBr, and HXeCCH compounds, the H-Xe stretching frequency was found to be higher (by >10 cm<sup>-1</sup>) in Ar matrix than in Kr matrix, while the opposite was observed for HXeI.<sup>117</sup> The performed hybrid quantum-classical simulations were found to successfully describe these experimental findings. For HXeI in the ⟨110⟩ (double substitution) site, the order of the calculated H-Xe stretching frequencies ( $\nu(\text{Xe}) < \nu(\text{Ar}) < \nu(\text{Kr})$ ) was found to be in accord with the experimental observations, and also the frequency shifts in Ar and Kr matrices compared to those in Xe matrix were well predicted.

Finally, Yu and co-workers<sup>118</sup> produced a series of novel noble gas molecules of NgBeSO<sub>2</sub> (Ng=Ne, Ar, Kr, Xe) type by laser-evaporated beryllium atom reactions with SO<sub>2</sub> in Ne, Ar, Kr, and Xe matrices. IR spectroscopy and theoretical calculations were used to confirm the band assignments proposed for these species, and the dissociation energies were predicted to be 0.9, 4.0, 4.7, and 6.0 kcal mol<sup>-1</sup> for NeBeSO<sub>2</sub>, ArBeSO<sub>2</sub>, KrBeSO<sub>2</sub>, and XeBeSO<sub>2</sub>, respectively, at the CCSD(T) level. Quantum chemical calculations demonstrated also that the Ng-Be bonds in NgBeSO<sub>2</sub> could be formed by the combination of electron-donation and ion-induced dipole interactions. The calculated Wiberg bond index (WBI) values of the Ng-Be bonds and the localized orbital locator profiles indicate that the Ng-Be bond exhibits a gradual increase in covalent character along Ne to Xe series.

## Acknowledgements

The authors thank the Portuguese Science Foundation (FCT; Project PTDC/QEQ-QFI/3284/2014-POCI-01-0145-FEDER-016617, also funded by FEDER/COMPETE 2020-EU). The Coimbra Chemistry Center (CQC) is supported by FCT, through the project UI0313/QUI/2013, and co-funded by FEDER/COMPETE 2020-EU. A. G.-Z. thanks the Argentinean Agency for Scientific and Technological Promotion (ANPCyT; Project PICT(2014)/0912) for financial support. A. G.-Z. is a member of the Research Career from the Argentinean National Research Council (CONICET). T. N. acknowledges FCT and FEDER/COMPETE 2020-EU for the post-doctoral grant running within the Project PTDC/QEQ-QFI/3284/2014-POCI-01-0145-FEDER-016617.

## References

- 1 R. Fausto and A. Gómez-Zavaglia, Light Induced Reactions in Cryogenic Matrices, in *Photochemistry, A Specialist Periodic Report*, ed. A. Albini, RSC Publishing, London, 2009, vol. 37, p. 72.
- 2 R. Fausto and A. Gómez-Zavaglia, Light Induced Reactions in Cryogenic Matrices, in *Photochemistry, A specialist Periodic Report*, ed. A. Albini, RSC Publishing, London, 2010, vol. 38, p. 37.
- 3 R. Fausto and A. Gómez-Zavaglia, Light Induced Reactions in Cryogenic Matrices, in *Photochemistry, A specialist Periodic Report*, ed. A. Albini, RSC Publishing, London, 2011, vol. 39, p. 1.
- 4 R. Fausto and A. Gómez-Zavaglia, Light Induced Reactions in Cryogenic Matrices (Highlights 2011–2012), in *Photochemistry, A specialist Periodic Report*, ed. A. Albini and E. Fasani, RSC Publishing, London, 2013, vol. 41, p. 12.
- 5 R. Fausto, A. Borba and A. Gómez-Zavaglia, Light Induced Reactions in Cryogenic Matrices (Highlights 2013–2014), in *Photochemistry, A specialist Periodic Report*, The Royal Society of Chemistry, 2016, vol. 43, p. 20.
- 6 B. Meyer, *Low Temperature Spectroscopy*, American Elsevier Publishers Company, New York, 1971.
- 7 *Chemistry and Physics of Matrix Isolated Species*, ed. L. Andrews and M. Moskovits, Elsevier, Amsterdam, 1989.
- 8 *Matrix Isolation Spectroscopy*, ed. A. Barnes, W. J. Orville-Thomas, R. Gaufrhs and A. Muller, Springer, 1981.
- 9 I. R. Dunkin, *Matrix Isolation Techniques: A Practical Approach*, Oxford University Press, 1998.
- 10 *Low Temperature Molecular Spectroscopy*, ed. R. Fausto, NATO-ASI Series C483, Kluwer, Amsterdam, 1996.
- 11 T. Bally, *Chimia*, 2007, **61**, 645.
- 12 R. Fausto, S. Breda and N. Kuş, *J. Phys. Org. Chem.*, 2008, **21**, 644–651.
- 13 Y. Zhao and M. Zhou, *Sci. China: Chem.*, 2010, **53**, 327–336.
- 14 N. Balucani, F. Zhang and R. I. Kaiser, *Chem. Rev.*, 2010, **110**, 5107–5127.
- 15 C. Wentrup, *Aust. J. Chem.*, 2010, **63**, 979.
- 16 M. Winkler and W. Sander, *Aust. J. Chem.*, 2010, **63**, 1013.
- 17 M. J. Almond and N. Goldberg, *Annu. Rep. Prog. Chem., Sect. C: Phys. Chem.*, 2007, **103**, 79–133.
- 18 Low temperature spectroscopy and radiation effects. On the anniversary of E. V. Savchenko, in *Fizika Nizkikh Temperatur*, ed. I. Arakawa and M. Räsänen, 2012, vol. 38, p. 671, (118 pages).
- 19 Special issue:Light-Induced Processes in Cryogenic Matrices, in *Journal of Molecular Structure*, ed. R. Fausto, L. Lapinski and I. Reva, 2012, vol. 1025, p. 159.
- 20 G. Bucher, Cryogenic Matrix Photochemistry, in *Handbook of Organic Photochemistry and Photobiology*, ed. A. Griesbeck, M. Oelgemöller and F. Ghetti, CRC Press, 3rd edn, 2012, vol. 1, ch. 12, pp. 277–291.
- 21 J. Cerkovnik and B. Plesničar, *Chem. Rev.*, 2013, **113**, 7930–7951.
- 22 L. M. T. Frija, M. L. S. Cristiano, A. Gómez-Zavaglia, I. Reva and R. Fausto, *J. Photochem. Photobiol., C*, 2014, **18**, 71–90.
- 23 A. F. Khlebnikov and M. S. Novikov, *Tetrahedron*, 2013, **69**, 3363–3401.
- 24 S. A. Reid, *Int. Rev. Phys. Chem.*, 2014, **33**, 341–370.
- 25 T. Hama and N. Watanabe, *Chem. Rev.*, 2013, **113**, 8783–8839.
- 26 L. N. Zack and J. P. Maier, *Chem. Soc. Rev.*, 2014, **43**, 4602–4614.
- 27 M. Bahou, P. Das, Y.-F. Lee, Y.-J. Wu and Y.-P. Lee, *Phys. Chem. Chem. Phys.*, 2014, **16**, 2200–2210.

- 28 *Physics and Chemistry at Low Temperatures*, ed. L. Khriachtchev, Pan Stanford Publishing, Singapore, 2012, p. 536.
- 29 A. V. Nemukhin, L. Y. Khriachtchev, B. L. Grigorenko, A. V. Bochenkova and M. Räsänen, *Russ. Chem. Rev.*, 2007, **76**, 1085–1092.
- 30 L. Khriachtchev, M. Räsänen and R. B. Gerber, *Acc. Chem. Res.*, 2009, **42**, 183–191.
- 31 R. B. Gerber, E. Tsivion, L. Khriachtchev and M. Räsänen, *Chem. Phys. Lett.*, 2012, **545**, 1–8.
- 32 D. S. Brock and G. J. Schrobilgen, *Annu. Rep. Prog. Chem., Sect. A: Inorg. Chem.*, 2013, **109**, 101–107.
- 33 L. Khriachtchev, *J. Phys. Chem. A*, 2015, **119**, 2735–2746.
- 34 V. I. Feldman, S. V. Ryazantsev, E. V. Saenko, S. V. Kameneva and E. S. Shiryeva, *Radiat. Phys. Chem.*, 2016, **124**, 7–13.
- 35 A. Halasa, L. Lapinski, H. Rostkowska and M. J. Nowak, *J. Phys. Chem. A*, 2015, **119**, 9262–9271.
- 36 A. Halasa, I. Reva, L. Lapinski, H. Rostkowska, R. Fausto and M. J. Nowak, *J. Phys. Chem. A*, 2016, **120**, 2647–2656.
- 37 A. J. Lopes Jesus, I. Reva, C. Araujo-Andrade and R. Fausto, *J. Am. Chem. Soc.*, 2015, **137**, 14240–14243.
- 38 S. Lopes, A. V. Domanskaya, M. Räsänen, L. Khriachtchev and R. Fausto, *J. Chem. Phys.*, 2015, **143**, 104307.
- 39 O. Ünsalan, N. Kuş, S. Jarmelo and R. Fausto, *Spectrochim. Acta, Part A*, 2015, **136**, 81–94.
- 40 C. M. Nunes, I. Reva, R. Fausto, D. Bégué and C. Wentrup, *Chem. Commun.*, 2015, **51**, 14712–14715.
- 41 C. M. Nunes, S. N. Knezz, I. Reva, R. Fausto and R. J. McMahon, *J. Am. Chem. Soc.*, 2016, **138**, 15287–15290.
- 42 J. Krupa, I. Kosendiak and M. Wierzejewska, *Phys. Chem. Chem. Phys.*, 2015, **17**, 22431–22437.
- 43 C. Zhu, M. Räsänen and L. Khriachtchev, *J. Chem. Phys.*, 2015, **143**, 74306.
- 44 Y. T. Angel Wong, S. Y. Toh, P. Djuricanin and T. Momose, *J. Mol. Spectrosc.*, 2015, **310**, 23–31.
- 45 S. G. Stepanian, A. Y. Ivanov and L. Adamowicz, *J. Mol. Spectrosc.*, 2016, **320**, 13–24.
- 46 L. Kócs, E. E. Najbauer, G. Bazsó, G. Magyarfalvi and G. Tarczay, *J. Phys. Chem. A*, 2015, **119**, 2429–2437.
- 47 S. Coussan and G. Tarczay, *Chem. Phys. Lett.*, 2016, **644**, 189–194.
- 48 E. E. Najbauer, G. Bazsó, R. Apóstolo, R. Fausto, M. Biczysko, V. Barone and G. Tarczay, *J. Phys. Chem. B*, 2015, **119**, 10496–10510.
- 49 J. A. Noble and S. Coussan, *J. Phys. Chem. A*, 2015, **119**, 1137–1145.
- 50 A. Canneva, M. F. Erben, R. M. Romano, Y. V. Vishnevskiy, C. G. Reuter, N. W. Mitzel and C. O. Della Védova, *Chem. – Eur. J.*, 2015, **21**, 10436–10442.
- 51 A. J. Lopes Jesus, I. Reva, C. Araujo-Andrade and R. Fausto, *J. Chem. Phys.*, 2016, **144**, 124306.
- 52 A. Halasa, L. Lapinski, I. Reva, H. Rostkowska, R. Fausto and M. J. Nowak, *J. Phys. Chem. A*, 2015, **119**, 1037–1047.
- 53 A. Halasa, I. Reva, L. Lapinski, M. J. Nowak and R. Fausto, *J. Phys. Chem. A*, 2016, **120**, 2078–2088.
- 54 M. Miyagawa, N. Akai and M. Nakata, *J. Mol. Struct.*, 2015, **1086**, 1–7.
- 55 A. Halasa, L. Lapinski, H. Rostkowska, I. Reva and M. J. Nowak, *J. Phys. Chem. A*, 2015, **119**, 2203–2210.
- 56 I. Reva, C. M. Nunes, M. Biczysko and R. Fausto, *J. Phys. Chem. A*, 2015, **119**, 2614–2627.

- 57 L. L. G. Justino, I. Reva and R. Fausto, *J. Chem. Phys.*, 2016, **145**, 14304.
- 58 R. F. G. Apóstolo, R. R. F. Bento and R. Fausto, *Croat. Chem. Acta*, 2015, **88**, 377–386.
- 59 R. F. G. Apóstolo, G. Bazsó, R. R. F. Bento, G. Tarczay and R. Fausto, *J. Mol. Struct.*, 2016, **1125**, 288–295.
- 60 A. Kwiatek and Z. Mielke, *Spectrochim. Acta, Part A*, 2015, **135**, 1099–1106.
- 61 S. Lopes, R. Fausto and L. Khriachtchev, *J. Chem. Phys.*, 2016, **144**, 84308.
- 62 Y. Berrueta Martínez, C. G. Reuter, Y. V. Vishnevskiy, Y. B. Bava, A. L. Picone, R. M. Romano, H.-G. Stammller, B. Neumann, N. W. Mitzel and C. O. Della Védova, *J. Phys. Chem. A*, 2016, **120**, 2420–2430.
- 63 P. Horta, N. Kuş, M. S. C. Henriques, J. A. Paixão, L. Coelho, F. Nogueira, P. M. O'Neill, R. Fausto and M. L. S. Cristiano, *J. Org. Chem.*, 2015, **80**, 12244–12257.
- 64 I. Reva, M. J. Nowak, L. Lapinski and R. Fausto, *Phys. Chem. Chem. Phys.*, 2015, **17**, 4888–4898.
- 65 L. Duarte, L. Khriachtchev, R. Fausto and I. D. Reva, *Phys. Chem. Chem. Phys.*, 2016, 16802–16811.
- 66 Y. Miyazaki, Y. Inokuchi, N. Akai and T. Ebata, *J. Phys. Chem. Lett.*, 2015, **6**, 1134–1139.
- 67 M. Avadanei, N. Kuş, V. Cozan and R. Fausto, *J. Phys. Chem. A*, 2015, **119**, 9121–9132.
- 68 M. C. Liu, S. C. Chen, C. H. Chin, T. P. Huang, H. F. Chen and Y. J. Wu, *J. Phys. Chem. Lett.*, 2015, **6**, 3185–3189.
- 69 A. Tajti, L. A. Mück, Á. L. Farkas, M. Krebsz, T. Pasinszki, G. Tarczay and P. G. Szalay, *J. Mol. Spectrosc.*, 2015, **310**, 8–15.
- 70 C. M. Nunes, I. Reva, M. T. S. Rosado and R. Fausto, *Eur. J. Org. Chem.*, 2015, 7484–7493.
- 71 S. Lopes, I. Reva and R. Fausto, *Vib. Spectrosc.*, 2015, **81**, 68–82.
- 72 S. K. Sarkar, A. Sawai, K. Kanahara, C. Wentrup, M. Abe and A. D. Gudmundsdottir, *J. Am. Chem. Soc.*, 2015, **137**, 4207–4214.
- 73 S. K. Sarkar, O. Osioma, W. L. Karney, M. Abe and A. D. Gudmundsdottir, *J. Am. Chem. Soc.*, 2016, **138**, 14905–14914.
- 74 A. Ismael, A. Borba, M. S. C. Henriques, J. A. Paixão, R. Fausto and M. L. S. Cristiano, *J. Org. Chem.*, 2015, **80**, 392–400.
- 75 C. M. Nunes, S. M. V. Pinto, I. Reva and R. Fausto, *Eur. J. Org. Chem.*, 2016, 4152–4158.
- 76 G. Deng, D. Li, Z. Wu, H. Li, E. Bernhardt and X. Zeng, *J. Phys. Chem. A*, 2016, **120**, 5590–5597.
- 77 H. Sun, B. Zhu, Z. Wu, X. Zeng, H. Beckers and W. S. Jenks, *J. Org. Chem.*, 2015, **80**, 2006–2009.
- 78 X. Zeng, H. Beckers, H. Willner, P. Neuhaus, D. Grote and W. Sander, *J. Phys. Chem. A*, 2015, **119**, 2281–2288.
- 79 H. Li, H. Wan, Z. Wu, D. Li, D. Bégué, C. Wentrup and X. Zeng, *Chem. – Eur. J.*, 2016, **22**, 7856–7862.
- 80 Q. Liu, H. Li, Z. Wu, D. Li, H. Beckers, G. Rauhut and X. Zeng, *Chem. – Asian J.*, 2016, **11**, 2953–2959.
- 81 P. Costa and W. Sander, *J. Phys. Org. Chem.*, 2015, **28**, 71–74.
- 82 P. Costa, T. Lohmiller, I. Trosien, A. Savitsky, W. Lubitz, M. Fernandez-Oliva, E. Sanchez-Garcia and W. Sander, *J. Am. Chem. Soc.*, 2016, **138**, 1622–1629.
- 83 S. N. Knezz, T. A. Waltz, B. C. Haenni, N. J. Burrmann and R. J. McMahon, *J. Am. Chem. Soc.*, 2016, **138**, 12596–12604.
- 84 G. Richter, E. Mendez-Vega and W. Sander, *J. Phys. Chem. A*, 2016, **120**, 3524–3532.

- 85 T. Butscher, F. Duvernay, P. Theule, G. Danger, Y. Carissan, D. Hagebaum-Reignier and T. Chiavassa, *Mon. Not. R. Astron. Soc.*, 2015, **453**, 1587–1596.
- 86 J. Krupa and M. Wierzejewska, *Chem. Phys. Lett.*, 2015, **618**, 219–224.
- 87 Y.-F. Lee, W.-T. Chou, B. A. Johnson, D. P. Tabor, E. L. Sibert and Y.-P. Lee, *J. Mol. Spectrosc.*, 2015, **310**, 57–67.
- 88 Y.-F. Lee and Y.-P. Lee, *Mol. Phys.*, 2015, **113**, 2148–2158.
- 89 F. M. Mutunga and D. T. Anderson, *J. Phys. Chem. A*, 2015, **119**, 2420–2428.
- 90 H. P. Reisenauer, J. Romański, G. Młostoiń and P. R. Schreiner, *Chem. Commun.*, 2015, **51**, 10022–10025.
- 91 S. Y. Toh, P. Djuricanin, T. Momose and J. Miyazaki, *J. Phys. Chem. A*, 2015, **119**, 2683–2691.
- 92 B. Zhu, X. Zeng, H. Beckers, J. S. Francisco and H. Willner, *Angew. Chem., Int. Ed.*, 2015, **54**, 11404–11408.
- 93 Y. A. Tsegaw, W. Sander and R. I. Kaiser, *J. Phys. Chem. A*, 2016, **120**, 1577–1587.
- 94 C. Zhu, L. Duarte and L. Khriachtchev, *J. Chem. Phys.*, 2016, **145**, 74312.
- 95 S. V. Ryazantsev and V. I. Feldman, *Phys. Chem. Chem. Phys.*, 2015, **17**, 30648–30658.
- 96 J. Mieres-Pérez, S. Henkel, E. Mendez-Vega, T. Schleif, T. Lohmiller, A. Savitsky and W. Sander, *J. Phys. Org. Chem.*, 2017, **30**, e3621.
- 97 L. Cluyts, A. Sharma, N. Kuş, K. Schoone and R. Fausto, *Spectrochim. Acta, Part A*, 2017, **171**, 207–212.
- 98 J. A. Gómez Castaño, R. M. Romano, A. R. Salamanca, G. Amésquita, H. Beckers, H. Willner and C. O. Della Védova, *J. Phys. Org. Chem.*, 2016, **29**, 636–644.
- 99 L. C. Juncal, M. V. Cozzarín and R. M. Romano, *Spectrochim. Acta, Part A*, 2015, **139**, 346–355.
- 100 T. Vörös, B. Pacsai, G. Magyarfalvi and G. Tarczay, *J. Mol. Spectrosc.*, 2015, **316**, 95–104.
- 101 N. Kuş, S. Sagdinc and R. Fausto, *J. Phys. Chem. A*, 2015, **119**, 6296–6308.
- 102 N. Kuş, A. Sharma and R. Fausto, *Tetrahedron*, 2016, **72**, 5914–5922.
- 103 R. W. Kugel and B. S. Ault, *J. Phys. Chem. A*, 2015, **119**, 312–322.
- 104 S. McMahon, S. Amirjalayer, W. J. Buma, Y. Halpin, C. Long, A. D. Rooney, S. Woutersen and M. T. Pryce, *Dalton Trans.*, 2015, **44**, 15424–15434.
- 105 A. Toumi, N. Piétri and I. Couturier-Tamburelli, *Phys. Chem. Chem. Phys.*, 2015, **17**, 30352–30363.
- 106 H. D. M. Sriyaratne, S. K. Sarkar, S. Hatano, M. Abe and A. D. Gudmundsdottir, *J. Phys. Org. Chem.*, 2017, **30**, 3638.
- 107 A. Borba, L. I. L. Cabral, R. Fausto and M. L. S. Cristiano, *Can. J. Chem.*, 2015, **93**, 1335–1344.
- 108 L. F. Pinelo, R. W. Kugel and B. S. Ault, *J. Phys. Chem. A*, 2015, **119**, 10272–10278.
- 109 L. F. Pinelo and B. S. Ault, *J. Mol. Struct.*, 2016, **1116**, 303–310.
- 110 H. D. M. Sriyaratne, A. D. Gudmundsdottir and B. S. Ault, *J. Phys. Chem. A*, 2015, **119**, 2834–2844.
- 111 R. W. Kugel, L. F. Pinelo and B. S. Ault, *J. Phys. Chem. A*, 2015, **119**, 2371–2382.
- 112 H.-F. Chen, M.-C. Liu, S.-C. Chen, T.-P. Huang and Y.-J. Wu, *Astrophys. J.*, 2015, **804**, 36.
- 113 S.-C. Chen, M.-C. Liu, T.-P. Huang, C.-H. Chin and Y.-J. Wu, *Chem. Phys. Lett.*, 2015, **630**, 96–100.
- 114 K. Willmann, T. Vent-Schmidt, M. Rasanen, S. Riedel and L. Khriachtchev, *RSC Adv.*, 2015, **5**, 35783–35791.

- 115 A. Domanskaya, A. V. Kobzarenko, E. Tsivion, L. Khriachtchev,  
V. I. Feldman, R. Benny Gerber and M. Räsänen, *Chem. Phys. Lett.*, 2009,  
**481**, 83–87.
- 116 C. Zhu, M. Räsänen and L. Khriachtchev, *J. Chem. Phys.*, 2015, **143**, 244319.
- 117 C. Zhu, K. Niimi, T. Taketsugu, M. Tsuge, A. Nakayama and L. Khriachtchev,  
*J. Chem. Phys.*, 2015, **142**, 54305.
- 118 W. Yu, X. Liu, B. Xu, X. Xing and X. Wang, *J. Phys. Chem. A*, 2016, **120**,  
8590–8598.

---

# The molecules of colour

J. Sérgio Seixas de Melo\*

DOI: 10.1039/9781788010696-00068

Indigo, alizarin, mauveine, brazilin and brazilein (the latter two being major colour constituents of Brazilwood) are molecules that have had a strong impact in our civilization. The colour and longevity of these molecules is linked to their photostability, which have different origins. In this contribution the photochemistry and photophysics of these and other molecules will be reviewed, and linked with relevant issues such as the photostability, photoisomerization, mechanisms of photodegradation, the origin of the colour, and the incorporation in different matrices. In some cases, stability is associated with excited state proton transfer, while in the case of indigo it also forms Maya Blue, the pigment of the ancient Central American civilizations, with the clay palygorskite.

## 1 Introduction

In the history of mankind, the exploitation of colour was a formidable achievement. Colour and the dyes, colorants or pigments that produce it have made it possible to turn the pale and drab into something shiny and invigorating. The capture of colours made by our ancestors was obtained using vegetal, mineral and animal sources. But behind these, the colour they produced came from molecules: the molecules of colour.

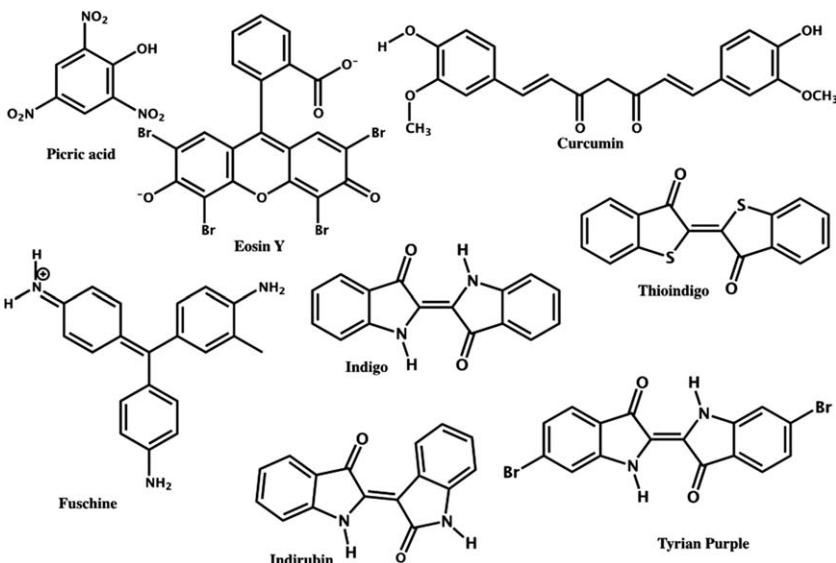
In this contribution we will focus on the chemistry (with some history) of both some of the most important and some forgotten molecules that have fingerprinted the origin and development of colours used for painting, dyeing, and generally colouring the world. The chemistry behind these molecules will include a special emphasis on the mythical blue indigo and the iconic colour of mauveine (a mixture of more than thirteen different methyl derivatives – C<sub>24</sub> to C<sub>28</sub> – of 7-amino-5-phenyl-3-(phenylamino)phenazin-5-i um compounds).

Several classifications of the molecules of colour can be made, based either on the colours they display or on their “appearance” to man over the ages. A brief outline of these will be made, aiming to give both chemical and historical perspectives.

Some of the colours, such as blue, were not readily accessible in prehistoric times. The grottos and caverns studied today lack this colour. Two of the important blues of antiquity were indigo, an organic molecule, and Ultramarine blue an inorganic sodium aluminosilicate complex, incorporating the blue S<sup>3-</sup> anions ( $\lambda_{\text{max}} = 600 \text{ nm}$ ). There are, however, many other important dyes, which can be considered both in terms of their colour and, in many cases, the impact they had in the history of mankind. Among these are the purples (Tyrian Purple, mauveine, and the triphenyl derivative fuschine, also known as a Hoffmann dye), yellows (picric acid, saffron (curcumin)), reds (alizarin, purpurin, eosin Y and the synthetic thioindigo), blues (indigo), etc.; see Schemes 1 and 8 (for the red

---

CQC, Department of Chemistry, University of Coimbra, P3004-535 Coimbra, Portugal. E-mail: sseixas@ci.uc.pt



**Scheme 1** Structures of some molecules of colour. For Eosin Y and Fuschine the counter-ions are omitted. For the red anthraquinones, see Scheme 8.

anthraquinone derivatives). Eosin is a dye, which was used by Vincent van Gogh (*e.g.* “Basket of pansies on a table”, 1886, Van Gogh museum).

## 2 The origin of electronic transitions: absorption and transmission of light

In atoms, molecules or extended atomic arrays the available energy levels are properties of the system as a whole. For a better visualization of these it is convenient to consider them as being of a particular type, *e.g.* of translational, rotational, vibrational and electronic nature. These have differences in energy spanning several orders of magnitude. For example, for an electronic transition of 335 nm (UV transition), which corresponds to an energy of 3.7 eV (or  $\Delta E = h\nu = hc/\lambda \approx 6 \times 10^{-19}$  J), we have associated with it vibrational energy levels typically at 1/10th of this energy (0.37 eV,  $\approx 3350$  nm and  $\Delta E \approx 6 \times 10^{-20}$  J) giving rise to transitions in the IR, while at 1/100th of this energy we have the rotational energetic levels (0.0037 eV,  $\Delta E \approx 6 \times 10^{-22}$  J and  $\approx 335$  130 nm). When considering colour and in the case of the molecules described here, we are only interested in materials with electronic energy in which the separation(s) of the energy levels are such that  $hc/\Delta E$  lies in the 400–700 nm visible (wavelength) range; however, the above indicates that a particular electronic transition brings with it a cluster of other transitions of lower energy.

## 3 Electronic transitions in molecules

Electronic transitions in the visible region (giving rise to colour) can be organized in terms of type of molecules and/or transitions. The latter can be discussed as follows: (i) transitions between energy levels localised on

atoms, *e.g.*, d-d transitions in metal salts (weak transitions of a forbidden nature, typically with molar extinction coefficients lower than  $10\text{ M}^{-1}\text{ cm}^{-1}$ ); (ii) transitions between “atomic” energy levels in mixed oxidation state transition metal complexes, *e.g.* metal–metal charge transfer transitions such as those occurring between  $\text{Fe}^{2+}$  and  $\text{Fe}^{3+}$  in the important pigment Prussian blue; (iii) transitions between molecular energy levels in transition metal complexes: metal–ligand (MLCT) and ligand–metal (LMCT) charge transfer transitions. These are the origin of the intense coloured transition in many metal complexes, such as chromates, permanganate, *etc.* In contrast to the first type (i) of transitions, these are not symmetry forbidden, which explains their intensity; (iv) transitions between molecular electronic energy levels in organic compounds. To understand the nature of the colour in organic dyes, such as indigo, one important type of transitions can be specified. In general in dyes, we find two constituent units: the chromophore, and the auxochrome. The chromophore group is responsible for basic colour, whereas the auxochromes allow its “enrichment”.<sup>1</sup> Dilthey and Wizinger<sup>2</sup> improved this concept when the chromophore has an electron accepting group, and the auxochromes an electron donating one, with these groups linked by a conjugated system.<sup>1,3</sup> This gives rise to the concept of the donor/acceptor dye type, which involve extensive charge-transfer. Other types of transitions include those (v) between electronic energy “bands” in semiconductors (semiconductor pigments) and (vi) between electronic energy levels in crystal impurities or dopants. Ruby for example is a perfect crystal with some  $\text{Al}^{3+}$  sites replaced by  $\text{Cr}^{3+}$ ; these are in the origin of the colours of some minerals.

#### 4 Processes occurring upon electronic excitation: photophysics and photochemistry

With organic and many inorganic molecules, following electronic excitation of a molecule to any upper singlet electronic electronic state ( $S_n$ ), deactivation occurs through internal conversion (IC) to higher vibrational levels of the lowest electronic singlet state,  $S_1$ , and from here, after vibrational relaxation (vr) to the lowest vibronic state of  $S_1$ , the molecule further decays to its ground electronic state through several slower deactivation processes, involving both radiative (fluorescence and phosphorescence) and radiationless (internal conversion and intersystem crossing) pathways, see Fig. 1. The investigation of these excited state deactivation processes is one of the key factors in the interpretation of correlations between reactivity, stability and molecular structure.<sup>4,5</sup>

Several parameters are associated with these deactivation process: energies (particularly of the lowest lying singlet and triplet excited states,  $S_1$  and  $T_1$  respectively), lifetimes ( $\tau_i$ ), quantum yields ( $\phi_i$ ) and rate constants ( $k_i$ ). After generation of an excited population of molecules A of concentration  $[A]_0$  in the lowest vibronic state of  $S_1$ , the concentration  $[A](t)$  at the time  $t$  after excitation decreases exponentially with time, according to  $[A](t) = [A]_0 \exp(-t/\tau_0)$ , where  $\tau_0$  is the reciprocal of the sum of the rate constants of all the decay processes available for this (excited) state. When time  $t$  is equal to  $\tau_0$ , the initial concentration  $[A]_0$  has fallen

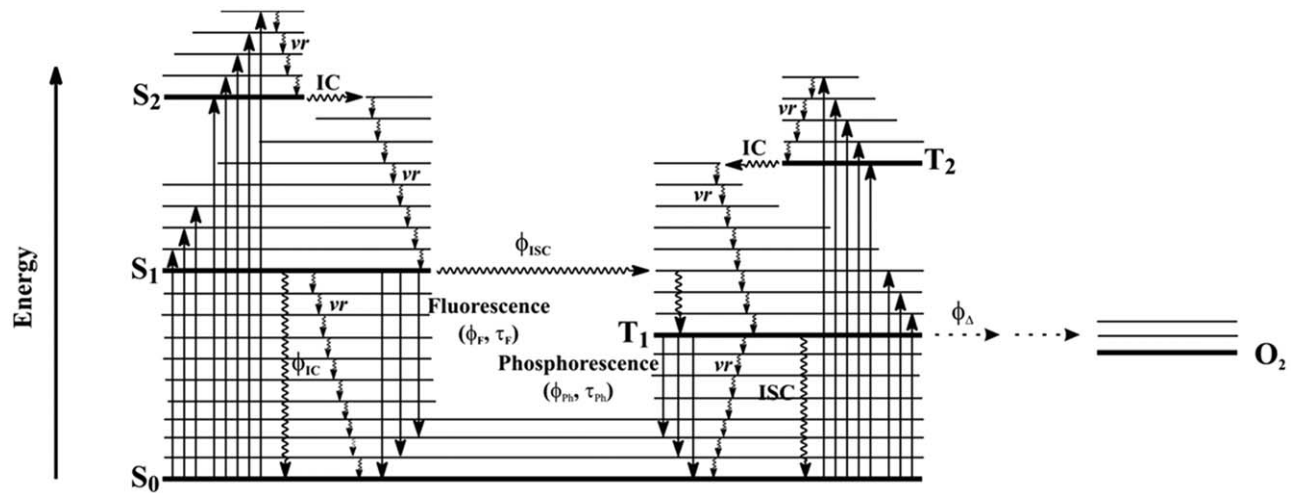


**Fig. 1** Jablonski-type diagram schematizing the overall set of deactivation processes occurring upon excitation. vr – vibrational relaxation; IC – internal conversion; ISC – interystem crossing. Adapted from ref. 4 with permission from The Royal Society of Chemistry.

to  $1/e$  of its initial value. The value of  $\tau_0$  is defined as the lifetime of the excited state (eqn (1)). When the excited state is fluorescent or phosphorescent, the most common method to measure the lifetime consists in recording the luminescence decay. In the latter case this may require low temperatures or/and high viscosity solvents. Since the luminescence intensity  $I(t)$  is proportional to  $[A](t)$ , it follows that  $I(t) = I_0 \exp(-t/\tau_0)$ , with

$$\tau_0 = \frac{1}{k_F + k_{IC} + k_{ISC} + k_q[Q]} \quad (1)$$

where  $k_F$ ,  $k_{IC}$  and  $k_{ISC}$  are the rate constants for fluorescence, internal conversion, and intersystem crossing, while the additional term, ( $k_q[Q]$ ), represents the possibility of deactivation by a quencher (Q). Oxygen, present in all solvents in equilibrium with air, acts as a very efficient quencher. This frequently is due to energy transfer to the ground-state of oxygen (a triplet) to generate singlet molecular oxygen (1270 nm,  $\approx 1$  eV).

This term,  $k_q[Q]$ , is absent when quenchers are removed, and only unimolecular decay of the excited state occurs. It is worth noting that this exponential law does not hold when higher vibronic levels are excited and the decay includes the fs-ps time region, where vibrational redistribution, relaxation and solvent orientation occurs.<sup>5</sup> Moreover, additional factors can influence and add new pathways for dissipation of energy, including the formation of new species (for example excimer formation or acid-base equilibrium).<sup>6</sup>

## 5 The chemistry of colour: the molecular origin

The perception of colour by humans and animals involves, in general, the specific vision mechanism. In essence, light absorption by molecules, with energetic levels and transitions in the visible region, is one of the main mechanisms responsible for colour.

### 5.1 Colour from dyes and pigments

The distinction of a colouring material as a dye or a pigment can be difficult. This bias frequently exists when discussing materials for different applications. For example it is common to find painters classify their materials as pigments, whereas for a textile dyer it is common to have them (sometimes the same material) named as dyes.

Pigments are classified as colouring materials, which are insoluble in the medium in which they are incorporated. The principal applications of pigments are in paints (particularly artist paints), printing inks and colorants for plastics. They have, however, widespread use, and are found for colouring paper, cosmetics, rubber, concrete, cement, ceramics and glass. Pigments are usually applied to a medium by a dispersion process, which aims to reduce the size of their molecular aggregates into a finely divided form, while still being insoluble in the medium.

The term dye is usually applied to materials that are soluble, either in the medium in which they are incorporated or, particularly with textiles,

in a dyeing solution, which is then applied to the medium in which they will be incorporated.

### 5.2 Molecules of colour: organic and inorganic

A further distinction can be made depending upon whether the colouring material is organic (including organic complex of metal atoms, such as those involving alumen and alizarin, carminic acid, laccaic acid, *etc.*, see below Scheme 8 for structures) or inorganic.

### 5.3 Inorganic origin

Inorganic colouring materials are almost all pigments. The most important examples of natural inorganic pigments are the white titanium dioxide, carbon black (black), metal oxides *e.g.* iron (yellow, brown, red, black) and chromium (green) oxides, cadmium/zinc sulphides/selenides (yellow/orange/red), lead chromates (yellows/oranges), cobalt aluminate (blue), ultramarine (blue) and Prussian blue.

The origin of the colour in these materials is diverse.  $\text{TiO}_2$ , titanium dioxide, exists in many polymorphic forms, of which the most common are anatase, rutile, and brookite, well known as minerals in nature; the band gaps of these vary from  $\sim 3.0$  eV for rutile,  $\sim 3.3$  eV for brookite and  $\sim 3.4$  eV for anatase, which means they absorb in the UV. It is used as a white pigment, because it has a high refractive index and, therefore, a high scattering efficiency over all visible wavelengths, excellent opacity, as well as good chemical properties.

Other natural inorganic pigments are the iron oxide based ones, such as yellow ochre and red haematite ( $\alpha\text{-Fe}_2\text{O}_3$ ). The blues comes from cobalt complexes. Lead chromates lead to the yellows such as the pure  $\text{PbCrO}_4$ . This and others are usually coated with silica in order to avoid darkening due to light exposition and atmospheric pollution (leading to formation of  $\text{PbS}$ ).

One example of the use, by ancient civilizations, of reds from the inorganic iron and lead derivatives are the ones found in the masks of the Yurupixunas tribe that lived in Brazil near the Pácos and Japurá (Amazon) rivers.<sup>7</sup> In his Philosophic Journey through Brazil in the late 18th century (1783–1792) through the Captaincies of Grão-Pará, Rio Negro, Mato Grosso and Cuiabá, the Portuguese explorer Alexandre Rodrigues Ferreira (ARF) was able, in his contact with this tribe, to send to Portugal, several ethnographic specimens, in which masks were included. Only in 1981 the masks were identified in the University of Coimbra as belonging to the catalogue sent by ARF to Portugal. In his memories ARF writes that the pigments used in the masks were ochre, urucu and carajuru. Whereas the two later ones are from organic origin, the first appears as a general designation for iron oxides. An analysis taken place in 2014 to one of these masks by X-ray fluorescence, HPLC-DAD, FTIR and Raman, showed that indeed,  $\text{Fe}_2\text{O}_3$ ,  $\text{CaCO}_3$  and  $\text{Pb}_3\text{O}_4$  were present in one of these masks (see Fig. 2)<sup>7</sup> No molecule of colour of organic origin was found in this mask in the 2014 analysis.<sup>7</sup>

Some of the most fascinating blues are the above-mentioned inorganic Ultramarine blue, which was originally obtained from mineral

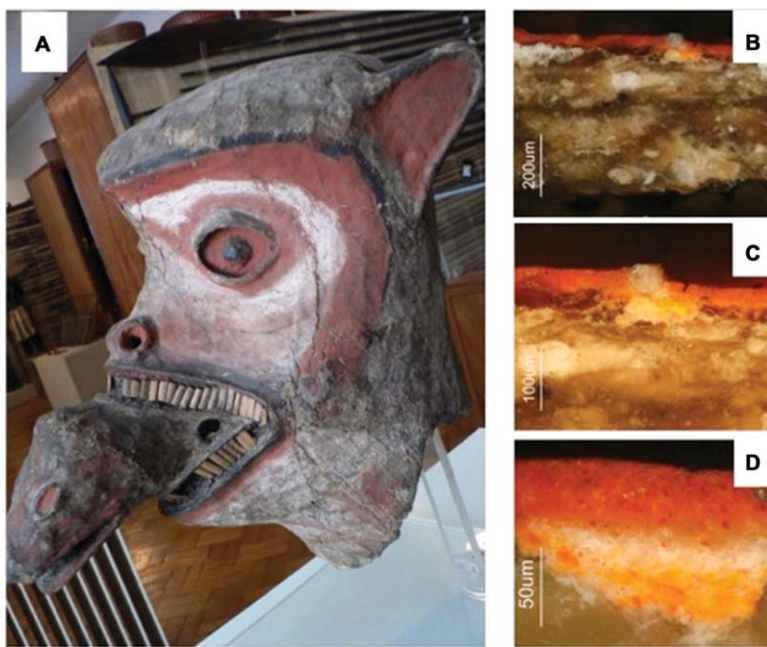


**Fig. 2** One of the masks of the Yurupixunas tribe from the Philosophic Journey of ARF (A), together with the analysis of three layers: (B) top layer: hematite ( $\text{Fe}_2\text{O}_3$ ) and calcium carbonate ( $\text{CaCO}_3$ ); (C) in-between layer: calcium carbonate ( $\text{CaCO}_3$ ); (D) bottom layer: calcium carbonate ( $\text{CaCO}_3$ ) and lead oxide ( $\text{Pb}_3\text{O}_4$ ). Pictures (A)–(C) taken with an optical microscope with magnifications of 10, 20 and 50 $\times$ , respectively, and F4 filter (for polarized light). Reproduced with permission from the author from ref. 7.

lapis lazuli –ultramarine (literally beyond the sea) – that could only be found in Afghanistan and was very costly. In the Italy of Renaissance the cost of a painting was determined not by how much gold leaf was on it, but by how much ultramarine was used for the blues. Nowadays this pigment is made synthetically and is known as the French ultramarine.

#### 5.4 Organic origin

**The Blue Indigo.** Indigo is a molecule charged with mysticism; it is probably the first known source of blue, is associated with the history of many different civilizations, and considered to be a link between Islam and Christianity.<sup>8</sup> Its use dates back to the Roman and Egyptian civilizations, where indigo has been found in, for example, wraps of mummies. Indigo was obtained (extracted after a biosynthetic process) from *Indigofera* plants and the richest in this dye was the *Indigofera tinctoria* (found in India); in Britain the plant extract was known as “woad”. Indigo is also one of the most stable organic dyes, which explains not only its wide use in antiquity and pre-modern times, but also its longevity as a colorant. The stability of indigo is also the reason why it was used in oil paintings by some of the great masters of the 17th and 18th centuries, such as Rubens, and of the 19th, such as

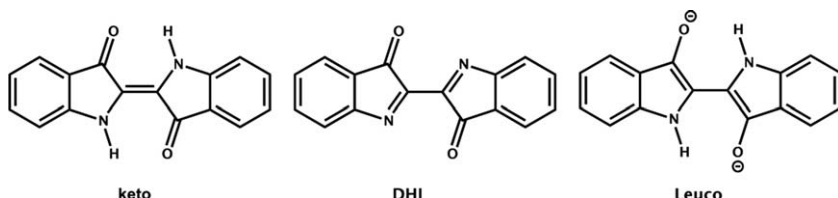
Vincent van Gogh;<sup>9</sup> it is also found in many Medieval illuminations from the 12–13th century.<sup>10,11</sup>

In *De bello Gallico* Julius Caesar describes the warrior skin paintings of his ancient Briton adversaries as being obtained from a blue juice; their faces were frightening and they believed that by this dyeing, the skin paintings, would protect them and turn them into invulnerable warriors!<sup>12</sup> Indigo's dibromo derivative, Tyrian Purple (Scheme 1), extracted by the Phoenician civilization from the gland of the shellfish *Murex Brandaris*, is one of the most important and powerful ancient dyes and is in the genesis of the development of the Mediterranean Tyrian city.<sup>13–16</sup>

The shellfish was found printed in what is believed to be one of the first existing coins. The exhaustive extraction of the dye – it is believed that 10 000 molluscs were needed in order to extract one gram of Tyrian Purple – led to the origin of what is considered as the first historically reported ecological catastrophe.<sup>16,17</sup> In addition to Tyrian Purple, indigo was also found to be present in the *Purpura* snails and, depending on the season and sex of the molluscs, gave a different hue to the blue of the Hebrews: the Tekhelet. Nowadays, indigo is still used to colour the world famous *blue jeans*.<sup>18,19</sup>

**Indigo: (some) relevant characteristics.** Indigo, being a dye known for millennia, obviously has an immense history and rich chemistry. A short systematic overview is needed to detail the chemistry of this molecule. The first, and, perhaps, most intriguing characteristic of indigo is its extraordinary blue colour (an unusually long absorption wavelength); the second is associated with this, the effect that substitution may have on its colour and properties. This is true both for substitution in the aromatic rings and replacing the hydrogen atom of the N-H group. The third is that, in addition to the neutral *keto* form, indigo has two other forms: the *leuco* (reduced) and dehydroindigo (oxidized) ones, Scheme 2. Finally, indigo presents a high (photo)stability which is related to its photophysics, as will be detailed in the next sections.

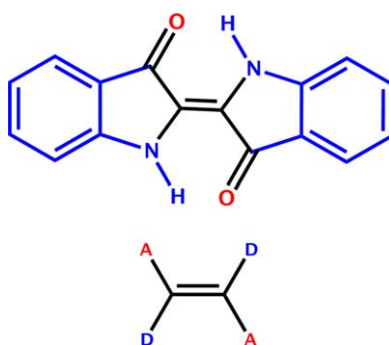
**Indigo: The H-Chromophore.** The explanation of the blue colour in indigo and its derivatives is intriguing and fascinating, and was explored with great detail and ingenuity during the nineteen seventies and eighties.<sup>20–23</sup> Its unusual (extraordinary!) blue colour is strongly associated with its molecular structure. However, and very interestingly for Bayer which pioneered the chemical synthesis of indigo, the *Z*-(*cis*)



**Scheme 2** The three forms of indigo: neutral blue (*keto*), oxidized reddish-brown (dehydroindigo, DHI) and reduced yellow (*leuco*).

configuration was thought to be the most stable and it was only in 1928 that Reis and Schneider,<sup>24</sup> using X-ray crystallography, established the correct structure as to be the *E*-(*trans*) isomer.<sup>3,25</sup>

Considering that we normally associate colour with extensive conjugation, we hope that the reader, like us, has become captivated with the fact that such a small molecule as indigo can have a deep colour in the visible region. Indeed, a unique and intriguing feature is that it absorbs at long wavelengths associated with the small energy difference between its ground and excited states.<sup>3</sup> For such a chromophore only involving one (central) double bond with no resonance extended to the two benzene rings, an additional explanation must be found. With similar structures such as merocyanines, even with a number of 6 (conjugated) double bonds, the absorption maximum is at 510 nm, 90–100 nm shorter wavelength than indigo. Indigo can be considered a donor–acceptor dye with the heterocyclic nitrogen atoms providing the electron donor groups and the carbonyl groups (C=O) the acceptors.<sup>3</sup> The origin of this peculiar behaviour was investigated in the 1970's with the synthesis of several derivatives.<sup>22</sup> It has been found that, the fundamental chromophore of indigo dyes includes the central double bond connecting the two rings, together with the nitrogen and carbonyl groups.<sup>22</sup> These and other studies showed that neither the benzene rings nor the double bonds in the five-member rings are essential for the characteristic indigo spectrum.<sup>3,25,26</sup> The basic chromophore of indigo consists of a central C=C bond with two donor (defined as N–H, or D in Scheme 3) and two acceptor groups (A, or O in Scheme 3). Further studies from the 1960s to 1980s confirmed this conclusion that the basic chromophore of the indigo dyes is the central C=C bond together with the adjacent C=O and N–H groups, which due to the particular design of indigo, where these groups are in a *trans* and H-like geometry lead to its designation as an H-chromophore.<sup>22,26–29</sup> More recently TD-DFT calculations have been used to support the H-chromophore theory.<sup>25,29,30</sup> The HOMO is essentially located in the central C=C bond and the nitrogen atoms and the LUMO in the central C=C bonds and oxygen atoms.<sup>28–30</sup> In a simplified approximation, the absorption of visible light may be explained by a narrow HOMO–LUMO separation, which is typical for systems like the H-chromophore. The donor groups raise the  $\pi$  orbital of the C=C double



**Scheme 3** The H-chromophore in indigo, with the donor (D) and acceptor (A) groups.

bond (HOMO), while the acceptor groups lower the  $\pi^*$  orbital (LUMO). Moreover the HOMO is delocalized over the N-C=C-N part of the molecule whereas the LUMO is delocalized over the fragment O=C-C=C=O.<sup>28</sup> Substitution in different ring positions of indigo promotes significant shifts in both the long-wavelength visible and UV bands.<sup>31,32</sup>

**Indigo: the effect of substitution on the colour.** The lowest absorption band (HOMO-LUMO energy gap) in indigo strongly depends on the solvent media, ranging from red (540 nm) in the gas phase, to violet (588 nm) in a nonpolar solvent such as CCl<sub>4</sub>, and to blue in polar solvents such as ethanol (606 nm) or in the solid state.<sup>26,27,32</sup> Moreover, substituents may affect the energy level of the excited state either by increasing or diminishing electron release from the nitrogen atom or electron withdrawal by the carbonyl group.<sup>32</sup> Substitutions at the 5,5'-positions lead to bathochromic shifts, while substitutions at 6,6' to hypsochromic shifts (Fig. 3).<sup>25,32,33</sup> Indeed, indigo derivatives with di-, tetra-, and hexa-substitution lead to absorption maxima in the wavelength range from 600 to 732 nm.<sup>33</sup>

**Indigo: Photophysics.** In 1994, George Wyman in a seminal work mentioned that indigo dyes showed no detectable emission, in contrast with the strongly fluorescent thioindigos.<sup>35</sup> However, as was shown later, indigo is weakly emissive with a fluorescence quantum yield of  $\phi_F = 0.0023$ , lifetime  $\tau_F \approx 0.14$  ns (ranging from ~117 ps in DMSO to

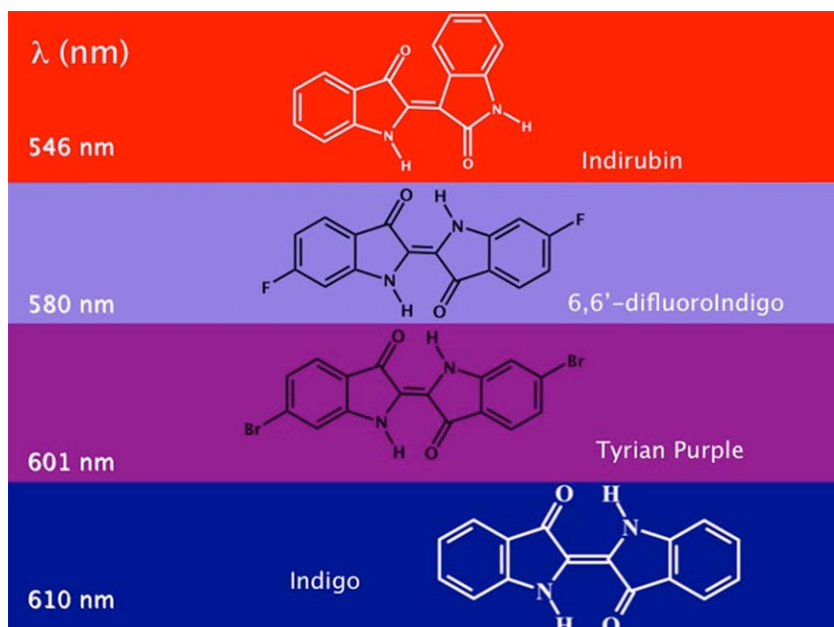


**Fig. 3** The Change in colour of indigo derivatives by replacement in the 6,6' positions and to the structural isomer (indirubin). Data is in DMF from ref. 33 and 34. The wavelength maxima shifts ~64 nm from indirubin to indigo. The color changes from red (indirubin in the top) to blue (indigo in the bottom) with the light purple (difluoroindigo) and deep (Tyrian) Purple in the middle.

**Table 1** Photophysical parameters for (*keto*) indigo, Tyrian Purple, indigocarmine and indirubin, including fluorescence, singlet oxygen sensitization and internal conversion quantum yields, together with fluorescence and radiationless rate constants<sup>33,34</sup>

Compound	$\phi_F$	$\tau_F$ (ns)	$k_F$ (ns <sup>-1</sup> )	$k_{NR}$ (ns <sup>-1</sup> )	$\phi_\Delta^a$	$\phi_{IC}^b$
Indigo	0.0023	0.14	0.0164	7.12	0.00117	0.9965
Tyrian Purple	0.0071	0.323	0.022	3.07	0.000552	0.9923
Indigocarmine	0.0015	0.110	0.0136	9.08	0.0008	0.9977
Indirubin	0.00027	0.030	0.009	33.3	0.00054	0.9992

<sup>a</sup>The data in Table 1 imply, as demonstrated for indigo, that the  $\phi_\Delta$  value is basically identical to the  $\phi_T$  (or  $\phi_{ISC}$ ) value.<sup>33,37</sup>

<sup>b</sup> $\phi_{IC} = 1 - \phi_F - \phi_T$  where  $\phi_T \sim \phi_\Delta$ .

135 ps in DMF)<sup>36</sup> and an energy of its first singlet excited state of 15 728 cm<sup>-1</sup>.<sup>33,34</sup>

The photophysical properties of indigo (*keto* form, Scheme 2) are summarized in Table 1 together with those of three other derivatives: Tyrian Purple, indirubin and indigocarmine.<sup>34</sup> The internal conversion from the first singlet excited state to the ground-state has been shown to be much faster than all the other S<sub>1</sub> deactivation processes (fluorescence, intersystem crossing and photochemistry).

With indigo, more than 99.99% of the *quanta* are lost through non-radiative channels. Its poor emission and absence of triplet signal (under conventional laser flash photolysis conditions) constituted a challenge to obtain the yields and rate constants for the radiationless deactivation (internal conversion,  $\phi_{IC}$  and singlet to triplet intersystem crossing,  $\phi_{ISC}$ ).

An initial attempt to obtain the triplet energy and yield was made by measuring the singlet oxygen sensitization by energy transfer from indigo. Sensitization of singlet oxygen necessary implies that the triplet energy of indigo is above 0.94 eV (1319 nm).<sup>33</sup> The  $\phi_\Delta$  (~0.0012) obtained were indicative of lower limits for the  $\phi_T$  value.<sup>33</sup>

The complete knowledge of the energy of the triplet state of indigo, intersystem crossing S<sub>1</sub> ↔ T<sub>1</sub> yield and  $\Delta E(S_1-T_1)$  energy splitting only came by obtaining the triplet energy with pulse radiolysis energy transfer experiments ( $E_T = 1.0 \pm 0.1$  eV) followed by the determination of the  $\phi_{ISC}$  value from photoacoustic calorimetry. This used the equation  $\phi_{ISC}E_T = (1 - \phi_1)E_{hv} - \phi_F E_{hv\ max}$  where the energy deposited in the triplet state ( $\phi_{ISC}E_T$ ) is equal to the energy of the laser pulse  $E_{hv}$  used minus the energies released as heat in the formation of the triplet state  $\phi_1 E_{hv}$  and the energy lost through fluorescence  $\phi_F E_{hv\ max}$ . Application of the above leads to a value of  $\phi_{ISC} = 0.0066$ .<sup>37</sup> Fig. 4 summarizes these findings. In the top of the figure the emission of singlet oxygen phosphorescence sensitized by indigo and several of other of its derivatives leading to an estimate of both the  $\phi_{ISC}$ , assumed to be approximately identical to  $\phi_\Delta$ , and the energy ( $E_T$ ) of the triplet state (above 0.94 eV). In the bottom part of the figure, schematic diagrams are given for the energy transfer (by pulse radiolysis) and the PAC experiments (with a typical photoacoustic wave together with the plot for obtaining the  $\phi_1$  value). The  $\Delta E(S_1 - T_1)$  was found experimentally to be  $0.91 \pm 0.1$  eV,<sup>37</sup> in excellent agreement with time-dependent density functional theory, TDDFT, calculations at 0.95 eV.<sup>38</sup>

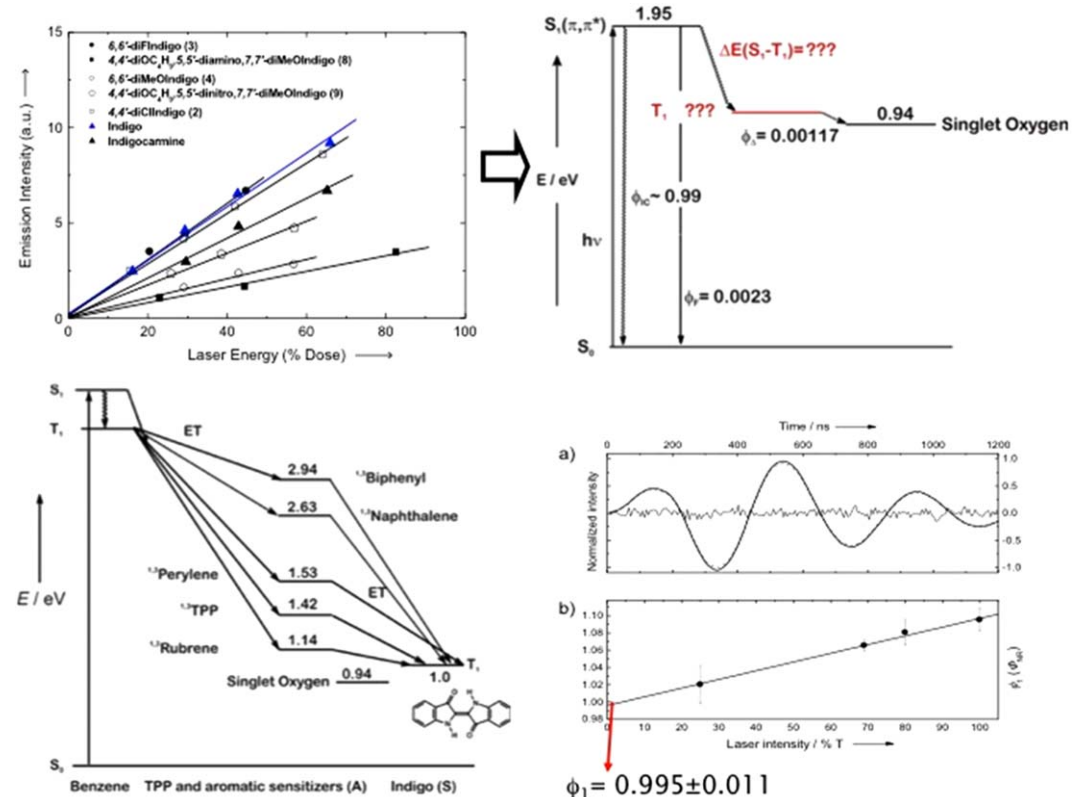


**Fig. 4** Figure schematizing the determination of the triplet energy ( $E_T$ ) and intersystem crossing yield ( $\phi_{ISc}$ ) in indigo. The top figures show (left) the determination of the singlet oxygen yield (a lower estimation of the  $\phi_{ISc}$  value) and (right) the remaining question in an energy diagram: what is the exact value of  $\phi_{ISc}$  and  $E_T$ ? The bottom panels represent (left) the determination (from pulse radiolysis experiments with the solvent benzene and several aromatic sensitizers) of the triplet energy and (right panel) with this value and from PAC experiments the energy deposited in the triplet state ( $\phi_{ISc}E_T$ ), the value of  $\phi_{ISc}$ . Reproduced from ref. 33, J. S. Seixas de Melo, R. Rondão, H. D. Burrows, M. J. Melo, S. Navaratnam, R. Edge and G. Voss, *ChemPhysChem*, John Wiley and Sons, Copyright © 2006 WILEY-VCH Verlag GmbH & Co. KGaA, Weinheim; and ref. 37, J. S. Seixas de Melo, C. Serpa, H. D. Burrows and L. G. Arnaut, *Angew. Chem., Int. Ed.*, John Wiley and Sons, Copyright © 2007 WILEY-VCH Verlag GmbH & Co. KGaA, Weinheim.

However, the question remaining is what is the mechanism behind the very efficient internal conversion deactivation channel? Two possible explanations have been proposed: (i) a proton transfer in the excited state (ESPT) or (ii) it is a consequence of the golden rule for radiationless transitions: when the energy difference between the ground and first singlet ( $\Delta E (S_1 - S_0)$ ) is very small, which is the case of indigo, it favours an efficient coupling between the  $S_0$  and  $S_1$  vibronic modes.<sup>33,36,39-42</sup>

**Indigo's high stability: (single) excited proton transfer involving the N–H and C=O groups.** In contrast to the behaviour of heteroatom derivatives,<sup>43,44</sup> such as thioindigo,<sup>45,46</sup> the remarkable stability of indigo and its ring-substituted derivatives has been attributed to intramolecular hydrogen-bonding between the two adjacent carbonyl and N–H groups which keeps the molecule in a trans planar configuration, preventing the photochemical *cis-trans* isomerization.<sup>39,47</sup>

Data in Table 1 may suggest that indigo and its derivatives decay by a single exponential. However, the fluorescence decay of indigo is more complicated. Indeed, Fig. 5 shows the fluorescence decays of indigo obtained with fits of one and two exponentials. Moreover, the decays obtained at two different emission wavelengths display identical decay components but different pre-exponential factors. This is related with the existence of two excited species which will be detailed in the next section at the light of the (photo)stability of indigo.

The explanation for the high stability of indigo, although linked with the very efficient internal conversion deactivation channel, is associated with a proton transfer in the excited state (ESPT).<sup>33,40-42</sup> This was demonstrated both from experiment<sup>33,41,42,47-52</sup> and theory,<sup>53,54</sup> although until recently there was still a dispute as to whether the excited proton transfer involves the concerted proton transfer between the two N–H and two C=O groups or from a single group,<sup>54</sup> and if this proton transfer is intra- or solvent assisted intermolecular.<sup>51</sup> According to some earlier works, methylation of the N–H group (to N-CH<sub>3</sub>) is reported to induce an additional deactivation pathway: photoisomerization.<sup>55</sup> The idea that the photostability of (*trans*) indigo was due to a ESPT in the singlet excited state rather than stability imparted to it by hydrogen bonds in the ground state has been for a long time a topic of debate and controversy.<sup>35,43,47-51,56</sup> Although there have been different views regarding the photostability of indigo, it now seems consensual that it is associated with its fast proton transfer in the excited state.<sup>33,40,51,54,56</sup> Indeed, in the recent literature the debate has now turned over as to whether a single or double ESIPT reaction could be involved in the very efficient internal conversion path. Some theoretical<sup>53,54</sup> and experimental studies using femtosecond time resolution<sup>48</sup> on indigo carmine, go in favor of a single ESIPT process, taking place in the subpicosecond-femtosecond time range, whereas with others the ESIPT occurs in the subpicosecond time range.<sup>33,41,42</sup> This ESPT can be schematically presented in Fig. 6, where the SPT and DBT are equated together with the possibility of reversibility (in the excited state) from the enol form to the keto form.

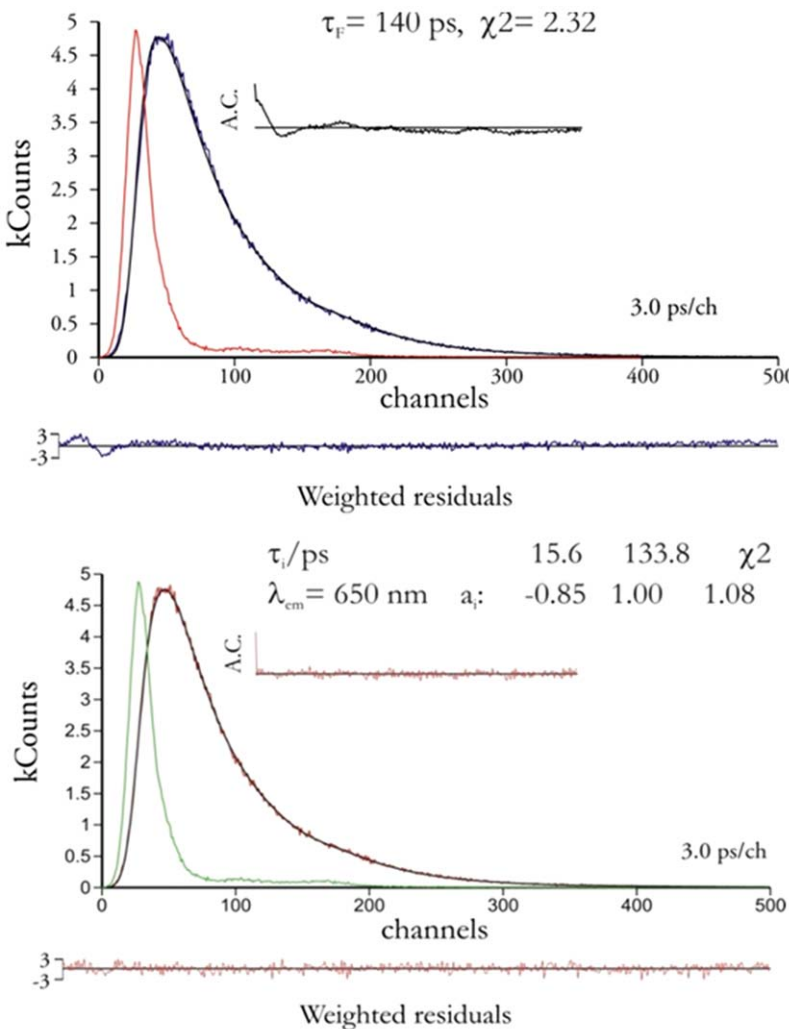


**Fig. 5** Fluorescence decay of indigo fit with a single exponential decay law (top) and with a double exponential decay law (bottom). The fluorescence decay times ( $\tau_i$ ) and the associated pre-exponential factors ( $a_i$ ) are presented in the inset. In the decays the pulse Instrument Response Function (IRF) are the gray lines. For a better judgment of the quality of the fits, the Weighted residuals, autocorrelation functions (A.C.), and chi-squared ( $\chi^2$ ) values are also shown.

Indeed, with indigo the absorption is due to its *keto* (neutral) form, whereas the emission (band) would result from the convoluted emission of this – instantaneously *keto* formed – species with that resulting from excited state proton transfer (from the N-H to the C=O group which could be intra- or solvent-assisted intermolecular) leading to the enol form;<sup>5,33,40–42</sup> the biexponential nature of the decays in indigo (and indigocarmine) further confirms the existence of these two excited state species.<sup>33,40–42</sup> For indigocarmine in DMF the instantaneously formed *keto* form of this indigo derivative transfers its proton to the solvent with an intermolecular rate constant of  $\sim 1.4 \times 10^{11} \text{ s}^{-1}$ , whereas for methanol

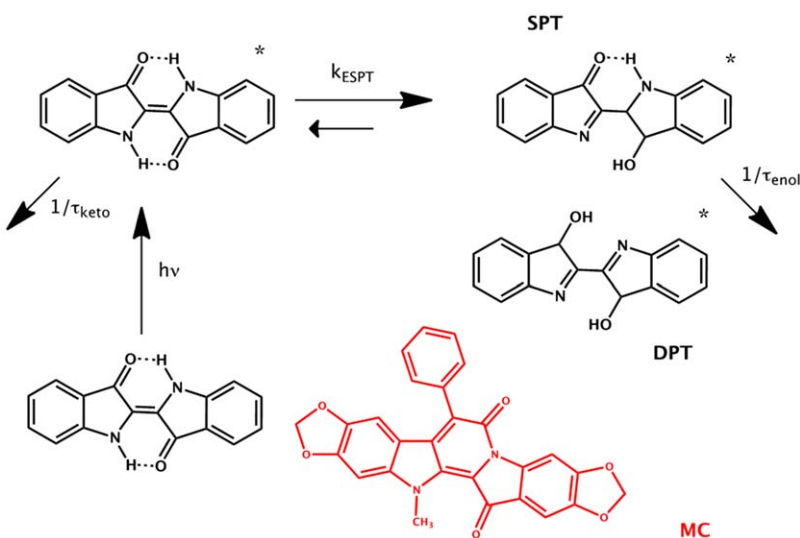


**Fig. 6** Schematic Presentation of the Kinetic Scheme for the ESPT with Indigo. In the scheme the two possibilities (involving a single proton transfer, SPT, or double proton transfer, DPT) are considered. The model compound used (MC, with an excited-state lifetime of 152 ps), where proton transfer is precluded, is also presented.<sup>36,40</sup>

this seems to change to an intramolecular proton transfer with a rate constant of  $\sim 1.2 \times 10^{11} \text{ s}^{-1}$ .<sup>41</sup> The difference between these two values is, however, inconclusive regarding the dominance of the intra- *vs.* intermolecular process.

In a recent work, combining experimental studies, including emission and absorption data as a function of solvent viscosity, polarity, and temperature, with theoretical data (TDDFT) for both indigo and its monohexyl-substituted derivative in solution showed that the proton transfer mechanism in the two compound is similar pointing out to a single proton transfer.<sup>36</sup> For indigo this ESPT rate constant has a value of  $\sim 8.4\text{--}9.2 \times 10^{10} \text{ s}^{-1}$ , while for its monohexyl-substituted derivative the value is  $\sim 7 \times 10^{10} \text{ s}^{-1}$ .<sup>36,40</sup>

**Indigo: the *leuco* form.** Indigo derivatives are known as vat dyes and are insoluble in water in their coloured form, the *keto* species.<sup>16,17,57</sup> A common characteristic of these vat dyes is the presence of one or more carbonyl groups which, when treated with a reducing agent in the presence of an alkali, form a water soluble species, known as the *leuco* form, which is the intermediate used in the dyeing process.<sup>18,58</sup> In the laboratory *leuco* indigo is obtained in a strong reducing media (aqueous  $\text{Na}_2\text{S}_2\text{O}_3/\text{NaOH}$  solution) in the absence of oxygen (see Fig. 7). It shows completely different spectral and photophysical behaviour when compared with the *keto* (neutral and blue) species.

For indigo in dioxane, the wavelength maximum changes from 610 nm (*keto* form) to 442 nm (*leuco* form). This extends to all other indigo derivatives and to the photophysical properties. Data is summarized in Table 2.

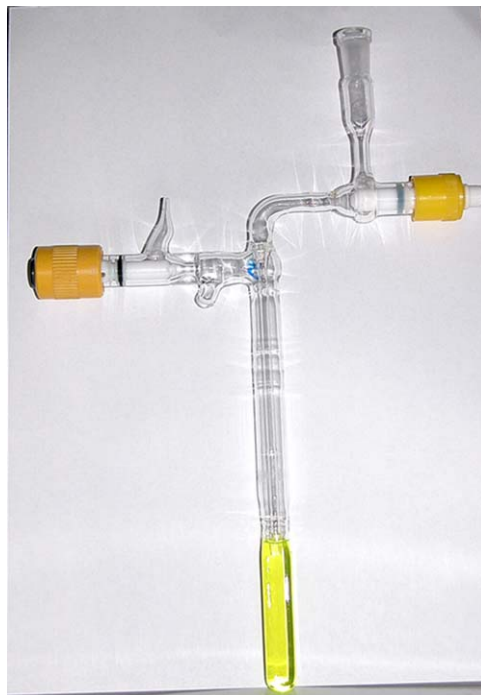


**Fig. 7** Picture of the *leuco* obtained from a solution of (neutral) keto indigo in a DMF–Na<sub>2</sub>S<sub>2</sub>O<sub>3</sub>/NaOH solution bubbled with argon (or N<sub>2</sub>) in a special designed cuvette to keep the solution in inert atmosphere for spectral and photophysical determinations.<sup>59</sup> The yellowish solution colour contrasts with the blue (keto) indigo which is obtained by simply open the cuvette taps and allowing air (oxygen) to be dissolved into the solvent.

**Table 2** Photophysical properties, including quantum yields of S<sub>1</sub>↔T<sub>1</sub> intersystem crossing ( $\phi_T$ ), fluorescence ( $\phi_F$ ) and internal conversion ( $\phi_{IC}$ ) together with the radiative ( $k_r$ ), intersystem crossing ( $k_{ISC}$ ) and internal conversion ( $k_{IC}$ ) rate constants for the *leuco* form of indigo, indigocarmine, indirubine and Tyrian Purple in DMF<sup>34</sup>

Compound	$\phi_T$	$\phi_F$	$\phi_{IC}$	$\tau_F$ (ns)	$k_r$ (ns <sup>-1</sup> )	$k_{IC}$ (ns <sup>-1</sup> )	$k_{ISC}$ (ns <sup>-1</sup> )
Indigo	0.125	0.348	0.527	3.15	0.111	0.167	0.040
Purple	0.190	0.225	0.585	3.77	0.060	0.155	0.050
Indigocarmine	0.250	0.292	0.458	3.50	0.083	0.131	0.070
Indirubin	0.171	0.0145	0.815	1.78	0.008	0.458	0.096

With the fully reduced *leuco*-indigo (and derivatives), the fluorescence, internal conversion and singlet-to-triplet intersystem crossing deactivation channels coexist (Table 2).<sup>34,58</sup>

One additional feature of *leuco* indigo is that it can undergo photoisomerization.<sup>60</sup> For *leuco* indigo (and its derivative 4,4'-dibutoxy-7,7'-dimethoxy-5,5'-dinitroindigo (DBMNI)) photoisomerisation of *trans* to *cis* forms of *leuco*-indigo was observed in the first excited singlet state. A study was made involving the fluorescence quantum yield ( $\phi_F$ ) dependence with the UV irradiation time, which was found to increase up to a value of  $\phi_F \approx 0.2$ –0.3 (plateauing after 16 min) for indigo (see Fig. 8) and  $\phi_F = 0.2$  (plateauing after  $\sim 150$  min) for DBMNI. This was further

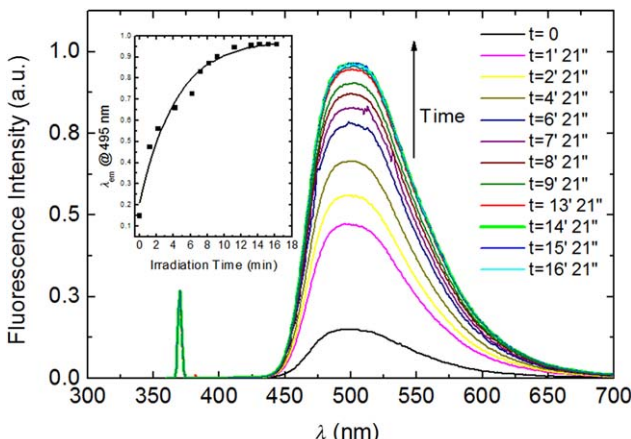
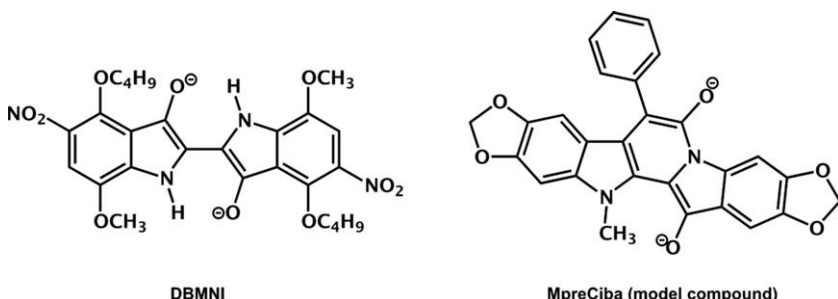


**Fig. 8** Fluorescence spectra of indigo's *leuco* species in dioxane obtained with different irradiation times at  $T = 293\text{ K}$ . Also shown as inset is the plot of intensity at 495 nm vs. the irradiation time. The *leuco* species was generated from a *keto* indigo solution as described in the experimental.<sup>60</sup> Reprinted with permission from R. Rondão, J. Seixas de Melo, M. J. Melo and A. J. Parola, *J. Phys. Chem. A*, 2012, **116**, 2826–2832. Copyright (2012) American Chemical Society.



**Scheme 4** Structures of the *leuco* forms of DBMNI and MpreCiba (model compound, where rotation around the central C–C bond is precluded), two derivatives used in the study of photoisomerization of indigo.

studied with a model compound, where rotation around the central C–C bond is obstructed, and the  $\phi_F$  value was found to be constant with the UV irradiation time. The structures of the *leuco* forms of DBMNI and of the model compound (MpreCiba) are presented in Scheme 4.

Quantum yields for the isomerisation photoreaction ( $\phi_R$ ) were also obtained for indigo and DBMNI with values of 0.9 and 0.007 respectively.<sup>60</sup>

Additional time-resolved fluorescence data obtained before and after 300 minutes of irradiation have revealed that initially the decays can be fitted with a bi-exponential law (with 0.12 ns and 2.17 ns), but afterwards have an almost mono-exponential decay (~2.17 ns). This was interpreted as the double exponential decays showing the initial presence of the *cis* and *trans* *leuco* forms which gradually lead into a single decay time (*cis* *leuco* form). This was also consistent with the steady-state data (Fig. 8). Fig. 9 shows the fluorescence decays obtained for DBMNI with no irradiation and after 300 minutes of irradiation, indicating completely different profiles.

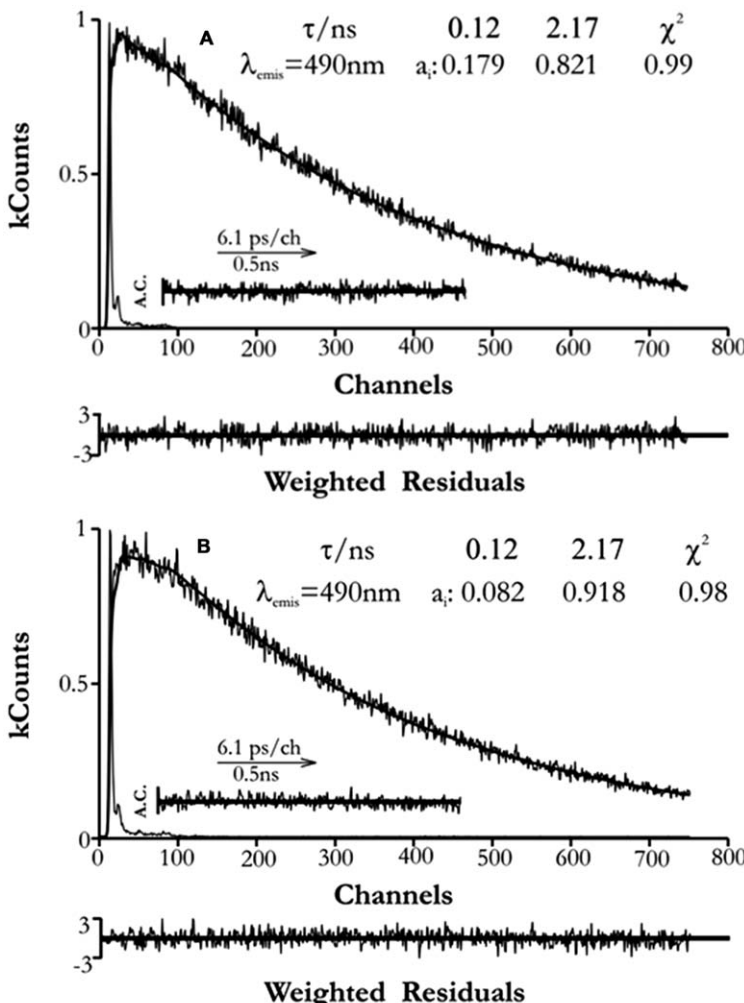
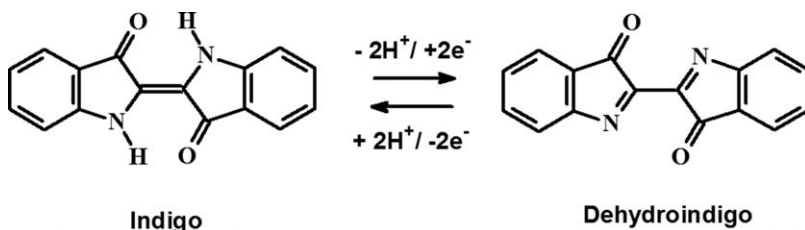


**Fig. 9** Fluorescence decays and pulse instrumental response for the *leuco* form of DBMNI in dioxane, at  $T = 293 \text{ K}$ , obtained immediately after the preparation of the solution (A) and (B) after 300 min of irradiation. Shown as insets are the decay times and pre-exponential factors. Also shown are the weighted residuals, autocorrelation functions (A.C.) and the  $\chi^2$  values for a better judgment of the quality of the fits. The excitation wavelength was  $\lambda_{\text{exc}} = 372 \text{ nm}$ .<sup>60</sup> The IRF is shown as a pulse in the first channels. Reprinted with permission from R. Rondão, J. Seixas de Melo, M. J. Melo and A. J. Parola, *J. Phys. Chem. A*, 2012, **116**, 2826–2832. Copyright (2012) American Chemical Society.

**Indigo: the oxidized form (Dehydroindigo, DHI).** Dehydroindigo (DHI) is the oxidized form of indigo and the one that has remained the most poorly studied. This is partly because it is very unstable and prone to capture protons (Scheme 5), and its isolation and consequent study has led it to be considered the forgotten species of indigo.<sup>61</sup> DHI readily converts into its neutral *keto* form, the blue indigo, in a process, which depends on the solvent and water content of the medium. Nevertheless, the resurgence of the importance of this species is strongly



**Scheme 5** Conversion of indigo into DHI and back reaction.

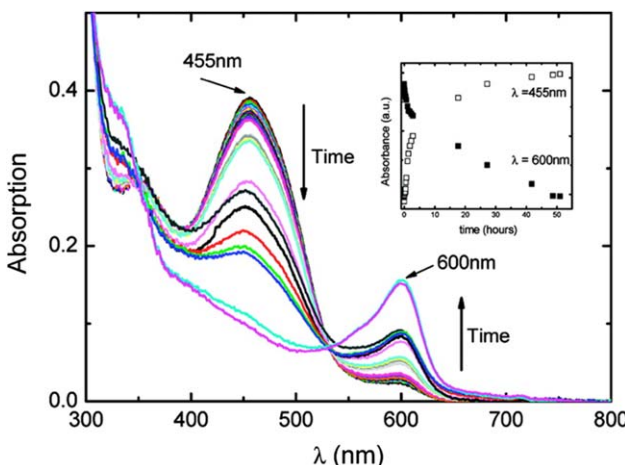


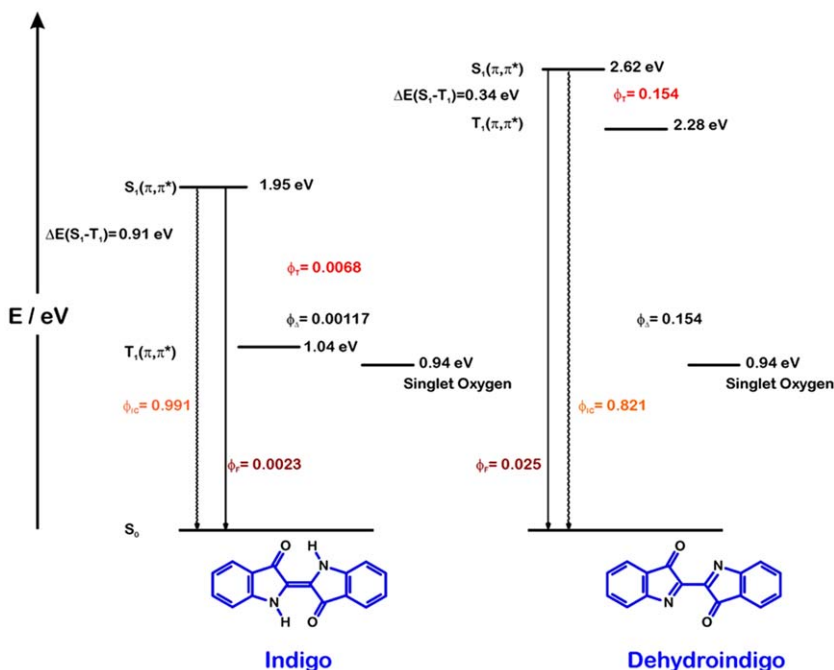
**Fig. 10** Dehydroindigo absorption spectra variation with time, in non dried toluene at  $T=293\text{ K}$ . Show as inset plot is the dependence with time of the absorption maxima of DHI and indigo.<sup>61</sup> Reprinted with permission from R. Rondão, J. S. Seixas de Melo, V. D. B. Bonifácio and M. J. Melo, *J. Phys. Chem. A*, 2010, **114**, 1699. Copyright (2010) American Chemical Society.

associated to the revival of interest in the Maya Blue pigment where it is believed to be involved.<sup>61,62</sup>

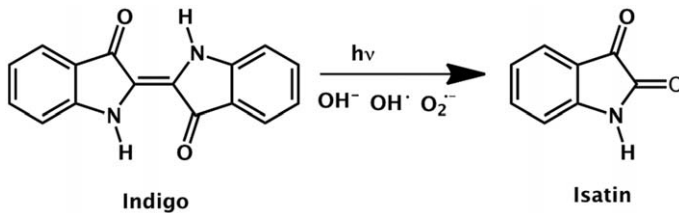
Although DHI readily converts into *keto* indigo with time, see Fig. 10, it was found that it shows particular and different properties when compared with the *keto* and *leuco* forms of indigo. In contrast with what has been found for the two other species of indigo (*keto* and *leuco*), in the case of DHI, the dominant excited state deactivation channel involves the triplet state. Indeed,  $\phi_T$  values of 0.7–0.8, with negligible fluorescence ( $\phi_F \leq 0.0003$ ) are observed in toluene and benzene.<sup>61</sup> In methanol the  $\phi_T$  value decreases to 0.15 with an increase of the  $\phi_F$  to 0.025, which makes these processes competitive with the  $S_1 \rightsquigarrow S_0$  internal conversion deactivation process.<sup>61</sup>

The comparison between the energies, excited state origin and quantum yields of fluorescence, intersystem crossing and internal conversion for indigo and DHI is summarized in Scheme 6.

**Indigo: (Photo)degradation.** Although indigo (and its derivatives) have a high (photo)stability imparted by the deactivation process



**Scheme 6** Diagrams depicting for indigo (left) and DHI in methanol (right) the different values for the quantum yields of excited state deactivation and energies (in eV) of the lowest lying singlet and triplet excited states.<sup>61</sup> Reprinted with permission from R. Rondão, J. S. Seixas de Melo, V. D. B. Bonifácio and M. J. Melo, *J. Phys. Chem. A*, 2010, **114**, 1699. Copyright (2010) American Chemical Society.



**Scheme 7**

associated to an ESPT, indigo fades. The main degradation product is consensual to be isatin (Scheme 7).<sup>10,63,64</sup> However, the presence of indirubin has also been reported.<sup>10,63</sup> Indeed, an analysis of ancient Andean textiles (dated from 200 BC to 200 AD.), from Paracas (South Peru), showed that besides indigo, indirubin is also present, in the range of 2% to 45%.<sup>63</sup> Since indirubin can be formed during the dyeing with indigo, namely when more oxygen is available, although not studied the photodegradation mechanism of indigo, it was there concluded that indirubin suffers a similar photodegradation process to that found for indigo, with isatin as the major resulting photodegradation compound.<sup>63</sup>

For indigo and indigo carmine, it was found that the mechanism associated to its photodegradation leading to isatin is likely to not be

mediated by singlet molecular oxygen.<sup>63</sup> Indeed, it was suggested that OH<sup>-</sup> like radicals (or other oxygen based reactive species such as O<sub>2</sub><sup>•-</sup> and OH<sup>•</sup> radicals) are involved in the degradation mechanism, which is linked to the attack to the central double bond in indigo. In a dry and protected from light environment, indigo was found to be very stable.<sup>63</sup> The photodegradation quantum yields ( $\phi_R$ ) were found to be in the order of 10<sup>-4</sup>, with the exception of aqueous media ( $\phi_R = 9 \times 10^{-6}$ ), and dependent on the irradiation wavelength thus showing the high stability of indigo.<sup>63</sup> The fact that as recently showed the stability associated to the ESPT in indigo involves a partial departure of the double character of the central double bond (to a single bond character) in order to promote the proton transfer, once more indicates that the process of degradation must be associated to a direct attack to the central double bond. Indeed, the central double bond may be considered the key for the stability of indigo since it assists a very fast non-radiative deactivation process, from the excited to the fundamental state, locking the molecule and protecting it from photodegradation. As has been shown from joint experimental and TDDFT calculations, in the deactivation of indigo an additional radiationless process, competing with ESPT, is involved.<sup>36</sup> This mechanism is attributed to rotation (in the excited state) about the central carbon–carbon bond, which brings the system close to a conical intersection (CI), of the sloped type, where the seam is reached through an OH stretching vibration.<sup>36</sup> In the forthcoming section we will discuss another mechanism found to stabilize indigo, the incorporation of this organic molecule into an inorganic host: Maya Blue.

## 6 On the track of Maya Blue

The stability towards hydrolysis, which can occur in acidic or alkaline media, is of great importance for all dyes, but this is particularly true for artist's materials. An example of protection against this potential hazard is found with the pigment dye Maya Blue.

In the sixteenth-century in Central America, the Spanish conquerors noted the local importance of fine textiles as gifts at festivals and weddings, and to signify status. Here, as in ancient Egypt, blue was a particularly admired colour.<sup>65</sup> The Aztecs also used indigo as medicine, and it is likely that its colour is responsible for the common name in the region for the 'blue herb', *iquilite*. The Mayans mixed indigo with a colourless mineral clay (attapulgite) to produce the "Maya Blue" pigment (MB), widely used for painting on murals and sculptures. This is probably the first report of man-made organic-inorganic hybrid (OIH). However, until 1966 the idea of this hybrid as responsible for the colour of Maya Blue was not at all consensual.<sup>66–68</sup> The Maya blue pigment was rediscovered in 1931 by Merwin<sup>69</sup> when analysing the pigments of a mural paint in the Chichén-Itzá archaeological site, in Mexico, and believed to be an inorganic pigment, with "an extraordinarily vivid shade similar to Prussian Blue", because of its high stability towards acids. The ancient blue color of the Maya Civilization, MB, has revealed extraordinary

properties towards stability and colour tunability which has led to the recent rediscovery of this dye as a strategy for a pigment of the future.<sup>70</sup>

At the molecular level, MB consists of a clay (palygorskite or attapulgite) to which indigo is attached (inside or at the surface is still a matter under debate) providing an extraordinary stability to severe environment conditions (humidity, acid attack, temperature, *etc.*).<sup>61,71-74</sup> One of the most elucidative ways of viewing Maya Blue is to consider it to consider it as a chessboard where the water (structural waters) may be replaced by indigo under heat, such as white replace the black pieces in a chess game.<sup>74</sup>

It is very interesting to note that DHI accompanies indigo in Maya Blue including in archeological specimens.<sup>61,75,76</sup> Host-guest systems have been investigated mimicking the process of dye stabilization established with MB.<sup>46,61,70,72,77</sup> Indeed, this includes the substitution of indigo with the synthetic derivatives thioindigo (TI) and Ciba Brilliant Pink (CBP) Christianized as "Maya Pink".<sup>46</sup> This shows a strategy of stabilization of synthetic dyes following what may mirror the recipe used by the ancient Maya civilization. It also tunes the color of the red (powder) TI into blue in attapulgite and purple in sepiolite, see Fig. 11.

Very interesting is to note that photophysical techniques may help to study the interaction between organic guest and inorganic host at a molecular level. Indeed, incorporation of TI and CBP in palygorskite and sepiolite clays has showed different photophysical properties with decrease of the fluorescence quantum yield; moreover, a single exponential decay for TI, which showed this to be incorporated into the clay channels, whereas and a multiexponential decay for CBP in palygorskite was found showing different locations and (*cis* and *trans*) conformers.<sup>46</sup> TI although being a synthetic parent of the blue indigo has red color and makes the liaison with the Reds in the next section.



**Fig. 11** Picture of powder TI (bottom) and mixed with attapulgite (top left) and with sepiolite (top right).

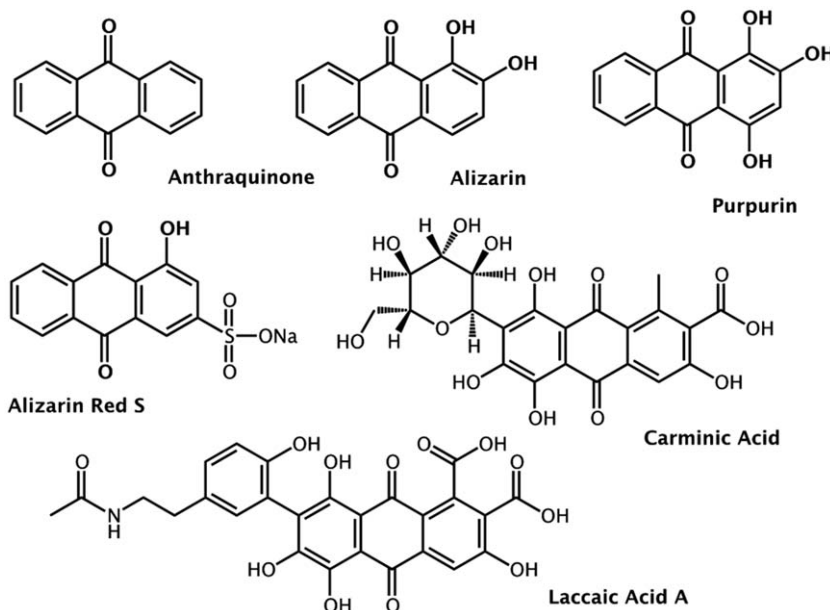
## 7 Reds

The molecules of colour red include a number of different structures. From these we place particular emphasis on Brazilin and Brazilein (both from Brazilwood),<sup>64,78,79</sup> madder components (the anthraquinone derivatives such as alizarin and its lakes),<sup>11,64</sup> and dracorhodin and dracoxylylum (from Dracaena Draco).<sup>80,81</sup>

Madder is the common name of the plant genus *Rubia* and family *Rubiaceae*, used since pre-historic times;<sup>82</sup> written accounts exist on its use as a dye in ancient Egypt.<sup>83,84</sup> Identification of madder dye in archaeological textiles<sup>85–87</sup> from a thousand years ago revealed the presence of purpurin and alizarin, which are among the organic dyes most resistant to light-induced fading,<sup>88</sup> and are the main chromophores in certain madder species. The red extracts were also prepared for use as pigments in painting, by precipitating the extract in solution with aluminium salts, such as alum. The pigments obtained are known as “lakes”. Madder-lake, a mixture of alizarin and purpurin lakes, which was first described by Heraclius in the 10th century,<sup>89</sup> was used in manuscript illuminations<sup>90,91</sup> and paintings.<sup>9,92</sup>

The part of the plant used for the dye is the root, which according to Cardon contains 28 anthraquinone derivatives,<sup>93</sup> with Alizarin as the major and main colourant, see Scheme 8 for structures.

Synthetic alizarin was the first of the new generation of synthetic reds. It was not created accidentally, since its chemical structure was discovered by Graebe and Liebermann at 1868, making it the first “copy” of a natural dye. Following the discovery, made simultaneously by Perkin (in his factory) and by chemists working for the German firm BASF in



**Scheme 8** Structures of the Anthraquinone-like compounds.

1869,<sup>94</sup> it took a few years (1874) for the dye to reach the market, but when it did it became a tremendous success. Alizarin red S (Scheme 6), is an industrially important anthraquinone dye coming from alizarin sulfonation. It is commonly used because it is water-soluble (like indigocarmine, the water soluble indigo), although it is a very polluting dye.<sup>95,96</sup> More recently alizarin, has found new and high-tech applications as a chromophore, namely in solar energy conversion, development of new imaging materials and in environmental strategies.<sup>97–101</sup>

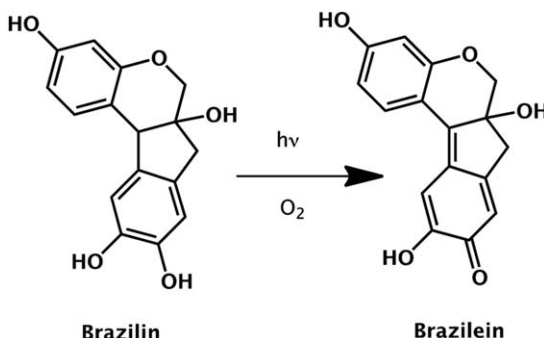
Lac dye is other red dye used since Antiquity. Native to India and Southeast Asia,<sup>102–106</sup> this was made from the insect *Kerria lacca* (from the *Kerriidae* family).<sup>93</sup> The colour was used to dye textiles, although European dyers found it expensive, a gummy substance hard to work with and restricted it primarily for dyeing leather.<sup>107</sup> Different shades could be obtained using alum (carmine hue), potassium dichromate, stannous chloride (scarlet hue), copper sulphate and iron salts (purple hue) which have also the function of improving colour fastness.<sup>108,109</sup> The colour of lac dye is due to the presence of different laccaic acid structures, with laccaic acid A being the main chromophore (Scheme 8).

Cochineal insects belong to the family Coccidae and has two distinct genus: the *Porphyrophora polonica* (Polish cochineal) or *hamelii* (Armenian cochineal), used in medieval Europe, and *Dactylopius*; the former are parasites hosted by diverse plant roots growing on the sandy soils of Central Europe,<sup>102</sup> while the latter are parasites of cacti belonging to the genera *Opuntia* and *Nopalea*.<sup>102</sup>

Cochineal (*Dactylopius coccus*) was used by Aztec, Maya and Incan civilizations. The Spanish people, who first thought that this was the kermes of their native Spain, were immediately impressed with its utility, starting a trade monopoly in the 16th century.<sup>110</sup> Collecting the mature cochineal (also called *grana*) was a patient process. Depending on the drying process, it could require *circa* 70 000 insects to obtain a single pound. The red dye is obtained from the eggs of the female. The females were cropped before depositing the eggs, leaving only sufficient to ensure the production.<sup>93,102</sup>

Cochineal substituted kermes, the most used red dye in Europe until then, in the 16th century. This was the result of the larger amount of carminic acid (Scheme 8) present on it.<sup>111</sup> Carminic acid is the main chromophore of cochineal, and could be extracted by different ways: handmade, by grinding the dry cochineal and boiling it in water, where it easily dissolved due to the presence of many free polar groups in the anthraquinone and glucose parts of the dye molecule,<sup>112</sup> or industrially where cochineal is transformed into a fine powder with intense purplish red colour.<sup>113</sup> The adult females of cochineal contained 19 to 24% carminic acid (in dry weight).<sup>111</sup> Carminic acid has widespread uses for red colouring; perhaps one of the most interesting is that it was the red dye used in the great majority of British (and Portuguese) postage stamps of the late XIXth and beginning of XXth centuries.<sup>114</sup>

The acidochromic effects in the excited state properties of alizarin and purpurin were reported by Milliani *et al.*<sup>115</sup> From these studies it was concluded that the substitution pattern of hydroxy anthraquinones is



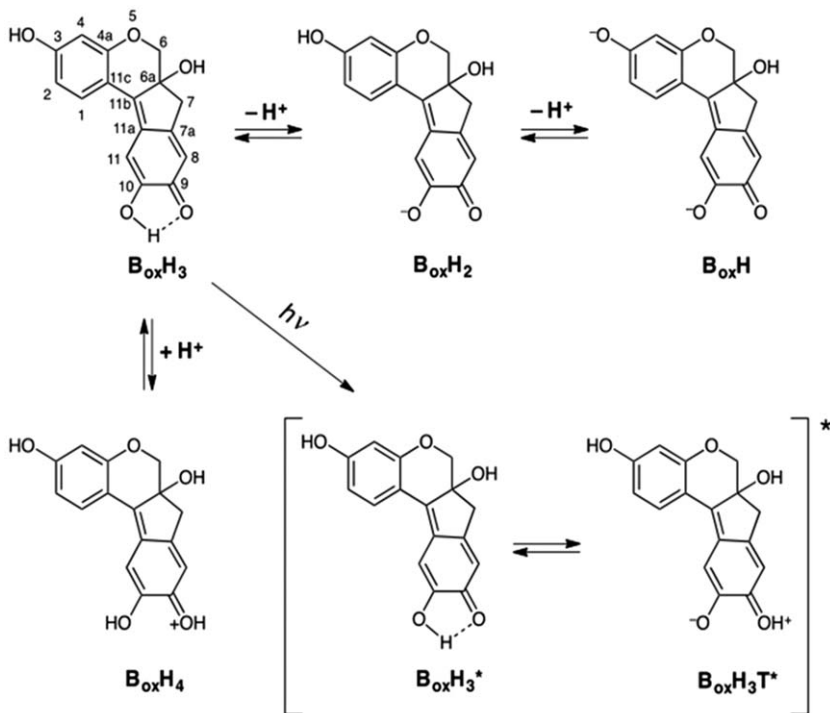
**Scheme 9** Oxidation under light exposure of brazilin to brazilein.

ruling their excited state properties, and that an efficient ( $S_1 \leftrightarrow S_0$ ) radiationless process, through an excited state intra- (ESPT) and intermolecular proton transfer (ESIPT) plays a fundamental role in the overall stability of the molecules. The ESIPT process can be extremely rapid (<300 fs) and is believed to involve proton tunnelling;<sup>116</sup> both ESPT and ESIPT, with excited-state tautomer formation, can be considered to induce a photoprotective mechanism for the molecule, enabling a very fast and effective dissipation of the energy excess of the excited state.

One last source of red colour considered in this text is brazilein from Brazilwood. Brazilein is formed from the oxidation under light exposure of brazilin, see Scheme 9.

While this last form has its wavelength maxima at 284 nm (therefore colourless), brazilein is at 445 nm and in solution reveals a yellow-orange color. More interesting is however the completely different photophysical characteristics displayed by brazilin and brazilein. The colourless species (brazilin) presents high fluorescence quantum yield ( $\phi_F = 0.33$ ) and competitive radiative channel ( $k_F = 1.3 \times 10^9 \text{ s}^{-1}$ ) over radiationless processes ( $k_{NR} = 2.6 \times 10^9 \text{ s}^{-1}$ ). In contrast with this behavior, brazilein displays a  $\phi_F$  value two orders of magnitude ( $\phi_F = 0.0068$ ) lower and a dominance of the radiationless decay pathways, which is linked to an excited state proton transfer leading to a quinoidal-like structure. This was further supported by time-resolved data (obtained in a ps time domain). The overall data indicates that brazilin is more prone to degradation than brazilein, mainly due to the high efficiency of the radiationless decay channel (likely through internal conversion), which confers a stabilizing inherent characteristic to this molecule.

Indeed, the *o*-hydroxyquinone moiety stabilizes its neutral form,  $B_{ox}H_3$  (see Scheme 10) through an intramolecular hydrogen bond (carbonyl oxygen and hydroxyl hydrogen). The fluorescence emission at  $pH \sim -1$  is due to the cationic  $B_{ox}H_4^+$  species, which apparently is stable at this pH and not prone to ESIPT (a monoexponential decay with a lifetime of 3.89 ns is obtained). At acidic pH (~1) this decay channel competes with fluorescence, promoting a strong decrease of the fluorescence intensity for  $pH \geq 0$  concomitant with the observed strong decrease in the decay



**Scheme 10** Acid–base equilibria of Brazilein ( $B_{ox}H_n$ ) and formation of Brazilein tautomers in the excited state.<sup>79</sup>

times (from 3.89 ns to 0.10 ns). The very efficient ESIPT is due to an excited state equilibrium between the neutral  $B_{ox}H_3^*$  and the zwitterionic  $B_{ox}H_3T^*$  tautomeric species, see Scheme 10.<sup>79</sup>

## 8 Mauveine: colour and stability

The genesis of the synthetic dye industry is commonly accepted to be founded upon the serendipitous discovery by William Henry Perkin in 1856 of a purple dye he called Aniline Purple, which later became known with the, more fashionable, name of Mauveine. This was also known as Tyrian Purple, following the name of the purple di-bromo indigo derivative, while other names were Phenanine, Indisine and Mauve dye.<sup>117</sup> Although the story has been described in detail in several textbooks and articles,<sup>94,118–127</sup> it can be summarized as follows. In 1856 the eighteen year-old William Perkin was asked by Hofmann, director of the “Royal College”, and who had been unsuccessful in trying to synthesise quinine, if he could manage this. However, while trying to find a synthesis for quinine, studying the dichromate oxidation of aromatic amines, Perkin obtained a black precipitate which gave an intense purple solution in alcohol: “On experimenting with the colouring matter thus obtained I found it to be a very stable compound dyeing silk a beautiful

purple which resisted light for a long time".<sup>128</sup> Perkin sent a sample to a Scottish dyer who replied:<sup>128</sup>

"If your discovery does not make the goods too expensive it is decidedly one of the most valuable that has come out for a very long time, this colour is one which has been very much wanted in all classes of goods and could not be had fast on silk, and only at great expense on cotton yams".

Perkin's synthesis of the dye only worked because the aniline used for the synthesis of what was intended to be the synthesis of quinine was highly impure with significant amounts of (*ortho* and *para*) toluidine in it.

Perkin stated: "In the early part of 1856, I commenced an investigation on the artificial formation of quinine. To obtain this base, I proposed to act on toluidine with iodide of allyl, so as to form allyl-toluidine, (...) thinking it not improbable that by oxidising this, I might obtain the desired result, thus:  $2(\text{C}_{10}\text{H}_3\text{N})$  (allyl-toluidine) +  $\text{O}_3 = \text{C}_{20}\text{H}_{24}\text{N}_2\text{O}_2$  (quinine) +  $\text{H}_2\text{O}$ ".<sup>117</sup>

However, what Perkin synthesized was a complex mixture of a core system consisting on the 7-amino-5-phenyl-3-(phenylamino)phenazin-5-ium with a varying number of methyl groups (two, three, or four) in peripheral positions leading to different methylated derivatives, *i.e.*, pseudo-mauveine ( $\text{C}_{24}$ ), mono ( $\text{C}_{25}$ ), di- ( $\text{C}_{26}$ ), tri- ( $\text{C}_{27}$ ) and tetramethylated ( $\text{C}_{28}$ ), see Fig. 12. Although Mauveine would dye protein based silk very well it would not dye cellulosic cotton and it took a year before a suitable mordanting process was reached which was developed with Pullar and consisted in the use of tannin and a metallic oxide.<sup>129</sup>

Purple (mauve) then became all the rage in French High Society. Perkin was only 18 yrs old when he made this discover of Aniline Purple (mauveine!). His dye business was to make him a millionaire, although this status was not obtained from Aniline Purple but, amongst other dyes, with Alizarin (for the UK market).

Perkin was unable to establish the correct composition of mauveine, although he was able to obtain the empirical formula for mauveine, which was defined as the base of mauve,  $\text{C}_{27}\text{H}_{24}\text{N}_4$ .<sup>129,130</sup> In 1994, Mandy Smith and Meth-Cohn identified in a museum sample of mauveine, two mauveine isomers:  $\text{C}_{26}$  and  $\text{C}_{27}$ .<sup>126</sup> However, the more complex mixture of  $\text{C}_{24}$  to  $\text{C}_{28}$  derivatives (in which the  $\text{C}_{26}$  and  $\text{C}_{27}$ , the mauveines A and B respectively, are found in major amounts) was only discovered in 2007 and 2008.<sup>118,120</sup> More recently and from a detailed chemical analysis of historical samples of both Perkin's and Caro's mauveine (from the Deutsches Museum), it was shown that Caro's mauveine contained a very high percentage of pseudomauveine ( $\text{C}_{24}$ ), whereas with Perkin's mauveine the major compounds were mauveine A ( $\text{C}_{26}$ ) and B ( $\text{C}_{27}$ ).<sup>114</sup> This means that at least two different recipes were used to produce mauveine.<sup>114,131</sup> Moreover, these two recipes were used to dye a small group of lilac 6d postage stamps in the 1867–1880 Victorian period, see Fig. 13.<sup>114</sup>

It is very interesting to note that the high stability of mauveine dyes is also linked to the high efficiency of its ( $\text{S}_1 \leftrightarrow \text{S}_0$ ) radiationless process with more than 99.9% of the *quanta* loss made through this process.<sup>120</sup>

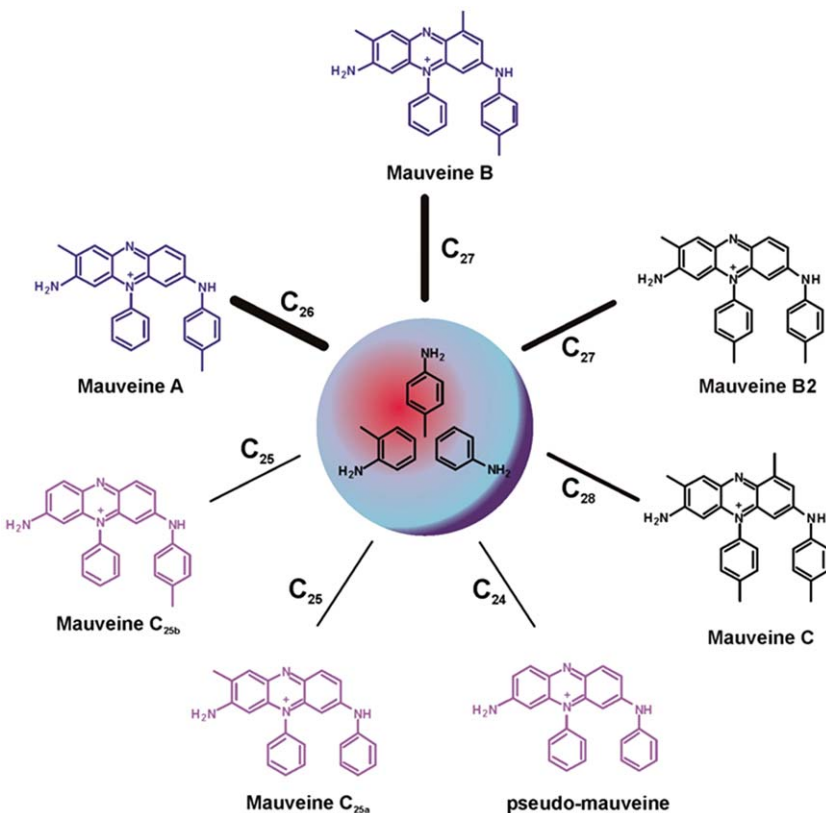


**Fig. 12** Mauveine structures isolated form historic samples. Reproduced with permission from ref. 118, M. M. Sousa, M. J. Melo, A. J. Parola, P. J. T. Morris, H. S. Rzepa and J. S. Seixas de Melo, *Chem. – Eur. J.*, John Wiley and Sons. Copyright © 2008 WILEY-VCH Verlag GmbH & Co. KGaA, Weinheim.



**Fig. 13** Victorian Postage stamps dyed with mauveine (the SG106 at the left with Caro's recipe and the SG107 at the right with Perkin's recipe). Reproduced with permission from ref. 114, M. Conceição Oliveira, A. Dias, P. Douglas and J. S. Seixas de Melo, *Chem. – Eur. J.*, John Wiley and Sons. Copyright © 2014 WILEY-VCH Verlag GmbH & Co. KGaA, Weinheim.

## 9 Conclusions

In this contribution we have highlighted some of the more historically important molecules of colour, with some of their stories, secrets, and impact they still have nowadays. A common feature presented by all them is the fact that the fluorescence deactivation is strongly diminished, with the exception of the synthetic thioindigo and the natural madder dye purpurin, while the internal conversion ( $S_1 \rightsquigarrow S_0$ ) radiationless decay dominates, either through the “Golden rule” (energy gap law) for the radiationless processes (mauveine) or through an excited state intra- and inter-molecular proton transfer (indigo, alizarin, brazilein, *etc.*).

## Acknowledgements

We acknowledge funding by FEDER (Fundo Europeu de Desenvolvimento Regional) through COMPETE (Programa Operacional Factores de Competitividade). The Coimbra Chemistry Centre is supported by the Fundação para a Ciência e a Tecnologia (FCT), Portuguese Agency for Scientific Research, through the programme UID/QUI/UI0313/2013.

This work was performed under the project “SunStorage - Harvesting and storage of solar energy”, with reference POCI-01-0145-FEDER-016387, funded by the European Regional Development Fund (ERDF), through COMPETE 2020 - Operational Programme for Competitiveness and Internationalisation (OPCI), and by national funds, through FCT.

## References

- 1 H. Zollinger, *Color Chemistry. Synthesis, Properties, and Applications of Organic Dyes and Pigments*, Verlag Helvetica Chimica Acta & Wiley-VCH, Zürich, 3rd edn, 2003.
- 2 W. Dilthey and R. Wizinger, *J. Prakt. Chem.*, 1928, **118**, 321.
- 3 R. M. Christie, *Biotech. Histochem.*, 2007, **82**, 51–56.
- 4 T. Costa, J. Pina and J. S. Seixas de Melo, in *Photochemistry*, ed. A. Albini, The Royal Society of Chemistry, 2009, vol. 37, pp. 44–71.
- 5 J. S. Seixas de Melo, J. Pina, F. B. Dias and A. L. Maçanita, in *Applied Photochemistry*, ed. R. C. Evans, P. Douglas and H. D. Burrows, Springer Netherlands, 2013, ch. 15, pp. 533–585, DOI: , DOI: 10.1007/978-90-481-3830-2\_15.
- 6 J. S. Seixas de Melo, T. Costa, C. S. de Castro and A. L. Maçanita, in *Photochemistry*, ed. A. Albini and E. Fasani, The Royal Society of Chemistry, 2013, vol. 41, pp. 59–126.
- 7 S. Takato, “The Molecules of Color: In the Masks of the Philosophical Journey (1783–1792) and in an Oriental Tissue (1880)”, Master’s Thesis, University of Coimbra, Coimbra, 2014.
- 8 J. Balfour-Paul, *Indigo in the Arab World*, RoutledgeCurzon, London, 1997.
- 9 M. R. v. Bommel, M. Geldof and E. Hendriks, *Art Matters: Netherlands Technical Studies in Art*, Waanders Zwolle, 2005, vol. 3, pp. 111–137.
- 10 P. Novotna, J. J. Boon, J. van der Horst and V. Pacakova, *Color. Technol.*, 2003, **119**, 121–127.
- 11 M. J. Melo, in *Handbook of Natural Colorants*, ed. T. Bechtold and R. Mussak, John Wiley & Sons, Ltd, 2009, pp. 1–20, DOI: 10.1002/9780470744970.ch1.
- 12 V. F. Fairbanks, *Mayo Clin. Proc.*, 1994, **69**, 889–892.

- 13 C. E. Steinhart, *J. Chem. Educ.*, 2001, **78**, 1444–1444.
- 14 P. E. McGovern and R. H. Michel, *Acc. Chem. Res.*, 1990, **23**, 152–158.
- 15 Z. C. Koren, *Microchim. Acta*, 2008, **162**, 381–392.
- 16 C. J. Cooksey, *Molecules*, 2001, **6**, 736–769.
- 17 R. J. H. Clark, C. J. Cooksey, M. A. M. Daniels and R. Withnall, *Endeavour*, 1993, **17**, 191–199.
- 18 T. M. Brown, C. J. Cooksey and A. T. Dronsfield, *Educ. Chem.*, 2001, **38**, 69–71.
- 19 J. Balfour-Paul, in *XXth International Congress of History of Science*, ed. G. Empotz and P. E. Aceves Pastrana, Brepols, Liège, Belgium, 1997, vol. II, pp. 29–39.
- 20 M. Klessinger, *Angew. Chem., Int. Ed. Engl.*, 1980, **19**, 908–909.
- 21 M. Klessinger and W. Luettke, *Tetrahedron*, 1963, **19**(Suppl. 2), 315–335.
- 22 E. Wille and W. Lüttke, *Angew. Chem., Int. Ed. Engl.*, 1971, **10**, 803–804.
- 23 G. Pfeifer, W. Otting and H. Bauer, *Angew. Chem., Int. Ed. Engl.*, 1976, **15**, 52–52.
- 24 A. Reis and W. Schneider, *Z. Kristallogr.*, 1928, **68**, 543.
- 25 L. Serrano-Andrés and B. O. Roos, *Chem. – Eur. J.*, 1997, **3**, 717–725.
- 26 M. Klessinger, *Dyes Pigm.*, 1982, **3**, 235–241.
- 27 W. Lüttke, H. Hermann and M. Klessinger, *Angew. Chem., Int. Ed. Engl.*, 1966, **5**, 598–599.
- 28 H. Bauer, K. Kowski, H. Kuhn, W. Luttke and P. Rademacher, *J. Mol. Struct.*, 1998, **445**, 277–286.
- 29 S. Yamazaki, A. L. Sobolewski and W. Domcke, *Phys. Chem. Chem. Phys.*, 2011, **13**, 1618–1628.
- 30 D. Jacquemin, J. Preat, V. Wathelet and E. A. Perpete, *J. Chem. Phys.*, 2006, **124**, 074104.
- 31 P. W. Sadler, *Spectrochim. Acta*, 1960, **16**, 1094–1099.
- 32 P. W. Sadler, *J. Org. Chem.*, 1956, **21**, 316–318.
- 33 J. S. Seixas de Melo, R. Rondão, H. D. Burrows, M. J. Melo, S. Navaratnam, R. Edge and G. Voss, *ChemPhysChem*, 2006, **7**, 2303–2311.
- 34 J. Seixas de Melo, A. P. Moura and M. J. Melo, *J. Phys. Chem. A*, 2004, **108**, 6975–6981.
- 35 G. M. Wyman, *EPA NewsL.*, 1994, **50**, 9–13.
- 36 J. Pina, D. Sarmento, M. Accoto, P. L. Gentili, L. Vaccaro, A. Galvão and J. S. Seixas de Melo, *J. Phys. Chem. B*, 2017, **121**, 2308–2318.
- 37 J. S. Seixas de Melo, C. Serpa, H. D. Burrows and L. G. Arnaut, *Angew. Chem., Int. Ed. Engl.*, 2007, **46**, 2094–2096.
- 38 V. T. Ngan, G. Gopakumar, T. T. Hue and M. T. Nguyen, *Chem. Phys. Lett.*, 2007, **449**, 11–17.
- 39 C. Miliani, A. Romani and G. Favaro, *Spectrochim. Acta, Part A*, 1998, **54**, 581–588.
- 40 J. Seixas de Melo, R. Rondão, H. D. Burrows, M. J. Melo, S. Navaratnam, R. Edge and G. Voss, *J. Phys. Chem. A*, 2006, **110**, 13653–13661.
- 41 A. L. Costa, A. C. Gomes, M. Pillinger, I. S. Gonçalves and J. S. Seixas de Melo, *Chem. – Eur. J.*, 2015, **21**, 12069–12078.
- 42 R. J. Rondão, J. S. Seixas de Melo, F. B. Schaberle and G. Voss, *Phys. Chem. Chem. Phys.*, 2012, **14**, 1778–1783.
- 43 G. M. Wyman and B. M. Zarnegar, *J. Phys. Chem.*, 1973, **77**, 1204–1207.
- 44 G. M. Wyman, B. M. Zarnegar and D. G. Whitten, *J. Phys. Chem.*, 1973, **77**, 2584–2586.
- 45 G. Boice, B. O. Patrick, R. McDonald, C. Bohne and R. Hicks, *J. Org. Chem.*, 2014, **79**, 9196–9205.
- 46 R. Rondão and J. S. Seixas de Melo, *J. Phys. Chem. C*, 2013, **117**, 603–614.
- 47 T. Kobayashi and P. M. Rentzepis, *J. Chem. Phys.*, 1979, **70**, 886–892.

- 48 I. Iwakura, A. Yabushita and T. Kobayashi, *Bull. Chem. Soc. Jpn.*, 2011, **84**, 164–171.
- 49 I. Iwakura, A. Yabushita and T. Kobayashi, *Chem. Phys. Lett.*, 2010, **484**, 354–357.
- 50 I. Iwakura, A. Yabushita and T. Kobayashi, *Chem. Lett.*, 2009, **38**, 1020–1021.
- 51 Y. Nagasawa, R. Taguri, H. Matsuda, M. Murakami, M. Ohama, T. Okada and H. Miyasaka, *Phys. Chem. Chem. Phys.*, 2004, **6**, 5370–5378.
- 52 M. Dittmann, F. F. Graupner, B. Maerz, S. Oesterling, R. de Vivie-Riedle, W. Zinth, M. Engelhard and W. Lüttke, *Angew. Chem., Int. Ed. Engl.*, 2014, **53**, 591–594.
- 53 M. Moreno, J. M. Ortiz-Sánchez, R. Gelabert and J. M. Lluch, *Phys. Chem. Chem. Phys.*, 2013, **15**, 20236–20246.
- 54 G. L. Cui and W. Thiel, *Phys. Chem. Chem. Phys.*, 2012, **14**, 12378–12384.
- 55 H. Gorner, J. Pouliquen and J. Kossanyi, *Can. J. Chem.*, 1987, **65**, 708–717.
- 56 T. Elsaesser, W. Kaiser and W. Lüttke, *J. Phys. Chem.*, 1986, **90**, 2901–2905.
- 57 M. Séquin-Frey, *J. Chem. Educ.*, 1981, **58**, 301–305.
- 58 R. Rondão, J. S. Seixas, de Melo and G. Voss, *ChemPhysChem*, 2010, **11**, 1903–1908.
- 59 J. Seixas de Melo, *Chem. Educ.*, 2005, **10**, 29–35.
- 60 R. Rondão, J. Seixas de Melo, M. J. Melo and A. J. Parola, *J. Phys. Chem. A*, 2012, **116**, 2826–2832.
- 61 R. Rondão, J. S. Seixas de Melo, V. D. B. Bonifácio and M. J. Melo, *J. Phys. Chem. A*, 2010, **114**, 1699.
- 62 A. Doménech-Carbó, M. Doménech-Carbó, F. Valle-Algarra, M. Domine and L. Osete-Cortina, *J. Mater. Sci.*, 2013, **48**, 7171–7183.
- 63 M. M. Sousa, C. Miguel, I. Rodrigues, A. J. Parola, J. Pina, J. S. Seixas de Melo and M. J. Melo, *Photochem. Photobiol. Sci.*, 2008, **7**, 1353–1359.
- 64 M. J. Melo, J. L. Ferreira, A. J. Parola and J. S. Seixas de Melo, in *Applied Photochemistry: When Light Meets Molecules*, ed. G. Bergamini and S. Silvi, Springer International Publishing, Cham, 2016, pp. 499–530, DOI: 10.1007/978-3-319-31671-0\_13.
- 65 J. Balfour-Paul, *Indigo*, British Museum Press, 1998.
- 66 R. J. Gettens, *Am. Antiq.*, 1962, **27**, 557–564.
- 67 A. O. Shepard, *Am. Antiq.*, 1962, **27**, 565–566.
- 68 H. van Olphen, *Science*, 1966, **154**, 645–646.
- 69 H. E. Merwin, in *The Temple of the Warriors at Chichen-Itza, Yucatan*, ed. E. H. Morris, J. Charlot and A. A. Morris, Carnegie Institution of Washington, Washington, 1931, pp. 355–356.
- 70 C. Dejoie, P. Martinetto, E. Dooryhee, P. Strobel, S. Blanc, P. Bordat, R. Brown, F. Porcher, M. S. del Rio and M. Anne, *ACS Appl. Mater. Interfaces*, 2010, **2**, 2308–2316.
- 71 C. Tsiantos, M. Tsampodimou, G. H. Kacandes, M. S. del Rio, V. Gionis and G. D. Chryssikos, *J. Mater. Sci.*, 2012, **47**, 3415–3428.
- 72 A. Domenech, M. T. Domenech-Carbo, C. Vidal-Lorenzo and M. L. V. de Agredos-Pascual, *Angew. Chem., Int. Ed. Engl.*, 2012, **51**, 700–703.
- 73 R. Giustetto, K. Seenivasan, F. Bonino, G. Ricchiardi, S. Bordiga, M. R. Chierotti and R. Gobetto, *J. Phys. Chem. C*, 2011, **115**, 16764–16776.
- 74 I. M. V. Leitao and J. Sergio Seixas de Melo, *J. Chem. Educ.*, 2013, **90**, 1493–1497.
- 75 A. Domenech, M. T. Domenech-Carbo and M. Pascual, *J. Phys. Chem. C*, 2007, **111**, 4585–4595.
- 76 A. Doménech-Carbó, F. M. Valle-Algarra, M. T. Doménech-Carbó, M. E. Domine, L. Osete-Cortina and J. V. Gimeno-Adelantado, *ACS Appl. Mater. Interfaces*, 2013, **5**, 8134–8145.

- 77 N. D'Elboux Bernardino, S. E. Brown-Xu, T. L. Gustafson and D. L. Araujo de Faria, *J. Phys. Chem. C*, 2016, **120**, 21905–21914.
- 78 M. J. Melo, V. Otero, T. Vitorino, R. Araujo, V. S. F. Muralha, A. Lemos and M. Picollo, *Appl. Spectrosc.*, 2014, **68**, 434–444.
- 79 R. Rondão, J. S. Seixas de Melo, J. Pina, M. J. Melo, T. Vitorino and A. J. Parola, *J. Phys. Chem. A*, 2013, **117**, 10650–10660.
- 80 M. J. Melo, M. Sousa, A. J. Parola, J. S. Seixas de Melo, F. Catarino, J. Marcalo and F. Pina, *Chem. – Eur. J.*, 2007, **13**, 1417–1422.
- 81 M. M. Sousa, M. J. Melo, A. J. Parola, J. S. Seixas de Melo, F. Catarino, F. Pina, F. E. M. Cook, M. S. J. Simmonds and J. A. Lopes, *J. Chromatogr. A*, 2008, **1209**, 153–161.
- 82 D. Cardon, in *Handbook of Natural Colorants*, John Wiley & Sons, Ltd, 2009, pp. 21–26, DOI: 10.1002/9780470744970.ch2.
- 83 E. R. Caley, *J. Chem. Ed.*, 1926, **3**, 1149–1166.
- 84 E. R. Caley, *J. Chem. Ed.*, 1927, **4**, 979–1002.
- 85 H. Schweppe and J. Winter, in *Artists' Pigments, a handbook of their history and characteristics*, ed. E. W. Fitzhugh, National Gallery of Art, Washington, 1997, vol. 3.
- 86 B. Szostek, J. Orska-Gawrys, I. Surowiec and M. Trojanowicz, *J. Chromatogr. A*, 2003, **1012**, 179–192.
- 87 X. Zhang and R. A. Laursen, *Anal. Chem.*, 2005, **77**, 2022–2025.
- 88 D. K. Palit, H. Pal, T. Mukherjee and J. P. Mittal, *J. Chem. Soc., Faraday Trans.*, 1990, **86**, 3861–3869.
- 89 M. Merrifield, *Medieval and Renaissance Treatises on the Arts of Painting*, Dover Publications, New York, 1999.
- 90 C. Cennini, *Il Libro dell' Arte*, Neri Pozza Editore, Vicenza, 2003.
- 91 S. Blondheim, *Jew. Q. Rev.*, 1928, **19**, 97–135.
- 92 N. Eastaugh, V. Walsh, T. Chaplin and R. Siddall, *The pigment compendium: optical microscopy of historical pigments*, Elsevier Butterworth-Heinemann, Oxford-UK, 2004.
- 93 D. Cardon, *Natural Dyes: Sources, Tradition, Technology and Science*, Arche-type, 2007.
- 94 S. Garfield, *MAUVE. How One Man Invented a Color That Changed the World*, W.W. Norton & Company, 2002.
- 95 P. Zucca, C. Vinci, F. Sollai, A. Rescigno and E. Sanjust, *J. Mol. Catal. A: Chem.*, 2008, **288**, 97–102.
- 96 G. C. H. Derkzen, G. P. Lelyveld, T. A. van Beek, A. Capelle and A. E. de Groot, *Phytochem. Anal.*, 2004, **15**, 397–406.
- 97 R. Huber, J. E. Moser, M. Gratzel and J. Wachtveitl, *J. Phys. Chem. B*, 2002, **106**, 6494–6499.
- 98 J. M. Kim, J. H. Kang, D. K. Han, C. W. Lee and K. D. Ahn, *Chem. Mater.*, 1998, **10**, 2332–2334.
- 99 F. R. Zaggout, A. Qarraman and S. M. Zourab, *Mater. Lett.*, 2007, **61**, 4192–4195.
- 100 V. K. Gupta, R. N. Goyal and R. A. Sharma, *Int. J. Electrochem. Sci.*, 2009, **4**, 156–172.
- 101 J. Fan, C. L. Wu, H. Z. Xu, J. J. Wang and C. Y. Peng, *Talanta*, 2008, **74**, 1020–1025.
- 102 R. A. Donkin, *Trans. Am. Philos. Soc.*, 1977, **67**, 5–84.
- 103 R. A. Donkin, *Anthropos*, 1977, **72**, 847–880.
- 104 C. Hatchett, *Philos. Trans. R. Soc. London*, 1804, **94**, 191.
- 105 E. Schafer, *J. Am. Orient. Soc.*, 1957, **77**, 129.
- 106 J. Kerr and J. Banks, *Philos. Trans. R. Soc. London*, 1781, **71**, 374.

- 107 A. B. Greenfield, *A Perfect Red – Empire, Espionage, and the Quest for the Color of Desire*, Harper Collins Publishers, New York, 2005.
- 108 M. Chairat, V. Rattanaphani, J. B. Bremner, S. Rattanaphani and D. F. Perkins, *Dyes Pigm.*, 2004, **63**, 141–150.
- 109 J. H. H. D. Graaff, *The Colourful Past – origins, Chemistry and Identification of Natural Dyestuffs*, Abegg-Stifung and Archetype Publications, Riggisberg and London, 2004.
- 110 H. Schweppe and H. Roosen-Rungue, in *Artists' Pigments, a Handbook of Their History and Characteristics*, ed. R. L. Feeler, National Gallery of Art, Washington, 1986, vol. 1, pp. 255–283.
- 111 C. Aldama-Aguilera, C. Lianderal-Cazares, M. Soto-Hernandez and L. E. Castillo-Marquez, *Agrociencia*, 2005, **39**, 161–171.
- 112 V. Golikov, in *Dyes in History and Archaeology*, ed. J. Kirby, Archetype Publications, Greenwich, 2001, vol. 16/17.
- 113 M. P. Sandy and R. Becerra, *Biodiversitas*, 2001, **31**, 1.
- 114 M. Conceição Oliveira, A. Dias, P. Douglas and J. S. Seixas de Melo, *Chem. – Eur. J.*, 2014, **20**, 1808–1812.
- 115 C. Miliani, A. Romani and G. Favaro, *J. Phys. Org. Chem.*, 2000, **13**, 141–150.
- 116 P. A. B. Marasinghe and G. D. Gillispie, *Chem. Phys.*, 1989, **136**, 249–257.
- 117 W. H. Perkin, *J. Chem. Soc.*, 1862, **14**, 230–255.
- 118 M. M. Sousa, M. J. Melo, A. J. Parola, P. J. T. Morris, H. S. Rzepa and J. S. Seixas de Melo, *Chem. – Eur. J.*, 2008, **14**, 8507–8513.
- 119 A. S. Travis, *Bull. Hist. Chem.*, 2007, **32**, 35–44.
- 120 J. Seixas de Melo, S. Takato, M. Sousa, M. J. Melo and A. J. Parola, *Chem. Commun.*, 2007, 2624–2626.
- 121 A. S. Travis, *Hist. Technol.*, 2006, **22**, 131–152.
- 122 P. J. T. Morris, *Hist. Technol.*, 2006, **22**, 119–130.
- 123 I. Holme, *Color. Technol.*, 2006, **122**, 235–251.
- 124 P. Ball, *Nature*, 2006, **440**, 429–429.
- 125 O. Meth-Cohn and A. S. Travis, *Chem. Br.*, 1995, **31**, 547–549.
- 126 O. Meth-Cohn and M. Smith, *J. Chem. Soc., Perkin Trans. 1*, 1994, 5–7.
- 127 A. S. Travis, *The rainbow makers – the origins of the synthetic dyestuffs industry in Western Europe*, Lehigh University Press, Bethlehem, 1993.
- 128 W. H. Perkin, *J. Chem. Soc., Trans.*, 1896, 596–637.
- 129 W. H. Perkin, *Proc. R. Soc. London*, 1862/63, **12**, 713–715.
- 130 W. H. Perkin, *Proc. R. Soc. London*, 1862/63, **13**, 170–176.
- 131 T. F. G. G. Cova, A. A. C. C. Pais and J. S. Seixas de Melo, *Sci. Rep.*, 2017.

DOI:10.1038/s41598-017-07239-z.

---

# Photochemical and photocatalytic properties of transition metal compounds

Valeria Amendola\* and Greta Bergamaschi

DOI: 10.1039/9781788010696-00101

This chapter reviews the most relevant results in the fields of photochemistry and photocatalysis by transition metal compounds published in 2015–2016; particular attention has been devoted to metal complexes. The structure of this chapter is similar to that adopted in our previous report, but the metals have been ordered according to the row they belong to in the periodic table. For each element, results are reviewed following a general sequence: (i) photocatalysis, e.g. CO<sub>2</sub>-to-CO photoreduction, H<sub>2</sub> photogeneration, water oxidation, etc.; (ii) photoreactivity; (iii) biomedical applications as e.g. photoCORMs and PDT agents.

## 1 Introduction

In the last years, because of climate change and rising global energy demand, the research into alternative and sustainable energy sources has been highly motivated.

As in previous years,<sup>1</sup> in 2015–2016, the development of systems for solar-to-fuel conversion based on inexpensive and earth-abundant elements has been pursued in many labs. Among transition metal compounds, polyoxometalates and decatungstate salts, in particular, found application in photocatalyzed organic synthesis, and were applied in sunlight induced C–H functionalization, C–X bond formation (X = C, N, O) and oxidations of organic compounds.<sup>2</sup> Catalysts using water, as both an earth-abundant and a solvent for proton reduction, are currently highly desirable.<sup>3</sup> The need for a green and sustainable energy source promoted the artificial photosynthesis approach consisting in the conversion of water and CO<sub>2</sub><sup>4</sup> into oxygen and solar fuels.

As an example, utilization of CO<sub>2</sub> as a C1 source in organic synthesis would help to mitigate global problems (e.g. energy shortage, environmental degradation, resource depletion) caused by fossil fuel and other natural resource consumption. In this context, transition metal compounds play a key role.<sup>5</sup>

The photochemical reactivity of transition metal complexes is also very attractive, in particular when associated to metal-hydrides due to their critical role in C–H bond activation.<sup>6</sup> In general, the chemical structure and electronic properties of the ligands are a key factor for obtaining an optimal catalyst performance. In the context of photocatalytic water splitting, transition metal complexes with *N*-heterocyclic carbene ligands gained attention because of their chemical stability and widely tunable activity.<sup>7</sup> Catalysts for the (photo)oxidation of water to oxygen (WOCs) based on earth-abundant first-row transition metals (e.g. Mn, Fe, Co and

---

*Dept. Chemistry, University of Pavia, via Taramelli 12, I-27100, Pavia, Italy.*  
E-mail: [amendola@unipv.it](mailto:amendola@unipv.it)

$\text{Cu}^{\text{II}}$ <sup>8</sup> are receiving considerable attention, despite their intrinsic lability compared to Ru or Ir based systems.

The hybridization of metal complexes with solid matrices has been recognized as a successful route for obtaining novel efficient photocatalysts. Hybrid photocatalysts were obtained using different methods, *e.g.* by encapsulation/immobilization of metal complexes within mesoporous matrices or onto nanoparticles.<sup>9</sup>

Releasing small molecules with a strong biological effect is also becoming an important application (singlet oxygen in photodynamic therapy, PDT; CO in the light-triggered release of carbon monoxide from the inner coordination sphere of transition metal complexes PhotoCORMs). As highlighted by several Authors, both photophysical properties and photochemical reactivity of transition metal compounds can be tailored by properly choosing the ligand set. This makes the compounds, *e.g.* versatile PDT agents, function by more than one mechanism, enhancing their effect on tumor cells while minimizing the impact on healthy cells.<sup>10</sup>

## 2 First-row transition metals

### 2.1 Manganese

In the biomimetic studies with transition metal-based WOCs, the generation of high-valent metal–oxo intermediates is one of the key points. However, the photocatalytic generation of non-heme Mn–oxo species with water as an oxygen source was obtained only recently by Nam and Sun.<sup>11</sup> The Authors obtained the  $\text{Mn}^{\text{IV}}$ –oxo complex,  $[\text{Mn}^{\text{IV}}(\text{O})(\text{BQCN})]^{2+}$  ( $\text{BQCN} = N,N'$ -dimethyl- $N,N'$ -bis(8-quinolyl)cyclohexanediamine), by photocatalytic reaction of  $[\text{Mn}^{\text{II}}(\text{BQCN})]^{2+}$  with  $[\text{Ru}^{\text{II}}(\text{bpy})_3]\text{Cl}_2$  as a photosensitizer,  $[\text{Co}^{\text{III}}(\text{NH}_3)_5\text{Cl}]^{2+}$  as a low-cost sacrificial electron acceptor, and water as an oxygen source (see Fig. 1). The reactive  $\text{Mn}^{\text{IV}}$ –oxo species could be applied in the photocatalytic oxidation of organic substrates, *e.g.* alcohols and sulfides, in both neutral and acidic media.

A visible-light induced copper catalyzed [3 + 2] azide–alkyne “click” reaction to give 1,2,3-triazoles was developed using a novel bimetallic Ru–Mn complex as photocatalyst by Jain *et al.*<sup>12</sup> The bimetallic complex consisted in a Ru unit (photosensitizer) and a catalytic Mn(i) moiety connected through a bipyrimidine (bpm) bridging ligand, which provided the rapid photochemical reduction of Cu(II) to Cu(I). This bimetallic complex exhibited enhanced activity compared to the photosensitizer and the Mn catalyst as separate components.

Notably, metal oxide/organic hybrid compounds are materials that combine some useful properties of organic ligands, *e.g.* molecular level tunability, with the robustness of metal oxides. Recently, Maggard *et al.* prepared Mn(II)–vanadate(V)/organic hybrids, containing N-donor organic ligands (*e.g.* *o*-phen and tpy).<sup>13</sup> Photocatalytic studies on these materials pointed out that their temperature-dependent photocatalytic activity increased with oxide/organic network connectivity. The Authors applied the Mn(II)–vanadate(V)/organic hybrids in the photocatalytic production of hydrogen under visible-light irradiation in 20% methanol solutions.

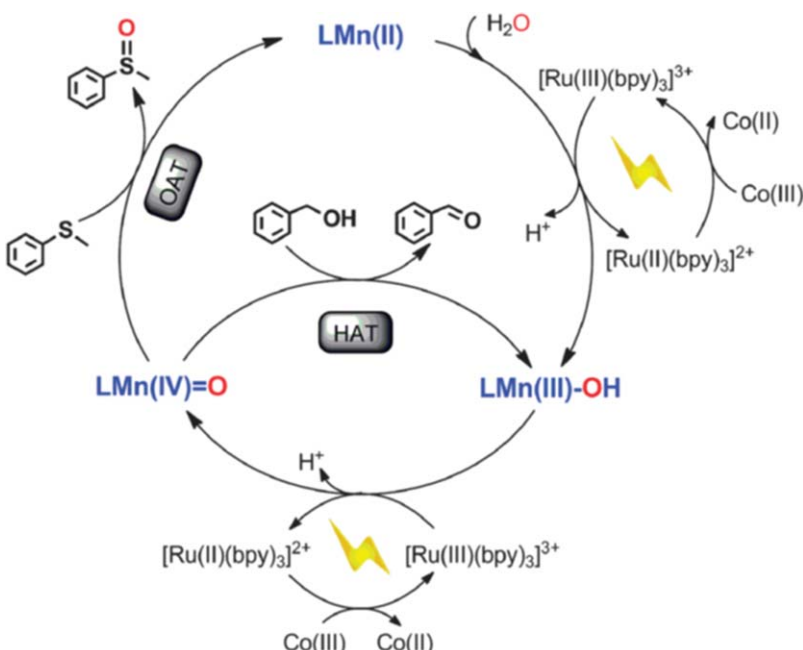


**Fig. 1** Proposed mechanisms of light-driven oxidation of organic substrates.  $[\text{Mn}^{\text{II}}(\text{BQCN})]^{2+}$  = catalyst,  $[\text{Ru}^{\text{II}}(\text{bpy})_3]^{2+}$  = photosensitizer, and  $[\text{Co}^{\text{III}}(\text{NH}_3)_5\text{Cl}]^{2+}$  = sacrificial electron acceptor. Reproduced from ref. 11 with permission from The Royal Society of Chemistry.

As recently remarked by Ruggi and Zobi, the realization of CO-releasing molecules, triggered by visible light within the phototherapeutic window, is an important goal to achieve, for therapeutic applications.<sup>14</sup> The Authors showed that carbonyl Mn(i) complexes, based on 2,2'-azopyridine ligands, were capable of releasing CO under red light ( $\geq 625$  nm) irradiation. The introduction of electron-donating or electron-withdrawing substituents on the ligand affected the electronic properties of the complexes, inducing a shift of the absorption bands. Electron-deficient ligands, in particular, could strongly decrease the HOMO – 1/LUMO gap. As a result, CO release was triggered also under irradiation in the NIR region (*i.e.* at 810 nm).

Compared to other photoCORMs previously reported in the literature, the new Mn(i) carbonyl complexes by Mascharak *et al.*, based on  $\alpha,\alpha'$ -diimine ligands (see Fig. 2), were highly sensitive to low-power (0.3–10 mW) visible light ( $\lambda \geq 520$  nm), rapidly releasing CO upon illumination even in the solid state. Such activity, which was influenced by the ligand structure, could find application in delivering high fluxes of CO to biological targets.<sup>15</sup> A series of tricarbonyl Mn(i) complexes with differently substituted terpyridyl ligands was synthesised by Chardon-Noblat *et al.* These compounds were shown to easily deliver CO under photoirradiation. The influence of bulky substituents was also investigated; thus, kinetics studies demonstrated that sterically hindered pyridyl groups significantly slowed down the photodecoordination rate.<sup>16</sup>

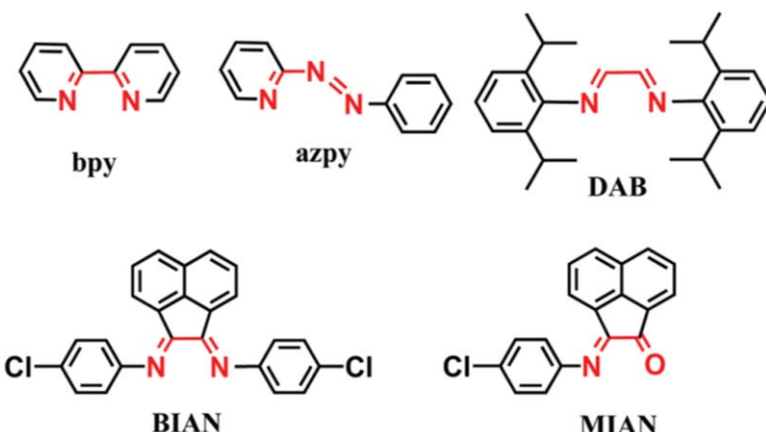


**Fig. 2** Proposed Mn(I) ligands: bipyridine (bpy), 2-phenylazopyridine (azpy), *N,N'*-bis(2,6-di-isopropylphenyl)-1,4-diaza-1,3-butadiene(iPr<sub>2</sub>Ph-DAB), bis(4-chlorophenylimino)-acenaphthene (BIAN) and 2-[(4-chlorophenyl)imino]acenaphthylene-1-one (MIAN). Reproduced from ref. 15 with permission from The Royal Society of Chemistry.

## 2.2 Iron

For the CO<sub>2</sub> photocatalytic reduction, both mono and heteronuclear iron-containing complexes have been recently investigated. The Beller's group disclosed for the first time the use of cyclopentadienone iron complexes as active photocatalysts in the reduction of CO<sub>2</sub> to CO under visible light, using an Ir complex as photosensitizer and TEOA as electron/proton donor. Thanks to Operando FTIR studies, a plausible reaction mechanism was proposed (see Fig. 3).<sup>17</sup>

Highly efficient and selective CO<sub>2</sub> reduction was obtained by Robert and Lau using Fe(II) and Co(II) quaterpyridine complexes as the photocatalysts, and the cheap organic dye purpurin as the photosensitizer. Notably, the obtained TONs and TOFs are among the highest reported to date for the homogeneous photocatalytic reduction of CO<sub>2</sub>.<sup>18</sup> On the side of macrocyclic complexes, the same Authors recently investigated the photocatalytic activity, toward CO<sub>2</sub> reduction, of the mononuclear Co(II) and Fe(III) complexes of a pentadentate N<sub>5</sub>-ligand (*i.e.* 2,13-dimethyl-3,6,9,12,18-pentaazabicyclo-[12.3.1]octadeca-1(18),2,12,14,16-pentaene).<sup>19</sup> Interestingly, using a photosensitizer under visible light excitation (>460 nm in acetonitrile), two different products were obtained: carbon monoxide with Co(II) and formic acid with Fe(III).

Light-induced catalytic CO<sub>2</sub> reduction to CO was achieved by Schwalbe *et al.*<sup>20</sup> with a series of complexes based on a phenanthroline-extended tetramesityl porphyrin ligand, containing FeCl (or Co) bound to the porphyrin, and a Ru(tbbpy)<sub>2</sub> unit linked to the phenanthroline.<sup>20</sup> Studies were performed in DMF with triethylamine as a sacrificial electron donor. Notably, a very high catalytic activity was observed with both Co and FeCl. In the case of FeCl, in particular, the turnover numbers (TONs) of CO obtained were twice as high as the TONs determined under the same conditions for CoTPP and FeClTPP (*i.e.* the most catalytically active porphyrins so far prepared).

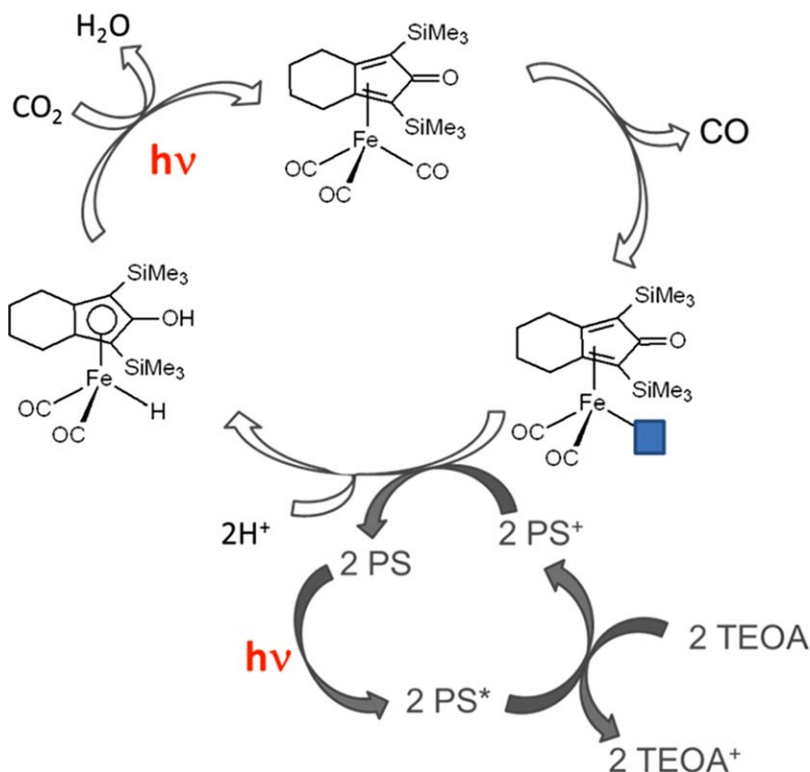


**Fig. 3** Proposed mechanism for the photoreduction of  $\text{CO}_2$  using the cyclopentadienone iron complex. Adapted from ref. 17 with permission from The Royal Society of Chemistry.

Production, storage and transportation of  $\text{H}_2$  are essential components for a future economy based on this high-energy fuel, thus  $\text{H}_2$  production from visible light-driven water splitting is considered a very important issue. In this field, the photochemical generation of  $\text{H}_2$  under visible light irradiation was successfully obtained by Na *et al.* with a three-component system, consisting of  $[\text{Ru}(\text{bpy})_3]^{2+}$ , a bio-inspired diiron dithiolate complex and EDTA, as electron donor in aqueous/organic media.<sup>21</sup> A robust photocatalytic system for proton reduction was obtained by McNamara *et al.* by mixing a mononuclear iron-based electrocatalyst with fluorescein (photosensitizer) and triethylamine (sacrificial donor). This system was very active, selective, and operated through a reductive quenching pathway.<sup>22</sup> Interesting results were also obtained by Dahrensbourg and Bengali, who proposed a mechanism of  $\text{H}_2$  release from amine-boranes by diiron complexes. In particular, compounds of structure  $(\mu-\text{SCH}_2\text{XCH}_2\text{S})\text{-}[\text{Fe}(\text{CO})_3]_2$  ( $\text{X} = \text{CH}_2, \text{CMe}_2, \text{CEt}_2, \text{NMe}, \text{NtBu}$ , and  $\text{NPh}$ ) were found to be effective photocatalysts for  $\text{H}_2$  release from solutions of amine-boranes in THF.<sup>23</sup>

Besides the reported examples, Fe complexes found also applications as visible-light-sensitive photoinitiators of polymerization processes, and as photocatalysts for controlled radical photopolymerizations.<sup>24</sup> The photochemical activation of iron complexes has attracted

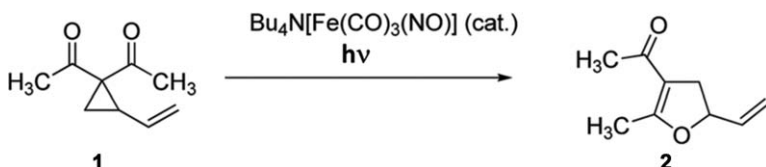


**Fig. 4** Cloke–Wilson rearrangement of vinyl cyclopropane using  $\text{Bu}_4\text{N}[\text{Fe}(\text{CO})_3(\text{NO})]$  as the catalyst.<sup>25</sup> Adapted from C. Lin, D. Pursley, J. E. M. N. Klein, J. Teske, J. A. Allen, F. Rami, A. Köhn and B. Plietker, *Chem. Sci.*, 2015, 6, 7034 – Published by The Royal Society of Chemistry.

significant interest in the field of organic synthesis. For instance, the  $\text{Bu}_4\text{N}[\text{Fe}(\text{CO})_3(\text{NO})]$  compound was found to catalyse the Cloke–Wilson rearrangement of aryl and vinyl cyclopropanes (**1** in Fig. 4) to give the corresponding aryl and vinyl dihydrafurans (**2** in Fig. 4), upon visible light irradiation (415 nm) at room temperature.<sup>25</sup>

Zanotti *et al.* reported for the first time the alkyne–thiocarbonyl migratory insertion in a bridging thiocarbonyl complex, *i.e.*  $[\text{Fe}_2(\text{CS})(\text{CO})_3(\text{Cp})_2]$ . The insertion, occurring under UV radiation, resulted in the formation of a peculiar bridging fragment,  $\text{S}=\text{C}-\text{CR}=\text{CR}$ , which could be further transformed by methylation of the S atom, followed by nucleophilic attack at the resulting thiocarbonyl group (Fig. 4). This is a promising approach to obtain new molecular fragments from the assembly of small molecular units on a diiron frame.<sup>26</sup>

High-valent Fe–oxo intermediates are active oxidants in enzymatic and synthetic catalytic oxidations. The Fe(IV)–oxo porphyrin radical cations, in particular, are intermediates in peroxidase and catalase enzymes as well as synthetic models. Depending on the electronic structure of the porphyrin ligand, Fe–oxo porphyrin radical cations or neutral Fe(IV)–oxo porphyrins can be obtained from bromate porphyrin–iron(III) salts under visible-light irradiation.<sup>27</sup> The oxidative reactivity of the photochemically generated Fe(IV)–oxo species, obtained from  $[\text{Fe}^{\text{II}}(\text{L})(\text{PY5Me}_2\text{-X})]^{2+}$  ( $\text{L} = \text{CH}_3\text{CN}$  or  $\text{H}_2\text{O}$ ) under blue light in the presence of  $[\text{Ru}(\text{bpy})_3]^{2+}$  and  $\text{K}_2\text{S}_2\text{O}_8$ , correlates with the electronic properties of the axial pyridine ligands. The Fe(IV)–oxo species are in fact capable of oxidizing (i) the C–H bonds of alkane and alcohol substrates *via* hydrogen atom transfer and (ii) an olefin substrate by oxygen atom transfer. However, even if the differences in reaction rates are relatively modest, the Fe(IV)–oxo derivatives with electron-poor axial ligands react faster than their counterparts containing electron-rich axial donors.<sup>28</sup>

Kondaiah and Chakravarty recently presented a series of ternary Fe(III) Schiff base complexes of vitamin B6, characterized by specific accumulation into cancer cells. These compounds, while inactive in the dark, exhibited remarkable photocytotoxicity under visible light irradiation. These studies also showed that cell death proceeded by the apoptotic pathway, due to the generation of ROS upon light exposure.<sup>29</sup>

The photoinduced CO release from half-sandwich Fe(II) carbonyl complexes,  $[\text{Fe}(\eta^5\text{-Cp})(\text{cis-CO})_2\text{X}]$  ( $\text{X}^- = \text{Cl}^-, \text{Br}^-, \text{I}^-$ ), can be induced by visible light irradiation. Liu *et al.* showed that CO release is significantly influenced by auxiliary ligands, and might involve the formation of an

intermediate species, *i.e.*  $\{\text{Fe}^{\text{II}}(\text{cis}-\text{CO})_2\}$ , by cyclopentadiene cleavage. The compounds showed good biocompatibility.<sup>30</sup>

### 2.3 Cobalt

Conventional Co-based catalysts (*e.g.* cobaloximes) are still widely applied in organic synthesis for the development of novel photocatalytic processes (*e.g.* in the oxidant-free aromatic C–H thiolation to construct C–S bonds).<sup>31</sup>

Co complexes as photocatalysts in CO<sub>2</sub>-to-CO conversion are frequently investigated, together with their Fe analogues, as in the studies by Schwalbe<sup>20</sup> and Lau.<sup>18</sup>

However, Co complexes have also attracted considerable attention, as highly active catalysts based on an earth-abundant metal, in the fields of oxygen reduction and hydrogen evolution reactions. For instance, a family of binuclear Co complexes based on a decadentate polypyridine ligand was applied by Llobet and Long in hydrogen evolution and oxygen reduction catalysis. These researchers have shown how small changes to the electronic and geometrical properties of the ligand might strongly influence the metal reactivity. In particular, a stable coordination environment, provided by the ligand in the coordination of Co in different oxidation states, has a crucial role in the performance of these complexes as photocatalysts.<sup>32</sup> Notably, a successful photocatalytic process was also achieved using Co-based complexes adsorbed on matrices. An example is the photocatalytic reduction of CO<sub>2</sub> to CO (and of H<sub>2</sub>O to H<sub>2</sub>) efficiently obtained with a Co(II) chlorin complex, as the reduction catalyst, adsorbed on multi-walled carbon nanotubes.<sup>33</sup>

Co-porphyrins are known to be active as water oxidation catalysts (WOCs), using  $[\text{Ru}(\text{bpy})_3]^{2+}$  as a photosensitizer and Na<sub>2</sub>S<sub>2</sub>O<sub>8</sub> as a sacrificial electron acceptor. In the series of Co-porphyrins synthesised by Sakai *et al.*, the modification of the aryl substituents on porphyrin rings was found to increase the stability of catalysts and change the water oxidation mechanism.<sup>34</sup>

Ott and Thapper investigated the  $[\text{Co}^{\text{II}}(\text{Py5OH})\text{Cl}](\text{BF}_4)$  complex as a catalyst for the photooxidation of water in the presence of m-CPBA, as the chemical oxidant.

These studies pointed out the role of the chloride ligand in preventing the formation of a binuclear Co(II) species, that would impede the catalytic turnover in wet CH<sub>3</sub>CN. A mechanism was proposed, in which the chloride ligand stays coordinated to the metal ion during catalysis, while one of the pyridine arms makes way for the substrate (see Fig. 5).<sup>35</sup>

Ding *et al.* proposed the mononuclear complex  $[\text{Co}^{\text{III}}(\text{DPK-OH})_2]\text{Cl}$ , as a stable WOC under visible light irradiation, using  $[\text{Ru}(\text{bpy})_3]^{2+}$  as photosensitizer and Na<sub>2</sub>S<sub>2</sub>O<sub>4</sub> as electron acceptor. Notably, the recorded turnover number, 1610, was the largest TON obtained for photocatalytic water oxidation with metal–organic complexes.<sup>36</sup> Even if cobalt complexes have been extensively studied as homogeneous WOCs for their remarkable performances, in some cases these complexes do not retain their integrity during catalysis. However, they can be alternatively employed as

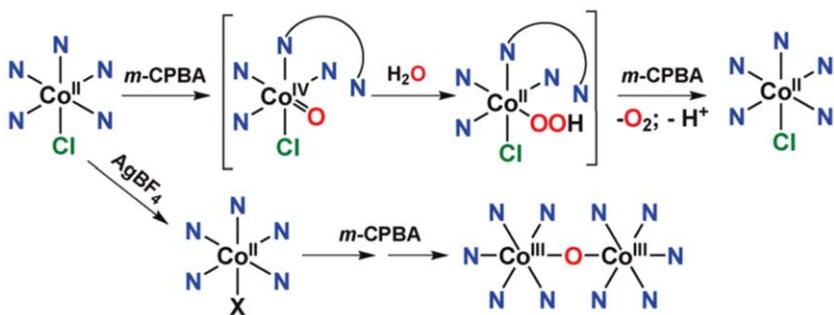


**Fig. 5** Mechanism proposed by Ott and Thapper for the photochemical oxidation of water and  $O_2$  evolution, using  $[\text{Co}^{\text{II}}(\text{Py5OH})\text{Cl}](\text{BF}_4)^-$  as the catalyst and m-CPBA, as the chemical oxidant. Reproduced from ref. 35 with permission from The Royal Society of Chemistry.

precursors of active heterogeneous WOCs. This is the case of the soluble dinuclear complex  $[(\text{TPA})\text{Co}^{\text{III}}(\mu\text{-OH})(\mu\text{-O}_2)\text{Co}^{\text{III}}(\text{TPA})](\text{ClO}_4)_3$  ( $\text{TPA} = \text{tris}(2\text{-pyridylmethyl})\text{-amine}$ ), which is not active as a WOC, but it decomposes in solution giving CoOx, which is the actual heterogeneous catalyst.<sup>37</sup>

A series of novel tetradentate ligands related to ppq ( $\text{ppq} = 8\text{-(1''},10''\text{-phenanthrol-2''-yl)-2-(pyrid-2'-yl)quinoline}$ ) and their corresponding Co(II) complexes have been synthesised. The light-driven  $H_2$ -evolving activity of these new complexes was investigated in aqueous solution under blue-light irradiation, with  $[\text{Ru}(\text{bpy})_3]^{2+}$  as the photosensitizer and ascorbic acid as a sacrificial electron donor. Studies suggested a catalytic pathway that involves the formation of Co(I)-aqua and Co(II)-H intermediates. Notably, an enhanced ligand rigidity favours the catalytic efficiency of these complexes.<sup>38</sup> A new class of tris(2-pyridylmethyl)-amine (TPMA) Co(II) complexes has been employed by Natali and Zonta, as  $H_2$  evolving photocatalysts, in the presence of  $[\text{Ru}(\text{bpy})_3]^{2+}$  and ascorbic acid (as the photosensitizer and the sacrificial electron donor, respectively).<sup>39</sup> The Authors showed that the introduction of different substituents at the catalyst periphery had little effect on the photocatalytic activity. However, good hydrogen-bonding groups (e.g. hydroxo), favouring the formation of a water network near the metal centre, were proven to accelerate the protonation step required in the  $H_2$ -evolving mechanism.

A perylene-Co(II) coordination polymer was recently coupled to reduced graphene oxide, *via* noncovalent interactions, to form a catalytically active composite for  $H_2$  evolving reactions (Fig. 6). The synergistic interactions between the two components promoted photocatalysis and enhanced the  $H_2$  yield in photoelectrochemical water splitting.<sup>40</sup>

Novel Bodipy dyes were used as photosensitizers for  $H_2$  photoevolution, in the presence of  $[\text{Co}^{\text{III}}(\text{dmgH})_2\text{pyCl}]$  ( $\text{dmgH} = \text{dimethylglyoximate}$ , py = pyridine) as the catalyst and triethanolamine as the sacrificial electron donor. These studies showed that only systems containing halogenated chromophores were active for  $H_2$  production; in fact, a long-lived triplet state was necessary for efficient bimolecular electron transfer.

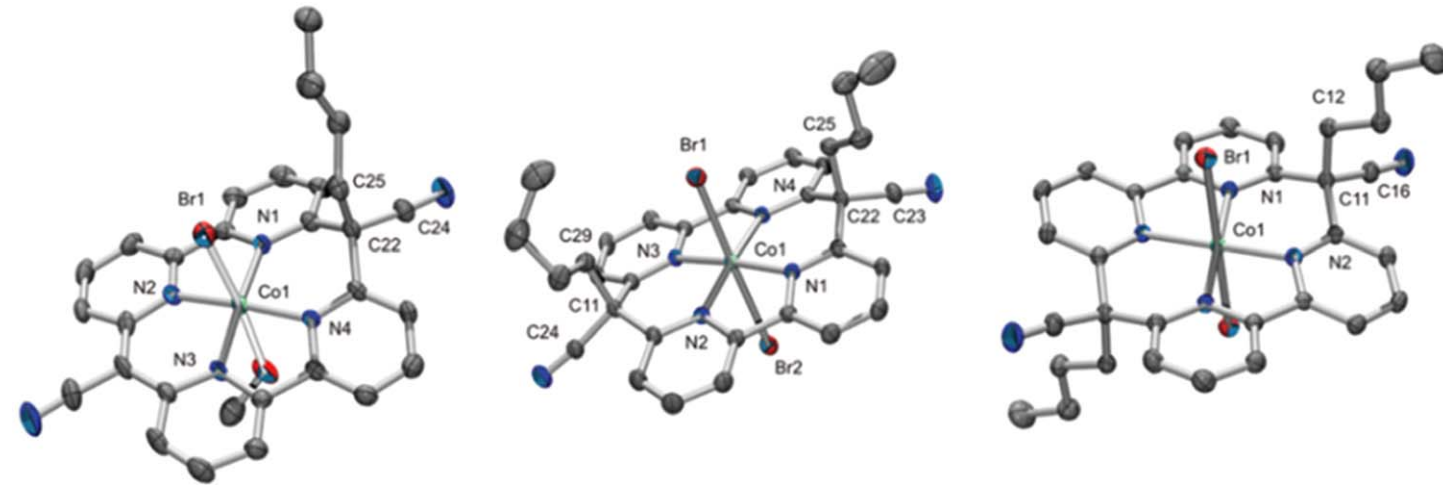


**Fig. 6** ORTEP representations for the novel Co(II) macrocyclic complexes investigated by the Alberto's group as proton reduction photocatalysts. Reproduced from ref. 42 with permission from The Royal Society of Chemistry.

Moreover, photostability was improved when the Bodipy dyes contained a mesityl group instead of phenyl, due to the electron donating properties of the former; notably, the obtained system was more active than Bodipy-Co(dmg)<sub>2</sub> linked dyads.<sup>41</sup> Co(II) complexes of pyridine-based macrocycles (see Fig. 6) were applied by the Alberto's group as catalysts in photocatalytic proton reduction processes.<sup>42</sup> The tetridentate macrocyclic ligands consisted in two 2,2'-bipyridine units linked twice by two cyano-methylene groups. The framework was modified by substituting the protons in the bridges with alkyl-chains. The corresponding Co(II) complexes enabled the efficient photoreduction of protons in aqueous solution, using [Ru(bpy)<sub>3</sub>]Cl<sub>2</sub> as a photosensitizer and TCEP/NaHasc as a sacrificial electron donor and shuttle (TONs, H<sub>2</sub>/Co ≤ 22 000).

Mindiola *et al.* reported a series of Co(II) complexes of a dianionic, bulky bis(pyrrolyl)pyridine pincer ligand. These compounds included an unusual azide adduct, consisting of an organic azide (N<sub>3</sub>Ad, Ad = 1-adamantyl) coordinated to the metal centre through the γ-N. The adduct photolysis resulted in N<sub>2</sub> extrusion and formation of the C–H insertion product, [(pyrppypyrrNHAd)Co].<sup>43</sup>

## 2.4 Nickel

A new strategy for accessing transient Ni(III) complexes through visible-light-mediated photoredox catalysis was developed by MacMillan *et al.* for the application in C–O cross-couplings. This method of modulating the transition metal oxidation state might be extended to other metal species in a series of challenging bond constructions.<sup>44</sup>

In 2015–2016, many examples were reported for the application of nickel complexes as catalysts in the photoreduction of protons to give H<sub>2</sub>. One of these catalysts is represented by the nickel bis-dithiocarbazate complex. Light-driven H<sub>2</sub> generation was obtained from this system (TON = 3300) in aqueous solution, with fluorescein as the photosensitizer and trimethylamine as the sacrificial donor.<sup>45</sup> A series of nickel bis-chelate complexes (containing *e.g.* 2-aminobenzenethiolate and 2-mercaptophenolate ligands) were found to be active photocatalysts for H<sub>2</sub> generation in water, using either fluorescein or CdSe quantum dots as the photosensitizers. Notable durability (>100 h) and overall photochemical stability were observed (TON ~ 6000).<sup>46</sup> For the photogeneration of H<sub>2</sub>, Kwong *et al.* investigated the metallosupramolecular triple-stranded helicate (Ni<sub>2</sub>L<sub>3</sub>, see Fig. 7) and tetrahedral cage (Ni<sub>4</sub>L<sub>6</sub>) complexes of bis-bidentate pyridine-based ligands (L).

These studies pointed out that the tetrahedral system was an active catalyst, while the helicate was not. This probably depended on the Ni<sup>II/III</sup> reduction of the tetrahedral complex, occurring at more negative potentials than in the other system.

Structural modifications of the ligand strands, in particular those of the bridging groups, were shown to affect the supramolecular architectures, as well as the redox potentials and the catalytic activities.<sup>47</sup>

The photogeneration of H<sub>2</sub> from HCl was obtained by Nocera *et al.* with the combination of a non-basic photoredox phosphine mediator and a Ni(II) trihalide catalyst. The phosphine mediator acted as a

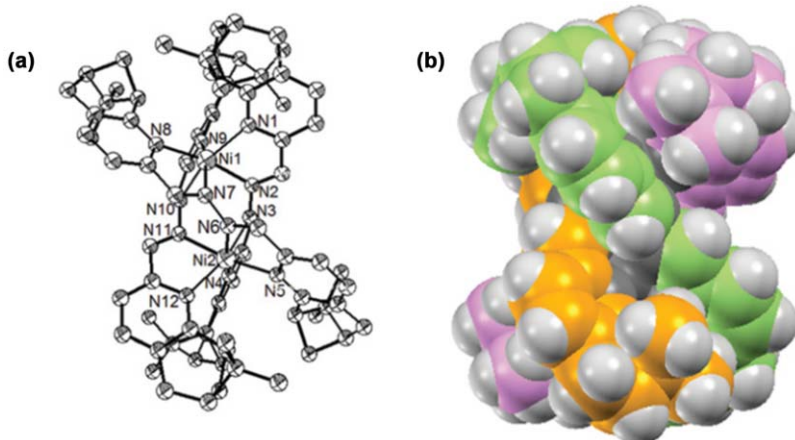


**Fig. 7** ORTEP representation (a) and space-filling model of the triple-stranded helicate  $[\text{Ni}_2\text{L}_3]^{4+}$  (b), applied by Kwong *et al.* for  $\text{H}_2$  photogeneration. Reproduced from ref. 47 with permission from The Royal Society of Chemistry.

photochemical H-atom donor to the Ni(II) complex, to deliver a Ni(I) centre. The catalytic cycle was closed by the sequential disproportionation of Ni(I) to Ni(0) and Ni(II), and the protolytic  $\text{H}_2$  evolution from the Ni(0) intermediate.<sup>48</sup> HX-splitting photocycles frequently require chemical traps to promote halogen extrusion. However, these traps inevitably reduce the utility of these processes in energy-storing catalysis. Nocera recently proposed an example of trap-free halogen photoelimination, based on mononuclear Ni(III) trihalide complexes supported by bidentate phosphine ligands. Studies in both solution and the solid state showed that the complexes participated in a clean halogen photoelimination. The process involved the formation of a Ni(II) complex as a photo-intermediate, in which the photoextruded chlorine radical interacted with the ligand. This step, involving the secondary coordination sphere, guided the halogen atom out of the primary coordination sphere, thus suppressing energetically favoured back-reactions.<sup>49</sup>

Benzene C–H activation was recently achieved using a photoactivated Ni(II)-azide complex,  $[\text{Ni}(\text{N}_3)(\text{PNP})]$  ( $\text{PNP} = 2,2'\text{-di(isopropylphosphino)-4,4'-ditolylamine}$ ).

Upon irradiation, this complex generated a nickel nitrido, that was efficiently trapped by insertion of the nitrogen into a Ni–P bond. The obtained coordinatively unsaturated Ni(II) imidophosphorane displayed an unprecedented reactivity toward the 1,2-addition of a C–H bond. As a consequence, the C–H activation of benzene occurred and the activated phenyl fragment was incorporated in the final complex.<sup>50</sup>

## 2.5 Copper

Cu-based complexes find application as photocatalysts in organic synthesis, such as in the preparation of poly-aromatic carbocycles. In this context, the heteroleptic Cu-based sensitizers, containing both bis-phosphine and diamine ligands, are promising photocatalysts with tuning

properties. Structural modifications of either bisphosphines or diamine ligands strongly influence the excited state oxidation/reduction potentials and optical absorbance.<sup>51</sup> Copper complexes, with the metal in both +1 and +2 oxidation states, have been recently applied for solar hydrogen production. The Cu(II) species [Cu(TMPA)Cl]Cl and [Cu(Cl-TMPA)Cl<sub>2</sub>] [TMPA = tris(2-pyridyl)methylamine; Cl-TMPA = 1-(6-chloropyridin-2-yl)-methyl-N,N-bis(pyridin-2-ylmethyl)methane-amine], for instance, represent the first examples of photocatalytic copper complex-based water reduction catalysts, exhibiting efficient photocatalytic H<sub>2</sub> evolution in aqueous mixture, with an Ir complex as the photosensitizer and triethylamine as the sacrificial reductant.

The higher photocatalytic activity of [Cu(Cl-TMPA)Cl<sub>2</sub>] compared to [Cu(TMPA)Cl]Cl was attributed to the peculiar features of the Cl-substituted ligand, acting at the same time as a mono-dentate ligand dissociation trigger, a proton relay and an electron relay.<sup>52</sup> Low cost Cu(I) cysteine complexes, obtained from Cu(II) and cysteine in aqueous solution, were found to greatly enhance the activity of CdSe photocatalysts for H<sub>2</sub>-production in water under visible light irradiation: the H<sub>2</sub>-production rate was actually increased by 150 times. Cu(I) cysteine played several roles, serving as a hole consumption co-catalyst, and suppressing electron-hole pair recombination in CdSe after photoexcitation. Notably, these low cost complexes could be also applied in other H<sub>2</sub>-production photocatalytic systems, in cooperation with proton reduction co-catalysts, e.g. Pt.<sup>53</sup> Copper complexes, such as copper tetrasulfonatophthalocyanine (CuPcTS), were also investigated as water oxidation photocatalysts (WOCs). The process, following a radical coupling mechanism, was found to be kinetically inhibited by chloride anions. Chloride, in fact, efficiently binds the axial position of CuPcTS, preventing the formation of the oxyl or hydroxyl intermediates.<sup>54</sup> Copper complexes have been also applied as catalysts in photocatalysed click reactions, visible-light-mediated atom transfer radical additions and allylation reactions. In particular, Mignard and Vincent recently applied the fluoro-surfactant, photoreducible complex [Cu<sup>II</sup>(trenRf)<sub>3</sub>-benzoylbenzoate]<sub>3</sub>-benzoylbenzoate as a catalyst in the Cu(I)-catalyzed alkyne-azide cycloadditions. The advantages of the proposed system were the following: (i) the catalytic reaction took place at the liquid/liquid interfaces (e.g. fluorous or organic phase/water); (ii) sodium ascorbate could be avoided; (iii) the purification from copper could be easily obtained by decantation.<sup>55</sup>

The Reiser's group recently proposed a family of heteroleptic Cu(I), [Cu(phenanthroline)-(bisisonitrile)]<sup>+</sup>, complexes as photoredox-catalysts in both visible-light-mediated atom transfer radical addition (ATRA) and allylation reactions. [Cu(dpp)(binc)]BF<sub>4</sub> (dpp = 2,9-diphenyl-1,10-phenanthroline; binc = bis(2-isocyanophenyl) phenylphosphonate), in particular, showed a high activity due to its enhanced excited-state lifetime compared to commonly employed, related, complexes.<sup>56</sup>

Cu-dioxygen intermediates have a key role in many chemical and biological processes. In the study by Karlin and Fukuzumi, the photo-excitation of the *trans*-μ-1,2-peroxo dicopper(II) complex, [(tmpa)<sub>2</sub>Cu<sup>II</sup><sub>2</sub>(O<sub>2</sub>)]<sup>2+</sup>, and of the side-one μ-η<sup>2</sup>:η<sup>2</sup>-peroxodicopper(II) species,

$[(N_5)Cu^{II}O_2]^{2+}$  and  $[(N_3)Cu^{II}O_2]^{2+}$ , at  $-80^\circ C$  in acetone, led to the one-photon two-electron peroxide-to-dioxygen oxidation. Notably, for the side-on complexes, photoexcitation brought about dioxygen release, whereas for the end-on species it did not. Spectroscopic studies pointed out that the reactions proceeded through a mixed-valent superoxide intermediate  $[Cu^{II}(O_2\cdot^-)Cu^{I}]^{2+}$  for all the complexes. However, for the end-on species, the intermediate underwent a fast intramolecular electron transfer, leading to an “O<sub>2</sub>-caged” dicopper(I) adduct, followed by a barrier-less stepwise back electron transfer to give the initial complex. For the side-on species, on the contrary, the intermediates underwent O<sub>2</sub> release. The different pathways probably resulted from a higher stability of the side-on species *vs.* the end-on one. The results reported by Karlin and Fukuzumi have both a biological relevance and a potential impact on the solar water splitting process.<sup>57</sup>

## 2.6 Vanadium, chromium, zinc and other first-row metals

Hirao and Soo obtained the selective photocatalytic cleavage of C–C bonds, under ambient conditions, using earth abundant vanadium complexes. In particular, the V(v)-oxo complex of a redox non-innocent salicylaldimine ligand acted as a photocatalyst in the cleavage of lignin model compounds under ambient conditions and visible light irradiation ( $>420$  nm). This mild and eco-friendly approach could find interesting applications in organic transformations and biomass valorisation.<sup>58</sup>

Ferreira and Shores reported, for the first time, Cr(III) complexes as photocatalysts in organic synthesis. The Authors, in particular, investigated selected Cr(III) complexes as reactive oxidizing alternatives to photocatalysts based on second-row metals, *e.g.* ruthenium. These studies brought about the discovery of photooxidizing chromium-catalyzed Diels–Alder cycloadditions *via* radical cation intermediates. The complexes chosen by the Authors showed, in fact, sufficiently long-lived excited states to oxidize electron-rich alkenes, initiating [4 + 2] cycloadditions. Notably, molecular oxygen was required for the reaction to occur.<sup>59</sup> Further studies elucidated the roles of oxygen in the process. According to the mechanism proposed, oxygen first quenches the Cr<sup>3+\*</sup> excited complex, producing singlet oxygen while protecting the catalyst from decomposition. In a second step, singlet oxygen returns the reduced catalyst to the Cr(III) ground state and produces superoxide. In the last step, superoxide reduces the Diels–Alder cyclo-adduct radical cation to the final product and reforms oxygen.<sup>60</sup> In biological and environmental processes, the importance of reactive oxygen species (*e.g.* singlet oxygen) production is already well established.

The Dabrowski’s group recently proposed the Zn(II) and Co(III) complexes of 5,10,15,20-tetrakis(2,6-difluoro-5-Nmethylsulfamylphenyl)porphyrin, as efficient photosensitizers for singlet oxygen production and as photocatalysts for the degradation of organic pollutants (see Fig. 8). In the case of the Zn(II) complex, ZnF<sub>2</sub>PMet, the mechanism of singlet oxygen generation involved an energy transfer process from the triplet excited state of the complex to the oxygen molecule. The Authors also

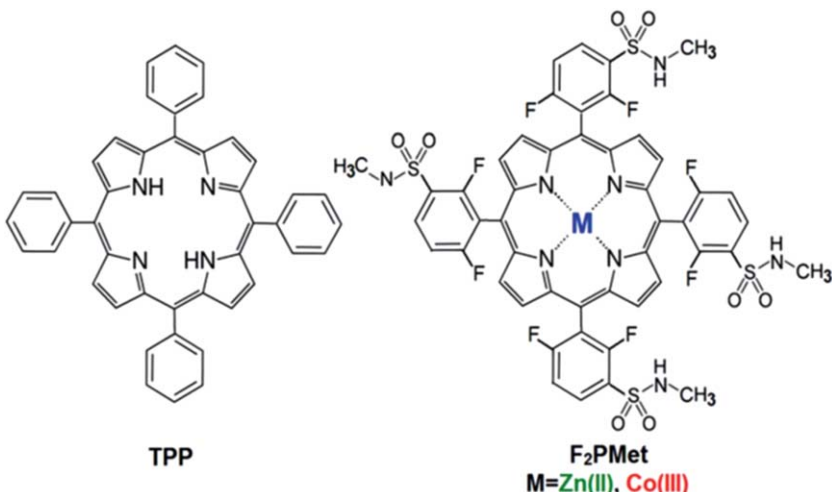


**Fig. 8** Chemical structures of TPP and metal (M) complexes of F<sub>2</sub>PMet. Reproduced from ref. 61 with permission from The Royal Society of Chemistry.

proposed the hybrid composite material, ZnF<sub>2</sub>PMet@TiO<sub>2</sub>, for the efficient degradation of organic pollutants under visible light irradiation. Due to its good photostability and photoactivity, this composite material may find also application in medicine, as a PDT agent, or for the photoinactivation of microorganisms and bacterial cells.<sup>61</sup>

### 3 Second- and third-row transition metals

#### 3.1 Ruthenium

**3.1.1 Advances in photocatalysis.** Ru-complexes find application as photosensitizers in many processes, *e.g.* CO<sub>2</sub> photoreduction<sup>62</sup> and H<sub>2</sub> photogeneration. Some examples have been already reported in this chapter.<sup>20,21</sup>

Recent advances in the application of Ru complexes in the photochemical reduction of CO<sub>2</sub> were presented by Ishida *et al.* The Authors synthesized a series of *trans*-(Cl)-[Ru(bpy)(CO)<sub>2</sub>Cl<sub>2</sub>]-type complexes, containing amide groups at the 5,5'-positions of the bpy ligands, by using a modified synthetic procedure. CO<sub>2</sub> photoreduction studies revealed that the total turnover frequency (TOF) was greatly affected by the substituents on the bpy. Moreover, the TOFs for CO and formate increased exponentially as the reduction potential shifted to the negative side. These results could prove useful to predict the catalytic activity of novel Ru-based catalysts.<sup>63</sup> Interesting results in the context of CO<sub>2</sub> photoreduction were obtained by Kitagawa *et al.* with a novel Zr(IV)-based porous coordination polymer, bearing the [Ru<sup>II</sup>(bpy)(tpy)(CO)](PF<sub>6</sub>)<sub>2</sub> complex as a metallo-linker. Porous coordination polymers, also known as MOFs, are a class of porous heterogeneous catalysts with highly tailorable features. The new composite turned out to be both a good CO<sub>2</sub> adsorbent and a reduction catalyst. High catalytic activity was obtained

even under low CO<sub>2</sub> concentrations, with a different product selectivity compared to the homogeneous counterpart.<sup>64</sup> Among heterogeneous photocatalysts for CO<sub>2</sub> reduction, the hybrid materials by Maeda *et al.* are worth mentioning. In particular, the hybrids consisting of carbon nitride (C<sub>3</sub>N<sub>4</sub>) and mononuclear Ru(II) complexes, *e.g.* *trans*(Cl)-[Ru(X<sub>2</sub>bpy)(CO)<sub>2</sub>Cl<sub>2</sub>] (X = COOH, PO<sub>3</sub>H<sub>2</sub>, or CH<sub>2</sub>PO<sub>3</sub>H<sub>2</sub> in the 4-positions), allowed for the photocatalytic reduction of CO<sub>2</sub> to CO and HCOOH, under visible light irradiation. Interestingly, CO/HCOOH selectivity was found to increase, when solvents with a relatively high donor number were employed (*e.g.* DMA, DMF, and DMSO) and when the electron injection efficiency from the conduction band of C<sub>3</sub>N<sub>4</sub> to the Ru(II) complex was low.<sup>65</sup> A high selectivity for HCOOH production (>99%) in DMA was obtained by the same Authors with a hybrid material consisting of CaTaO<sub>2</sub>N (a perovskite oxy-nitride semiconductor, with a band gap of 2.5 eV) and a binuclear Ru(II) complex. HCOOH was produced *via* catalytic CO<sub>2</sub> photoreduction under visible light. The reaction was driven according to the two-step photoexcitation of CaTaO<sub>2</sub>N and the Ru photosensitizer. The modification of CaTaO<sub>2</sub>N with Ag nanoparticles, with optimal distribution, was essential to mediate the interfacial electron transfer from the conduction band of CaTaO<sub>2</sub>N to the binuclear Ru(II) complex.<sup>66</sup> The selective reduction of CO<sub>2</sub> to HCOOH was also obtained, under visible light in aqueous solution, with a hybrid consisting of carbon nitride, modified with Ag nanoparticles and a Ru(II) binuclear complex (RuRu'). In the presence proper electron donors, the RuRu'/Ag/C<sub>3</sub>N<sub>4</sub> hybrid photocatalyst exhibited a very high turnover number (>33 000 with respect to the amount of RuRu') and a high selectivity for HCOOH production (87–99%). Notably, the obtained turnover number was 30 times greater than that obtained with the C<sub>3</sub>N<sub>4</sub>/mononuclear Ru(II)-complex hybrid and, according to the Authors, this was also “the highest among the metal-complex/semiconductor hybrid systems reported”.<sup>67</sup> Ishitani and Maeda also developed a new Z-scheme photocatalyst, consisting of a semiconductor material (*i.e.* yttrium–tantalum oxynitride) and a binuclear Ru(II) complex. The highly selective (>99%) photoreduction of CO<sub>2</sub> to HCOOH was obtained with these systems at room temperature in a DMA:TEOA mixture (4 : 1 v/v).<sup>68</sup>

The Ru(III) complex [Ru<sup>III</sup>(edta)]<sup>−</sup> was found to catalyse the conversion of bicarbonate to formate over non-metal (*i.e.* carbon, nitrogen and sulfur) doped TiO<sub>2</sub> semiconductor photocatalyst particles, under visible-light irradiation. The mechanism involved the activation of bicarbonate, through coordination to the metal centre, followed by the photochemical reduction of the substrate to give formate at the surface of the semiconductor particles. Notably, the process efficacy decreased along the order C-TiO<sub>2</sub>>N-TiO<sub>2</sub>>S-TiO<sub>2</sub>.<sup>69</sup>

Ru complexes, in particular [Ru(bpy)<sub>3</sub>]<sup>2+</sup>, find application as photosensitizers in many H<sub>2</sub> photogeneration processes.<sup>21</sup> However, the design of Ru(II) complexes with red-shifted absorption is still a challenge. Hanan and Marvaud synthesised a Ru(II) quaterpyridine complex, characterized by a high quantum yield, a long excited-state lifetime and an extended absorption in the visible region. These features made this species an

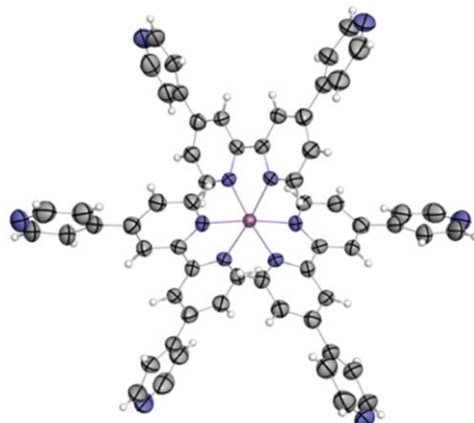


**Fig. 9** ORTEP view of  $[\text{Ru}(\text{qpy})_3]^{2+}$  complex, synthesised and applied by Hanan and Marvaud as a photosensitizer in  $\text{H}_2$ -evolution reactions. Reproduced from ref. 70 with permission from The Royal Society of Chemistry.

excellent candidate as a photosensitizer in artificial photosynthetic systems.  $[\text{Ru}(\text{qpy})_3]^{2+}$  (see Fig. 9), in particular, showed better photophysical properties than  $[\text{Ru}(\text{bpy})_3]^{2+}$ , and an excellent activity as photosensitizer in  $\text{H}_2$ -evolution reactions.<sup>70</sup>

Monomeric Ru(II) complexes, based on substituted pyridine and bpy ligands, found also applications as water oxidation photocatalysts.<sup>71</sup> Recent studies in the field were performed by Murata *et al.*<sup>72</sup> The stabilisation of the metal centre, in a variety of different redox states, is of fundamental importance in the design of new catalysts for the multi-electron oxidation of  $\text{H}_2\text{O}$ . In order to obtain an efficient  $\text{H}_2\text{O}$  oxidation photocatalyst, Åkermark *et al.* appropriately designed the ligand scaffold in order to stabilize the Ru centres of a binuclear Ru complex in the high oxidation states. This approach was actually successful, and the obtained system could promote both chemical and photochemical  $\text{H}_2\text{O}$  oxidations with mild one-electron oxidants.<sup>73</sup>

Sakai and Brudvig recently reported the first example of light-induced water oxidation, catalysed by a  $\mu$ -oxido-bridged Ru–O–Ru–O–Ru trinuclear complex. Water oxidation was obtained with the photocatalyst in aqueous borate buffer at pH 8, in the presence of  $[\text{Ru}(\text{bpy})_3]^{2+}/\text{S}_2\text{O}_8^{2-}$ . The trinuclear complex was found to be stable all over the course of the catalytic process.<sup>74</sup> Efficient photoinduced water oxidation was obtained by Llobet *et al.*, at neutral pH in a RuPS– $\text{S}_2\text{O}_8^{2-}$  type system, using novel diruthenium complexes based on the 4-methylbis(bipyridyl)pyrazolate ligandas the photocatalysts. Heterogenization strategies, aimed at anchoring the catalysts onto metal oxide surfaces to obtain a photo-anode, are likewise under investigation.<sup>75</sup>

In this context, visible light-driven WO was obtained by Imahori and Sun, using a covalently-linked molecular catalyst–sensitizer dyad assembled on a  $\text{TiO}_2$  electrode (Fig. 10).

The dyad consisted into a porphyrin unit (photosensitizer), covalently bound to a Ru(II) complex (water oxidation catalyst). The performance

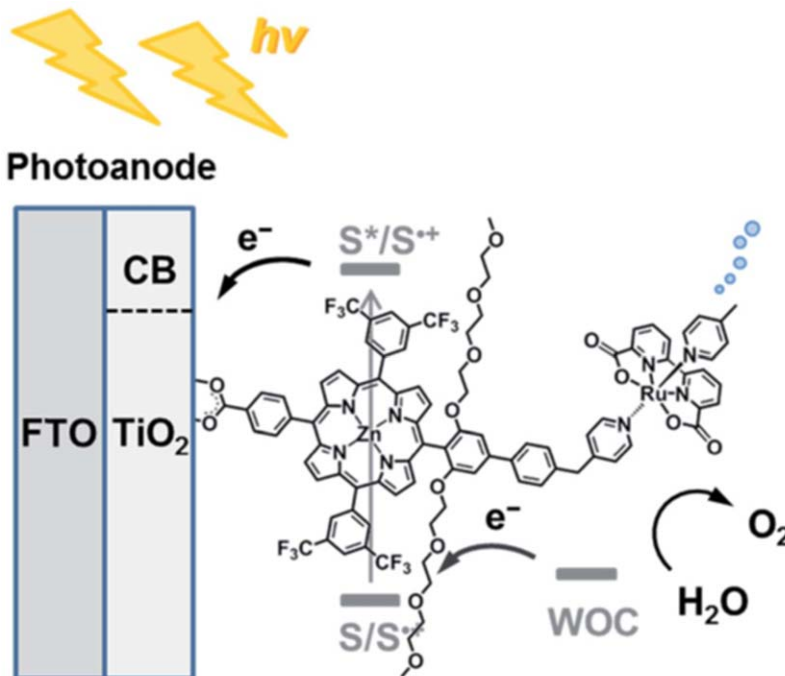


**Fig. 10** Schematic diagram of visible light-driven water oxidation using TiO<sub>2</sub> functionalized with a ruthenium WOC–porphyrin linked dyad as the photoanode. Reproduced from ref. 76 with permission from The Royal Society of Chemistry.

was better than that obtained with co-adsorption of individual Ru-complex and Zn-porphyrin (ZnP) as well as with ZnP alone. This result showed up the advantage of the covalent linking approach over the non-covalent one.<sup>76</sup> A reduced graphene oxide-immobilized tris(bipyridine)-ruthenium(II) complex (*i.e.* [Ru(bpy)<sub>3</sub>]-rGO) was successfully applied as a heterogeneous catalyst in visible-light-driven reductive dehalogenation reactions. This system is easily recyclable and works under mild conditions, showing a comparable reactivity to homogeneous [Ru(bpy)<sub>3</sub>]Cl<sub>2</sub>. Its successful performance was attributed by the Authors to the bi-dimensional sheet-like structure, which diminishes the diffusion resistance of reactants.<sup>77</sup>

A Ru-based trinuclear cluster photocatalyst was employed in the photocatalytic oxygenation of sulfide and alkenes in neutral water. The reaction occurred under visible light and in the presence of [Co(NH<sub>3</sub>)<sub>5</sub>Cl]Cl<sub>2</sub>, as an electron acceptor. The trinuclear cluster contained two Ru(II) photosensitizers and one Ru(II) reaction centre. The presence of two dicationic photoredox units enabled the formation of the reactive Ru<sup>V=O</sup> intermediate at relatively low potential.<sup>78</sup>

**3.1.2 Photoreactivity of Ru-based complexes.** Under visible light irradiation, Ru complexes may undergo photochemical processes, such as those involving the substitution of ligands with solvent molecules. The Alary's group recently investigated the mechanism of methylthioethanol

(Hmte) photocleavage for the complexes  $[\text{Ru}(\text{tpy})(\text{N}^{\wedge}\text{N})(\text{Hmte})]^{2+}$  ( $\text{N}^{\wedge}\text{N} = \text{bpy}$ , 2,2'-biquinoline, *etc.*) through density functional theory. This study highlighted the existence of several different mechanistic schemes. In particular, the population of a pentacoordinate  ${}^3\text{MC}$  photo-reactive intermediate, more accessible for solvent attack, seemed to give a strong contribution to the photosubstitution quantum yield.<sup>79</sup> In the case of the triazole-containing complex  $[\text{Ru}(\text{pytz})-(\text{btz})_2]^{2+}$  [ $\text{pytz} = 1\text{-benzyl-4-(pyrid-2-yl)-1,2,3-triazole}$ ,  $\text{btz} = 1,1'\text{-dibenzyl-4,4'-bi-1,2,3-triazolyl}$ ], studied by Elliott *et al.*, photoreactivity was increased by the proximity in energy of  ${}^3\text{MLCT}$  and  ${}^3\text{MC}$  states. The population of the  ${}^3\text{MC}$  state actually favoured the photochemical reactivity of the complex and, in particular, the light-activated ligand ejection.<sup>80</sup> Chemical bonds activation through external triggers (*e.g.* light) may lead to new molecules with catalytic and switchable functions. Sarkar *et al.* prepared a series of Ru( $\text{n}$ ) complexes of formula  $[\text{Ru}(\text{bident})(\text{tripod})]^{2+}$  (bident, tripod = bidentate and tripodal ligand, respectively), characterised by different numbers of pyridine/triazole groups on the ligands. The Authors demonstrated that the stepwise substitution of pyridine with “click” triazoles had a significant effect on both the thermo- and photoreactivity of the complexes. In particular, in complexes featuring neither steric interactions nor axial triazoles, reactivity was suppressed.<sup>81</sup> In the case of the  $[\text{Ru}(\text{L})(\text{Cl})(\text{X})]^+$  complexes ( $\text{X} = \text{DMSO}$ ,  $\text{PPh}_3$ , or  $\text{CH}_3\text{CN}$ ), containing different numbers of py/triazole arms on the tripodal ligand L, Sarkar *et al.* showed again that py/triazole substitution as well as substituents at triazoles affected both Ru( $\text{n}$ )/Ru( $\text{m}$ ) oxidation potentials and photoreactivity. In the catalytic oxygenation of alkanes (*e.g.* from cyclooctane to cyclooctanone with MCPBA), in particular, yields increased with the number of triazole arms, in both DMSO and  $\text{PPh}_3$  containing complexes. This result was attributed to a higher stability of the triazole-rich complexes towards degradation, and demonstrates that “click-derived ligands can be tuned on demand for catalytic processes”.<sup>82</sup> The addition of steric bulk may accelerate photochemical ligand dissociation. This was observed by Kodanko and Turro in a series of Ru-caged nitrile complexes of the ligand TPA [*i.e.* tris(2-pyridylmethyl)amine], where steric effects were shown to accelerate the photochemical dissociation of the nitrile donors.<sup>83</sup>

The photochemistry of novel diruthenium oxyanion complexes was investigated by Berry *et al.*  $\text{Ru}_2(\text{chp})_4\text{ONO}_2$  (chp = 6-chloro-2-hydroxy-pyridinate), for instance, was found to release  $\text{NO}_2\cdot$  upon photolysis, leading to the metal oxo intermediate  $[\text{Ru}_2(\text{chp})_4\text{O}]^+$ . In the presence of excess  $\text{PPh}_3$ , the process yielded  $\text{OPPh}_3$  by oxygen atom transfer.<sup>84</sup> Novel diruthenium tetrahydride complexes, containing cyclopentadienyls as auxiliary ligands, were studied by Takao *et al.* with the aim of clarifying the reaction mode of polyhydride-bridged complexes. The diruthenium tetrahydride species reacted with tetrahydrofuran under UV irradiation, leading to peculiar bridging cyclic Fischer-type carbene complexes, *via* consecutive hydrogen abstraction from the coordinated tetrahydrofuran. The cyclic structures of the bridging carbene ligands were determined by X-ray diffraction studies.<sup>85</sup>

### 3.1.3 Application of photoreactive Ru-based complexes in medicine.

Photoactivated chemotherapy is a cancer treatment that uses activation by light. In this context, Ru(II) complexes are of great interest because of their ability to undergo both photoinduced ligand exchange and  $^1\text{O}_2$  generation upon visible-light irradiation. As a consequence, the photorelease of drugs can be coupled to the activity of singlet oxygen, thus efficiently promoting cell death *via* two different mechanisms (*i.e.* dual photoreactivity).<sup>86</sup> In 2015–2016, new Ru-based complexes have been synthesized and studied as potential photosensitizers in photodynamic therapy (PDT), such as the pincer-like Ru(II)-complexes developed by Tabrizi and Chiniforoshan.<sup>87</sup> Among chemotherapy agents with long photoactivation wavelengths, Zhou and Wang recently proposed a series of Ru(arene) complexes,  $[(\eta^6-p\text{-cymene})\text{Ru}(\text{dpb})(\text{py-R})]^{2+}$  ( $\text{dpb} = 2,3\text{-bis}(2\text{-pyridyl})\text{benzoquinoxaline}$ ,  $\text{py-R} = 4\text{-substituted pyridine}$ ,  $\text{R} = \text{N}(\text{CH}_3)_2$ ,  $\text{NH}_2$ ,  $\text{OCH}_3$ ,  $\text{H}$ ,  $\text{COOCH}_3$  and  $\text{NO}_2$ ). By varying the push/pull properties of the group at the 4-position of pyridine (*i.e.* R), the Authors could tune the photoinduced ligand dissociation and  $^1\text{O}_2$  generation, as well as the DNA photobinding and photocleavage capabilities of the complexes. These results depend on the substituents' effects on the energy levels of  $^3\text{MC}$  and  $^3\text{MLCT}$  excited states, as well as on the energy gaps between  $^3\text{MC}$ ,  $^3\text{MLCT}$  and dpb-based states. The highest phototoxicity against human lung carcinoma A-549 cells was obtained for  $\text{R} = \text{H}$ .<sup>88</sup> Another promising complex,  $[\text{Ru}(\text{pydppn})(\text{biq})(\text{py})]^{2+}$  ( $\text{pydppn} = 3\text{-}(p\text{-pyrid-2-yl})\text{benzo}[i]\text{dipyrido}[3,2-a:2',3'-c]\text{phenazine}$ ;  $\text{biq} = 2,2'\text{-biquinoline}$ ;  $\text{py} = \text{pyridine}$ ), was synthesised by Turro *et al.*. This species acted as a dual action photochemotherapy agent, releasing py and producing  $^1\text{O}_2$  under irradiation. Transient absorption data revealed that the  $^3\text{MLCT}$  state of  $[\text{Ru}(\text{pydppn})(\text{biq})(\text{py})]^{2+}$  is characterised by a shorter lifetime and a lower quantum yield for ligand exchange, as compared to the model complex  $[\text{Ru}(\text{tpy})(\text{biq})(\text{py})]^{2+}$ . The difference between these two structurally similar complexes may be attributed to the existence of a second deactivation pathway, in the case of  $[\text{Ru}(\text{pydppn})(\text{biq})(\text{py})]^{2+}$ , involving the long-lived  $^3\pi-\pi^*$  state, and consequently to the competitive population of  $^3\text{LF}$  states (involved in the ligand dissociation).<sup>89</sup>

The DNA-binding properties of Ru(II) complexes have gained interest in relation to anticancer drugs, DNA structural probes and sequence-specific DNA cleaving agents.<sup>90</sup> The dinuclear Ru(II) polypyridyl complexes with bridging alkyl linkers, reported by Wang *et al.*, partially intercalate between the base pairs of DNA and enter HeLa cells efficiently, localizing within lysosomes. The lengths of the alkyl linkers tune the biological properties of these dinuclear complexes. The inhibition of HeLa cell proliferation was observed under these conditions, and this was attributed to the combination of the induction of apoptosis and cell cycle arrest.<sup>91</sup> On the other hand, in the case of the photoreactive  $[\text{Ru}(\text{TAP})_2(\text{phen})]^{2+}$  complex conjugated to the TAT peptide, efficient vectorization inside HeLa cells was obtained without phototoxicity.

The TAT peptide, in fact, was found to transport the Ru complex mainly into vesicles and cytoplasm, thus far enough from the DNA or RNA targets. As a consequence, 100% cellular survival was observed.<sup>92</sup>

### 3.2 Rhodium

In seeking novel efficient supramolecular photocatalysts for H<sub>2</sub> generation, Ru(II)-Rh(III) polynuclear systems were investigated by several Authors.<sup>93</sup> A trinuclear Ru(II)-Rh(III)-Ru(II) complex was synthesized by Rogers *et al.* as a new photocatalyst for H<sub>2</sub>O reduction to H<sub>2</sub>. This system, containing hydroxide labile ligands at the Rh(III) centre, was proved to be more active than the halide analogues in different solvents (*i.e.* DMF, CH<sub>3</sub>CN, and H<sub>2</sub>O). As a matter of fact, the formation of ion pairs between halides and the complex, as it cycles from Rh(III)/(II)/(I), was found to prevent the interaction of the photocatalyst with the H<sub>2</sub>O substrate, thus negatively affecting the H<sub>2</sub> production yield.<sup>94</sup> The 5,10,15,20-tetrakis(4-methoxyphenyl)porphyrin rhodium iodide, (TAP)Rh-I, complex was proved to catalyse the visible-light-driven hydrolysis of silanes into silanols and H<sub>2</sub> under mild conditions. (TAP)Rh-H was shown to be a key intermediate, obtained through activation of the Si-H bond by (TAP)Rh-I. The addition of water provides a novel pathway, converting the stoichiometric Si-H activation into catalysis.<sup>95</sup>

Rh-based complexes have been also applied in organic synthesis. Meggers *et al.*, for example, successfully applied a chiral bis-cyclometalated rhodium complex as a photoredox catalyst in the enantioselective addition of alkyl radicals to alkenes under visible light irradiation (99% ee).<sup>96</sup> The new Rh(I) silyl carbonyl complex, [Rh{Si(OEt)<sub>3</sub>}](CO)(dippe)] (dippe = 1,2-bis-(diisopropylphosphino)ethane), reported by Braun *et al.* was found to react with fluorinated aromatic compounds under irradiation, leading to the corresponding C-F and C-H activation products.<sup>96,97</sup>

### 3.3 Rhenium

The photochemical reactions of common Re-based compounds, *e.g.* photochemical ligand substitution in fac-rhenium(I) tricarbonyl complexes, are still of interest for their applications in synthesis.<sup>98</sup> In 2015–2016 new mono-, bi- and hetero-nuclear Re complexes have been proposed for the photocatalytic reduction of CO<sub>2</sub>.<sup>99</sup> Selective and efficient photochemical conversion of CO<sub>2</sub> into CO was obtained by Robert and Ko, using N,O and N,S-NHC-containing dicarbonyl Re(I) bipyridine systems.<sup>100</sup> In particular, the replacement of one CO ligand with a weaker π-accepting ligand in tricarbonyl Re(I) complexes was proved to be a successful strategy for catalysing CO<sub>2</sub> reduction through low-energy visible light. Among mononuclear Re(I) photocatalysts, studies on the photocatalytic mechanism of CO<sub>2</sub> reduction were performed by Farrokhpour *et al.* with the fac-[Re(phendione)(CO)<sub>3</sub>Cl] complex.<sup>101</sup>

Among binuclear systems, Ishitani *et al.* recently proposed binuclear Re(I) diimine tricarbonyl photocatalysts for the photochemical reduction of CO<sub>2</sub> in the presence a Ru(II) tris-diimine complex as photosensitizer.<sup>62</sup> Dinuclear Re(I) complexes, containing diimine ligands connected through alkyl chains of various lengths, exhibited improved durability compared to systems based on the corresponding mononuclear species. A greater durability was, in particular, obtained using shorter alkyl chains

in the bridging ligands. Ishitani also proposed a supramolecular Ir-Re heteronuclear photocatalyst, showing a higher photocatalytic activity compared to the corresponding mixed system of mononuclear complexes. BNAH was used as the reductant.<sup>102</sup>

In the literature, there are only few examples of heteronuclear complexes combining a Re(i) bipyridine tricarbonyl unit with a porphyrin. In 2015, George and Perutz reported novel zinc porphyrin-Re bipyridine tricarbonyl dyads, active for the photocatalytic reduction of CO<sub>2</sub> to CO upon visible light (>520 nm) irradiation (see the example reported in Fig. 11).<sup>103</sup> The photoreduction of these complexes resulted in the hydrogenation of porphyrin to give a chlorin. Moreover, the dyads reacted with triethanolamine yielding the Re(OCH<sub>2</sub>CH<sub>2</sub>NR<sub>2</sub>)bpy(CO)<sub>3</sub> species, which underwent CO<sub>2</sub> insertion. The Authors suggested that “the active photocatalyst is formed by a combination of reaction of triethanolamine at rhenium and photoreduction of the porphyrin”.

The same year, Schwalbe *et al.* developed binuclear complexes, M–L–Re (M = H<sub>2</sub>, Zn, Cu, Pd, Co, and FeCl; L = ligand), consisting of a phenanthroline-extended metal porphyrin unit, linked to Re(i) tricarbonyl chloride through a phen moiety.<sup>104</sup> These systems were applied for the photocatalytic reduction of CO<sub>2</sub> to CO in DMF, using trimethylamine as a sacrificial electron donor. Compared to the parent M–L compounds, the catalytic activity of the binuclear complexes was independent from the redox activity of the porphyrin metal. The catalytic active centre, in fact, seemed to be the Re(i) moiety and not the porphyrin. Notably, the highest activity in the series was obtained for Zn–L–Re.

Recently, the Ishitani's group studied the photocatalytic activity of a binuclear supramolecular complex, Ru(II)–Re(I), in which the Ru(II) photosensitizer and the Re(I) catalyst were connected through a bridging ligand. The complex was shown to photocatalyze the reduction of CO<sub>2</sub> to formic acid, using ascorbate as an electron donor. Unfortunately, the efficiency of the photocatalytic reaction in aqueous solution was relatively low, due to the rapid back-electron transfer from the photosensitizer unit to oxidized ascorbate, and the decomposition of the photosensitizer

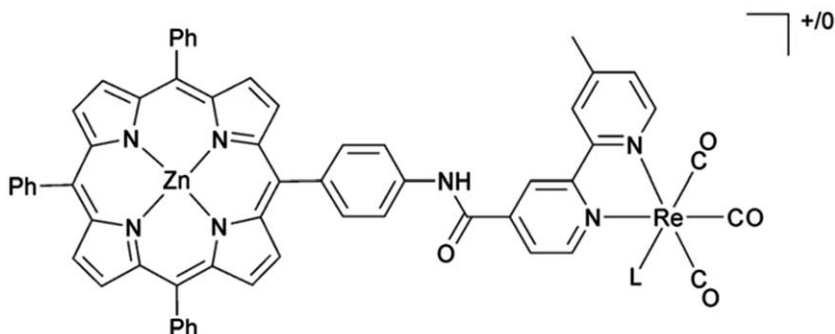


**Fig. 11** Example of zinc porphyrin-Re bipyridine tricarbonyl dyad reported by George and Perutz for the photocatalytic reduction of CO<sub>2</sub> to CO.<sup>103</sup> Adapted from C. D. Windle, M. W. George, R. N. Perutz, P. A. Summers, X. Z. Sun and A. C. Whitwood, *Chem. Sci.*, 2015, 6, 6847 – Published by The Royal Society of Chemistry.

itself.<sup>62</sup> Improvements in the photocatalytic ability were obtained by the same Authors using hetero-multinuclear Ru(II)-Re(I) complexes. These multinuclear systems were synthesised through the Mizoroki-Heck reaction in a single step, using photofunctional complexes possessing vinyl or bromo groups as building blocks.<sup>105</sup>

Re(I) N-heterocyclic carbene (NHC) complexes of the type fac-[Re(CO)<sub>3</sub>(NHC)L] (L = azide or triazolate), reported by Massi *et al.*, were proved to be photoreactive, undergoing photochemical CO dissociation in acetonitrile.<sup>106</sup> The rate was significantly greater in the case of the azide complex. This result could be of potential benefit for the development of new CO-releasing molecules.

An interesting application of Re(I) complexes as photoCORMs was reported by Mascharak *et al.*<sup>107</sup> The Authors described the first case of a CO-releasing complex acting as a “two-tone” theranostic agent. In particular, under low-power UV illumination, the complex rapidly released CO, and the luminescence changed from orange to deep blue.

These two distinct signals were employed to track both the entry of the complex into cancer cells and the end of CO release.

### 3.4 Iridium

Novel Ir-based complexes have been proposed as both photosensitizers and photocatalysts in many photochemical processes. An example is represented by the fluorinated Ir(III)-terpyridine-phenylpyridine-X complexes (X = anionic ligand), synthesised and studied by Bernhard *et al.* These were applied as photosensitizers for photocatalytic H<sub>2</sub>-generation from water and as redox photocatalysts for decarboxylative fluorination of carboxylic acids.<sup>108</sup> Another example of Ir-based photosensitizers is represented by the series of cyclometalated Ir(III) complexes, synthesised by same Authors, containing the new cyclometalating ligand 2-(4-cyano-phenyl)-5-methylpyridine. This cyano-decorated molecule proved to be a good alternative to the commonly used fluorinated ligands. The corresponding bis-cyclometalated Ir(III) complexes showed a remarkable photosensitizing ability for water reduction with Pt colloids, achieving ~2000 turnovers under optimized conditions.<sup>109</sup> On the other hand, photochemical formic acid dehydrogenation in aqueous solution was achieved by the Miller's group using Cp\*Ir-based complexes. [Cp\*Ir(bpy)(Cl)]<sup>+</sup> and [Cp\*Ir(bpy-OMe)(Cl)]<sup>+</sup>, in particular, operated with a good turnover frequency in a wide pH range. According to the Authors, the turnover-limiting step was the light-triggered H<sub>2</sub>-release from the photohydride intermediate [Cp\*Ir(bpy)(H)]<sup>+</sup>. Deactivation pathways were also identified. Thanks to these findings, the Authors could obtain the photochemical release of pure H<sub>2</sub> under visible light irradiation at room temperature.<sup>110</sup> Cp\*Ir-based cyclometalated complexes were examined by the Pandey's group as water oxidation photocatalysts.

These new systems, containing tert-butyl and Cp\* groups, present an electron rich environment around the metal centre, that stabilizes the Ir(IV) and Ir(V) species involved in the catalytic process. Good stability was observed even at very low pH values under LED light (440 nm) irradiation, and impressive TONs were obtained at neutral pH.<sup>111</sup> Meggers *et al.*

recently proposed a unique catalytic asymmetric process, which combined a single electron transfer between a donor substrate and a catalyst-activated acceptor substrate with a stereo-controlled radical–radical recombination. In the presence of a chiral Ir complex, as a dual Lewis acid/photoredox catalyst, this process enabled the visible-light-driven catalytic enantioselective synthesis of 1,2-amino alcohols from trifluoromethyl ketones and tertiary amines (99% ee).<sup>112</sup> The same Authors also proposed a chiral Ir complex, as both a catalytically active chiral Lewis acid and a precursor, for a visible-light-triggered photoredox catalyst in the enantioselective trichloromethylation of 2-acyl imidazoles and 2-acylpyridines (99% ee).<sup>113</sup>

A single component Ir(III) photoredox catalyst, able of catalysing the hydrotrifluoromethylation of terminal alkenes with sodium triflinate, was developed by Zhu and Zhang. With this new system, various trifluoromethylated aliphatic compounds could be easily synthesised at room temperature under blue LED irradiation. According to the proposed mechanism (shown in Fig. 12), the sulfinate anion quenches the excited  $^*\text{Ir}(\text{III})$  catalyst, producing the trifluoromethyl radical. The latter reacts with an olefin giving a methylene radical, which oxidizes Ir(II) to Ir(III) and closes the cycle.<sup>114</sup>

Recyclable catalysts, with excellent performances in batch as well as in flow reactions, were obtained by immobilizing fac-Ir(ppy)<sub>3</sub> on a polymer. This result was successfully achieved by Reiser *et al.* with a poly-isobutylene-polymer-tagged, Ir(III) photocatalyst.<sup>115</sup> The photosensitizing activity of a series of new pH-activated cyclometalated Ir(III) compounds was recently investigated by Aoki *et al.* These red-emitting complexes, whose intensity increased by protonation, were able to generate singlet oxygen upon photoirradiation at 465 nm, inducing the necrosis-like cell death of HeLa-S3 cells. Photoinduced cell death in cancer tissues was

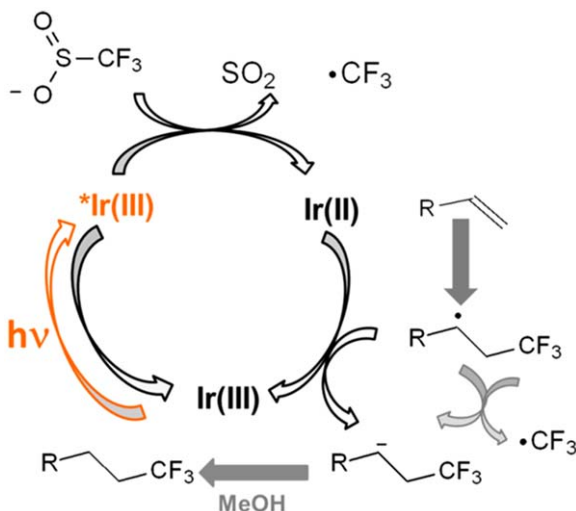


**Fig. 12** Mechanism proposed by Zhu and Zhang. Adapted from ref. 114 with permission from The Royal Society of Chemistry.

extensively investigated.<sup>116</sup> The organometallic chemistry of Ir complexes and their photoreactivity has been also receiving attention. In their studies on iridacyclopentene complexes, Paneque and Poveda found out that the complex  $[TpIr\{\kappa^2(C,C)-CH_2CH_2C(R)=C(R)\}(THF)]$  ( $Tp$  = hydrotris(pyrazolyl)borate;  $R = CO_2Me$ ) was photochemically unstable. In particular, under UV irradiation, the intermolecular  $[2 + 2]$  cyclo-addition of the double bonds of two complex molecules occurred. The proposed mechanism involved the initial photodissociation of THF from one complex. The resulting intermediate, probably in the excited state, reacted with another complex molecule *via*  $[2 + 2]$  cycloaddition. The final product was a dimeric species (*i.e.* a tetrasubstituted cyclobutane derivative), in which the metal centres completed their coordination sphere by interaction with the carboxylates' keto groups. The crystal structure of the dimer was reported.<sup>117</sup>

### 3.5 Palladium and platinum

The first example of aerobic oxidation of monomethyl Pd(II) complexes in water was reported by Vedernikov *et al.* The reaction led to ethane, methanol and methylhydroperoxide as the products. Selectivity could be tuned to favour the formation of ethane or methanol, by varying the reaction pH and the substrate concentration. The hypothesized mechanism involved the reaction of the excited methyl Pd(II) complex with O<sub>2</sub>, leading to the corresponding monomethyl Pd(IV) transient species, which was responsible for the subsequent methyl group transfer to nucleophiles, *e.g.* water.<sup>118</sup> The stereoselective synthesis of 1,3-diaminotruxillic acid derivatives was recently obtained through the combination of C-H-*ortho*-palladation and  $[2 + 2]$ -photocycloaddition in micro-reactors. This process first involved the *ortho*-palladation of (*Z*)-2-aryl-4-arylidene-5(4H)-oxazolones to give dinuclear complexes with bridging carboxylates. In the second stage, the  $[2 + 2]$ -photocycloaddition of the C=C bonds of oxazolones occurred under LED light in flow micro-reactors and gave the corresponding dinuclear *ortho*-palladated cyclobutanes.  $\epsilon$ -1,3-Diaminotruxillic acids as single isomers were finally obtained by depalladation.<sup>119</sup> An interesting example of Pt-based photocatalysts was reported by Park *et al.*, who proposed the Pt(II) complex of 4,4'-bis[4-(triphenylsilyl)phenyl]-2,2'-bipyridine for water reduction in the presence of a conventional Ir(III) photosensitizer and *N,N*-dimethylaniline as the sacrificial electron donor. This Pt(II) complex, with a turnover number of  $5.1 \times 10^5$ , represented a large improvement compared to unsubstituted Pt(II) water reduction catalysts.<sup>120</sup> A general method for the cyclo-metallation of aromatic compounds, containing an N-donor hetero-aromatic moiety as directing groups, was introduced by González-Herrero *et al.* Starting from a common Pt(II) precursor, under visible-light at room temperature, the Authors observed an unprecedented C-H oxidative addition, followed by the formation of a Pt(IV) methyl hydride intermediate. This latter underwent C-H reductive elimination of methane to afford the bis-cyclometalated complex. As an example, starting from  $[PtMe(C^N)(N^CH)]$  (where  $N^CH$  is 2-phenylpyridine and  $C^N$  is the corresponding cyclometalated ligand),

the Authors obtained the bis-cyclometalated complex *cis*-[Pt(C<sup>N</sup>)<sub>2</sub>] as the final product.<sup>121</sup> Sharp *et al.* obtained some interesting results in studying the photolysis of Pt(IV)-hydroxido complexes, containing H-bonding groups (*e.g.* acetate) into the coordination sphere. Through H-bonding interactions, the photogenerated hydroxyl radicals were directed to abstract a hydrogen atom from the ethyl group of a triethylphosphine. This process occurred even at room temperature and led to phosphaplatinacycle complexes.<sup>122</sup>

Pt complexes are well known also in medicine as photodynamic therapy (PDT) agents. For instance, 2-(phenylazo)pyridyl Pt(II) catecholates, such as [Pt(pap)(an-cat)] (pap = 2-(phenylazo)pyridine, H<sub>2</sub>an-cat = 4-[2-[(anthracen-9-ylmethylene)amino]ethyl]benzene-1,2-diol), have been studied by Kondaiah and Chakravarty as photoactive prodrugs. Within cancer cells, intracellular GSH reacts with the Pt(II)-bound pap ligand, promoting the delivery of the photoactive catecholate moiety responsible of cellular toxicity. As a result, the [Pt(pap)(an-cat)] complex shows a remarkable PDT effect, with a 10-fold enhancement of cytotoxicity in HaCat and MCF-7 cells under visible-light.<sup>123</sup>

The same Authors presented the curcumin-bound<sup>124</sup> *cis*-diamminePt(II) complex, [Pt(cur)(NH<sub>3</sub>)<sub>2</sub>](NO<sub>3</sub>), as a novel photoactivated chemotherapeutic agent, releasing two anticancer agents, *i.e.* curcumin and an active Pt(II) species, under visible light irradiation. Through this compound a dual action was obtained, permitting the controlled generation of diamminePt(II), as a DNA crosslinking/transcription inhibitor agent, and curcumin, as a PDT agent. A remarkable phototoxic activity was observed in cancer cells, while a low toxicity in the dark.<sup>125</sup>

The photoactivation of nontoxic Pt(IV)-azido complexes may lead to highly cytotoxic species. Kasparkova *et al.* recently synthesised a new prodrug, consisting of a Pt(IV) complex conjugated with suberoyl-bis-hydroxamic acid. After photoactivation, this system was able to play different roles, as a Pt(II) anticancer drug and a histone deacetylase inhibitor in cancer cells. This approach, based on two different mechanisms of action, is a valuable way to design chemotherapeutic agents of strong efficacy.<sup>126</sup>

### 3.6 Properties of other transition metal complexes

The luminescent complex Zr(MePDP)<sub>2</sub> (MePDP = 2,6-bis(5-methyl-3-phenyl-1H-pyrrol-2-yl)pyridine), characterised by intense LMCT bands in the visible region, is quenched by mild reductants leading to a powerful electron transfer reagent. Thanks to these properties, the complex was proposed by Milsmann *et al.* as an earth-abundant metal substitute for Ru-based photosensitizers in reductive photoredox catalysis with visible light (*e.g.* in dehalogenation reactions and in the reduction of electron-poor olefins).<sup>127</sup> A Mo-based dithiolene-oxo complex was applied by Fontecave and Li as a model of the active sites of some Mo/W-dependent enzymes. The complex was proved to be an active photoreduction catalyst of protons with excellent turnover numbers (~500) and good stability in aqueous/organic media.

The oxo ligand seemed to have an active role in the proton exchange, in facilitating protonation of the hydrido  $[Mo^{IV}OH(H)-(LH)(L)]$  intermediate and in further  $H_2$  formation.<sup>128</sup> Cationic mono- and poly-nuclear Ag-based complexes of Buchwald-type phosphane (XPhos) and cyclooctatetraene (COT) ligands were recently synthesised, displaying a remarkable catalytic activity for the photochemical C–C bond cleavage of coordinated acetonitrile. This process resulted in the formation of well-defined cyanide bridged Ag clusters.<sup>129</sup>

Han and Jin recently applied photochemical [2 + 2] cycloadditions at olefinic groups within metal–carbene metallacycles. In particular, the Authors observed that dinuclear Ag(I) carbene-based metallacycles could be quantitatively converted into the corresponding dinuclear cyclobutane–carbene complexes under UV-light irradiation.<sup>130</sup> Vittal *et al.* studied the light-induced motility of the crystals of a series of structurally related Ag(I) complexes, *i.e.*  $AgL_2X_2$  ( $L = 4$ -styrylpyridine, 2'-fluoro-4-styrylpyridine, and 3'-fluoro-4-styrylpyridine,  $X = BF_4^-$ ,  $ClO_4^-$  and  $NO_3^-$ ), undergoing [2 + 2] photocycloaddition under UV light. The Authors found out that the occurrence of photosalient effects depended on both the nature of the ligand and the crystal packing. The latter, in particular, “directs the magnitude, direction, and rate of volume expansion during the photoreaction”.<sup>131</sup> New hybrid silver bromides,  $K[M(bpy)_3]_2Ag_6Br_{11}$  and  $[M(bpy)_3]_2Ag_{13}Br_{17}$  ( $M = Ni, Co, Zn, Fe$ ), were synthesised, possessing tunable band gaps of 1.73–2.71 eV and efficient photocatalytic activities under visible-light irradiation. The transition complex cation was found to play a key role in both the photocatalytic activities and photochemical stabilities of the corresponding material.<sup>132</sup>

$[Os(N^N)_3]^{2+}$ -type complexes are typically highly inert and require drastic conditions for ligand exchange. However, Elliot *et al.* recently reported the first known procedure for the photochemical ligand substitution in the homoleptic complex  $[Os(btz)_3]^{2+}$  ( $btz = 1,1'$ -dibenzyl-4,4'-bi-1,2,3-triazolyl). The Authors also characterized the ligand-loss intermediate species by  $^1H$ -NMR spectroscopy and mass spectrometry. These results may be of interest for the development of novel Os(II)-based (pro)drugs and light-initiated DNA coordinating agents.<sup>133</sup>

Homogeneous Au-based catalysis has emerged as a powerful tool in organic synthesis. In particular, Au(I) or Au(III) complexes have been used to selectively activate unsaturated molecules, such as alkynes towards nucleophilic attack. By merging gold and visible-light photoredox catalyses, Glorius *et al.* developed a new strategy for selective alkyne difunctionalisation, avoiding homocoupling and overcoming conventional hydrofunctionalisation.<sup>134</sup> The same Authors also developed a visible-light-promoted method for the oxidative addition of aryl-diazonium salts to Au(I) complexes. This process enabled to access a series of (C,N)-cyclometalated Au(III) compounds with a variety of phosphine and N-heterocyclic carbene ligands.<sup>135</sup>

In the last years, interesting examples of Au-based pincer complexes with unusual photochemical and redox properties have been reported.<sup>136</sup> The Au(II) pincer complex  $[(C^N^C)Au]_2$ , for instance, was shown to undergo a photochemically (not thermally) induced disproportionation,

leading to the mixed-valence aggregate  $[Au(I)_4Au(III)_4]$ . This product consisted of a 20-membered macrocycle based on Au(I) C–Au–N building blocks, each of which was decorated with an Au(III) pincer moiety.<sup>137</sup> Shin *et al.* recently employed catalytically generated vinyl Au-complexes in cross-coupling reactions with arenediazonium salts. Interestingly, the Au(I)–Au(III) redox cycle could be accessed under both visible-light photoredox and thermal conditions.<sup>138</sup>

Bis-cyclometalated Au(III) acetylides complexes, coupled with Co or Rh catalysts and TEOA (electron donor), were successfully applied by Yu *et al.* as sensitizers in the photocatalytic H<sub>2</sub> production in acetone/water mixture.<sup>139</sup> The photocatalytic system showed a long lifetime, and a turnover number 4-fold higher than those reported in the literature for H<sub>2</sub>O reduction with gold complexes. Polynuclear Au(I) complexes were applied by Barriault and Scaiano as photoredox catalysts for the light-driven-reduction of carbon–halogen bonds. This process provides a mild new pathway for the generation of C–H and C–C bonds.<sup>140</sup>

## References

- 1 V. Amendola, G. Bergamaschi and M. Licchelli, *Photochemistry*, 2016, **43**, 103–147.
- 2 D. Ravelli, S. Prottì and M. Fagnoni, *Acc. Chem. Res.*, 2016, **49**, 2232–2242.
- 3 D. Z. Zee, T. Chantarojsiri, J. R. Long and C. J. Chang, *Acc. Chem. Res.*, 2015, **48**, 2027–2036.
- 4 Y. Yamazaki, H. Takeda and O. Ishitani, *J. Photochem. Photobiol., C*, 2015, **25**, 106–137.
- 5 K. Kobayashi and K. Tanaka, *Inorg. Chem.*, 2015, **54**, 5085–5095.
- 6 R. N. Perutz and B. Procacci, *Chem. Rev.*, 2016, **116**, 8506–8544.
- 7 S. Kaufhold, L. Petermann and R. S. S. Rau, *Coord. Chem. Rev.*, 2015, 73–87; Y. Liu, P. Persson, V. Sundström and K. Wärnmark, *Acc. Chem. Res.*, 2016, **49**, 1477–1485.
- 8 M. D. Kärkäs and B. Åkermark, *Dalton Trans.*, 2016, **45**, 14421–14461.
- 9 K. Mori and H. Yamashita, *Chem. – Eur. J.*, 2016, **22**, 11122–11137.
- 10 J. D. Knoll and C. Turro, *Coord. Chem. Rev.*, 2015, 110–126; E. Ruggiero, S. Alonso-De-Castro, A. Habtemariam and L. Salassa, *Struct. Bonding*, 2015, **165**, 69–107; E. Ruggiero, S. Alonso-de Castro, A. Habtemariam and L. Salassa, *Dalton Trans.*, 2016, **45**, 13012–13020.
- 11 X. Wu, X. Yang, Y. M. Lee, W. Nam and L. Sun, *Chem. Commun.*, 2015, **51**, 4013–4016.
- 12 P. Kumar, C. Joshi, A. K. Srivastava, P. Gupta, R. Boukherroub and S. L. Jain, *ACS Sustainable Chem. Eng.*, 2016, **4**, 69–75.
- 13 L. Luo, Y. Zeng, L. Li, Z. Luo, T. I. Smirnova and P. A. Maggard, *Inorg. Chem.*, 2015, **54**, 7388–7401.
- 14 E. Kottelat, A. Ruggi and F. Zobi, *Dalton Trans.*, 2016, **45**, 6920.
- 15 S. J. Carrington, I. Chakraborty and P. K. Mascharak, *Dalton Trans.*, 2015, **44**, 13828.
- 16 J. D. Compain, M. Stanbury, M. Trejo and S. Chardon-Noblat, *Eur. J. Inorg. Chem.*, 2015, 5757–5766.
- 17 A. Rosas-Hernández, P. G. Alsabeh, E. Barsch, H. Junge, R. Ludwig and M. Beller, *Chem. Commun.*, 2016, **52**, 8393.

- 18 Z. Guo, S. Cheng, C. Cometto, E. Anxolabéhère-Mallart, S. M. Ng, C. C. Ko, G. Liu, L. Chen, M. Robert and T. C. Lau, *J. Am. Chem. Soc.*, 2016, **138**, 9413–9416.
- 19 L. Chen, Z. Guo, X. G. Wei, C. Gallenkamp, J. Bonin, E. A. Mallart, K. C. Lau, T. C. Lau and M. Robert, *J. Am. Chem. Soc.*, 2015, **137**, 10918–10921.
- 20 C. Matlachowski and M. Schwalbe, *Dalton Trans.*, 2015, **44**, 6480.
- 21 Y. Na, P. Wei and L. Zhou, *Chem. – Eur. J.*, 2016, **22**, 10365–10368.
- 22 C. L. Hartley, R. J. DiRisio, M. E. Screen, K. J. Mayer and W. R. McNamara, *Inorg. Chem.*, 2016, **55**, 8865–8870.
- 23 A. M. Lunsford, J. H. Blank, S. Moncho, S. C. Haas, S. Muhammad, E. N. Brothers, M. Y. Darensbourg and A. A. Bengali, *Inorg. Chem.*, 2016, **55**, 964–973.
- 24 P. Xiao, J. Zhang, D. Campolo, F. Dumur, D. Gigmes, J. Pierre Fouassier and J. Lalevée, *J. Polym. Sci., Part A: Polym. Chem.*, 2015, **53**, 2673–2684; S. Telitel, F. Dumur, D. Campolo, J. Poly, D. Gigmes, J. Pierre Fouassier and J. Lalevée, *J. Polym. Sci., Part A: Polym. Chem.*, 2016, **54**, 702–713.
- 25 C. H. Lin, D. Pursley, J. E. M. N. Klein, J. Teske, J. A. Allen, F. Rami, A. Köhn and B. Plietker, *Chem. Sci.*, 2015, **6**, 7034.
- 26 F. Marchetti, S. Zacchini and V. Zanotti, *Organometallics*, 2016, **35**, 2630–2637.
- 27 T. H. Chen, N. Asiri, K. W. Kwong, J. Malone and R. Zhang, *Chem. Commun.*, 2015, **51**, 9949.
- 28 T. Chantarojsiri, Y. Sun, J. R. Long and C. J. Chan, *Inorg. Chem.*, 2015, **54**, 5879–5887.
- 29 U. Basu, I. Pant, A. Hussain, P. Kondaiah and A. R. Chakravarty, *Inorg. Chem.*, 2015, **54**, 3748–3758.
- 30 X. Jiang, L. Chen, X. Wang, L. Long, Z. Xiao and X. Liu, *Chem. – Eur. J.*, 2015, **21**, 13065–13072.
- 31 G. Zhang, C. Liu, H. Yi, Q. Meng, C. Bian, H. Chen, J. X. Jian, L. Z. Wu and A. Lei, *J. Am. Chem. Soc.*, 2015, **137**, 9273–9280.
- 32 C. Di Giovanni, C. Gimbert-Suriçach, M. Nippe, J. Benet-Buchholz, J. R. Long, X. Sala and A. Llobet, *Chem. – Eur. J.*, 2016, **22**, 361–369.
- 33 S. Aoi, K. Mase, K. Ohkubo and S. Fukuzumi, *Catal. Sci. Technol.*, 2016, **6**, 4077.
- 34 T. Nakazono, A. R. Parent and K. Sakai, *Chem. – Eur. J.*, 2015, **21**, 6723–6726.
- 35 B. Das, A. Orthaber, S. Ott and A. Thapper, *Chem. Commun.*, 2015, **51**, 13074–13077.
- 36 Y. Zhao, J. Lin, Y. Liu, B. Ma, Y. Ding and M. Chen, *Chem. Commun.*, 2015, **51**, 17309–17312.
- 37 J. W. Wang, P. Sahoo and T. B. Lu, *ACS Catal.*, 2016, **6**, 5062–5068.
- 38 L. Tong, A. Kopecky, R. Zong, K. J. Gagnon, M. S. G. Ahlquist and R. P. Thummel, *Inorg. Chem.*, 2015, **54**, 7873–7884.
- 39 M. Natali, E. Badetti, E. Deponti, M. Gamberoni, F. A. Scaramuzzo, A. Sartorel and C. Zonta, *Dalton Trans.*, 2016, **45**, 14764–14773.
- 40 J. Balapanuru, G. Chiu, C. Su, N. Zhou, Z. Hai, Q. Xu and K. Ping Loh, *ACS Appl. Mater. Interfaces*, 2015, **7**, 880–886.
- 41 R. P. Sabatini, B. Lindley, T. M. McCormick, T. Lazarides, W. W. Brennessel, D. W. McCamant and R. Eisenberg, *J. Phys. Chem. B*, 2016, **120**, 527–534.
- 42 E. Joliat, S. Schnidrig, B. Probst, C. Bachmann, B. Spingler, K. K. Baldridge, F. von Rohr, A. Schilling and R. Alberto, *Dalton Trans.*, 2016, **45**, 1737.
- 43 L. N. Grant, M. E. Carroll, P. J. Carroll and D. J. Mindiola, *Inorg. Chem.*, 2016, **55**, 7997–8002.

- 44 J. A. Terrett, J. D. Cuthbertson, V. W. Shurtleff and D. W. C. MacMillan, *Nature*, 2015, **524**, 330–334.
- 45 C. F. Wise, D. Liu, K. J. Mayer, P. M. Crossland, C. L. Hartley and W. R. McNamara, *Dalton Trans.*, 2015, **44**, 14265.
- 46 A. Das, Z. Han, W. W. Brennessel, P. L. Holland and R. Eisenberg, *ACS Catal.*, 2015, **5**, 1397–1406.
- 47 C. S. Tsang, L. Chen, L. W. Li, S. M. Yiu, T. C. Lau and H. L. Kwong, *Dalton Trans.*, 2015, **44**, 13087–13092.
- 48 S. J. Hwang, D. C. Powers, A. G. Maherab and D. G. Nocera, *Chem. Sci.*, 2015, **6**, 917.
- 49 S. J. Hwang, B. L. Anderson, D. C. Powers, A. G. Maher, R. G. Hadt and D. G. Nocera, *Organometallics*, 2015, **34**, 4766–4774; S. J. Hwang, D. C. Powers, A. G. Maher, B. L. Anderson, R. G. Hadt, S. L. Zheng, Y. S. Chen and D. G. Nocera, *J. Am. Chem. Soc.*, 2015, **137**, 6472–6475.
- 50 V. Vreeken, M. A. Siegler, B. de Bruin, J. N. H. Reek, M. Lutz and J. Ivar van der Vlugt, *Angew. Chem., Int. Ed.*, 2015, **54**, 7055–7059.
- 51 A. C. Hernandez-Perez and S. K. Collins, *Acc. Chem. Res.*, 2016, **49**, 1557–1565.
- 52 J. Wang, C. Li, Q. Zhou, W. Wang, Y. Hou, B. Zhang and X. Wang, *Dalton Trans.*, 2016, **45**, 5439–5443.
- 53 Y. Peng, L. Shang, Y. Cao, G. I. N. Waterhouse, C. Zhou, T. Bian, L. Z. Wu, C. H. Tung and T. Zhang, *Chem. Commun.*, 2015, **51**, 12556–12559.
- 54 R. Terao, T. Nakazono, A. Rene Parent and K. Sakai, *ChemPlusChem*, 2016, **81**, 1064–1067.
- 55 Q. Jochyms, P. Guillot, E. Mignard and J. M. Vincent, *Dalton Trans.*, 2015, **44**, 19700.
- 56 M. Knorn, T. Rawner, R. Czerwieniec and O. Reiser, *ACS Catal.*, 2015, **5**, 5186–5193; O. Reiser, *Acc. Chem. Res.*, 2016, **49**, 1990–1996.
- 57 C. Saracini, K. Ohkubo, T. Suenobu, G. J. Meyer, K. D. Karlin and S. Fukuzumi, *J. Am. Chem. Soc.*, 2015, **137**, 15865–15874.
- 58 S. Gazi, W. K. Hung Ng, R. Ganguly, A. M. P. Moeljadi, H. Hirao and H. S. Soo, *Chem. Sci.*, 2015, **6**, 7130–7142.
- 59 S. M. Stevenson, M. P. Shores and E. M. Ferreira, *Angew. Chem., Int. Ed.*, 2015, **54**, 6506–6510.
- 60 R. F. Higgins, S. M. Fatur, S. G. Shepard, S. M. Stevenson, D. J. Boston, E. M. Ferreira, N. H. Damrauer, A. K. Rappe and M. P. Shores, *J. Am. Chem. Soc.*, 2016, **138**, 5451–5464.
- 61 J. M. Dabrowski, B. Pucelik, M. M. Pereira, L. G. Arnaut, W. Macyk and G. Stochel, *RSC Adv.*, 2015, **5**, 93252.
- 62 Y. Tamaki, D. Imori, T. Morimoto, K. Koike and O. Ishitani, *Dalton Trans.*, 2016, **45**, 14668–14677; A. Nakada, K. Koike, T. Nakashima, T. Morimoto and O. Ishitani, *Inorg. Chem.*, 2015, **54**, 1800–1807.
- 63 Y. Kuramochi, K. Fukaya, M. Yoshida and H. Ishida, *Chem. – Eur. J.*, 2015, **21**, 10049–10060.
- 64 T. Kajiwara, M. Fujii, M. Tsujimoto, K. Kobayashi, M. Higuchi, K. Tanaka and S. Kitagawa, *Angew. Chem., Int. Ed.*, 2016, **55**, 2697–2700.
- 65 R. Kuriki, O. Ishitani and K. Maeda, *ACS Appl. Mater. Interfaces*, 2016, **8**, 6011–6018.
- 66 F. Yoshitomi, K. Sekizawa, K. Maeda and O. Ishitani, *ACS Appl. Mater. Interfaces*, 2015, **7**, 13092–13097.
- 67 R. Kuriki, H. Matsunaga, T. Nakashima, K. Wada, A. Yamakata, O. Ishitani and K. Maeda, *J. Am. Chem. Soc.*, 2016, **138**, 5159–5170.

- 68 K. Muraoka, H. Kumagai, M. Eguchi, O. Ishitani and K. Maeda, *Chem. Commun.*, 2016, **52**, 7886.
- 69 T. Mondal and D. Chatterjee, *RSC Adv.*, 2016, **6**, 63488.
- 70 E. Rousset, D. Chartrand, I. Ciofini, V. Marvaud and G. S. Hanan, *Chem. Commun.*, 2015, **51**, 9261–9264.
- 71 L. X. Xue, T. T. Meng, W. Yang and K. Z. Wang, *J. Photochem. Photobiol., B*, 2015, **152**, 95–105.
- 72 Y. Sato, S. Takizawa and S. Murata, *Eur. J. Inorg. Chem.*, 2015, 5495–5502; Y. Sato, S. Takizawa and S. Murata, *J. Photochem. Photobiol., A*, 2016, **321**, 151–160.
- 73 M. D. Kärkäs and B. Åkermark, *Chem. Rev.*, 2016, **16**, 940–963; T. M. Laine, M. D. Kärkäs, R. Z. Liao, T. Åkermark, B. L. Lee, E. A. Karlsson, P. E. M. Siegbahn and B. Åkermark, *Chem. Commun.*, 2015, **51**, 1862–1865.
- 74 Y. Tsubonouchi, S. Lin, A. R. Parent, G. W. Brudvig and K. Sakai, *Chem. Commun.*, 2016, **52**, 8018–8021.
- 75 S. Berardi, L. Francàs, S. Neudeck, S. Maji, J. Benet-Buchholz, F. Meyer and A. Llobet, *ChemSusChem*, 2015, **8**, 3688–3696.
- 76 M. Yamamoto, L. Wang, F. Li, T. Fukushima, K. Tanaka, L. Sun and H. Imahori, *Chem. Sci.*, 2016, **7**, 1430–1439.
- 77 X. Li, Z. Hao, F. Zhang and H. Li, *ACS Appl. Mater. Interfaces*, 2016, **8**, 12141–12148.
- 78 S. Phungsripheng, K. Kozawa, M. Akita and A. Inagaki, *Inorg. Chem.*, 2016, **55**, 3750–3758.
- 79 A. J. Göttle, F. Alary, M. Boggio-Pasqua, I. M. Dixon, J. L. Heully, A. Bahreman, S. H. C. Askes and S. Bonnet, *Inorg. Chem.*, 2016, **55**, 4448–4456.
- 80 P. A. Scattergood, U. Khushnood, A. Tariq, D. J. Cooke, C. R. Rice and P. I. P. Elliott, *Inorg. Chem.*, 2016, **55**, 7787–7796.
- 81 F. Weisser, S. Plebst, S. Hohloch, M. van der Meer, S. Manck, F. Führer, V. Radtke, D. Leichnitz and B. Sarkar, *Inorg. Chem.*, 2015, **54**, 4621–4635.
- 82 F. Weisser, H. Stevens, J. Klein, M. van der Meer, S. Hohloch and B. Sarkar, *Chem. – Eur. J.*, 2015, **21**, 8926–8938.
- 83 K. Arora, J. K. White, R. Sharma, S. Mazumder, P. D. Martin, H. Bernhard Schlegel, C. Turro and J. J. Kodanko, *Inorg. Chem.*, 2016, **55**, 6968–6979.
- 84 A. R. Corcos, J. S. Pap, T. Yang and J. F. Berry, *J. Am. Chem. Soc.*, 2016, **138**, 10032–10040.
- 85 R. Shimogawa, G. Konishi, T. Takao and H. Suzuki, *Organometallics*, 2016, **35**, 1446–1457.
- 86 J. D. Knoll, B. A. Albani and C. Turro, *Acc. Chem. Res.*, 2015, **48**, 2280–2287.
- 87 L. Tabrizi and H. Chiniforoshan, *Dalton Trans.*, 2016, **45**, 18333–18345.
- 88 Y. Chen, W. Lei, Y. Hou, C. Li, G. Jiang, B. Zhang, Q. Zhou and X. Wang, *Dalton Trans.*, 2015, **44**, 7347–7354.
- 89 L. M. Loftus, J. K. White, B. A. Albani, L. Kohler, J. J. Kodanko, R. P. Thummel, K. R. Dunbar and C. Turro, *Chem. – Eur. J.*, 2016, **22**, 3704–3708.
- 90 P. M. Keane, F. E. Poynton, J. P. Hall, I. P. Clark, I. V. Sazanovich, M. Towrie, T. Gunnlaugsson, S. J. Quinn, C. J. Cardin and J. M. Kelly, *Faraday Discuss.*, 2015, **185**, 455.
- 91 P. Liu, B.-Y. Wu, J. Liu, Y.-C. Dai, Y.-J. Wang and K.-Z. Wang, *Inorg. Chem.*, 2016, **55**, 1412–1422.
- 92 L. Marcélis, S. Kajouj, J. Ghesquière, G. Fettweis, I. Coupienne, R. Lartia, M. Surin, E. Defrancq, J. Piette, C. Moucheron and A. Kirsch-De Mesmaeker, *Eur. J. Inorg. Chem.*, 2016, 2902–2911.

- 93 R. Zhou, G. F. Manbeck, D. G. Wimer and K. J. Brewer, *Chem. Commun.*, 2015, **51**, 12966–12969.
- 94 H. Mallalieu Rogers, S. M. Arachchige and K. J. Brewer, *Chem. – Eur. J.*, 2015, **21**, 16948–16954.
- 95 M. Yu, H. Jing, X. Liu and X. Fu, *Organometallics*, 2015, **34**, 5754–5758.
- 96 H. Huo, K. Harms and E. Meggers, *J. Am. Chem. Soc.*, 2016, **138**, 6936–6939.
- 97 L. Zámostná, S. Sander, T. Braun, R. Laubenstein, B. Braun, R. Herrmann and P. Kläring, *Dalton Trans.*, 2015, **44**, 9450.
- 98 S. Sato and O. Ishitani, *Coord. Chem. Rev.*, 2015, **282–283**, 50–59; K. Saita, Y. Harabuchi, T. Taketsugu, O. Ishitani and S. Maeda, *Phys.Chem.Chem.-Phys.*, 2016, **18**, 17557.
- 99 F. Franco, C. Cometto, C. Garino, C. Minero, F. Sordello, C. Nervi and R. Gobetto, *Eur. J. Inorg. Chem.*, 2015, 296–304; T. G. Fenton, M. E. Louis and G. Li, *J. Mol. Catal. A: Chem.*, 2016, **411**, 272–278.
- 100 A. Maurin, C. Ng, L. Chen, T. C. Lau, M. Robert and C. C. Ko, *Dalton Trans.*, 2016, **45**, 14524–14529.
- 101 J. Shakeri, H. Farrokhpour, H. Hadadzadeh and M. Joshaghani, *RSC Adv.*, 2015, **5**, 41125.
- 102 Y. Kuramochi and O. Ishitani, *Inorg. Chem.*, 2016, **55**, 5702–5709.
- 103 C. D. Windle, M. W. George, R. N. Perutz, P. A. Summers, X. Zhong Sun and A. C. Whitwood, *Chem. Sci.*, 2015, **6**, 6847–6864.
- 104 C. Matlachowski, B. Braun, S. Tscherlei and M. Schwalbe, *Inorg. Chem.*, 2015, **54**, 10351–10360.
- 105 Y. Yamazaki, T. Morimoto and O. Ishitani, *Dalton Trans.*, 2015, **44**, 11626; Y. Yamazaki, A. Umemoto and O. Ishitani, *Inorg. Chem.*, 2016, **55**, 11110–11124.
- 106 P. V. Simpson, B. W. Skelton, P. Raiteria and M. Massi, *New J. Chem.*, 2016, **40**, 5797.
- 107 S. J. Carrington, I. Chakraborty, J. M. L. Bernard and P. K. Mascharak, *Inorg. Chem.*, 2016, **55**, 7852–7858.
- 108 J. A. Porras, I. N. Mills, W. J. Transue and S. Bernhard, *J. Am. Chem. Soc.*, 2016, **138**, 9460–9472.
- 109 I. N. Mills, H. N. Kagalwala and S. Bernhard, *Dalton Trans.*, 2016, **45**, 10411–10419.
- 110 S. M. Barrett, S. A. Slattery and A. J. M. Miller, *ACS Catal.*, 2015, **5**, 6320–6327.
- 111 S. Mukhopadhyay, R. Shikha Singh, A. Biswas and D. Shankar Pandey, *Chem. Commun.*, 2016, **52**, 3840.
- 112 C. Wang, J. Qin, X. Shen, R. Riedel, K. Harms and E. Meggers, *Angew. Chem., Int. Ed.*, 2016, **55**, 685–688; C. Wang, J. Qin, X. Shen, R. Riedel, K. Harms and E. Meggers, *Angew. Chem.*, 2016, **128**, 695–698; A. G. Amador and T. P. Yoon, *Angew. Chem., Int. Ed.*, 2016, **55**, 2304–2306.
- 113 H. Huo, C. Wang, K. Harms and E. Meggers, *J. Am. Chem. Soc.*, 2015, **137**, 9551–9554.
- 114 L. Zhu, L. S. Wang, B. Li, B. Fu, C. P. Zhang and W. Li, *Chem. Commun.*, 2016, **52**, 6371–6374.
- 115 D. Rackl, P. Kreitmeier and O. Reiser, *Green Chem.*, 2016, **18**, 214–219.
- 116 A. Kando, Y. Hisamatsu, H. Ohwada, T. Itoh, S. Moromizato, M. Kohno and S. Aoki, *Inorg. Chem.*, 2015, **54**, 5342–5357.
- 117 Á. Vivancos, N. Rendón, M. Paneque, M. L. Poveda and E. Álvarez, *Organometallics*, 2015, **34**, 5438–5453.
- 118 A. V. Sberegaeva, P. Y. Zavalij and A. N. Vedernikov, *J. Am. Chem. Soc.*, 2016, **138**, 1446–1455.

- 119 E. Serrano, A. Juan, A. García-Montero, T. Soler, F. Jiménez-Márquez, C. Cativiela, M. Victoria Gomez and E. P. Urriolabeitia, *Chem. – Eur. J.*, 2016, **22**, 144–152.
- 120 D. R. Whang and S. Y. Park, *ChemSusChem*, 2015, **8**, 3204–3207.
- 121 F. J. P. González-Herrero, *J. Am. Chem. Soc.*, 2016, **138**, 5276–5282.
- 122 L. A. Wickramasinghe and P. R. Sharp, *Organometallics*, 2015, **34**, 3451–3454.
- 123 K. Mitra, S. Patil, P. Kondaiah and A. R. Chakravarty, *Inorg. Chem.*, 2015, **54**, 253–264.
- 124 S. Banerjee and A. R. Chakravarty, *Acc. Chem. Res.*, 2015, **48**, 2075–2083.
- 125 K. Mitra, S. Gautam, P. Kondaiah and A. R. Chakravarty, *Angew. Chem., Int. Ed.*, 2015, **54**, 13989–13993.
- 126 J. Kasparkova, H. Kostrhunova, O. Novakova, R. Kříkavová, J. Vančo, Z. Trávníček and V. Brabec, *Angew. Chem., Int. Ed.*, 2015, **54**, 14478–14482.
- 127 Y. Zhang, J. L. Petersen and C. Milsmann, *J. Am. Chem. Soc.*, 2016, **138**, 13115–13118.
- 128 J.-P. Porcher, T. Fogeron, M. Gomez-Mingot, E. Derat, L.-M. Chamoreau, Y. Li and M. Fontecave, *Angew. Chem., Int. Ed.*, 2015, **54**, 14090–14093.
- 129 A. Grirrane, E. Álvarez, J. Albero, H. García and A. Corma, *Dalton Trans.*, 2016, **45**, 5444.
- 130 C. X. Wang, Y. Gao, Y. X. Deng, Y. J. Lin, Y. F. Han and G. X. Jin, *Organometallics*, 2015, **34**, 5801–5806.
- 131 R. Medishetty, S. C. Sahoo, C. E. Mulijanto, P. Naumov and J. J. Vittal, *Chem. Mater.*, 2015, **27**, 1821–1829.
- 132 C. Y. Yue, X. W. Lei, Y. F. Han, X. X. Lu, Y. W. Tian, J. Xu, X. F. Liu and X. Xu, *Inorg. Chem.*, 2016, **55**, 12193–12203.
- 133 P. A. Scattergood, D. A. W. Ross, C. R. Rice and P. I. P. Elliott, *Angew. Chem., Int. Ed.*, 2016, **55**, 10697–10701.
- 134 A. Tlahuext-Aca, M. N. Hopkinson, R. A. Garza-Sánchez and F. Glorius, *Chem. – Eur. J.*, 2016, **22**, 5909–5913.
- 135 A. Tlahuext-Aca, M. N. Hopkinson, C. G. Daniliuc and F. Glorius, *Chem. – Eur. J.*, 2016, **22**, 11587–11592.
- 136 M. C. Gimeno, J. M. López-de-Luzuriaga, E. Manso, M. Monge, M. E. Olmos, M. Rodríguez-Castillo, M. T. Tena, D. P. Day, E. J. Lawrence and G. G. Wildgoose, *Inorg. Chem.*, 2015, **54**, 10667–10677.
- 137 D.-A. Roșca and M. Bochmann, *Organometallics*, 2016, **35**, 27–31.
- 138 D. V. Patil, H. Yun and S. Shin, *Adv. Synth. Catal.*, 2015, **357**, 2622–2628.
- 139 Z. T. Yu, X. L. Liu, Y. J. Yuan, Y. H. Li, G. H. Chen and Z. G. Zou, *Dalton Trans.*, 2016, **45**, 17223–17232.
- 140 C. D. McTiernan, M. Morin, T. McCallum, J. C. Scaiano and L. Barriault, *Catal. Sci. Technol.*, 2016, **6**, 201–207.

---

# Photophysics of transition metal complexes

Valeria Amendola\*

DOI: 10.1039/9781788010696-00133

Due to their rich luminescence, transition metal complexes find applications in multiple fields, spanning from photochemistry and photocatalysis (see Chapter 4) to molecular electronics, OLEDs, intracellular sensors and bioimaging reagents. However, the practical application of novel luminescent complexes cannot ignore a profound knowledge of the fundamentals of their photophysical properties. In 2015–2016, much research has been actually addressed to this issue and this chapter will attempt to summarize the major advances in the scope of the photophysics of d-block metal complexes.

## 1 Introduction

Besides photochemistry and photocatalysis, which have been illustrated in Chapter 4, transition metal complexes find applications in many other fields, such as molecular electronics, OLEDs, solar energy conversion, *etc.* Luminescent transition metal complexes have also attracted attention in the biomedicine as intracellular sensors and bioimaging reagents. The main advantages are the high photostability, long-lived luminescence (allowing time-resolved detection) and large Stokes shifts. The latter, in particular, enables to minimize the self-quenching effects.<sup>1</sup> Wolf *et al.* recently reviewed the photophysical properties and applications of metal complexes containing pyrene moieties. Beside acting as an efficient fluorescent label, pyrene can actually affect the photophysical properties of metal complexes *e.g.* by extending excited state lifetimes as a consequence of the  ${}^3\text{MLCT}^*/{}^3\text{LC}_{\text{pyr}}^*$  equilibrium.<sup>2</sup>

## 2 First-row transition metals

Nowadays, the most widely used devices and photochemical processes are based on the scarcely abundant second/third row transition metals, thus generating expensive costs. In the last years, there has been a great interest in developing systems based on earth-abundant first-row transition metal species; the development of ultrafast spectroscopies has brought about a better understanding of the photophysical properties of these cheaper compounds.<sup>3,4</sup>

### 2.1 Iron

Dixon *et al.* investigated a series of organometallic Fe(II) complexes based on polypyridine, bis(phosphine) and carbon-bound ligands. The Authors verified the potentialities of the density functional theory (DFT) in foreseeing the photophysical properties of Fe(II) complexes, and identified on

---

*Dept. Chemistry, University of Pavia, via Taramelli 12, I-27100, Pavia, Italy.*

*E-mail:* amendola@unipv.it

this basis those pertaining to the lowest excited state of  $^3\text{MLCT}$  nature. Through DFT studies, Jablonski diagrams were also obtained, showing the lowest singlet, triplet, and quintet states for all the investigated complexes.<sup>5</sup> A new heteroleptic Fe( $\text{n}$ ) complex, containing one 2,2'-bipyridine (bpy) unit and the mesoionic 4,4'-bis(1,2,3-triazol-5-ylidene) ligand, was characterized by static and ultrafast spectroscopies. These studies pointed out a bathochromic shift of the absorption bands compared to homoleptic analogues. The strongly  $\sigma$ -donating 4,4'-bis(1,2,3-triazol-5-ylidene) ligand was found to destabilize the  $\text{MC}^*$  states relative to the  $\text{MLCT}^*$  state, and the corresponding lifetime (13 ps) was the longest obtained with a stable Fe( $\text{n}$ ) complex.<sup>6</sup> Among polynuclear complexes, Chen and Wu recently synthesised an emissive triple helical dinuclear Fe( $\text{m}$ ) complex, using a novel bis- $\beta$ -diketone ligand, *i.e.* the 3,5-bis-(3-oxobutanoyl)benzoic acid (BOBA). Compared to the free ligand, which exhibited a weak emission with an intra-molecular charge-transfer of  $n-\pi^*$  character, the  $\text{Fe}_2(\text{BOBA})_3$  helicate displayed a remarkable fluorescence in solution ( $\lambda_{\text{exc}} = 289 \text{ nm}$ ;  $\lambda_{\text{em}} = 359 \text{ nm}$ ), attributed to the charge-transfer  $\pi-\pi^*$  character of the emission.<sup>7</sup>

## 2.2 Copper

Emitting devices based on Cu( $\text{l}$ ) have attracted great attention due to the low toxicity of the metal. Novel luminescent Cu( $\text{l}$ ) complexes, characterized by high quantum yields and long-lifetimes in the solid state, were proposed by several authors as potential materials for electroluminescent devices. In most cases, the Cu( $\text{l}$ ) complexes were heteroleptic and displayed a distorted tetrahedral geometry.

Great attention was given, in particular, to heteroleptic Cu( $\text{l}$ ) complexes of N-heterocyclic (*e.g.* carbenes,<sup>8–11</sup> pyridine-1,2,4-triazoles,<sup>12</sup> phenanthroline<sup>13,14</sup> imidoyl-indazols,<sup>10</sup>) and phosphines ligands. The absorption bands of these compounds generally corresponded to LC and MLCT transitions and were influenced by the nature of the ligands.

Due to competitive non-radiative deactivations of excited states, the emission was generally weak in solution, while the enhanced emission in the solid state was ascribed to phosphorescence or delayed fluorescence processes. For instance, the polynuclear (*i.e.* tetra- and di-nuclear) Cu( $\text{l}$ ) complexes of a novel type of heterocyclic pyridylphospholane ligands showed a phosphorescence emission in the solid state, with bands in the 471–615 nm range.<sup>15</sup>

## 2.3 Zinc

The photophysical properties of Zn-based compounds have achieved a considerable interest<sup>16</sup> for the development of new luminescent materials, such as coordination polymers<sup>17</sup> and composites, *e.g.* the composite of polyaniline with Zn( $\text{n}$ ) bis(8-hydroxyquinolate) by Rafiqi *et al.*<sup>18</sup>

The coordination of Zn( $\text{n}$ ) generally enhances the ligand's luminescence, *e.g.* for Schiff-base ligands, and the corresponding complexes find applications in many fields, *e.g.* as OLEDs and luminescent chemosensors.

Das, Frontera, Escudero *et al.* recently studied the photophysical properties of the dinuclear Zn complexes with novel phenol-based “end-off” compartmental imino-ligands. The complexes displayed similar structural features, consisting of a dizinc cationic complex  $[\text{Zn}_2\text{L}(\text{CH}_3\text{COO})_2]^{2+}$  and a  $[\text{Zn}(\text{NCS})_4]^{2-}$  counter-anion [ $\text{L} = 2,6\text{-bis-(N-ethylmorpholine-iminomethyl)-4-R-phenol}$ ;  $R = -\text{CH}_3, \text{Cl}, t\text{Bu}$ ]. Moreover, the compounds were found to be fluorescent in solution at room temperature and phosphorescent in the solid state (*i.e.* in transparent KBr medium), with the *para*-substituents R playing a role in the emission properties.<sup>19</sup>

The Zn(II) complexes of the 2,4-dimethyl-6-((quinolin-8-ylimino)methyl)phenol Schiff-base ligand were synthesised using different Zn(II):ligand ratios. The emission of the free ligand was attributed to an excited state intramolecular/intermolecular proton transfer and was partially quenched by substituents through a PET mechanism. Upon Zn(II) coordination, an increase in the emission was observed. The coordination of more Zn(II) ions had a stronger effect, with the highest fluorescence observed in the trinuclear species. Due to the d<sup>10</sup> configuration of metal ion, the emission could not be attributed to MC\*, MLCT\* or LMCT\* states and was ascribed to a  $\pi-\pi^*$  intra-ligand transition (ILCT). The higher polarity of the excited state ( $S_1$ ) compared to the ground state ( $S_0$ ) was consistent with the bathochromic effect observed in polar solvents (see Fig. 1).<sup>20</sup>

A new series of Zn(II) and Hg(II) Schiff-base complexes were synthesised by Yang *et al.* The photophysical properties of these systems, such as emission colours, were found to depend on the ligand flexibility; in fact, by increasing the ligand rigidity, the emission wavelength of Zn(II) and Hg(II) complexes gradually changed from blue to red. Zn(II) complexes were all very emissive in solution, with an emission efficiency depending on molecular structure. Notably, for the corresponding Hg(II) complexes, the emission was reduced by the heavy atom effect.<sup>21</sup>

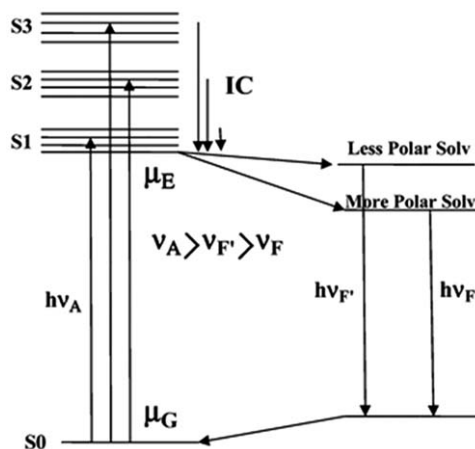


**Fig. 1** The Jablonski diagram is shown for the fluorescence emission with solvent relaxation. Reproduced from ref. 20 with permission from The Royal Society of Chemistry.

Eight bis(imino)acenaphthene Zn complexes, containing *para*-substituted aryl groups, were synthesised by Cowley *et al.* Most of the investigated complexes were emissive in the solid state, but not in solution, with emission colours spanning a range from red to yellow. The colour was connected to the electronic properties of the *para*-substituents, *e.g.* electron donating groups promoted emissions in the red region of the spectrum.<sup>22</sup>

New luminescent Zn and Cd-based octahedral complexes were synthesised by Rissanen *et al.* using a terpyridine-diphenylacetylene containing ligand. The blue fluorescence of the ligand was attributed to an intramolecular charge transfer from diphenylacetylene to terpyridine. By coordination of two ligands around a Zn (or Cd) centre, a distorted octahedral  $MN_6$ -like complex was obtained with a notable green emission from an intra-ligand charge transfer state. A strong dependence of emission maxima from solvent polarity was observed.<sup>23</sup>

The Zn(II) and Co(II) complexes of new phthalocyanines, containing four calixpyrrole arms, were synthesised and studied for their anion binding properties. Notably, the calixpyrrole units had no influence on the spectroscopic properties of the metal-phthalocyanine group. At the ground state, the interaction with the anions mainly involved the calixpyrrole units; while, at the triplet excited state, formed upon laser excitation, the binding of halides involved the metal-phthalocyanine moiety. This triplet excited state could be monitored by a 10 nm shift of the Q-band.<sup>24</sup> A new supramolecular 1:1 system was recently obtained, formed by both a crown ether-appended Zn-phthalocyanine (electron donor) and an ammonium group linked to fullerene (electron acceptor). Transient absorption experiments allowed for a better understanding of the excited-state interaction in the supramolecular complex. In particular, an intermolecular charge separation was found to develop from the photo-excited Zn-phthalocyanine to fullerene, leading to short-lived charge-separated states. This intermolecular charge separation was also obtained by photoexcitation of Zn-phthalocyanine dimers (and aggregates) and involved vicinal phthalocyanines.<sup>25</sup>

New substituted Zn(II)-phthalocyanines have been proposed by several authors as potential photodynamic therapy (PDT) agents. The coordination of Zn(II) (or other diamagnetic metal ions) to phthalocyanine derivatives generally leads to high quantum yields and long triplet lifetimes, thus making these systems suitable as photosensitizers in photodynamic therapy.<sup>26</sup> Tetrapyridoporphyrazines (TPyPz) are a type of phthalocyanines, in which the benzene rings are replaced by pyridines. The Zn(II) complex of alkylsulfanyl TPyPz, with the Q-band centred at ~730 nm, was found to promote high singlet oxygen production and it is thus a promising photosensitizer for photodynamic therapy (PDT).<sup>27</sup>

Through computational studies, Mazzone *et al.* recently elucidated the effects of heavy substituents (*e.g.* iodine atoms) on the photophysical properties of Zn(II)-phthalocyanines. In particular, the Authors showed that the substitution pattern significantly affected the absorption spectrum, but had little influence on the singlet-triplet energy gap. In addition, iodine substituents enhanced the spin-orbit coupling values,

increased the efficiency of singlet–triplet intersystem crossing and promoted singlet oxygen production.<sup>28</sup>

#### 2.4 Other first row metals

Among other first row metals, chromium and manganese gained a particular attention.

New organometallic dyads were recently obtained by Sierra and Fernandez, by attaching Cr(0) and W(0)-based Fischer carbene complexes to BODIPY chromophores, through a *p*-aminophenyl group linked to the C8 position of the BODIPY core. The absorption properties of these systems were similar to that of 4-anilinyl-substituted BODIPY, while the fluorescence emissions were reduced due to a Förster-type energy transfer involving the carbene unit. The replacement of the carbene with a carbonyl group led, in fact, to a higher emission intensity. The low fluorescence of these systems was also tuned by remote groups at the C8 position through  $\pi$ -conjugation.<sup>29</sup>

A  $\eta^6$ -coordinated species was obtained by complexation of [9]CPP or [12]CPP, cycloparaphenylenes (CPPs) to M(CO)<sub>6</sub> (M = Cr, Mo, W). Crystals suitable for X-ray diffraction studies were obtained for [9]CPP–Cr(CO)<sub>3</sub>, despite the poor stability of the complex toward ambient light and/or oxygen. The structural studies showed that metal coordination took place at the convex surface of the ligand. The weak absorption in solution was attributed to a weak HOMO–LUMO transition, as confirmed by TD-DFT calculations. The complexes showed a remarkable reactivity, leading to a rapid, one-pot and highly monoselective functionalization of the CPP ligand.<sup>30</sup>

A luminescent polynuclear Mn compound, [Mn<sub>4</sub>(ThiaSO<sub>2</sub>)<sub>2</sub>F][K(18-crown-6)] (ThiaSO<sub>2</sub> = *p*-*tert*-butylsulphonylcycl[4]arene), was recently obtained by Suffren *et al.*<sup>31</sup> The X-ray crystal structure showed a square of four Mn(II) ions sandwiched between two ThiaSO<sub>2</sub> units. The strong orange luminescence was attributed to a Mn(II)-centred  ${}^4T_1(t_{2g}^4e_g^1) \rightarrow {}^6A_1(t_{2g}^3e_g^2)$  transition. The quenching by molecular dioxygen was ascribed to an energy transfer process from the excited complex to O<sub>2</sub>, which then led to the excitation of O<sub>2</sub> to the  ${}^1\Sigma_g^+$  state. The high efficiency of quenching in the solid state depends on the open pore structure of [Mn<sub>4</sub>(ThiaSO<sub>2</sub>)<sub>2</sub>F][K(18-crown-6)], which allows fast diffusion of O<sub>2</sub> into the crystal lattice.

### 3 Second- and third-row transition metals

Transition metal complexes, in particular those containing metals of the second- and third-row with d<sup>6</sup> and d<sup>8</sup> electronic configurations [*i.e.* Ir(III), Re(I), Pt(II), Os(II) and Ru(II)], display a bright phosphorescence at room temperature, both in solution and in the solid state, thanks to the strong spin-orbit coupling (SOC) exerted by the heavy-atom, which promotes a fast intersystem crossing, between single and triplet excited states, and partially removes the spin-forbidden nature of the T<sub>1</sub>–S<sub>0</sub> radiative relaxation. These compounds find application as intracellular sensors and

bioimaging reagents,<sup>1</sup> but are also good candidates for NLO materials and OLEDs.

The direct involvement of the heavy-atom d orbital in the T<sub>1</sub> state can enhance the SOC effects in the T<sub>1</sub>-S<sub>0</sub> transition, resulting in a drastic decrease of the radiative lifetime. A large MLCT contribution thus reduces the possibility of a non-radiative decay. The S<sub>1</sub>-T<sub>1</sub> energy gap also influences the spin-orbit coupling: to a low energy gap corresponds, in fact, a high radiative rate constant and thus a higher quantum yield [ $k_r = \Phi \times \tau_{\text{em}}$ ,  $\tau_{\text{em}} = \text{emission decay time, } i.e. (k_r + k_{\text{nr}})^{-1}$ ].<sup>32</sup> Notably, metal-centred (<sup>3</sup>MC\*, d-d\*) excited states represent an important deactivation pathway of the phosphorescent emission; large separations between <sup>3</sup>MLCT\*/π-π\* and <sup>3</sup>MC\*/d-d\* states are actually associated to higher phosphorescence quantum yields.

### 3.1 Ruthenium

Over the last years, Ru-based coordination compounds have been applied in lots of light-induced electron and energy transfer processes, in new technologies and biomedical devices.<sup>33,34</sup> Between 2015 and 2016, hundreds of new ruthenium complexes have been synthesised, and their photophysical properties have been investigated for applications such as *e.g.* (bio)imaging<sup>35–37</sup> and PDT agents,<sup>38</sup> DNA intercalators,<sup>39</sup> theranostic agents<sup>40</sup> and sensitizers for solar cells.<sup>41</sup>

Ru(II) polypyridyl complexes are of particular interest because of their high luminescence, due to the little changes in bond parameters following the metal to ligand charge transfer.<sup>42</sup> Upon excitation by LED light in flow micro-reactors the <sup>1</sup>MLCT state is first populated, then it undergoes an efficient and fast intersystem crossing (ISC;  $\Phi_{\text{ISC}} \sim 1$ ) to give the triplet <sup>3</sup>MLCT\* state. In the absence of an external quencher, deactivation may occur *via* either emission or non-radiative pathway. Depending on the crystal field and thus on the energy gap between the excited states, thermal activation to a higher lying metal-centred (<sup>3</sup>MC\*) state is also possible. In this case, a non-radiative deactivation might be expected, due to the high reactivity of the metal centre.

Substituent groups on the pyridine ligands may strongly influence the photophysical and electrochemical properties of Ru(II) complexes, as well as their photo-catalytic activity (*e.g.* toward water oxidation). In a series of Ru(II) complexes [Ru(bda)(pyR)<sub>2</sub>] (H<sub>2</sub>bda = 2,2'-bipyridine-6,6'-dicarboxylic acid, pyR = pyridine with a substituent R at the 4-position), an increase in the electron-withdrawing tendencies of R promoted the red-shift of the MLCT absorption band, and increased the oxidation potential of the corresponding complexes.<sup>43</sup>

This is related to the variation of the energy level of molecular orbitals promoted by the substituent. For instance, due to the mesomeric effect of the hydroxy group, bpyOH and phenOH are poorer π-acceptors and possess higher-lying π\* orbitals compared to the unsubstituted analogues. This results in the destabilisation of the π(Ru) orbitals, and in the red-shift of <sup>1</sup>MLCT transitions ( $\lambda_{\text{abs}} = 461\text{--}488\text{ nm}$ ) compared to *e.g.* [Ru(bpy)<sub>3</sub>]<sup>2+</sup> ( $\lambda_{\text{abs}} = 422\text{ nm}$ ). The electron-richness of the ligands

increases upon the hydroxy group deprotonation, due to the delocalisation of the negative charge. The  $^1\text{MLCT}$  bands are consequently further red-shifted. For the complex  $[\text{Ru}(\text{bpy})_2(\text{phenOH})]^{2+}$ , DFT studies showed that the HOMO is mainly composed of the  $\text{d}\pi(\text{Ru})$  orbital, while the LUMO is a mixture of  $\pi^*(\text{bpy})$  and  $\pi^*(\text{phenOH})$  orbitals. This result is consistent with the attribution of the lowest-energy band to a  $^1\text{MLCT}$  transition. On the other hand, the HOMO of the deprotonated complex is a mixture of  $\text{d}\pi(\text{Ru})$  and  $\pi(\text{phenO}^-)$  orbitals, while the LUMO is mainly composed of  $\pi^*(\text{bpy})$ . In this situation, the lowest-energy transition has a mixture of MLCT and LLCT characters. At room temperature, in acetonitrile, the emission spectra showed broad and structureless bands centred between 622–688 nm, which underwent a red-shift under deprotonation.<sup>44</sup>

In a series of 3,5-difluorophenyl-substituted Ru(II) complexes, synthesised and studied by Zhu *et al.*, the electron-withdrawing 3,5-difluorophenyl group was found to extend the  $\pi$ -conjugation of bpy and phen ligands, facilitating the MLCT excited states and inducing red-shifts in the emission spectra. All the complexes showed an orange-red phosphorescent emission with the maxima between 605 and 638 nm.<sup>45</sup>

Datta *et al.* demonstrated how little differences in the ligand conformation could dramatically affect the photophysical properties of Ru(II) polypyridyl complexes, determining the nature of the electronic states. The Authors investigated, in particular,  $[\text{Ru}(\text{bpy})_2\text{L}]^{2+}$  and  $[\text{Ru}(\text{phen})_2\text{L}]^{2+}$  complexes, where L was the dihydrazone of 2,6-diacylpyridine. In the case of  $[\text{Ru}(\text{bpy})_2\text{L}]^{2+}$ , the HOMO was localized on L, thus a  $\text{L}(\pi)\text{-bpy}(\pi^*)$  charge transfer state (LLCT) was obtained upon excitation. The emission involved a  $^3\text{LLCT}^*$  state, which is rather uncommon in Ru(II) polypyridyl species. On the other hand, the  $[\text{Ru}(\text{phen})_2\text{L}]^{2+}$  complex was characterized by a metal centred HOMO and the emission occurred from the usual  $^3\text{MLCT}^*$ . Studies at 77 K showed that  $^3\text{LLCT}^*$  and  $^3\text{MLCT}^*$  states were in thermal equilibrium, thus the nature of the lowest excited state strongly depended on the conformation adopted by L in the two complexes.<sup>46</sup> Persson *et al.* recently synthesised and studied a series of homoleptic Ru(II) complexes based on asymmetric quinoline-pyrazole ligands [*i.e.* 8-(1-pyrazol)-quinoline, 8-(3-pyrazol)-quinoline, bis(quinolinyl)-1,3-pyrazole].<sup>47</sup> These studies pointed out that the orientation of the pyrazole unit, in relation to quinolone, could affect the geometric and electronic structures of the complexes, thus influencing the photophysical and photochemical properties of these systems. Rau *et al.* recently reported the optimized synthesis of the ligand tpphz(tbp)<sub>2</sub> [3,16-di(*tert*-butyl-phenyl)-tetrapyrido[3,2-*a*:2',3'-*c*:3'',2''-*h*:2''',3''',*f*]phenazine] as well as of the two regio-isomeric complexes Ru(tbp)<sub>2</sub>tpphz and Rutpphz(tbp)<sub>2</sub> (see Fig. 2).<sup>48</sup>

For the Ru(tbp)<sub>2</sub>tpphz isomer, compared to Rutpphz(tbp)<sub>2</sub>, emission studies pointed out that the *tert*-butyl-phenyl groups on the phen ligand had a stabilising effect on both  $^1\text{MLCT}$  and  $^3\text{MLCT}^*$  states, significantly affecting the absorption and emission spectra.

Wolf *et al.* studied a series of homoleptic and heteroleptic Ru(II) complexes, bearing thiienyl groups bound to a bpy ligand through direct, secondary and tertiary amide linkages. These studies showed that the

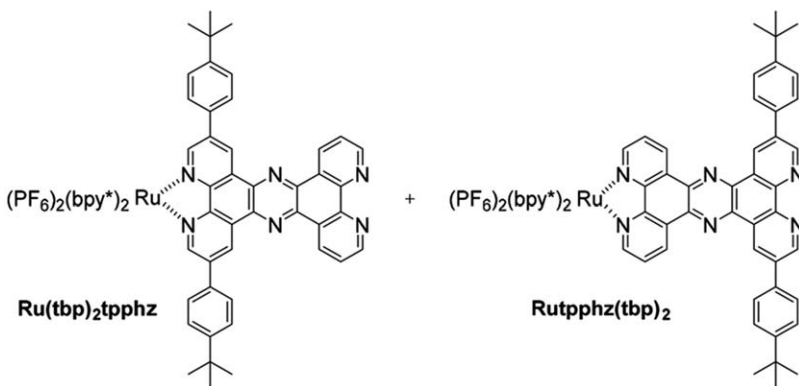


**Fig. 2**  $\text{Ru}(\text{tbp})_2\text{tpphz}$  and  $\text{Rutpphz}(\text{tbp})_2$  regio-isomeric complexes synthesised by Rau *et al.* Reproduced from ref. 48 with permission from The Royal Society of Chemistry.

amide bridge did not act as a direct conjugation path between  $[\text{Ru}(\text{bpy})_3]^{2+}$  and the peripheral thiaryl groups. On the other hand, the red-shift of the MLCT absorption bands, observed for the complexes with directly bound thiaryl and bithiaryl substituents, was attributed to a higher degree of conjugation from the periphery to the metal centre. The complexes bearing amide-linked thiophene substituents had quantum yields similar to  $[\text{Ru}(\text{bpy})_3]^{2+}$ ; while, for the directly bound analogues, the quantum yields were three times higher. Notably, much delocalized MLCT excited states resulted in a longer-lived excited state.<sup>49</sup>

The triazole-containing complex  $[\text{Ru}(\text{pytz})(\text{btz})_2]^{2+}$  (pytz = 1-benzyl-4-(pyrid-2-yl)-1,2,3-triazole, btz = 1,1'-dibenzyl-4,4'-bi-1,2,3-triazolyl), characterized by pytz- and btz-centred  $^1\text{MLCT}$  absorption bands at 365 and 300 nm, was found to undergo ligand loss upon irradiation in MeCN solution. The proximity in energy of  $^3\text{MLCT}^*$  and  $^3\text{MC}^*$  states, demonstrated by TD-DFT calculations, facilitated the efficient population of the latter, accounting for the observed photochemical reactivity.<sup>50</sup>

Rochfort *et al.* studied a series of bis-heteroleptic Ru(II) bisbipyridyl N-(carboxyaryl)amidoquinolate (CAQN) complexes with different degree of N-carboxyaryl fluorination. In these systems, both bonding and anti-bonding levels contained a significant mixture of metal and ligand contributions. As a result of this  $\text{Ru}(\text{d}\pi)\text{-CAQN}(\pi)$  mixing, the HOMO  $\rightarrow$  LUMO charge-transfer excitation, accessible with lower energy irradiation, was more properly described as a singlet (metal-ligand)-to-ligand charge-transfer ( $^1\text{MLLCT}$ ) transition. The absorption spectra were thus dominated by  $^1\text{MLLCT}$  electronic transitions, with a major contribution from  $[\text{Ru}(\text{d}\pi)\text{-CAQN}(\pi)] \rightarrow \text{CAQN}(\pi^*)$ . Fluorination of the N-carboxy-aryl group scarcely affected the absorption properties, while the first oxidation potential was tuned over a range of 0.92 V compared to  $[\text{Ru}(\text{bpy})_3]^{2+}$ .<sup>51</sup>

Solar cell dyes of the type  $[\text{Ru}(\text{L})_2(\text{NCS})_4]$  (with  $\text{L} = \text{dcb}, \text{dab}, \text{dpb}$ ;  $\text{dcb} = 4,4'\text{-dicarboxylato-2,2'-bipyridine}$ ;  $\text{dab} = 4,4'\text{-dianthracenethenyl-2,2'-bipyridine}$ ;  $\text{dpb} = 4,4'\text{-diphenylethenyl-2,2'-bipyridine}$ ) were investigated by George, Gordon *et al.*. The lowest energy absorption bands of

these systems corresponded to  $\{\text{Ru}(\text{NCS})_2\} \rightarrow \text{L}$  transitions, with strong contributions of the NCS ligands. Relatively short-living  $\{\text{Ru}(\text{NCS})_2\} \rightarrow \text{L}$  excited states were found for all the complexes, except for  $[\text{Ru}(\text{dcb})(-\text{dab})(\text{NCS})_2]$ . The latter system showed significantly different and long-lived excited state peaks, consistent with a LCCT (ligand centred charge transfer) transition, in which both the excited state electron and hole were located on the dab ligand.<sup>52</sup>

Commonly, the emission lifetime of polypyridyl Ru(II) complexes decreases upon temperature increase, due to the thermal population of  ${}^3\text{MC}^*$  states from  ${}^3\text{MLCT}^*$ , followed by the fast non-radiative decay of  ${}^3\text{MC}^*$  to the ground state. Nevertheless, Kitamura *et al.* found that, for the complex  $[\text{Ru}(\text{phen})_2\{4-(\text{dimesityl})\text{borylduryl}\text{ethynyl-phen}\}]^{2+}$ , the emission lifetime was almost independent of temperature. In the 4-(dimesityl)borylduryl-ethynyl-phen ligand, in fact, the  $\pi$ -orbital of the aryl group [ $\pi(\text{aryl})$ ] gives a CT interaction with the vacant p-orbital on the boron atom [ $\text{p(B)}$ ,  $\pi(\text{aryl})-\text{p(B)}$  CT]. In the Ru(II) complex, synergistic MLCT/ $\pi(\text{aryl})-\text{p(B)}$  CT interactions induced the stabilization of  ${}^3\text{MLCT}^*$  relative to  ${}^3\text{MC}^*$ , thus inhibiting the thermal activation of the non-radiative state.<sup>53,54</sup>

Synergistic MLCT/ $\pi(\text{aryl})-\text{p(B)}$  CT interactions were also observed in a series of Ru(II) complexes, containing a number ( $n$ ,  $n=1-3$ ) of triarylborane-appended 2,2'-bipyridine ligand(s). In the excited states of these complexes, intramolecular  $\pi(\text{aryl})-\text{p(B)}$  CT transitions synergistically interacted with MLCT transitions, enhancing both  $\epsilon(\text{MLCT})$  and emission quantum yields. This effect was found to increase with increasing  $n$ .<sup>55</sup> The heteroleptic Ru(II) complexes of bidentate 2-[ $(\text{alkylthio})\text{methyl}$ ]pyridine ( $\text{N}^{\text{S}}$ ) ligands and diimines ( $\text{N}^{\text{N}}$ ) co-ligands, *i.e.*  $[\text{Ru}(\text{N}^{\text{N}})_2(\text{N}^{\text{S}})]^{2+}$ , showed strong emissions from the  ${}^3\text{MLCT}^*$  states governed by the  $\text{N}^{\text{N}}$  donors, at both room temperature and 80 K. Higher non-radiative decay rates were rather attributed to  $\text{N}^{\text{S}}$  ligands. The latter also increased the oxidation potential of the  $\text{Ru}^{2+}/\text{Ru}^{3+}$  couple, resulting in a blue-shift of the absorption maxima compared to the homoleptic  $[\text{Ru}(\text{N}^{\text{N}})_3]^{2+}$  analogues.<sup>56</sup>

A bridged di-Ru compound,  $[(\text{bpy})_2\text{Ru}(\mu-\text{L})\text{Ru}(\text{bpy})_2]\text{Cl}_4 \cdot 6\text{H}_2\text{O}$ , was obtained by reacting the *cis*-bis(2,2'-bipyridine)dichloro Ru(II) hydrate with a new bipyridyl macrocycle (see L in Fig. 3). X-ray diffraction studies revealed that the macrocycle adopted a bowl-like conformation in the crystal, with a distance between the exo-coordinated Ru(II) ions of 7.29 Å. The dinuclear complex displayed the typical absorption bands of ruthenium polypyridyl species (*i.e.*  $\pi-\pi^*$  from 260–320 nm,  ${}^1\text{MLCT}$  at 451 nm), and a  ${}^3\text{MLCT}^*$  band at 610 nm in the emission spectrum ( $\tau = 706$  ns,  $\Phi_{\text{PL}} = 0.021$ ). No triplet-triplet annihilation between the adjacent  $[\text{Ru}(\text{bpy})_3]^{2+}$  units was observed, under the relatively mild excitation conditions used by the Authors. This system was also found to be a selective photocatalyst for the radical cation Diels–Alder reaction between *trans*-anethole and isoprene.<sup>57</sup> A series of new dinuclear and mono-nuclear complexes, *i.e.*  $[(\text{bpy})_2\text{Ru}(\text{L})\text{Ru}(\text{bpy})_2]^{4+}$  and  $[(\text{bpy})_2\text{Ru}(\text{L})]^{2+}$  with  $\text{L} = 2,6\text{-di}(1\text{H-imidazo}[4,5-f][1,10]\text{phenanthrolin-2-yl})\text{aryl}$  ligands, were synthesised and studied by Maynadié *et al.*<sup>58</sup> The Authors analysed the

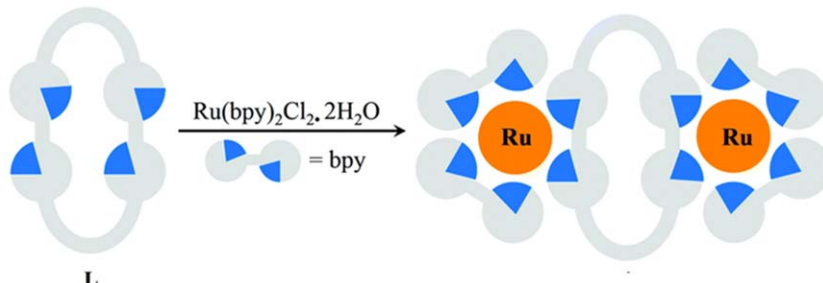
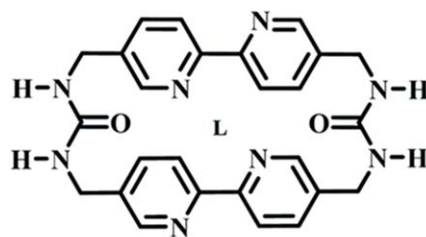


**Fig. 3** Bridged di-Ru complex,  $[(\text{bpy})_2\text{Ru}(\mu\text{-L})\text{Ru}(\text{bpy})_2]^{4+}$ , obtained by reacting the *cis*-bis(2,2'-bipyridine)dichloro Ru(II) hydrate with the bipyridyl macrocycle L by Shimizu *et al.* Reproduced from ref. 57 with permission from The Royal Society of Chemistry.

connection between the nature of the aryl core (*i.e.* benzene, pyridine, 4-*tert*-butyl phenol) and the photophysical properties of the corresponding Ru complexes. The comparison between mononuclear and dinuclear species, bearing the same ligands, showed no difference in the absorption spectra, except for the intensity of the MLCT band, which was twice for the dinuclear species. This demonstrated that the two Ru(II) centres were independent whatever the nature of the aryl core. Notably, upon oxidation of the Ru(II) centres, the MLCT bands were replaced by LMCT bands. Moreover, a new broad band appeared at 1260 nm, attributable to the inter-valence charge-transfer (IVCT) transition of the mixed-valence Ru(II)/Ru(III) species. Notably, for all the investigated complexes, both emission maxima and luminescence lifetimes were close to those of  $[\text{Ru}(\text{bpy})_3]^{2+}$ .

A family of  $[(\text{Ru}(\text{bpy})_2)_n(\text{L})][(\text{PF}_6)_{2n}]$  complexes [with  $n = 1\text{--}3$  and L = tris-2'',4'',6''-(2,2'-bipyridin-4-yl)-1'',3'',5''-triazine] were studied by Ciofini, Hannan *et al.*

Interestingly, the triazine containing ligand was found to induce a bathochromic shift of the MLCT absorption band compared to  $[\text{Ru}(\text{bpy})_3]^{2+}$ . The lower energy of the  $^1\text{MLCT}$  transition was attributed to a greater  $\pi$ -acceptor ability of the bpy subunit attached to triazine. Similarly, emission studies pointed out the red-shift of the  $^3\text{MLCT}^*$  band from 608 nm to 712 nm. A shorter excited-state lifetime was also observed; in fact, the lower energy of the excited state promoted a faster non-radiative decay.<sup>59</sup>

Hayvali *et al.* proposed a new interesting Ru(bpy)<sub>3</sub>-rhodamine triad, in which the rhodamine was the acid-responsive unit with a reversible spirolactam↔open-amide conversion. The Ru(II) centre was instead responsible for the triplet state generation upon excitation. In the absence of acid, a quenched  $^3\text{MLCT}^*$  state was obtained ( $\tau = 103.6$  ns), due to a PET from the rhodamine to the Ru(II) subunit. Upon

acidification, the open-amide form of rhodamine was generated and the PET was thus inhibited. In this situation, a triplet excited state ( $^3\text{IL}^*$ ) was obtained, located on the rhodamine moiety. Intramolecular singlet-triplet energy transfer and triplet-triplet energy transfer (TTET,  $^3\text{MLCT}^* \rightarrow ^3\text{IL}^*$ ) were observed for this system using femtosecond and nanosecond transient absorption spectroscopies.<sup>60</sup>

New Ru(II) bis(terpyridine) methanofullerene and pyrrolidinofullerene dyads were developed by Crowley *et al.* Notably, the absorption spectra of the dyads were mainly a superposition of the single units' spectra, thus showing that only weak interactions between the Ru- and C<sub>60</sub>-based subunits occurred in the ground state.

On the other hand, strong interactions were found in the excited state. In fact, the  $^3\text{MLCT}^*$  state, obtained upon excitation of the Ru-based  $^1\text{MLCT}$  transition, was rapidly depopulated to give the lower lying triplet excited state  $^3\text{C}_{60}^*$ . The energy transfer process showed a dependence on both linker type and distance.<sup>61</sup> The photophysical properties of a Ru 4H-imidazole complex, bearing a carboxyl group as an anchoring moiety [*i.e.* bis(4,4'-di-*tert*-butyl-2,2'-bipy- $\kappa^2\text{N},\text{N}'$ )-[2-(4-carboxyphenyl)-4,5-bis(*p*-tolylimino- $\kappa\text{N}$ )imidazolato]Ru(II)hexafluorophosphate] were investigated both in solution and on a nanocrystalline TiO<sub>2</sub> film support. When the unprotonated complex was anchored to TiO<sub>2</sub>, a photoinduced electron injection to the semiconductor took place from thermally non-relaxed  $^3\text{MLCT}^*$  states, with a time constant of 0.5 ps and an injection efficiency of about 25%. Notably, the electron injection did not involve the thermalized  $^3\text{MLCT}^*$  state, probably because its energy is lower than the conduction band edge of TiO<sub>2</sub>.<sup>62</sup>

Novel metallocene-functionalized chlorin complexes were synthesised by Kahnt and Juho Helaja. The ruthenocene derivatives, in particular, were found to be stable under irradiation.

Transient absorption studies pointed out the formation of charge-separated states, from the ruthenocene unit to the singlet excited state of chlorin (lifetimes of 152–1029 ps), followed by recombination into the first excited triplet state.<sup>63</sup>

### 3.2 Rhenium

Tricarbonyl Re(I) complexes of the type *fac*-[Re(N<sup>+</sup>N)(CO)<sub>3</sub>(L)]<sup>0/+</sup> (N<sup>+</sup>N = phen, bpy; L = monodentate ancillary ligand) find applications in a number of contexts, including optical probes/biomarkers, singlet oxygen producing devices<sup>64</sup> and photocatalysis. The lowest excited states of these complexes generally derive from MLCT transitions, which can be variably mixed to LLCT transitions depending on the nature of the ancillary ligands. Massi *et al.* studied a series of Re(I) tetrazolato complexes, *fac*-[Re(N<sup>+</sup>N)(CO)<sub>3</sub>(L)] (see Fig. 4), obtained by methylation of a *para* substituted 5-aryltetrazolate (L). Before methylation, the excited state was ascribed to mixed  $^3\text{MLCT}^*$  and  $^3\text{LLCT}^*$ , whereas after methylation it became a pure  $^3\text{MLCT}^*$ . Methylation, in fact, removed the contribution of the tetrazole  $\pi$ -orbitals from the HOMO. The photophysical properties of the methylated complex were found improved in terms of

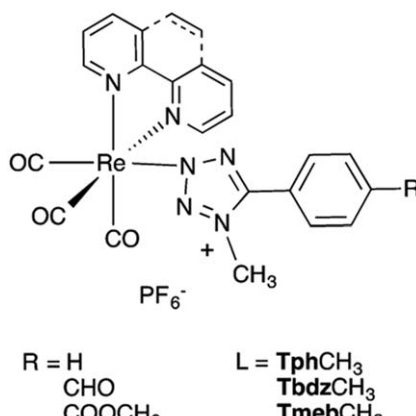


**Fig. 4** Methylated *fac*-[Re(diim)(CO)<sub>3</sub>(L)]<sup>+</sup> complexes, synthesised by Massi *et al.* Reproduced from ref. 65 with permission from The Royal Society of Chemistry.

quantum yields. Longer excited state lifetimes and blue-shifted emission maxima were also observed.<sup>65</sup>

Vega *et al.* investigated the photophysical properties of the new complex  $P,N\{(\text{C}_6\text{H}_5)_2(\text{C}_5\text{H}_4\text{N})\text{P}\}\text{Re}(\text{CO})_3\text{Br}$ . These studies pointed out the existence of two emissive  $d\pi \rightarrow \pi^*$  pyridine and  $d\pi \rightarrow \pi^*$  phenyl excited states, different in nature but close in energy, responsible for the biexponential luminescent decay observed. TD-DFT calculations allowed the identification of the participating orbitals. The conformational flexibility of the pyridylphosphine ligand, which favours a radiation-less decay, is probably responsible of the low emission quantum yield observed for the complex.<sup>66</sup>

The series of dicarbonyl Re(i) complexes, [Re(phen)(CO)<sub>2</sub>L]<sup>+</sup> (with L = alkynyl(aryl)phosphanes), studied by Koshevoy *et al.*, displayed a strong phosphorescence due to <sup>3</sup>MLCT\* excited states, independently of the nature of the phosphane ligands, L. For the tricarbonyl analogues, a strong dependence of the emission efficiency on L was instead observed, promoted by the pronounced  $\pi - \pi^*$  contribution of L to the electronic transitions of the complex. These observations were supported by TD-DFT studies.<sup>67</sup>

Ko *et al.* reported a new series of luminescent isocyanoRe(i) complexes, with chelating acyclic diaminocarbene ( $\text{N}^{\text{C}}$ ) ligands, characterized by a phosphorescence spanning from blue to red. The emission maxima depended on the number of isocyanide ligands, as well as on the substituents of diaminocarbene units. In  $\text{CH}_2\text{Cl}_2$  solution, the lowest-energy absorption and the phosphorescence derived from the predominant MLCT [ $d\pi(\text{Re}) \rightarrow \pi^*(\text{N}^{\text{C}})$ ] transition.<sup>68</sup>

In collaboration with Lau *et al.*, Ko also synthesised a new family of neutral isocyanoborato Re(i) diimine complexes, presenting iso-cyanoborate and diimine ligands of diverse electronic and steric features ([Re(CO)<sub>3</sub>(N<sup>N</sup>)(CNBR<sub>3</sub>)]; N<sup>N</sup>=bpy, Me<sub>2</sub>bpy, phen, Me<sub>2</sub>phen, *etc.*; R = C<sub>6</sub>F<sub>5</sub>, C<sub>6</sub>H<sub>5</sub>, Cl, *etc.*). At room temperature in  $\text{CH}_2\text{Cl}_2$ , upon excitation into the lowest-energy absorption, these complexes displayed a long-lived bluish-green to yellow phosphorescence ( $\lambda_{\text{exc}} < 400$  nm;  $\lambda_{\text{em}} = 481 - 554$  nm) with quantum yields up to 0.67. DFT and TD-DFT calculations

revealed that the lowest-energy electronic transition derived from a mixture of MLCT [ $d\pi(\text{Re}) \rightarrow \pi^*(\text{N}^{\wedge}\text{N})$ ] and LLCT [ $\pi(\text{CNBR}_3) \rightarrow \pi^*(\text{N}^{\wedge}\text{N})$ ] contributions. Complexes with the same isocyanoborate ligand showed, in fact, a dependence of the absorption energy on the electronic nature of the  $\text{N}^{\wedge}\text{N}$  subunit. The improved quantum efficiency and the blue-shifted emission energy, compared to their cyano precursors, are effects of the stronger  $\pi$ -accepting capabilities of isocyanoborate ligands, which stabilize the  $d\pi(\text{Re})$  orbitals and raise the energy of the deactivating ligand-field states.<sup>69</sup>

New phosphorescent mononuclear and binuclear  $\text{Re}(\text{i})$  polypyridine ( $\text{N}^{\wedge}\text{N}$ ) complexes, containing a 1,2,4,5-tetrazine ligand, were synthesised and studied by Lo *et al.* as phosphorogenic bioorthogonal probes. These complexes showed intense  $^1\text{IL}$  ( $\pi-\pi^*$ ) absorption bands in the range 260–339 nm, weaker  $^1\text{MLCT}$  [ $d\pi(\text{Re})-\pi^*(\text{N}^{\wedge}\text{N})$ ] shoulders, between 371 and 390 nm, and a weak band around 540 nm assigned to the tetrazine moiety ( $n-\pi^*$ ). The  $^3\text{MLCT}$  [ $d\pi(\text{Re})-\text{p}^*(\text{N}^{\wedge}\text{N})$ ] emission was quenched by fluorescence resonance energy transfer (FRET) from the  $\text{Re}(\text{i})$ -subunit to tetrazine, hence the luminescence quantum yields were much lower ( $\Phi_{\text{PL}} < 0.05$ ) than those of common  $\text{Re}(\text{i})$  polypyridine species. These complexes showed a substantial dienophile-induced emission enhancement, allowing the Authors to target dienophile-modified proteins in living cells.<sup>70</sup>

### 3.3 Iridium

In 2015–2016, the photophysical properties of  $\text{Ir}(\text{m})$  complexes, especially cyclometalated ones, have raised great interest for applications in the fields of light emitting devices, *e.g.* as OLEDs phosphors,<sup>71–82</sup> light-emitting electrochemical cells,<sup>83,84</sup> dye-sensitized solar cells,<sup>85</sup> chemosensors,<sup>86</sup> and bioimaging agents.<sup>87,88</sup> In contrast to the narrow orange-red emission range of  $\text{Ru}(\text{n})$  polypyridyl complexes, the phosphorescence of cyclometalated  $\text{Ir}(\text{m})$  complexes spans the whole visible spectrum. Moreover, a greater ligand-field stabilisation energy imparts a higher photostability to the complexes of third-row metals, such as  $\text{Ir}(\text{m})$ , compared to the corresponding stability of the second-row ions. For the latter, the population of the  $^3\text{MC}^*$  states might lead to photo-decomposition, *e.g.* light-induced ligand loss.

In the complexes of type  $[\text{Ir}(\text{C}^{\wedge}\text{N})_2(\text{N}^{\wedge}\text{N})]^+$  ( $\text{C}^{\wedge}\text{N}$  = cyclometalating ligand, *e.g.* 2,5-diaryl-1,3,4-oxadiazoles<sup>89</sup> and 2-phenylpyridine;  $\text{N}^{\wedge}\text{N}$ : diimine ancillary ligand, *e.g.* substituted 2,2'-bpy), the desired emitting colour can be arrived at by modifying  $\text{C}^{\wedge}\text{N}$  and  $\text{N}^{\wedge}\text{N}$  ligands. The emissive excited states of these complexes are, in fact, a mixture of  $^3\text{MLCT}^*$  [between  $\text{Ir}(\text{m})$  and  $\text{N}^{\wedge}\text{N}$  ligands] and  $^3\text{LLCT}^*$  states [between the phenyl rings of the  $\text{C}^{\wedge}\text{N}$  ligands and the  $\text{N}^{\wedge}\text{N}$  ligands]. Consequently, HOMOs and LUMOs' energies can be modulated independently, by choosing the appropriate substituents for  $\text{C}^{\wedge}\text{N}$  and  $\text{N}^{\wedge}\text{N}$  ligands.

For systems of the type  $[\text{Ir}(\text{ppy})_2(\text{N}^{\wedge}\text{N})]^+$  (Hppy = 2-phenylpyridine), the HOMO is composed of a mixture of  $\text{Ir}(\text{m})$ - $d\pi$  orbitals and phenyl(ppy)- $\pi$  orbitals, while the LUMO is completely localized over the diimine ligand

(N<sup>+</sup>N). A high conjugation of N<sup>+</sup>N is expected to promote the LUMO stabilization and the HOMO–LUMO gap decrease. This is not the case for the series of Ir(III) complexes containing *p*-phenylethynyl-1,10-phenanthroline ligands of different length, for which the photophysical properties showed only a little dependence on the conjugation extent.<sup>90</sup> Theoretical studies by Bai, Zhang *et al.* demonstrated that there exists a striking correlation between the π-conjugation on C<sup>+</sup>N ligands and the radiative/nonradiative decay rate. According to the Authors, the larger π-conjugation, “the faster radiative decay rate (due to the stronger intersystem crossing by SOC interaction) and the slower nonradiative decay rate (due to the larger energy gap between the excited triplet state and the ground state)”.<sup>91</sup>

Electron-withdrawing substituents, such as fluorine atoms<sup>92</sup> –CF<sub>3</sub>, –OCF<sub>3</sub>, –SCF<sub>3</sub><sup>93</sup> or sulfonyl groups<sup>94</sup> on the phenyl moiety of ppy-type C<sup>+</sup>N ligands are able to stabilize the iridium pseudo-t<sub>2g</sub> orbitals and consequently the HOMO level, without affecting the LUMO. This increases the emission energy of the related complexes, and represents a good starting point for the development of new Ir(III)-based blue-emitting phosphors, which are more unusual than red and green-emitting ones. The 2-(2,4-difluorophenyl)pyridine (dfppy) ligand, for instance, is known to provide short emission wavelength Ir(III) complexes.

For the cyclo-metalating C<sup>+</sup>N ligands, the replacement of the pyridine moiety with fragments characterized by a higher lying LUMO could raise the energy of both MLCT and LC transitions. Blue-emitting complexes were also obtained by attaching electron-donating groups to the pyridine moiety of ppy-type C<sup>+</sup>N ligands; this structural variation actually increases the energy of the triplet <sup>3</sup>(π–π\*) state.<sup>95</sup> The emission from this excited state can be ensured by using electron-rich/non-conjugated ancillary ligands.

The complex [Ir(dph-oxd)<sub>2</sub>(bpy)]<sup>+</sup>, with dph-oxd (2,5-diphenyl-1,3,4-oxadiazole) as the C<sup>+</sup>N ligand, showed a largely stabilized HOMO caused by the electron-deficient 1,3,4-oxadiazole (oxd) fragment. This stabilization brought about a larger HOMO–LUMO gap, compared *e.g.* to [Ir(ppy)<sub>2</sub>(bpy)], and consequently a blue-shifted emission.<sup>96</sup> On the other hand, the synergistic effect of steric hindrance and electron-donating substituents on C<sup>+</sup>N ligands was shown to improve the emission quantum yields of new yellow and red emitting phosphorescent Ir(III) complexes, containing 2-thienyl quinazoline C<sup>+</sup>N ligands.<sup>97</sup> Notably, the HOMO–LUMO gap could be increased also by employing strong-field ancillary ligands, such as cyanide, carbonyl, phosphine, and carbene (NHC) units, which destabilise the MC\* states and thus favour the radiative deactivation pathway.<sup>98,99</sup>

Among ancillary ligands, aryl isocyanides offer a versatile control thanks to the selective substitution at the aryl ring periphery. Teets *et al.*, studying a series of new bis-cyclometalated bis(aryl isocyanide)Ir(III) complexes, demonstrated that aryl isocyanide ligands (CNAr) lead to redox-stable luminescent Ir compounds, with emission colours spanning from blue, *i.e.* [Ir(dfppy)<sub>2</sub>(CNAr)<sub>2</sub>]<sup>+</sup>, to orange, *i.e.* [Ir(btp)<sub>2</sub>(CNAr)<sub>2</sub>]<sup>+</sup> (btp = 2-benzothienylpyridine). In most cases, the photophysical

properties of the complexes showed a little dependence on the CNAr ligand structure, and the emission generally involved a 3LC\* state with minimal contribution from 3MLCT.<sup>100</sup> The same Authors showed that the fluorination of  $\beta$ -ketoiminate (acNac) and  $\beta$ -diketiminate (NacNac) ancillary ligands significantly change the redox and photophysical properties of the corresponding bis-cyclometalated Ir(III) complexes [*i.e.*  $[\text{Ir}(\text{C}^{\text{N}}\text{N})_2(\text{LL}')]$  with LL' = acNac or NacNac]. The Ir(IV)/Ir(III) redox potential, for instance, showed a dependence on the degree of fluorination on the ancillary ligand. Fluorination of NacNac also altered the excited-state properties of the corresponding complexes. In the presence of backbone CF<sub>3</sub> groups, for instance, the complexes displayed a luminescence in the red and near-infrared regions out of a  $\pi \rightarrow \pi^*$  NacNac-centred triplet state.<sup>101</sup>

New orange-emitting ( $\lambda_{\text{em}} = 606$  nm), water-soluble compounds of the formula  $[(\text{ppy})_2\text{Ir}(\text{bpy})]\text{X}$  ( $\text{X}^- = \text{EtO}^-$ ,  $\text{OH}^-$ ,  $\text{EtOCH}_2\text{CO}_2^-$ ,  $\text{MeOCH}_2\text{CO}_2^-$ , see Fig. 5) were obtained by Godbert *et al.* from the cyclometalated Ir(III) chloro-bridged dimeric precursor,  $[(\text{ppy})_2\text{Ir}(\mu\text{-Cl})]_2$ , through a new microwave-assisted procedure. The chloro-bridged complex was first converted into the corresponding hydroxy-bridged dimer, which was then employed for the synthesis of all the complexes. The intermediate  $[(\text{ppy})_2\text{Ir}(\mu\text{-OH})]_2$  showed a strong base character and an unexpected oxidative ability towards the alcoholic function of glycol ethers. Notably, all of the new compounds displayed gelation tendencies, forming gel phases upon increasing the concentration in water.<sup>102</sup>

The cyclometalated Ir(III) carbene complexes of formula  $[\text{Ir}(\text{C}^{\text{N}}\text{N})_2(\text{C}^{\text{C}}\text{:})]$ , containing a naphthalimide chromophore bound to the N-heterocyclic carbene ligand, are characterised by a deep-red phosphorescent emission. These new compounds also showed an envelope of absorption bands above 350 nm and a long low-intensity tail around 500 nm. The latter was attributed to the direct singlet-triplet absorption, promoted by the large SOC of iridium. The emission spectra of the complexes, dispersed in polymeric film, displayed a structured emission above 630 nm (*i.e.* deep-red).<sup>103</sup> A bichromophore, consisting of a bis-cyclometalated Ir(III) complex covalently bound to a 4-piperidinyl-1,8-naphthalimide (PNI) unit through a phen ligand, was recently synthesised by Castellano *et al.* The emission studies pointed out that the initially excited PNI unit (<sup>1</sup>LC) transferred its energy to the Ir(III) chromophore through a Förster resonance energy-transfer process. Following

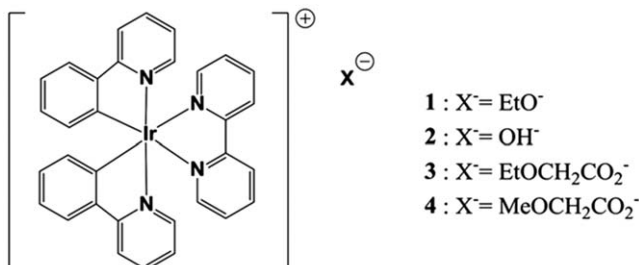


**Fig. 5** Chemical structures of the  $[(\text{ppy})_2\text{Ir}(\text{bpy})]\text{X}$  complexes by Godbert *et al.* Reproduced from ref. 102 with permission from The Royal Society of Chemistry.

a fast ISC and the formation a  $^3\text{MLLCT}^*$  state centred on the Ir(III) chromophore, the energy was transferred back to the PNI unit leading to a  $^3\text{LC}^*$  state. The thermal equilibrium between the  $^3\text{LC}^*$  and  $^3\text{MLLCT}^*$  states is responsible of the remarkable room-temperature excited-state lifetimes ( $\tau = 8.8$  ms).<sup>104</sup>

The bis(cyclometalated) complexes of the formula  $[\text{Ir}(\text{ppy})_2(\mu-\kappa\text{C}^\alpha:\eta^2-\text{C}=\text{CR})]_2$  ( $\text{R} = \text{e.g. } 4\text{-MeC}_6\text{H}_4, 4\text{-OMeC}_6\text{H}_4, 1\text{-naphthyl}$ ), stabilized by a double alkynyl bridging system, were prepared by alkynylation of the dichloro-bridged complex  $[\text{Ir}(\text{ppy})_2(\mu\text{-Cl})]_2$ . In most cases, only one diastereoisomer (*i.e.*  $\Lambda\Lambda/\Delta\Delta$ ) was obtained from the synthesis. All of the complexes displayed a green emission ( $\lambda_{\text{em}} = 505\text{--}515$  nm) in solution at 298 K, with higher quantum yields ( $\Phi = 0.007\text{--}0.024$ ) than the precursor  $[\text{Ir}(\text{ppy})_2(\mu\text{-Cl})]_2$  ( $\Phi = 0.0037$ ). The emission was attributed by the Authors to a mixed charge transfer  $^3\text{MLCT}^*/^3\text{L}'\text{LCT}^*$  ( $\text{L} = \text{ppy}; \text{L}' = \text{C}\equiv\text{CR}$ ) state. For the naphthylacetylide derivative, a switch from the  $^3\text{MLCT}^*/^3\text{L}'\text{LCT}^*$  state to a long-lived low lying  $^3\text{LC}^*$  state, centred on the naphthalene moiety, was observed at 77 K.<sup>105</sup>

### 3.4 Platinum and palladium

The photophysical properties of cyclo-metallated Pt(IV)<sup>106</sup> and Pt(II) complexes are of great interest due to potential applications as luminescent labels for bio-imaging,<sup>107</sup> in dye-sensitised solar cells<sup>108</sup> and as triplet emitters in OLEDs.<sup>109–112</sup> In the latter context, in particular, square-planar Pt(II) complexes with N-heterocyclic carbenes and cyclo-metallated fragments ( $\text{C}^\wedge\text{C}$ ) are very efficient systems. The electronic properties of these complexes can be tuned by modifying the  $\text{C}^\wedge\text{C}$  units, while steric features are usually varied through the auxiliary ligands (*e.g.*  $\beta$ -diketonato,  $\beta$ -ketoimimates, amidinate).<sup>113–117</sup>

In the absence of intermolecular Pt(II)/Pt(II) interactions, phosphorescence generally originates from  $^3\text{LC}^*$ ,  $^3\text{LLCT}^*$  or/and  $^3\text{MLCT}^*$  states. Cyclo-metallated and NHC-carbene ligands, being strong  $\sigma$ -donors, increase the energy gap between occupied and unoccupied orbitals, and consequently have a hypso-chromic effect on the emission. The use of strong-field ligands has also the advantage of raising the energy of the quenching states (*i.e.* MC\* and LMCT\*), resulting from the population of metal d $\sigma^*$  orbitals. It has to be reminded that the population of d $\sigma^*$  orbitals implicates a significant geometry distortion of the complex, leading to ligand dissociation or causing the metal centre reduction.

New blue/green phosphorescent Pt(II) complexes have been obtained by Strassert, De Cola *et al.* using a new bidentate NHC $^\wedge$ pyrazolate ligand precursor, consisting of a benzimidazol-2-ylidene and a pyrazolate unit linked together through a methylene spacer. The electronic and steric environments of these complexes, as well as the *cis/trans* configurations adopted, could be modified by introducing proper substituents of the ligands frame. In particular, the Pt(II) complex, containing both the NHC $^\wedge$ pyrazolate ligand and a bulky adamantyl functionalized pyridine-triazole luminophore, showed an intense blue phosphorescence ( $\lambda_{\text{em}} = 470$  nm) with high quantum yields in the solid state.<sup>118</sup>

For Pt(II) complexes, intermolecular face-to-face d-d interactions are rather common, promoting the splitting of the z-oriented  $5d_{z^2}$  and  $6p_z$  atomic orbitals (which are occupied and unoccupied, respectively) into filled  $d\sigma/d\sigma^*$  and unfilled  $p\sigma/p\sigma^*$  molecular orbitals. These interactions are favoured, as they lead to an overall energy stabilization. Upon irradiation, an electron can be promoted from a  $d\sigma^*$  antibonding orbital to the weakly bonding  $p\sigma$  orbital. The excited dimer is thus characterised by a new emissive  $^3\text{MMLCT}^*$  (metal–metal-to-ligand charge transfer) state, corresponding to a red-shifted transition (compared to that caused by the combined LC and MLCT excited states) in the emission spectrum. Besides these excited dimers, excimers can be also observed.

Cyclo-metalated Pt(II) complexes with pincer ligands have attracted attention for their rich photophysical properties. Among pincer-type Pt(II) complexes, tridentate cyclo-metalated Pt(II) acetylides compounds have gained attention for their rich luminescence properties. Thanks to their less-distorted square-planar geometry, these complexes are better emitters in solution than the Pt-tpy analogues. Moreover, aryl/alkyl acetylides and NHC carbene ligands, being  $\sigma$ -donors, raise the energy of the Pt(II)  $d_{x^2-y^2}$  orbital, thus promoting the radiative decay from the  $^3\text{MLCT}^*/^3\text{LLCT}^*$  states in solution at room temperature. Many new phosphorescent pincer-type complexes have been developed in 2015–2016, with applications in various fields *e.g.* for anion-binding, as anti-cancer and PDT agents.<sup>119,120</sup>

The introduction of electron-withdrawing substituents, in particular carborane, on  $\sigma$ -alkynyl auxiliary ligands, was found to promote the stabilisation of the HOMO level in Pt(II) [and Pd(II)] complexes with cyclo-metalating  $\text{N}^{\wedge}\text{C}^{\wedge}\text{N}$  ligands (see Fig. 6). This is accompanied by the increase of the HOMO–LUMO gap and, consequently, by the blue-shift of the emission.<sup>121</sup>

A new Pt(II) and Pt(II) complexes were synthesised by Moussa, Amouri *et al.*, using a  $\text{N}^{\wedge}\text{C}^{\wedge}\text{N}$  tridentate ligand characterised by two lateral pyridines and a central 6-membered carbene unit. In the solid state at room temperature, the Pt(II) complex showed an orange luminescence ( $\lambda_{\text{em}} = 570 \text{ nm}$ ) while the Pd(II) analogue did not.

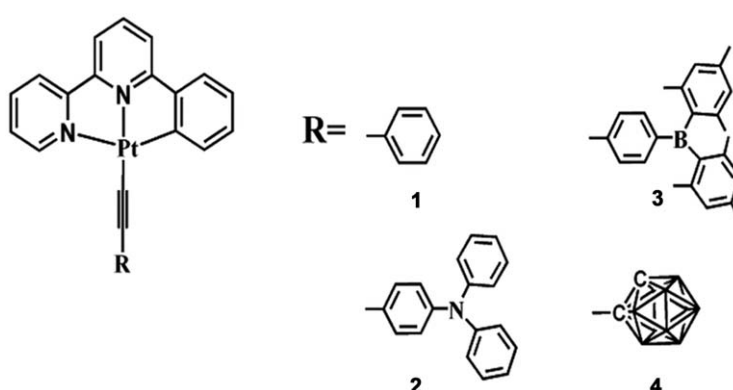


**Fig. 6** Chemical structures of the  $\text{C}^{\wedge}\text{N}^{\wedge}\text{N}$  platinum complexes presented by Shen *et al.* Reproduced from ref. 121 with permission from The Royal Society of Chemistry.

The long lifetime ( $\tau = 480$  ns) of the emission was consistent with a triplet nature of the excited state. The crystal structures of the two complexes displayed 1-dimensional chains, with short M $\cdots$ M and  $\pi$ - $\pi$  and interactions.<sup>122</sup>

Supramolecular gels based on a new series of cyclo-metalated N $\wedge$ C $\wedge$ N Pt(II) complexes of 1,3-bis(1-*n*-alkylpyrazol-3-yl)benzene (bpzb) ligands have been obtained by Li, Yam *et al.* The driving forces of gelation were Pt(II) $\cdots$ Pt(II) and  $\pi$ - $\pi$  stacking interactions, and the sol-to-gel transition was accompanied by emission changes due to aggregation-deaggregation processes.<sup>123</sup>

Intermolecular Pt(II) $\cdots$ Pt(II) interactions may be suppressed by appending bulky substituents on the auxiliary ligands. For instance, an imidazopyridine ligand combined with a sterically demanding counter-ligand leads to excellent single-molecule emitters, whereas less bulky groups may enhance the excimer formation.<sup>124</sup> A correlation between photophysical properties, OLED performances, solid-state packing and the substituents was also found by Chi, Chang *et al.*, in a series of Pt(II) complexes with substituted isoquinolinyl pyrazolate ligands. In the presence of bulky groups (e.g. 5,7-di-*t*-butyl), which prevented intermolecular stacking interactions, the complexes showed identical spectra in both solution and the solid state. On the other hand, with less bulky substituents (e.g. 6-*t*-butyl), aggregation was not hampered. Consequently, the corresponding Pt(II) complexes showed a red-shifted emission in both the solid state and poly(methylmethacrylate) matrix at higher concentrations, due to the population of  $^3\text{MLCT}^*$  states.<sup>125</sup> De Cola *et al.* synthesised a series of Pt(II) complexes containing the tridentate ligand 2,6-bis-(1H-1,2,3-triazol-5-yl)pyridine (N $\wedge$ N $\wedge$ N) combined with Cl $^-$ /CN $^-$  ancillary ligands. By changing either the substitution pattern on the 1,2,3-triazoles or the ancillary ligand, the intermolecular Pt(II) $\cdots$ Pt(II) interactions could be modified, as well as the emission properties of the complexes. In the case of (N $\wedge$ N $\wedge$ N)Pt(II)CN, the  $\pi$ -accepting CN $^-$  ligand was found to promote Pt(II) $\cdots$ Pt(II) interactions, irrespectively of the bulky substituents on N $\wedge$ N $\wedge$ N.<sup>126</sup> As for Ir(III) analogues, the photophysical properties of cyclo-metalated Pt(II) complexes withppy and thpy [Hthpy=2-(2'-thienyl)pyridine] are influenced by the substituents on the C $\wedge$ N ligand. In particular, in a series of Pt-ppy and Pt-thpy complexes, containing acetylacetone as the counter-ligand, the substitution of the benzene unit with a more electron-rich thiophene resulted in the decrease of the HOMO-LUMO gap and in a red-shift of phosphorescence. Moreover, for the Pt-thpy complex, a fluorescence emission was observed in addition to phosphorescence. In fact, when the thpy ligand is extended with a thiophene unit, the metal contribution to S<sub>1</sub> and T<sub>1</sub> becomes smaller and the  $\Delta E(S_1 - T_1)$  gap is enlarged. As a consequence, the metal-induced ISC is reduced and the k<sub>ISC</sub> rates are low enough for the occurrence of a dual (fluorescence/phosphorescence) emission.<sup>127</sup>

Differently from Ir(III) and Pt(II)-analogues, for cyclo-metalated Pt(IV) (d<sup>6</sup>) complexes, the emissive  $^3\text{LC}^*$  states are only scarcely mixed with  $^3\text{MLCT}^*$  states.

The poor MLCT\* contribution is due to the very low energy of the occupied Pt(IV) d-orbitals. On the other hand, the LMCT\* states are thermally accessible and can provide an efficient non-radiative deactivation.

New luminescent bis-cyclometalated Pt(IV) complexes, based on either a  $C_2$ -symmetrical or an unsymmetrical {Pt-(ppy)<sub>2</sub>} unit, and containing different ancillary ligands (*e.g.* Cl<sup>-</sup>, Br<sup>-</sup>, OAc<sup>-</sup>, OTf<sup>-</sup>), were synthesised by Gonzalez-Herrero *et al.* Interestingly, the complexes *sym*-[Pt(ppy)<sub>2</sub>X<sub>2</sub>], except for X=I<sup>-</sup>, displayed a phosphorescence emission from a <sup>3</sup>LC\* state in solution at RT. The highest quantum yield was obtained for X=F<sup>-</sup>, because of the high <sup>3</sup>MLCT\* contribution to the emitting state. Notably, for the other *sym*-[Pt(ppy)<sub>2</sub>X<sub>2</sub>] derivatives, this contribution decreased and the non-radiative deactivation became more important due to the highly accessible, deactivating LMCT\* and LLCT\* states. For the complexes *unsym*-[Pt(ppy)<sub>2</sub>X<sub>2</sub>], the emission from <sup>3</sup>LC states only occurred at 77 K. The significantly lower energies of dσ\*(Pt) orbitals resulted in low-lying deactivating LMCT\* states, non-emissive at room temperature and promoting photoisomerization processes.<sup>128</sup>

Compared to platinum, examples of outstanding emissive Pd(II) complexes are still uncommon. This is due to the lower ligand-field splitting of Pd(II) complexes, compared to the Pt(II) analogues, which facilitates the population of the d<sub>x<sup>2</sup>-y<sup>2</sup></sub> antibonding orbital. The resulting distortion of the square-planar geometry towards tetrahedron promotes the efficient deactivation of the excited state. As a consequence, Pd(II) luminescent complexes generally display low efficient emissions, only detectable at low temperatures. A way to prevent the population of non-radiative excited states is to use strong-field ligands, which raise the energy of both d-d transitions and MC\* states. For the cyclo-metalated Pd(II) complexes with ppy-type ligands, this can be obtained by introducing proper substituents on ppy or by replacing the pyridine ring with a smaller N-heterocycle. As for platinum, inter-molecular M···M or π-π\* stacking interactions may tune the photophysical properties of Pd(II) complexes.

In a series of compounds reported by Santana *et al.*, strong Pd···Pd or π-π\* interactions were found in the solid state (see Fig. 7), thus the emission disclosed the mixed contributions of <sup>3</sup>MMLCT\*, <sup>3</sup>MLCT\* and <sup>3</sup>LLCT\* states. Notably, low-energy dσ(Pd···Pd)\*→π(L)\* MMLCT transitions, red-shifted from the MLCT, were also observed in the absorption spectra.<sup>129</sup> Very interestingly, a number of luminescent Pd(0) (d<sup>10</sup>) complexes of the type [Pd(L)(L')], bearing NHC and PR<sub>3</sub> ligands, were synthesised by Cazin, Zysman-Colman *et al.* In these compounds, the strong NHC σ-donors raise the energy of <sup>3</sup>MC\* states and favour a radiative deactivation pathway. At the same time, the π-accepting ability of NHC ligands promotes MLCT transitions. The obtained Pd(0) systems, showing bright, tunable and short-lived emissions, are proved useful for OLEDs applications.<sup>130</sup>

### 3.5 Gold

Luminescent square-planar Au(III) complexes, stabilized by strong σ-donating cyclo-metalating ligands (*e.g.* alkynes), have gained increasing

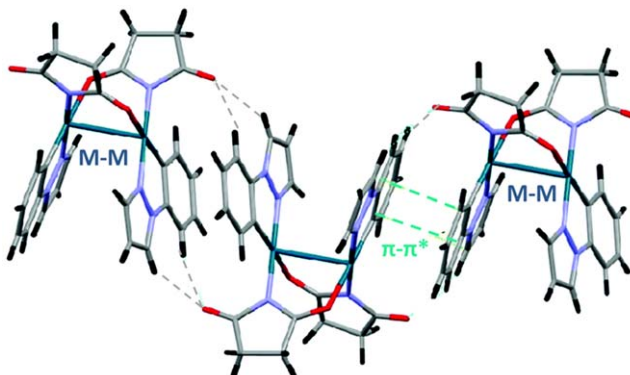


**Fig. 7** Molecular packing diagram of one of the complexes synthesised by Santana *et al.* The chains of molecules are linked through H-bonding and  $\pi \cdots \pi^*$  interactions. Reproduced from ref. 129 with permission from The Royal Society of Chemistry.

attention in the last years for both the fabrication of OLEDs (as potential triplet phosphors) and the development of organic memory devices.<sup>131</sup> In most cases, stable luminescent Au(III) complexes are of the bis-cyclometalated type.<sup>132</sup> As a matter of fact, mono-cyclometalated Au(III) complexes generally display a high degree of reductive elimination, especially when  $\sigma$ -donors are bound in a *cis* fashion. Moreover, due to the low-lying Au (5d $\sigma^*$ ) orbital, the deactivating LMCT and/or MC excited states are usually close in energy to the emitting state, thus leading to an efficient quenching of luminescence.

McMillin, Sharp *et al.* recently reported a series of biphenyl bis-cyclometalated Au(III) compounds containing diethyl dithiocarbamate ancillary ligands. These systems are phosphorescent both in solution and solid state. Emission originates from a metal-perturbed  $^3\text{IL}$  ( $\pi-\pi^*$ ) excited state of the biphenyl ligand, with a minor contribution from LLCT\*. The partial deactivation in solution was attributed to the population of a distorted  $^3\text{LMCT}^*$  state, which is more accessible in solution than in solid state and low-temperature glass.<sup>133</sup>

Stable and luminescent mono-cyclometalated Au(III) complexes have been recently obtained Venkatesan *et al.*, using ancillary ligands with  $\pi$ -accepting properties (*i.e.* cyanide). Besides their good stability, these new systems showed long-lived emissions, in both solution and solid-state, due to metal-perturbed  $^3\text{IL}^*$  ( $\pi-\pi^*$ ) states delocalized over the cyclometalating ligand. The good  $\sigma$ -donating and  $\pi$ -accepting properties of this set of ligands increased the chemical stability of the complexes and also split the non-emissive MC\* states, thus favouring the radiative decay.<sup>134</sup> Luminescent Au(III) compounds were also obtained by reacting bidentate phosphines with the  $[\text{Au}(\text{C}_6\text{F}_5)_3(\text{tht})]$  complex (tht = tetrahydrothiophene).

The compounds,  $[\{\text{Au}(\text{C}_6\text{F}_5)_3\}_2(1,4\text{-PPh}_2(\text{C}_6\text{H}_4)_n\text{PPh}_2)]$  ( $n=1-3$ ) and  $[\{\text{Au}(\text{C}_6\text{F}_5)_3\}_2(\text{PPh}_2\text{C}\equiv\text{C}(\text{C}_6\text{H}_4)_n\text{C}\equiv\text{CPPh}_2)]$  ( $n=0-2$ ) showed different emission colours, spanning from violet to yellow, according to the number of phenylene/alkynyl-phenylene spacers in the diphosphine ligand.<sup>135</sup>

The first examples of luminescent non-cyclometalated Au(III) complexes were synthesised by Venkatesan *et al.*, using  $[\text{Au}(\text{C}_6\text{F}_5)_3(\text{tht})]$  as the precursor (see Fig. 8). The obtained  $[(\text{L})\text{Au}(\text{C}_6\text{F}_5)_3]$  neutral systems [with L = 2-(2,4-difluorophenyl)pyridine, 4- or 2-phenylpyridine, 2-phenylisoquinoline or 2-thienylpyridine] are phosphorescent at room temperature in the solid state, at 77 K in 2-MeTHF, and displayed a widely tunable emission over the visible range (*i.e.* 400–650 nm).<sup>136</sup>

Nevado *et al.* recently obtained new stable  $\text{C}(\text{sp}^2)\text{-Au(III)}$  fluorides, using the  $(\text{N}^{\wedge}\text{C}^{\wedge}\text{C})$  platform instead of classical  $(\text{C}^{\wedge}\text{N}^{\wedge}\text{C})$  pincer ligands. Notably, these new systems represent the first examples of  $\text{C}(\text{sp}^2)\text{-Au(III)}$  fluorides obtained using a mild Cl/F ligand exchange reaction. The  $[(\text{N}^{\wedge}\text{C}^{\wedge}\text{C})\text{Au(III)}]$ -containing systems also displayed improved photochemical properties compared to common  $(\text{C}^{\wedge}\text{N}^{\wedge}\text{C})\text{-Au}$  complexes.<sup>137</sup>

Among Au-based phosphorophores, those containing corrole-type ligands are also of interest;<sup>138</sup> recent examples display near-IR phosphorescence, even at room temperature, and find applications in photodynamic therapy and dye-sensitized solar cells.<sup>139</sup>

Gold complexes, especially those with carbon-donor ligands, are of interest for the rich chemistry of the Au-C bond. In 2015–2016, novel luminescent organo-Au(I) complexes have been synthesised and studied, using *e.g.* alkynyl<sup>140,141</sup> and N-heterocyclic allenylidene ligands.<sup>142</sup> Also gold–heterometal interactions, with heterometals of the main groups, have been explored; for instance, Lúpez-de-Luzuriaga investigated the photophysical properties of novel tetrahedral Au(I) complexes of formula  $[\text{Au}(\text{GeCl}_3)\text{L}_3]$  ( $\text{L} = \text{e.g. PMe}_3, \text{PMe}_2\text{Ph}, \text{PPh}_3$ ).

The peculiar photophysical properties of Au(I) complexes, where the metal has a  $d^{10}$  electronic configuration, are strongly influenced by the so-called “aurophilic interactions”. These, made strong by the large

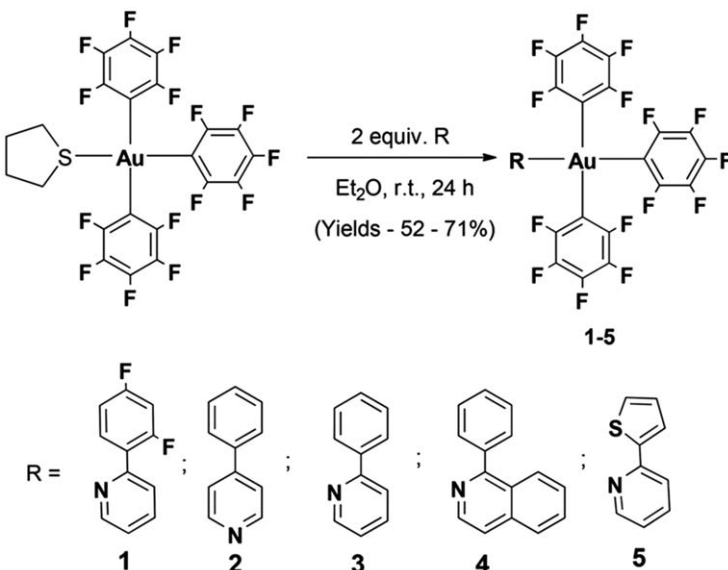


**Fig. 8** Luminescent non-cyclometalated Au(III) complexes synthesised by Venkatesan *et al.* Reproduced from ref. 136 with permission from The Royal Society of Chemistry.

relativistic effects, can operate inter-molecularly and/or intra-molecularly and can be modulated by counter-ions, solvent, temperature and pressure. Au(i)···Au(i) interactions are also promoted by proper ligand architectures, *e.g.* bridging ligands.

Among stimuli-responsive gold complexes, the novel Au(i) diphosphine-based dimers by Deák *et al.* are worth mentioning.  $[Au_2(nixantphos)_2]^{2+}$  [nixantphos = 4,6-bis(diphenylphosphino)-phenoxazine] cations displayed different emission colours, according to their counter-anions, and exhibited a distinct reversible vapo-, thermo- and mechanochromic luminescence. In the crystals, short Au···Au and N-H···X ( $X=O$  and N) interactions were observed. H-bonding interactions, in particular, were found to be involved in the stimuli-responsive luminescent behaviour of these systems.<sup>143</sup>

In the last years, a series of luminescent, homo- and hetero-nuclear Au(i) complexes have been developed using N-heterocyclic carbene (NHC) ligands.

Notably, common NHC moieties are good  $\sigma$ -donors and lead to stable M-C<sub>NHC</sub> bonding interactions, besides the weak  $\pi$ -accepting ability of the NHC-carbene unit due to high-lying  $\pi^*$ -orbitals. By adding functionalised side chains, containing *e.g.* phosphine groups, to the nitrogen atom of NHC moieties, new polydentate systems were obtained, which could be used as building blocks for polynuclear complexes.<sup>144</sup>

Au(i)/carbene complexes are generally easily obtained by *trans*-metalation from Ag(i) analogues.<sup>145</sup> Homo- and hetero-bimetallic [*e.g.* Ag(i)<sub>2</sub>, Au(i)<sub>2</sub> and Au(i)-Ag(i)] complexes were obtained by Barnard *et al.*, using a bis-NHC pincer ligand. These bimetallic species were found to be emissive in the crystalline state, at RT and at 77 K, where the adopted twisted conformation favoured short M···M interactions. On the other hand, no luminescence was observed in solution, where the conformational fluxionality brought about a loss of the M···M interactions and promoted non-radiative deactivations.<sup>146</sup>

Danopoulos, Braunstein *et al.* recently obtained stable polynuclear chain [*i.e.* Au(i)<sub>3</sub>, Ag(i)Au(i)<sub>2</sub> and Au(i)<sub>2</sub>] complexes with the rigid *N,N'*-diphosphanyl-imidazol-2-ylidene ligand (L), characterized by a phosphorus donor and two NHC units. The ligand's hetero-functionality was found to generate an anisotropic charge distribution in the chain. As a consequence, the Au(i)···Au(i) interactions presented a significant electrostatic component, contributing to the short distance between the Au centres, especially in the case of  $[Au_3L_2]^{3+}$ . This trinuclear species showed excellent photophysical properties in solution, with a narrow emission band centred at 445 nm ( $\phi = 80\%$ ). DFT studies on the dinuclear complex  $[Au_2L_2]^{2+}$  pointed out that the excited state was stabilized by coordination changes, associated to the binding of a dangling P donor to gold.<sup>147</sup>

### 3.6 Other metals of the second and third row

Metal-metal quadruply bonded complexes of Mo(II) and W(II) have raised significant interest for their peculiar features. Complexes of the type

$M_2L_4$ , with  $L =$  carboxylate or amidinate (*i.e.*  $\pi$ -accepting) ligands, are also known as paddle-wheel compounds and generally show photoluminescence from both the  $S_1$  and  $T_1$  excited states. Their most peculiar feature is the presence of a long-living  $S_1$  state (1–20 ps) deriving from a  $M_2\delta \rightarrow L\pi^*$  transition ( $^1\text{MLCT}$ ). The long lifetime of the  $^1\text{MLCT}$  state is surprising, especially if compared to that of  $d^6$  and  $d^8$  transition metal complexes, for which the  $^1\text{MLCT}$  states ( $\sim 100$  fs) rapidly undergo ISC, leading to longer-living  $^3\text{MLCT}$  states. In the case of  $M_2L_4$  compounds,  $T_1$  states are of the  $^3\text{MLCT}^*$  or  $^3\text{MM}\delta\delta^*$  types, with lifetimes of 1–100 ns and 1–100  $\mu$ s, respectively. Even if the M–M quadruple bond was recognized more than 50 years ago, these compounds are still revealing some remarkable features, and much work has to be done for a better understanding of their photophysical properties.<sup>148,149</sup>

The tetra-*n*-butylammonium salts of  $[\{Mo_6I_8\}(RCOO)_6]^{2-}$  complexes showed bright and long-lived red phosphorescence in both solution (*i.e.* degassed acetonitrile) and solid state. Interestingly, a linear correlation was found between the  $E_{\text{ox}}/E_{\text{red}}$  potentials of the complexes and the  $pK_a$  value of the terminal carboxylate ligands. As a consequence, a correlation could be also found between the emission energy ( $\nu_{\text{em}}$ ) of the complexes and the  $pK_a$ ; in fact,  $(E_{\text{ox}} - E_{\text{red}})$  corresponds to the HOMO/LUMO energy gap, which is proportional to  $\nu_{\text{em}}$ .<sup>150</sup>

Among luminescent  $d^6$  transition-metal complexes, those based on Os(**ii**) and Rh(**iii**) have gained significant interest. Compared to Ru(**ii**) complexes with polypyridyl ligands, the Os(**ii**) analogues are better photosensitizers because of their lower absorption energy in the visible spectrum. However, even if the price of Osmium is now close to those of ruthenium and iridium, Os-based photosensitisers are still underutilized compared to Ru and Ir analogues.<sup>151,152</sup>

New emitting isomeric  $MC_4$  Rh-based metallacycles were obtained by reactions of  $[\text{Rh}(\kappa^2-O,O-\text{acac})(\text{PMe}_3)_2]$  (acac = acetylacetoneato) with  $\alpha,\omega$ -bis(arylbutadiynyl)alkanes. Isomer distribution was controlled by changing the bis-(diyne) linker length. The corresponding isomeric 2,5-bis(arylethyynyl)rhodacyclopentadienes and 2,2'-biphenyl complexes showed very different photophysical properties, with the former exhibiting an intense fluorescence and the latter a pure phosphorescence. This stark difference was attributed to a higher contribution of the metal d-orbitals to the frontier molecular orbitals in the Rh 2,2'-biphenyl isomer, allowing for a more efficient ISC ( $S_1 \rightarrow T_n$  and  $T_1 \rightarrow S_0$ ).<sup>153</sup> In the field of metallo-porphyrins, novel near-IR emitting complexes have been obtained by linking an aza-BODIPY chromophore to a Rh(**iii**)-porphyrin moiety, through an axial Rh–C(aryl) bond. The new systems combine the advantages of aza-BODIPY and Rh(**iii**)-porphyrin, *i.e.* absorption/emission in the NIR region and long-lived triplet states, respectively. Notably, the emission occurs at about 720 nm whatever the excitation wavelength. This approach represents an useful strategy for the development of new NIR-absorbing triplet-state materials, with applications in *e.g.* photodynamic therapy, OLEDs and photocatalysis.<sup>154</sup>

## References

- 1 K. K.-W. Lo, *Acc. Chem. Res.*, 2015, **48**, 2985.
- 2 A. J. Howarth, M. B. Majewski and M. O. Wolf, *Coord. Chem. Rev.*, 2015, **282–283**, 139.
- 3 M. Chergui, *Acc. Chem. Res.*, 2015, **48**, 801.
- 4 D. Z. Zee, T. Chantarojsiri, J. R. Long and C. J. Chang, *Acc. Chem. Res.*, 2015, **48**, 2027.
- 5 I. M. Dixon, G. Boissard, H. Whyte, F. Alary and J.-L. Heully, *Inorg. Chem.*, 2016, **55**, 5089.
- 6 Y. Liu, K. S. Kjær, L. A. Fredin, P. Chábera, T. Harlang, S. E. Canton, S. Lidin, J. Zhang, R. Lomoth, K.-E. Bergquist, P. Persson, K. Wärnmark and V. Sundström, *Chem. – Eur. J.*, 2015, **21**, 3628.
- 7 F. Zou, X. Tang, Y. Huang, S. Wan, F. Lu, Z. N. Chen, A. Wu and H. Zhang, *CrystEngCommun*, 2016, **18**, 6624–6631.
- 8 Z. Wang, C. Zheng, W. Wang, C. Xu, B. Ji and X. Zhang, *Inorg. Chem.*, 2016, **55**, 2157.
- 9 R. Molteni, K. Edkins, M. Haehnel and A. Steffen, *Organometallics*, 2016, **35**, 629.
- 10 A. R. Cabrera, I. A. Gonzalez, D. Cortés-Arriagada, M. Natali, H. Berke, C. G. Daniliuc, M. B. Camarada, A. Toro-Labbé, R. S. Rojas and C. O. Salas, *RSC Adv.*, 2016, **6**, 5141.
- 11 J. Föller, M. Kleinschmidt and C. M. Marian, *Inorg. Chem.*, 2016, **55**, 7508.
- 12 Y. Sun, V. Lemaur, J. I. Beltrán, J. Cornil, J. Huang, J. Zhu, Y. Wang, R. Fröhlich, H. Wang, L. Jiang and G. Zou, *Inorg. Chem.*, 2016, **55**, 5845.
- 13 C. Yi, S. Xu, J. Wang, F. Zhao, H. Xia and Y. Wang, *Eur. J. Inorg. Chem.*, 2016, 4885.
- 14 M. Nishikawa, S. Sawamura, A. Haraguchi, J. Morikubo, K. Takao and T. Tsubomura, *Dalton Trans.*, 2015, **44**, 411.
- 15 E. I. Musina, A. V. Shamsieva, I. D. Strelnik, T. P. Gerasimova, D. B. Krivolapov, I. E. Kolesnikov, E. V. Grachova, S. P. Tunik, C. Bannwarth, S. Grimme, S. A. Katsyuba, A. A. Karasik and O. G. Sinyashin, *Dalton Trans.*, 2016, **45**, 2250.
- 16 N. K. Al Rasbi and J. Husband, *J. Photochem. Photobiol., A*, 2016, **314**, 96.
- 17 R. Y. Huang, H. Jiang, C. H. Zhu and H. Xu, *RSC Adv.*, 2016, **6**, 3341.
- 18 F. A. Rafiqi and K. Majid, *RSC Adv.*, 2016, **6**, 22016.
- 19 P. Chakraborty, J. Adhikary, S. Samanta, I. Majumder, C. Massera, D. Escudero, S. Ghosh, A. Bauza, A. Frontera and D. Das, *Dalton Trans.*, 2015, **44**, 20032.
- 20 A. Hens and K. K. Rajak, *RSC Adv.*, 2015, **5**, 4219.
- 21 X. M. Wang, S. Chen, R. Q. Fan, F. Q. Zhang and Y. L. Yang, *Dalton Trans.*, 2015, **44**, 8107.
- 22 D. A. Evans, L. M. Lee, I. Vargas-Baca and A. H. Cowley, *Dalton Trans.*, 2015, **44**, 11984.
- 23 B. N. Ghosh, F. Topić, P. K. Sahoo, P. Mal, J. Linnera, E. Kalenius, H. M. Tuononen and K. Rissanen, *Dalton Trans.*, 2015, **44**, 254.
- 24 Z. N. Erol, P. Atienzar, Y. Arslanoglu, E. H. and H. García, *RSC Adv.*, 2015, **5**, 55901.
- 25 M. Lederer, U. Hahn, J. M. Strub, S. Cianferani, A. Van Dorsselaer, J. F. Nierengarten, T. Torres and D. M. Guldi, *Chem. – Eur. J.*, 2016, **22**, 2051.
- 26 V. Çakır, D. Çakır, M. Göksel, M. Durmuş, Z. Biyiklioglu and H. Kantekin, *J. Photochem. Photobiol., A*, 2015, **299**, 138.

- 27 L. Vachova, M. Machacek, R. Kučera, J. Demuth, P. Cermak, K. Kopecky, M. Miletin, A. Jedlickova, T. Simunek, V. Novakova and P. Zimcik, *Org. Biomol. Chem.*, 2015, **13**, 5608.
- 28 M. E. Alberto, B. C. De Simone, G. Mazzone, E. Sicilia and N. Russo, *Phys. Chem. Chem. Phys.*, 2015, **17**, 23595.
- 29 G. M. Chu, A. Guerrero-Martínez, C. Ramírez de Arellano, I. Fernández and M. A. Sierra, *Inorg. Chem.*, 2016, **55**, 2737.
- 30 N. Kubota, Y. Segawa and K. Itami, *J. Am. Chem. Soc.*, 2015, **137**, 1356.
- 31 Y. Suffren, N. O'Toole, A. Hauser, E. Jeanneau, A. Brioude and C. Desroches, *Dalton Trans.*, 2015, **44**, 7991.
- 32 X. Shang, D. Han, Q. Zhan, D. Zhou and G. Zhang, *New J. Chem.*, 2015, **39**, 2588.
- 33 Q. Sun, S. Mosquera-Vazquez, Y. Suffren, J. Hankache, N. Amstutz, L. M. L. Daku, E. Vauthay and A. Hauser, *Coord. Chem. Rev.*, 2015, **282–283**, 87.
- 34 B. Colasson, A. Credi and G. Ragazzon, *Coord. Chem. Rev.*, 2016, **325**, 125.
- 35 A. Boulay, C. Deraeve, L. V. Elst, N. Leygue, O. Maury, S. Laurent, R. N. Muller, B. Mestre Voegtle and C. Picard, *Inorg. Chem.*, 2015, **54**, 1414.
- 36 T. S. M. Tang, A. M. H. Yip, K. Y. Zhang, H. W. Liu, P. L. Wu, K. F. Li, K. W. Cheah and K. K. W. Lo, *Chem. – Eur. J.*, 2015, **21**, 10729.
- 37 M. Wenzel, A. de Almeida, E. Bigaeva, P. Kavanagh, M. Picquet, P. Le Gendre, E. Bodio and A. Casini, *Inorg. Chem.*, 2016, **55**, 2544.
- 38 C. Mari, H. Huang, R. Rubbiani, M. Schulze, F. Würthner, H. Chao and G. Gasser, *Eur. J. Inorg. Chem.*, 2016, DOI: 10.1002/ejic.201600516.
- 39 S. Mardanya, S. Karmakar, D. Maity and S. Baitalik, *Inorg. Chem.*, 2015, **54**, 513.
- 40 P. D. Harvey, S. Tasan, C. P. Gros, C. H. Devillers, P. Richard, P. Le Gendre and E. Bodio, *Organometallics*, 2015, **34**, 1218.
- 41 F. Nisic, A. Colombo, C. Dragonetti, E. Garoni, D. Marinotto, S. Righetto, F. De Angelis, M. G. Lobello, P. Salvatori, P. Biagini and F. Melchiorre, *Organometallics*, 2015, **34**, 94.
- 42 R. Horvath, G. S. Huff, K. C. Gordo and M. W. George, *Coord. Chem. Rev.*, 2016, **325**, 41.
- 43 Y. Sato, S. Takizawa and S. Murata, *Eur. J. Inorg. Chem.*, 2015, **33**, 5495.
- 44 F. Yu, C. Shen, T. Zheng, W. K. Chu, J. Xiang, Y. Luo, C. C. Ko, Z. Q. Guo and T. C. Lau, *Eur. J. Inorg. Chem.*, 2016, 3641.
- 45 Y. Zhu, T. Fei and Y. Ma, *ChemPlusChem*, 2016, **81**, 73.
- 46 N. K. Shee, M. G. B. Drew and D. Datta, *New J. Chem.*, 2016, **40**, 5002.
- 47 J. H. Wallenstein, L. A. Fredin, M. Jarenmark, M. Abrahamsson and P. Persson, *Dalton Trans.*, 2016, **45**, 11723.
- 48 K. Ritter, C. Pehlken, D. Sorsche and S. Rau, *Dalton Trans.*, 2015, **44**, 8889.
- 49 M. B. Majewski, J. G. Smith, M. O. Wolf and B. O. Patrick, *Eur. J. Inorg. Chem.*, 2016, **10**, 1470.
- 50 P. A. Scattergood, U. Khushnood, A. Tariq, D. J. Cooke, C. R. Rice and P. I. P. Elliott, *Inorg. Chem.*, 2016, **55**, 7787.
- 51 K. T. Ngo, N. A. Lee, S. D. Pinnace, D. J. Szalda, R. T. Weber and J. Rochford, *Inorg. Chem.*, 2016, **55**, 2460.
- 52 R. Horvath, M. G. Fraser, C. A. Clark, X. Z. Sun, M. W. George and K. C. Gordon, *Inorg. Chem.*, 2015, **54**, 11697.
- 53 E. Sakuda, Y. Ando, A. Ito and N. Kitamura, *Inorg. Chem.*, 2011, **50**, 1603.
- 54 E. Sakuda, C. Matsumoto, Y. Ando, A. Ito, K. Mochida, A. Nakagawa and N. Kitamura, *Inorg. Chem.*, 2015, **54**, 3245.

- 55 A. Nakagawa, E. Sakuda, A. Ito and N. Kitamura, *Inorg. Chem.*, 2015, **54**, 10287.
- 56 J. H. Wallenstein, J. Sundberg, C. J. McKenzie and M. Abrahamsson, *Eur. J. Inorg. Chem.*, 2016, **6**, 897.
- 57 S. R. Salpage, A. Paul, B. Som, T. Banerjee, K. Hanson, M. D. Smith, A. K. Vannucci and L. S. Shimizu, *Dalton Trans.*, 2016, **45**, 9601.
- 58 V. Goudy, J. Maynadié, X. Le Goff, D. Meyer and M. Fontecave, *New J. Chem.*, 2016, **40**, 1704.
- 59 B. Laramée-Milette, F. Lussier, I. Ciofini and G. S. Hanan, *Dalton Trans.*, 2015, **44**, 11551.
- 60 X. Cui, J. Zhao, A. Karatay, H. G. Yaglioglu, M. Hayvali and B. Küçüköz, *Eur. J. Inorg. Chem.*, 2016, **32**, 5077.
- 61 K. Barthelmes, J. Kübel, A. Winter, M. Wächtler, C. Friebel, B. Dietzek and U. S. Schubert, *Inorg. Chem.*, 2015, **54**, 3159.
- 62 J. Schindler, S. Kupfer, M. Wächtler, J. Guthmüller, S. Rau and B. Dietzek, *ChemPhysChem*, 2015, **16**, 1061.
- 63 T. Nikkonen, M. Moreno Oliva, S. Taubert, M. Melchionna, A. Kahnt and J. Helaja, *Chem. – Eur. J.*, 2015, **21**, 12755.
- 64 R. M. Spada, M. Cepeda-Plaza, M. L. Gómez, G. Günther, P. Jaque, N. Pizarro, R. E. Palacios and A. Vega, *J. Phys. Chem. C*, 2015, **119**, 10148.
- 65 M. V. Werrett, G. S. Huff, S. Muzzioli, V. Fiorini, S. Zacchini, B. W. Skelton, A. Maggiore, J. M. Malicka, M. Cocchi, K. C. Gordon, S. Stagni and M. Massi, *Dalton Trans.*, 2015, **44**, 8379.
- 66 N. Pizarro, M. Duque, E. Chamorro, S. Nonell, J. Manzur, J. R. de la Fuente, G. Günther, M. Cepeda-Plaza and A. Vega, *J. Phys. Chem. A*, 2015, **119**, 3929.
- 67 I. Kondrasenko, K. S. Kisel, A. J. Karttunen, J. Jänis, E. V. Grachova, S. P. Tunik and I. O. Koshevoy, *Eur. J. Inorg. Chem.*, 2015, **5**, 864.
- 68 C. O. Ng, S. C. Cheng, W. K. Chu, K. M. Tang, S. M. Yiu and C. C. Ko, *Inorg. Chem.*, 2016, **55**, 7969.
- 69 W. K. Chu, X. G. Wei, S. M. Yiu, C. C. Ko and K. C. Lau, *Chem. – Eur. J.*, 2015, **21**, 2603.
- 70 A. W. T. Choi, K. K. S. Tso, V. M. W. Yim, H. W. Liu and K. K. W. Lo, *Chem. Commun.*, 2015, **51**, 3442.
- 71 T. Duan, T. K. Chang, Y. Chi, J. Y. Wang, Z. N. Chen, W. Y. Hung, C. H. Chen and G. H. Lee, *Dalton Trans.*, 2015, **44**, 14613.
- 72 T. Yu, X. Wang, W. Su, C. Zhang, Y. Zhao, H. Zhang and Z. Xu, *RSC Adv.*, 2015, **5**, 80572.
- 73 J. Zhuang, W. Li, W. Wu, M. Song, W. Su, M. Zhou and Z. Cui, *New J. Chem.*, 2015, **39**, 246.
- 74 A. Baschieri, S. Muzzioli, E. Matteucci, S. Stagni, M. Massi and L. Sambri, *Dalton Trans.*, 2015, **44**, 37.
- 75 J. Li, L. Wang, K. Sun and J. Zhang, *Dalton Trans.*, 2016, **45**, 3034.
- 76 A. J. Howarth, M. B. Majewski, C. M. Brown, F. Lelj, M. O. Wolf and B. O. Patrick, *Dalton Trans.*, 2015, **44**, 16272.
- 77 S. Sinha, S. Mandal and P. Gupta, *RSC Adv.*, 2015, **5**, 99529.
- 78 Y. Si, N. Qu, L. Cui, B. Gao and Z. Wu, *Dalton Trans.*, 2016, **45**, 12587.
- 79 T. Yu, Z. Xu, W. Su, Y. Zhao, H. Zhang and Y. Bao, *Dalton Trans.*, 2016, **45**, 13491.
- 80 X. Yang, Z. Feng, J. Zhao, J. S. Dang, B. Liu, K. Zhang and G. Zhou, *ACS Appl. Mater. Interfaces*, 2016, **8**, 33874.
- 81 H. T. Mao, C. X. Zang, L. L. Wen, G. G. Shan, H. Z. Sun, W. F. Xie and Z. M. Su, *Organometallics*, 2016, **35**, 3870.

- 82 X. Yang, X. Xu, J. S. Dang, G. Zhou, C. L. Ho and W. Y. Wong, *Inorg. Chem.*, 2016, **55**, 1720.
- 83 P. Dreyse, I. Gonzalez, D. Cortés-Arriagada, O. Ramirez, I. Salas, A. Gonzalez, A. Toro-Labbe and B. Loeb, *New J. Chem.*, 2016, **40**, 6253.
- 84 C. D. Ertl, L. Gil-Escriv, J. Cerdá, A. Pertegás, H. J. Bolink, J. M. Junquera-Hernández, A. Prescimone, M. Neuburger, E. C. Constable, E. Ortí and C. E. Housecroft, *Dalton Trans.*, 2016, **45**, 11668.
- 85 Y. Wang, C. P. Cabry, M. Xiao, L. Male, S. J. Cowling, D. W. Bruce, J. Shi, W. Zhu and E. Baranoff, *Chem. – Eur. J.*, 2016, **22**, 1618.
- 86 W. Shen, Z. Qi, L. Yan, W. Tian, X. Cui, H. Yao and Y. Sun, *RSC Adv.*, 2016, **6**, 16482.
- 87 T. S. M. Tang, K. K. Leung, M. W. Louie, H. W. Liu, S. H. Cheng and K. K. W. Lo, *Dalton Trans.*, 2015, **44**, 4945.
- 88 Y. Hisamatsu, A. Shibuya, N. Suzuki, T. Suzuki, R. Abe and S. Aoki, *Bioconjugate Chem.*, 2015, **26**, 857.
- 89 X. Shang, Y. Li, Q. Zhan and G. Zhang, *New J. Chem.*, 2016, **40**, 1111.
- 90 J. Ponce, J. Aragó, I. Vayá, J. Gómez Magenti, S. Tatay, E. Ortí and E. Coronado, *Eur. J. Inorg. Chem.*, 2016, **12**, 1851.
- 91 L. M. Xie, F. Q. Bai, W. Li, Z. X. Zhang and H. X. Zhang, *Phys. Chem. Chem. Phys.*, 2015, **17**, 10014.
- 92 J. A. Porras, I. N. Mills, W. J. Transue and S. Bernhard, *J. Am. Chem. Soc.*, 2016, **138**, 9460.
- 93 A. K. Pal, D. B. Cordes, A. M. Z. Slawin, C. Momblona, E. Ortí, I. D. W. Samuel, H. J. Bolink and E. Zysman-Colman, *Inorg. Chem.*, 2016, **55**, 10361.
- 94 H. Benjamin, Y. Zheng, A. S. Batsanov, M. A. Fox, H. A. Al-Attar, A. P. Monkman and M. R. Bryce, *Inorg. Chem.*, 2016, **55**, 8612.
- 95 L. He, Z. Wang, L. Duan, C. Yang, R. Tang, X. Song and C. Pan, *Dalton Trans.*, 2016, **45**, 5604.
- 96 Z. Wang, L. He, L. Duan, J. Yan, R. Tang, C. Pan and X. Song, *Dalton Trans.*, 2015, **44**, 15914.
- 97 Q. Mei, J. Weng, Z. Xu, B. Tong, Q. Hua, Y. Shi, J. A. Song and W. Huang, *RSC Adv.*, 2015, **5**, 97841.
- 98 I. González, P. Dreyse, D. Cortés-Arriagada, M. Sundararajan, C. Morgado, I. Brito, C. Roldán-Carmona, H. J. Bolink and B. Loeb, *Dalton Trans.*, 2015, **44**, 14771.
- 99 X. Shang, D. Han, H. Zhang, L. Zhou and G. Zhang, *Eur. J. Inorg. Chem.*, 2016, **10**, 1541.
- 100 A. Maity, L. Q. Le, Z. Zhu, J. Bao and T. S. Teets, *Inorg. Chem.*, 2016, **55**, 2299.
- 101 R. A. Maya, A. Maity and T. S. Teets, *Organometallics*, 2016, **35**, 2890.
- 102 F. Scarpelli, A. Ionescu, L. Ricciardi, P. Plastina, I. Aiello, M. La Deda, A. Crispini, M. Ghedinia and N. Godbert, *Dalton Trans.*, 2016, **45**, 17264.
- 103 P. H. Lanoë, J. Chan, G. Gontard, F. Monti, N. Armaroli, A. Barbieri and H. Amouri, *Eur. J. Inorg. Chem.*, 2016, **11**, 1631.
- 104 J. E. Yarnell, C. E. McCusker, A. J. Leeds, J. M. Breaux and F. N. Castellano, *Eur. J. Inorg. Chem.*, 2016, **12**, 1808.
- 105 J. Fernández-Cestau, N. Giménez, E. Lalinde, P. Montaño, M. T. Moreno and S. Sánchez, *Organometallics*, 2015, **34**, 1766.
- 106 F. Juliá and P. González-Herrero, *Dalton Trans.*, 2016, **45**, 10599.
- 107 A. Colombo, F. Fiorini, D. Septiadi, C. Dragonetti, F. Nisic, A. Valore, D. Roberto, M. Mauro and L. De Cola, *Dalton Trans.*, 2015, **44**, 8478.
- 108 P. A. Scattergood, P. Jesus, H. Adams, M. Delor, I. V. Sazanovich, H. D. Burrows, C. Serpa and J. A. Weinstein, *Dalton Trans.*, 2015, **44**, 11705.

- 109 K. Li, G. S. Ming Tong, Q. Wan, G. Cheng, W. Y. Tong, W. H. Ang, W. L. Kwong and C. Ming Che, *Chem. Sci.*, 2016, **7**, 1653.
- 110 B. Wang, F. Liang, H. Hu, Y. Liu, Z. Kang, L. S. Liao and J. Fan, *J. Mater. Chem. C*, 2015, **3**, 8212.
- 111 T. T. Feng, F. Q. Bai, L. Ming Xie, Y. Tang and H. X. Zhang, *RSC Adv.*, 2016, **6**, 11648.
- 112 M. Jamshidi, S. M. Nabavizadeh, H. R. Shahsavari and M. Rashidi, *RSC Adv.*, 2015, **5**, 57581.
- 113 M. Tenne, S. Metz, G. Wagenblast, I. Münster and T. Strassner, *Organometallics*, 2015, **34**, 4433.
- 114 M. Tenne, S. Metz, G. Wagenblast, I. Münster and T. Strassner, *Dalton Trans.*, 2015, **44**, 8444.
- 115 H. Leopold and T. Strassner, *Organometallics*, 2016, **35**, 4050.
- 116 H. Leopold, M. Tenne, A. Tronnier, S. Metz, I. Münster, G. Wagenblast and T. Strassner, *Angew. Chem., Int. Ed.*, 2016, **55**, 15779.
- 117 T. Strassner, *Acc. Chem. Res.*, 2016, **49**, 2680.
- 118 A. R. Naziruddin, A. Galstyan, A. Iordache, C. G. Daniliuc, C. A. Strassert and L. De Cola, *Dalton Trans.*, 2015, **44**, 8467.
- 119 K. Li, T. Zou, Y. Chen, X. Guan and C. M. Che, *Chem. – Eur. J.*, 2015, **21**, 7441.
- 120 A. Jana, L. McKenzie, A. B. Wragg, M. Ishida, J. P. Hill, J. A. Weinstein, E. Baggaley and M. D. Ward, *Chem. – Eur. J.*, 2016, **22**, 4164.
- 121 W. Zhang, Y. Luo, Y. Xu, L. Tian, M. Li, R. He and W. Shen, *Dalton Trans.*, 2015, **44**, 18130.
- 122 J. Moussa, K. Haddouche, L. M. Chamoreau, H. Amouri and J. A. G. Williams, *Dalton Trans.*, 2016, **45**, 12644.
- 123 Y. Ai, Y. Li, H. Ma, C. Y. Su and V. W. W. Yam, *Inorg. Chem.*, 2016, **55**, 11920.
- 124 P. Pinter, H. Mangold, I. Stengel, I. Münster and T. Strassner, *Organometallics*, 2016, **35**, 673.
- 125 H. Y. Ku, B. Tong, Y. Chi, H. C. Kao, C. C. Yeh, C. H. Chang and G. H. Leed, *Dalton Trans.*, 2015, **44**, 8552.
- 126 N. K. Allampally, C. G. Daniliuc, C. A. Strassert and L. De Cola, *Inorg. Chem.*, 2015, **54**, 1588.
- 127 M. Z. Shafikov, D. N. Kozhevnikov, M. Bodensteiner, F. Brandl and R. Czerwieniec, *Inorg. Chem.*, 2016, **55**, 7457.
- 128 F. Juliá, M. D. García-Legaz, D. Bautista and P. González-Herrero, *Inorg. Chem.*, 2016, **55**, 7647.
- 129 M. D. Santana, L. López-Banet, G. Sánchez, J. Pérez, E. Pérez, L. García, J. L. Serrano and A. Espinosa, *Dalton Trans.*, 2016, **45**, 8601.
- 130 A. F. Henwood, M. Lesieur, A. K. Bansal, V. Lemaur, D. Beljonne, D. G. Thompson, D. Graham, A. M. Z. Slawin, I. D. W. Samuel, C. S. J. Cazin and E. Zysman-Colman, *Chem. Sci.*, 2015, **6**, 3248.
- 131 V. K. M. Au, D. Wu and V. W. W. Yam, *J. Am. Chem. Soc.*, 2015, **137**, 4654.
- 132 G. S. Ming Tong, K. T. Chan, X. Chang and C. Ming Che, *Chem. Sci.*, 2015, **6**, 3026.
- 133 L. Nilakantan, D. R. McMillin and P. R. Sharp, *Organometallics*, 2016, **35**, 2339.
- 134 A. Szentkuti, J. A. Garg, O. Blacque and K. Venkatesan, *Inorg. Chem.*, 2015, **54**, 10748.
- 135 V. Fernández-Moreira, J. Cámarra, E. S. Smirnova, I. O. Koshevoy, A. Laguna, S. P. Tunik, M. C. Blanco and M. Concepción Gimeno, *Organometallics*, 2016, **35**, 1141.

- 136 M. Bachmann, O. Blacque and K. Venkatesan, *Dalton Trans.*, 2015, **44**, 10003.
- 137 R. Kumar, A. Linden and C. Nevado, *Angew. Chem., Int. Ed.*, 2015, **54**, 14287.
- 138 M. Soll, K. Sudhakar, N. Fridman, A. Müller, B. Röder and Z. Gross, *Org. Lett.*, 2016, **18**, 5840.
- 139 A. B. Alemanyehu, N. U. Day, T. Mani, A. B. Rudine, K. E. Thomas, O. A. Gederaas, S. A. Vinogradov, C. C. Wamser and A. Ghosh, *ACS Appl. Mater. Interfaces*, 2016, **8**, 18935.
- 140 F. K. W. Hau and V. W. W. Yam, *Dalton Trans.*, 2016, **45**, 300.
- 141 M. E. S. Moussa, H. Chen, Z. Wang, M. Srebro-Hooper, N. Vanthuyne, S. Chevance, C. Roussel, J. A. G. Williams, J. Autschbach, R. Réau, Z. Duan, C. Lescop and J. Crassous, *Chem. – Eur. J.*, 2016, **22**, 6075.
- 142 X. S. Xiao, C. Zou, X. Guan, C. Yang, W. Lu and C. M. Che, *Chem. Commun.*, 2016, **52**, 4983.
- 143 A. Deák, C. Jobbág, G. Marsi, M. Molnár, Z. Szakács and P. Baranyai, *Chem. – Eur. J.*, 2015, **21**, 11495.
- 144 S. Bestgen, M. T. Gamer, S. Lebedkin, M. M. Kappes and P. W. Roesky, *Chem. – Eur. J.*, 2015, **21**, 601.
- 145 M. Monticelli, C. Tubaro, M. Baron, M. Basato, P. Sgarbossa, C. Graiff, G. Accorsi, T. P. Pell, D. J. D. Wilson and P. J. Barnard, *Dalton Trans.*, 2016, **45**, 9540.
- 146 T. P. Pell, D. J. D. Wilson, B. W. Skelton, J. L. Dutton and P. J. Barnard, *Inorg. Chem.*, 2016, **55**, 6882.
- 147 P. Ai, M. Mauro, C. Gourlaouen, S. Carrara, L. De Cola, Y. Tobon, U. Giovanella, C. Botta, A. A. Danopoulos and P. Braunstein, *Inorg. Chem.*, 2016, **55**, 8527.
- 148 M. H. Chisholm, S. E. Brown-Xu and T. F. Spilker, *Acc. Chem. Res.*, 2015, **48**, 877.
- 149 S. E. Brown-Xu, M. H. Chisholm, C. B. Durr, T. F. Spilker and P. J. Young, *Chem. Sci.*, 2015, **6**, 1780.
- 150 M. A. Mikhailov, K. A. Brylev, P. A. Abramov, E. Sakuda, S. Akagi, A. Ito, N. Kitamura and M. N. Sokolov, *Inorg. Chem.*, 2016, **55**, 8437.
- 151 Y. H. Li, X. L. Liu, Z. T. Yu, Z. S. Li, S. C. Yan, G. H. Chen and Z. G. Zou, *Dalton Trans.*, 2016, **45**, 12400.
- 152 J. Habermehl, D. Sorsche, P. Murszat and S. Rau, *Eur. J. Inorg. Chem.*, 2016, **21**, 3423.
- 153 C. Sieck, M. G. Tay, M. H. Thibault, R. M. Edkins, K. Costuas, J. F. Halet, A. S. Batsanov, M. Haehnel, K. Edkins, A. Lorbach, A. Steffen and T. B. Marder, *Chem. – Eur. J.*, 2016, **22**, 10523.
- 154 J. Zhou, L. Gai, Z. Zhou, W. Yang, J. Mack, K. Xu, J. Zhao, Y. Zhao, H. Qiu, K. S. Chan and Z. Shen, *Chem. – Eur. J.*, 2016, **22**, 13201.



# Highlights in Photochemistry



# Photoredox systems for building C–C bonds from carbon dioxide

Yutaka Amao\*

DOI: 10.1039/9781788010696-00165

In this review, some studies on the visible-light induced photoredox systems consisting of a photosensitizer, an electron mediator and a biocatalyst for building C–C bonds from CO<sub>2</sub> as a feedstock are introduced.

## 1 Introduction

Greenhouse gases are chemical compounds, which induce the greenhouse effect. The rapidly increase in Earth's atmospheric concentrations of the three main human-made greenhouse gases – carbon dioxide (CO<sub>2</sub>), methane (CH<sub>4</sub>), and nitrous oxide (NO<sub>x</sub>) – is clear from the data sets for these gases over the last 400 000 years.

Among the greenhouse gasses, CO<sub>2</sub> produced by human activities, primarily through the combustion of fossil fuels is the most important. Its concentration in the Earth's atmosphere has risen by more than 30% since the Industrial Revolution.

Thus, the development of technology for CO<sub>2</sub> gas reduction is drastically important for the future. CO<sub>2</sub> reduction and fixation are the potential technology for the realization of photoinduced catalytic CO<sub>2</sub> reduction and the synthesis of organic compounds starting from CO<sub>2</sub> as the feedstock. Many researches on CO<sub>2</sub> reduction and fixation have been focused on ultra-visible light induced photocatalysis by semiconductors in heterogeneous water media.<sup>1,2</sup>

On the other hand, biological CO<sub>2</sub> reduction and fixation systems have also received much attention, since organic compounds are produced in homogenous water media by using biocatalysts with CO<sub>2</sub> reduction or fixation function. The production of organic molecules based on the biocatalytic approach has been paid much attention because of the regio- and stereo-selectivity, and of physiological conditions employed. Biocatalytic production competes with conventional chemical methods, especially in the case of organic molecules that are not able to be successfully carried out by chemical catalysts.

Examples of beneficial biocatalytic reactions are the oxidations of alkanes, alkenes, and aromatics.<sup>3</sup> Moreover, since the biocatalytic reactions proceed in aqueous solution as the reaction medium, these are attractive for the production of organic molecules under sustainable conditions.

The concept of the visible-light induced and biocatalytic CO<sub>2</sub> reduction and fixation system is shown in Fig. 1.<sup>4–10</sup>

*Research Centre for Artificial Photosynthesis, Osaka City University, Sugimoto3-3-138, Sumiyoshi-ku, Osaka, Japan. E-mail: amao@ocarina.osaka-cu.ac.jp*

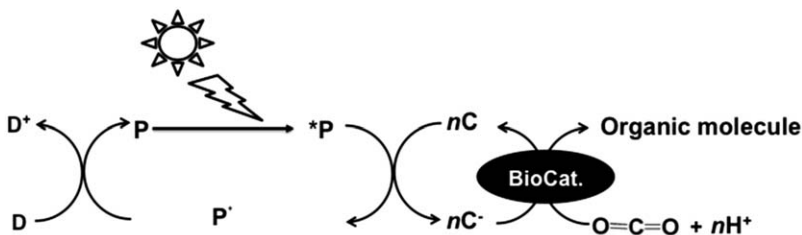


**Fig. 1** The concept for the visible light-induced and biocatalytic  $\text{CO}_2$  reduction and fixation system consisting of an electron donor (D), a photosensitizer (P), an electron mediator (C), and biocatalyst (BioCat.).

In this review, the recent studies on the visible light-induced biocatalytic building C–C bonds from  $\text{CO}_2$  as a feedstock by means of a photoredox catalytic system are introduced.

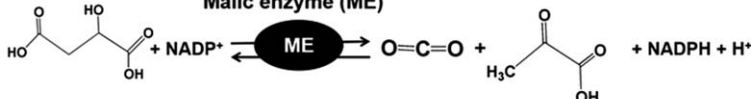
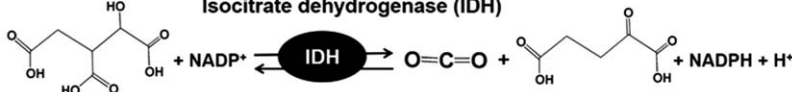
## 2 Biocatalysts for $\text{CO}_2$ reduction and fixation

Enzymes belonging to the class of *oxidoreductases* catalyze the transfer of electrons from one molecule, the reductant, (also defined as the electron donor), to another, the oxidant, also called the electron acceptor. Among these enzymes, some biocatalysts have the function of  $\text{CO}_2$  reduction and fixation. In this section, biocatalysts for the photoredox system of  $\text{CO}_2$  reduction and fixation are introduced.

Biocatalyst for the  $\text{CO}_2$  reduction with the photoredox system is a set of enzyme that catalyze the oxidation of  $\text{C}_1$  materials such as formic acid and CO to  $\text{CO}_2$ , while donating, at the same time, the electrons to a second substrate (e.g.  $\text{NAD}^+$ ) and the reverse reaction of  $\text{CO}_2$  reduction, donating the electrons to a second substrate ( $\text{NADH}$ ). In this case, formate dehydrogenase (FDH) and carbon-monoxide dehydrogenase (CODH) are the typical biocatalysts employed.

On the other hand, biocatalyst for the  $\text{CO}_2$  fixation with the photoredox system is a set of enzyme that catalyze the decarboxylation or carboxylation with redox reaction in the presence of  $\text{NADP}^+$  or  $\text{NADPH}$ . Malic enzyme (ME) and isocitrate dehydrogenase (IDH) are typical biocatalysts for the  $\text{CO}_2$  fixation. Typical pathways for the  $\text{CO}_2$  reduction and fixation are shown in Fig. 2.

For example, formic acid is produced from  $\text{CO}_2$  with a photoredox system consisting of an electron donor (D), a photosensitizer (P), and  $\text{NAD}^+$  in the presence of formate dehydrogenase (FDH). In this case, the formation of NAD dimer occurs in the reaction of the one-electron reduced form of  $\text{NAD}^+$  with a photosensitizer.<sup>11</sup> Since the NAD dimer is an inactive coenzyme for  $\text{NAD}^+$ -dependent dehydrogenases, the combination of  $\text{NAD}^+$  photoreduction and FDH for the conversion of  $\text{CO}_2$  to formic acid is hardly to achieve. To resolve this problem for the  $\text{NAD}^+$ -dependent dehydrogenase, 2,2'- or 4,4'-bipyridinium salt ( $\text{BP}^{2+}$ ; Fig. 3) is used as the electron carrier as its one-electron reduced form ( $\text{BP}^+$ ) is easily produced by reaction with the photoexcited photosensitizer.

**Biocatalyst for CO<sub>2</sub> reduction****Formate dehydrogenase (FDH)****Carbon-monoxide dehydrogenase (CODH)****Biocatalyst for CO<sub>2</sub> fixation****Malic enzyme (ME)****Isocitrate dehydrogenase (IDH)**

**Fig. 2** Typical biocatalytic pathways for the CO<sub>2</sub> reduction and fixation.

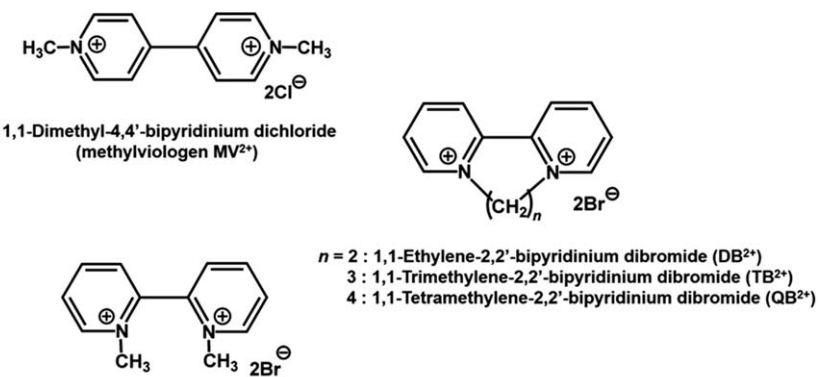


**Fig. 3** Chemical structures of 2,2'- and 4,4'-bipyridinium salts (BP<sup>2+</sup>) for the photoredox system with photosensitizer and FDH.

On the other hand, since BP<sup>+</sup> is an effective coenzyme for NAD<sup>+</sup>-dependent dehydrogenase, formic acid is produced from CO<sub>2</sub> by means of the photoredox system consisting of an electron donor (D), a photosensitizer (P), and BP<sup>2+</sup> in the presence of FDH as shown in Fig. 4.

The visible light-induced photoredox systems for CO<sub>2</sub> reduction to formic acid with tris(bipyridine)ruthenium(II) (Ru(bpy)<sub>3</sub><sup>2+</sup>) as the photosensitizer, 2,2'- or 4,4'-bipyridinium salt in the presence of FDH have been reported.<sup>12–15</sup>

Systems using water-soluble zinc tetraphenylporphyrin tetrasulfonate (ZnTPPS) or zinc tetrakis(4-methylpyridyl)porphyrin (ZnTMPyP) as the photosensitizer have also been reported.<sup>16–24</sup> Some of the results

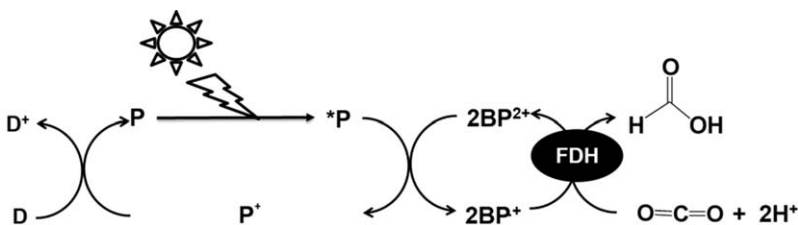


**Fig. 4** Visible light-induced photoredox systems consisting of an electron donor (D), a photosensitizer (P), and 2,2'- or 4,4'-bipyridinium salt ( $\text{BP}^{2+}$ ) in the presence of FDH for  $\text{CO}_2$  reduction to formic acid.

**Table 1** Visible light-induced formic acid production from  $\text{CO}_2$  with FDH and photoreduction of various 4,4'- or 2,2'- $\text{BP}^{2+}$ s with a system using ZnTPPS.<sup>a</sup>

$\text{BP}^{2+}$	Rate of formic acid production ( $\mu\text{M h}^{-1}$ )	Ref.
$\text{MV}^{2+}$	52.5	20
$\text{DM}^{2+}$	40.0	20
$\text{DB}^{2+}$	62.5	20
$\text{TB}^{2+}$	60.0	20
$\text{QB}^{2+}$	42.5	20

<sup>a</sup> Reaction condition: TEOA (0.3 M), ZnTPPS (10  $\mu\text{M}$ ),  $\text{BP}^{2+}$  (0.1 mM), and FDH (9.3  $\mu\text{M}$ ) in 3  $\text{CO}_2$  saturated sodium pyrophosphate buffer under visible light irradiation.

obtained from such systems with ZnTPPS and various 2,2'- or 4,4'-bipyridinium salts are summarized in Table 1.

### 3 Photoredox/biocatalytic systems for the formation of C–C bonds from $\text{CO}_2$

As mentioned previous section, photoredox systems for the reduction of  $\text{CO}_2$  to formic acid production in the presence of FDH as the biocatalyst have been reported in literature.

The system is only  $\text{CO}_2$  reduction based on the multi-electrons-protons coupling reaction with visible light energy. Now, let us focus on systems with biocatalyst for C–C bonds formation by using  $\text{CO}_2$  as the carbon feedstock with visible light energy. ME and IDH are attractive biocatalyst for this target, and  $\text{CO}_2$  is bonded to the organic molecule as a carboxyl group.

A photoredox system with ME catalyst that exploit reduction of  $\text{NADP}^+$  to  $\text{NADPH}$  as the electron carrier has been described for the first time. In this case, the use of  $\text{Ru}(\text{bpy})_3^{2+}$ ,  $\text{MV}^{2+}$ , ferredoxin- $\text{NADP}^+$  reductase (FNR) and mercaptoethanol (RSH) led to malic acid production from  $\text{HCO}_3^-$  and pyruvic acid, as shown in Fig. 5. In this approach, the quantum yield value for malic acid production from  $\text{HCO}_3^-$  and pyruvic acid has been estimated to be 3.6% after 2 h irradiation.<sup>12</sup>

IDH biocatalyst coupled with a photoredox system consisting in  $\text{NADP}^+$  with a system containing visible light photoredox catalyst  $\text{Ru}(\text{bpy})_3^{2+}$ ,  $\text{MV}^{2+}$  as the electron acceptor, FNR and RSH for isocitric acid production from  $\text{HCO}_3^-$  and  $\alpha$ -oxoglutaric acid shown in Fig. 6 also has been reported. In this system, the quantum yield for isocitric

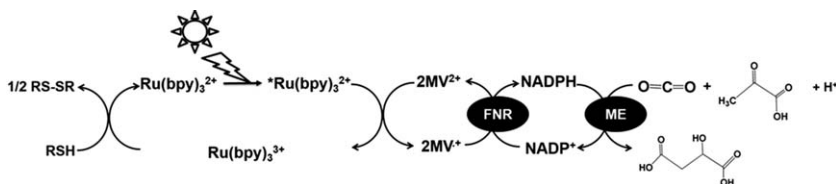


**Fig. 5** Photoredox system with ME and reduction of NADP<sup>+</sup> with a system containing Ru(bpy)<sub>3</sub><sup>2+</sup>, MV<sup>2+</sup>, ferredoxin-NADP<sup>+</sup> reductase (FNR) and mercaptoethanol (RSH) for malic acid production from HCO<sub>3</sub><sup>-</sup> and pyruvic acid.

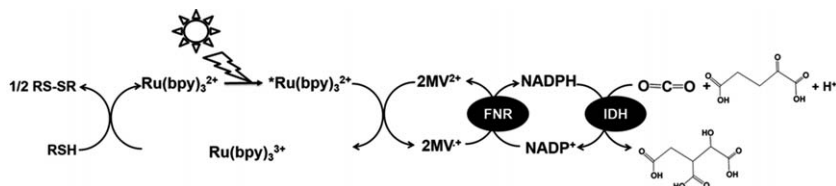


**Fig. 6** Photoredox system with IDH and reduction of NADP<sup>+</sup> with a system containing Ru(bpy)<sub>3</sub><sup>2+</sup>, MV<sup>2+</sup>, FNR and RSH for isocitric acid production from HCO<sub>3</sub><sup>-</sup> and α-oxoglutaric acid.

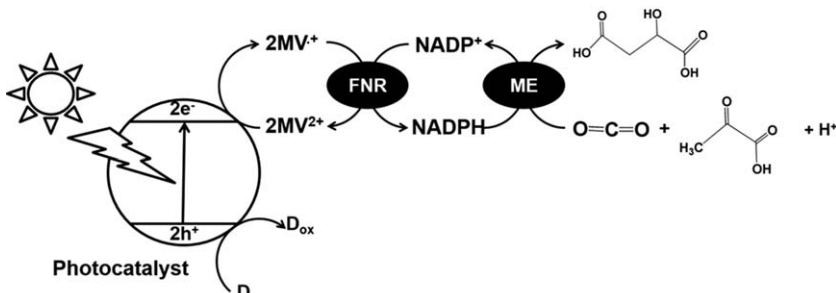


**Fig. 7** Photoredox system with ME and reduction of NADP<sup>+</sup> with a system containing photocatalyst, MV<sup>2+</sup>, FNR and an electron donor for malic acid production from CO<sub>2</sub> and pyruvic acid.

acid production from HCO<sub>3</sub><sup>-</sup> and α-oxoglutaric acid is estimated to be 1.9% after 2 h irradiation.<sup>12</sup>

A different approach involving ME as the biocatalyst and reduction of NADP<sup>+</sup> with a system containing TiO<sub>2</sub> semiconductor or CdS photocatalyst, MV<sup>2+</sup>, FNR and an electron donor (in this case lactic acid) for the malic acid production from CO<sub>2</sub> and pyruvic acid (Fig. 7). It is thought that at these stages, *ca.* 50% of pyruvic acid is converted to malic acid at CdS and *ca.* 15% at TiO<sub>2</sub> semiconductor, respectively.<sup>25</sup>

By means of a catalytic system consisting of NADH as the electron donor, Zn Chl-e<sub>6</sub> (chlorine-e<sub>6</sub>, formed by the hydrolysis of chlorophyll-a) as the photosensitizer, MV<sup>2+</sup>, FNR, NADP<sup>+</sup> as the electron carrier, and biocatalyst ME (see Fig. 8), the malic acid production is 0.65 mM after 3 h visible light irradiation. The ratio of pyruvic acid (initial concentration: 10 mM) to malic acid is about 6.5%. In contrast, no production of malic acid is observed without FNR, MV<sup>2+</sup> or irradiation.<sup>26,27</sup>

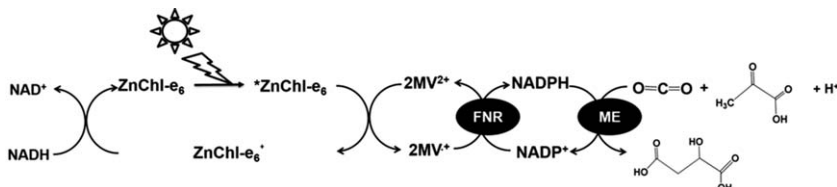


**Fig. 8** Photoredox system with ME and reduction of  $\text{NADP}^+$  with a system containing  $\text{ZnChl-e}_6$ ,  $\text{MV}^{2+}$ , FNR and NADH for malic acid production from  $\text{HCO}_3^-$  and pyruvic acid.

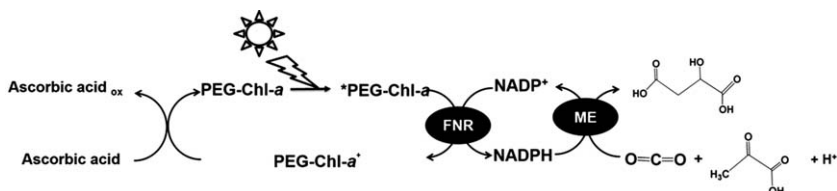


**Fig. 9** Photoredox system with a system containing ascorbate, PEG-Chl- $\alpha$ , FNR,  $\text{NADP}^+$ , and ME.

These results show that the malic acid production proceeds by coupling the  $\text{NADP}^+$  reduction using the photosensitization of dye molecule or photocatalyst and enzymatic conversion of pyruvic acid and  $\text{CO}_2$  to malic acid with ME *via* the enzymatic function of FNR in water media.

The photoredox system with ME and reduction of  $\text{NADP}^+$  with a system containing ascorbate as an electron donor, the polyethylene glycol modified chlorophyll- $\alpha$  (PEG-Chl- $\alpha$ ) as a photosensitizer, FNR,  $\text{NADP}^+$ , and ME as shown Fig. 9 has been exploited for the production of malic acid from  $\text{HCO}_3^-$  and pyruvic acid. As  $\text{NADP}^+$  directly is reduced with FNR and PEG-Chl- $\alpha$  in this reaction, it is not necessary to add the  $\text{MV}^{2+}$  as an electron carrier. The concentration of malic acid produced is estimated to be 75  $\mu\text{M}$  after 3 h visible light irradiation. The conversion yield of pyruvic acid to malic acid is estimated to be 0.041% under excess  $\text{HCO}_3^-$  (180 mM) condition.<sup>28</sup>

However, as these systems are very complicated and FNR is an expensive biological reagent, it is necessary to simplify it by using a novel electron mediator (C) instead of  $\text{NADP}^+$  reduction system with FNR, as shown in Fig. 10.

In order to develop the simplified visible light-induced photoredox system as shown in Fig. 10, the electron mediator that shows the same behavior as NADPH is necessary. 1,1'-Diphenyl-4,4'-bipyridinium salt derivatives ( $\text{PV}^{2+}$ s) have received much attention, because  $\text{PV}^{2+}$ s have a lower first and second reduction potentials compared with the 2,2'- or 4,4'-bipyridinium salts (BP $^{2+}$ s) such as a  $\text{MV}^{2+}$  and so on. Since both the first and the second reduction state of 1,1'-diphenyl-4,4'-bipyridinium salt ( $\text{PV}^{2+}$ ) are insoluble in an aqueous media, however,  $\text{PV}^{2+}$  is not suitable for homogenous visible light-induced processes shown in Fig. 10. Thus, the water-soluble derivative, 1,1'-bis(*p*-sulfonylphenyl)-4,4'-bipyridinium dichloride ( $\text{PSV}^{2+}$ )<sup>29</sup> is used as an electron carrier in this reaction. Fig. 11 shows the first and second reduction state of  $\text{PSV}^{2+}$ .

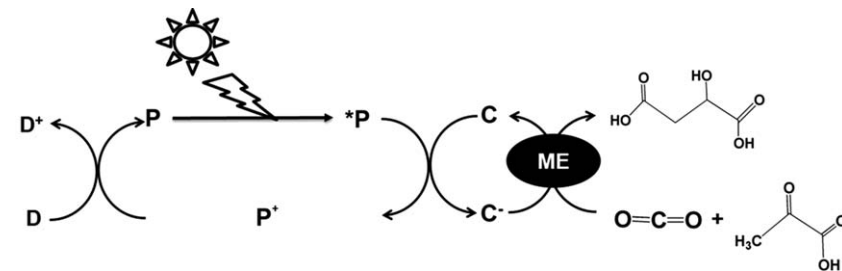


**Fig. 10** Photoredox system with ME and reduction of novel electron mediator (C) with a system containing a photo-sensitizer (P) and an electron donor (D) for malic acid production from CO<sub>2</sub> and pyruvic acid.

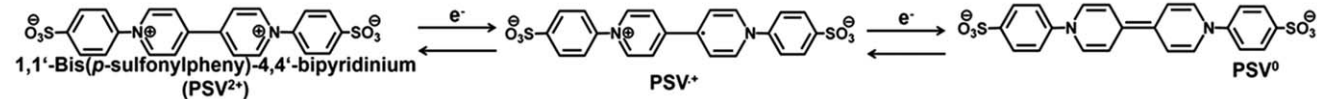


**Fig. 11** The oxidized (PSV<sup>2+</sup>), first (PSV<sup>+</sup>) and second reduction state (PSV<sup>0</sup>) of PSV<sup>2+</sup>.

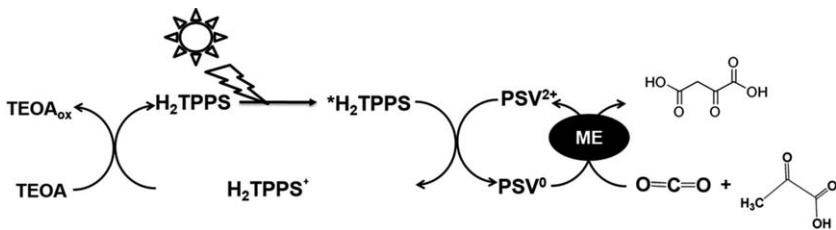


**Fig. 12** Photoredox system with ME and reduction of  $\text{PSV}^{2+}$  with a system containing  $\text{H}_2\text{TPPS}$  and TEOA for oxaloacetic acid production from  $\text{CO}_2$  and pyruvic acid.

The reduction potentials for such compounds are estimated to be  $-0.34$  and  $-0.64$  V (vs. Ag/AgCl) using electrochemical approach, respectively.

The visible-light induced formation of C–C bonds from pyruvic acid and  $\text{CO}_2$  with ME by exploiting  $\text{PSV}^{2+}$  as the electron mediator, in the presence of water soluble photoredox catalyst tetraphenylporphyrinetransulfonate ( $\text{H}_2\text{TPPS}$ ) and TEOA as the electron donor is achieved, as shown in Fig. 12.<sup>30</sup> The redox potentials of the exited triplet state of  $\text{H}_2\text{TPPS}$  in buffer aqueous,  $E(\text{H}_2\text{TPPS}^+/\text{H}_2\text{TPPS}^*)$  and  $E(\text{H}_2\text{TPPS}^*/\text{H}_2\text{TPPS})$  are estimated to be  $-0.70$  V and  $0.40$  V using electrochemical and optical measurements, respectively, thus allowing for the production of the one- or two-electron reduced states of  $\text{PSV}^{2+}$ .

When a reaction mixture containing  $\text{H}_2\text{TPPS}$ ,  $\text{PSV}^{2+}$ , and TEOA is irradiated with visible light by using 250 W halogen lamp as the light source, the absorbance attributed to the absorption band of two-electron reduced state of  $\text{PSV}^{2+}$  ( $\text{PSV}^0$ ) around at 688 nm increased with irradiation time.

As the visible-light induced reduction of  $\text{PSV}^{2+}$  to  $\text{PSV}^0$  with the sensitization of  $\text{H}_2\text{TPPS}$  is accomplished, the visible-light induced malic acid production from pyruvic acid and  $\text{CO}_2$  with ME *via* the photoreduction of  $\text{PSV}^{2+}$  with the sensitization of  $\text{H}_2\text{TPPS}$  in the presence of TEOA is attempted. When the reaction mixture containing  $\text{H}_2\text{TPPS}$ ,  $\text{PSV}^{2+}$ , TEOA and ME in  $\text{CO}_2$  saturated buffer aqueous solution is irradiated with visible light, oxaloacetic acid production is exclusively observed. Indeed, after 2 h visible-light irradiation,  $60 \mu\text{M}$  oxaloacetic acid is produced with increasing irradiation time. In contrast, with the examined catalytic system, no malic acid is observed.<sup>30</sup>

However, in the presence of  $\text{Mg}^{2+}$ , that acts as a co-factor for ME, the production of malic acid is observed. From these results,  $\text{PSV}^0$  is used for building C–C bonds from  $\text{CO}_2$ , oxaloacetic acid production and  $\text{PSV}^+$  is used for the reduction of carbonyl group of oxaloacetic acid to malic acid, respectively. The possible mechanism in the photoredox system is shown in Fig. 13. At first, the hydrogen in pyruvic acid is abstracted by  $\text{PSV}^0$  and then  $\text{CO}_2$  is bonded to pyruvic acid derivative as a carboxy group based on the building C–C bonds from  $\text{CO}_2$ , resulting the oxaloacetic acid production. Finally, the oxaloacetic acid is reduced to malic acid by  $\text{PSV}^+$ .

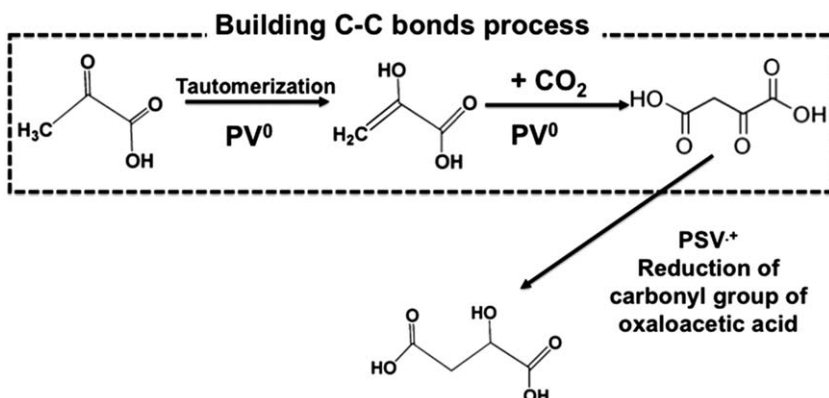


**Fig. 13** Possible mechanism for oxaloacetic acid and malic acid production from  $\text{CO}_2$  and pyruvic acid using the reduced state of  $\text{PSV}^{2+}$ .

## 4 Conclusions

In this review, some studies on the visible-light induced photoredox systems consisting of a photosensitizer, an electron mediator and a biocatalyst for building C–C bonds from  $\text{CO}_2$  as a feedstock are introduced. Many approaches focused on the visible-light induced systems for  $\text{CO}_2$  reduction to C1 molecules are mainstream. In viewpoint of the photoredox systems for  $\text{CO}_2$  utilization based on the artificial photosynthesis, building C–C bonds from  $\text{CO}_2$  as a feedstock with the photoredox system using visible light energy, mimicking natural photosynthesis of glucose production from  $\text{CO}_2$  is more important technology. The studies introduced in this review is opened the new avenue for the approach building C–C bonds from  $\text{CO}_2$  as a feedstock with the biocatalyst and a photosensitizer.

## Acknowledgements

This work was partially supported by Precursory Research for Embryonic Science and Technology (PRESTO, Japan Science and Technology Agency JST), Grant-in-Aid for challenging Exploratory Research (Japan Society for the Promotion of Science) (15K14239), and Grant-in-Aid for Scientific Research on Innovative Areas “Artificial Photosynthesis (2406).”

## References

- 1 T. Inoue, A. Fujishima, S. Konishi and K. Honda, *Nature*, 1979, **277**, 637–638.
- 2 B. Aurian-Blajeni, M. Halmann and J. Manassen, *Sol. Energy*, 1980, **25**, 165–170.
- 3 K. Faber, *Biotransformations in Organic Chemistry*, 3rd edn, Springer, Berlin, 1997, vol. 201.
- 4 Y. Amao, *ChemCatChem*, 2011, **3**, 458–474.
- 5 Y. Amao, *Curr. Top. Biotechnol.*, 2009, **5**, 71–81.
- 6 Y. Amao, *Curr. Nanosci.*, 2008, **4**, 45–52.
- 7 Y. Amao, *Chem. Lett.*, 2017, **46**, 780–788.
- 8 Y. Amao and T. Watanabe, *Chem. Lett.*, 2004, **33**, 1544–1545.

- 9 Y. Amao and T. Watanabe, *Appl. Catal., B*, 2009, **86**, 109–113.
- 10 Y. Amao, *Prepr. Pap. – Am. Chem. Soc., Div. Fuel Chem.*, 2010, **55**, 91.
- 11 K. Hironaka, S. Fukuzumi and T. Tanaka, *J. Chem. Soc., Perkin Trans. 2*, 1984, 1705.
- 12 D. Mandler and I. Willner, *J. Chem. Soc., Perkin Trans. 2*, 1988, 997–1003.
- 13 I. Willner and D. Mandler, *J. Am. Chem. Soc.*, 1989, **111**, 1330–1336.
- 14 I. Willner, N. Lapidot, A. Riklin, R. Kasher, E. Zahavy and E. Katz, *J. Am. Chem. Soc.*, 1994, **116**, 1428–1441.
- 15 I. Willner, I. Willner and N. Lapidot, *J. Am. Chem. Soc.*, 1990, **112**, 6438–66439.
- 16 R. Miyatani and Y. Amao, *Biotechnol. Lett.*, 2002, **24**, 1931–1934.
- 17 R. Miyatani and Y. Amao, *J. Mol. Catal. B: Enzym.*, 2004, **27**, 121–125.
- 18 R. Miyatani and Y. Amao, *J. Jpn. Pet. Inst.*, 2004, **47**, 27–31.
- 19 I. Tsujisho, M. Toyoda and Y. Amao, *Catal. Commun.*, 2006, **7**, 173–176.
- 20 Y. Amao, R. Abe and S. Shiotani, *J. Photochem. Photobiol., A: chemistry*, 2015, **313**, 149–153.
- 21 Y. Amao and S. Ikeyama, *Chem. Lett.*, 2015, **44**, 1182–1184.
- 22 S. Ikeyama, R. Abe, S. Shiotani and Y. Amao, *Chem. Lett.*, 2016, **45**, 979–981.
- 23 S. Ikeyama and Y. Amao, *Chem. Lett.*, 2016, **45**, 1259–1261.
- 24 S. Ikeyama and Y. Amao, *ChemCatChem*, 2017, **9**, 833–838.
- 25 H. Inoue, M. Yamachika and H. Yoneyama, *J. Chem. Soc., Faraday Trans.*, 1992, **88**, 2215–2219.
- 26 Y. Amao and M. Ishikawa, *J. Jpn. Pet. Inst.*, 2007, **50**, 272–277.
- 27 Y. Amao and M. Ishikawa, *Catal. Commun.*, 2007, **8**, 423–512.
- 28 T. Itoh, H. Asada, K. Tobioka, Y. Kodera, A. Matsushima, M. Hiroto, H. Nishimura, T. Kamachi, I. Okura and Y. Inada, *Bioconjugate Chem.*, 2000, **11**, 8–13.
- 29 H. Kamogawa and S. Sato, *Bull. Chem. Soc. Jpn.*, 1991, **64**, 321–323.
- 30 Y. Amao, S. Ikeyama, T. Katagiri and K. Fujita, *Faraday Discuss.*, 2017, **198**, 73–81.

---

# Pushing the limits of photoactivatable compounds

Tomáš Slanina\*

DOI: 10.1039/9781788010696-00175

The text summarizes selected chapters from my dissertation thesis which was awarded by the 2016 European Photochemistry Association PhD Prize. It reports on the development of first fully-organic visible light absorbing photoremoveable protecting group and carbon-monoxide releasing compounds. These dye-based molecules were rationally designed, carefully synthetized and their properties were investigated in detail. Some of them were also used for *in vivo* and *in vitro* biological studies.

## 1 Introduction

*“Photochemistry is the branch of chemistry concerned with the chemical effects of light (far UV to IR).”<sup>1</sup>* This rather brief definition of IUPAC covers immense amount of transformations which are found in many, often unexpected, fields of life.

Starting with photodynamic therapy of neonatal jaundice<sup>2</sup> and ending with high-power laser engraving on marble,<sup>3</sup> photochemistry accompanies humans in their whole life. The history of photochemistry is older than the written historical sources.

The earliest written records of the use of dyestuffs and pigments in China are from 2600 B.C.<sup>4</sup> The famous tale from the history of photochemistry about photochromic materials used by the army of Alexander the Great (356–323 B.C.) as a tool for determination of the precise time and synchronizing the army attacks turned out to be a hoax. It was published on 5th August 1961 in an American weekly magazine *Saturday Review* as a joke of a columnist and since that it has spread into scientific publications and chemistry textbooks.<sup>5</sup> In 1669, Henning Brand prepared white phosphorus from urine which was the first material known to exhibit phosphorescence.<sup>6</sup> Fluorescein, a famous fluorescent dye, has been synthetized by Alexander von Baeyer in 1871 from phthalic anhydride and resorcinol.<sup>7</sup> Modern photochemistry that studies the interaction of molecules with light was established by pioneering works by Giacomo Ciamician at the beginning of 20th century.<sup>8</sup>

## 2 Photoremoveable protecting groups

In 1962, Barltrop and Schofield introduced the first “traceless” deprotection of a protecting group.<sup>9</sup> They observed the cleavage of benzyloxy-carbonyl group, a commonly used protecting group for amines, by irradiation with UV light (254 nm).

---

*Institute of Organic Chemistry and Chemical Biology, Goethe University Frankfurt, Frankfurt am Main, Germany. E-mail: slanina.tomas@seznam.cz*

Their work initiated the development of photoremoveable protecting groups (PPGs) and caged compounds. Photoremoveable protecting groups are protecting groups used for temporary blocking of functional groups in organic synthesis which are released by the action of light. Caged compounds are based on the same derivatives as PPGs, but are used for suppressing the activity of biologically relevant molecules and releasing them in cell or in tissue by light. Caged compounds help to investigate biochemical and biological processes by regulating them in a high temporal and spatial precision. The activity of an enzyme, neuron synapsis or cell metabolism can be precisely controlled by lasers focused into small volume. All previously known PPGs used bioincompatible UV light for uncaging and their use was therefore limited.

The design of a visible light-absorbing PPG has always been a substantial challenge for photochemists. Classical PPGs were modified by different substituents in order to shift their absorption into the visible region, but the longest-wavelength-absorbing pHPs<sup>10</sup> and coumarins<sup>11</sup> absorb only up to 400 nm. Most of the known UV-absorbing PPGs have sufficient energy in the excited state (4–5 eV) to break the chemical bond between PPG and the leaving group. The energy of visible-light photons is substantially lower (2–3 eV) and, therefore, other mechanisms must be applied for the bond cleavage. The most common processes are intramolecular or intermolecular electron transfer and energy transfer.

The first attempts to design a visible-light-absorbing PPG were based on organometallic ruthenium complexes used for caging of GABA.<sup>12–14</sup>

Our approach in designing a visible light-absorbing PPG is based on coumarin-4-yl methyl moiety (Fig. 1) which absorbs up to 400 nm.<sup>11</sup> Formal extension of the coumarin chromophore leads to the xanthene-based PPG (**1**, Fig. 1). In analogy to its structural analogue, fluorescein,

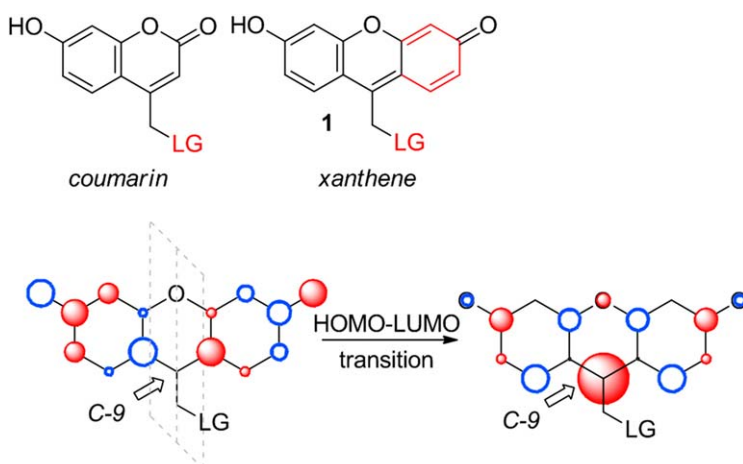
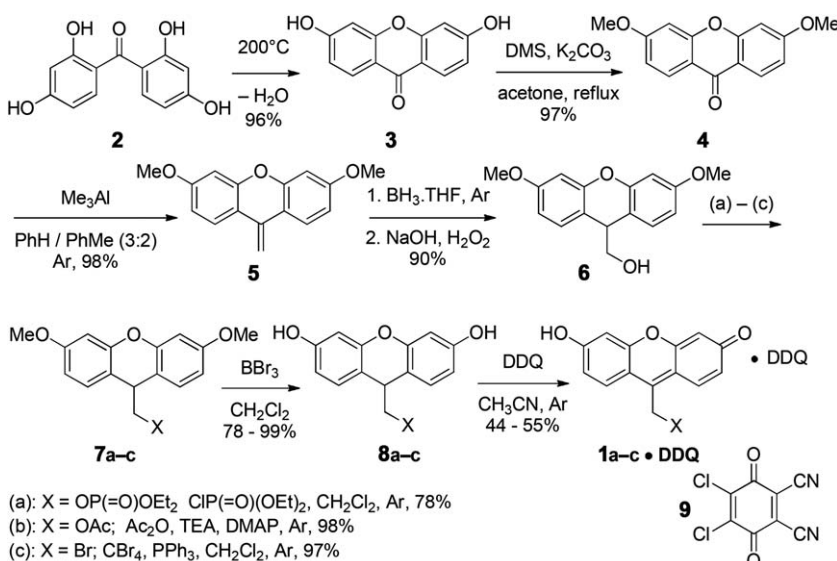


**Fig. 1** Design of a new photoremoveable protecting group by extension of the coumarin chromophore to xanthene. Depiction of its frontier MOs (middle: HOMO, right: LUMO) using the Hückel MO theory (software HuLiS). The C-9 position is indicated by an arrow. The nodal plane in HOMO is depicted by gray dashed lines. The size of the circle is proportional to the orbital coefficient and its shading represents the sign of the wavefunction.

the proposed structure **1** should have high molar absorption coefficient, bright fluorescence, good solubility in aqueous media, and lowest absorption maximum close to 500 nm.<sup>15</sup>

The behavior of **1** in the excited state was predicted by calculation of its molecular orbitals (MO) by Hückel theory (predicted by software HuLiS; Fig. 1). In HOMO (Fig. 1), the C-9 position together with the bridging oxygen atom are parts of a nodal plane and therefore have zero coefficients. On the contrary, the LUMO orbital (Fig. 1) has a large coefficient at the position C-9. The excitation of one electron from HOMO to LUMO induces a strong charge transfer to the position C-9 which should favor the heterolytic release of an attached leaving group (LG).<sup>16</sup>

We designed a novel synthetic route of preparation of xanthene moiety from 2,2',4,4'-tetrahydroxybenzophenone **2** (Scheme 1). The condensation reaction in water in an autoclave at 200 °C led to very stable 3,6-dihydroxy-9*H*-xanthen-9-one **3**.<sup>15</sup> The carbonyl functionality in C-9 position of **3** was transformed, after protection of phenolic hydroxyls by dimethyl sulfate (**4**), by a Wittig-like reaction with trimethylaluminium into a derivative with the exocyclic double bond **5**.<sup>17</sup> The hydroboration-oxidation reduced the xanthene moiety into its *leuco* form and installed the hydroxyl functionality in an anti-Markovnikov fashion to give the alcohol **6**. The leaving group was installed to the xanthene PPG by reaction of the alcohol **6** with acid chloride or anhydride to give diethyl phosphate **7a** and acetate **7b**<sup>18</sup> or by Appel reaction to give bromide **7c**.<sup>19</sup> The diethyl phosphate was chosen as a model for ATP and other biogenic phosphates and acetate as a model for amino acids. The deprotection of methoxy groups by BBr<sub>3</sub> gave the 9*H*-xanthene diol derivatives **8a–c**. These compounds were oxidized to the final products **1a–c** by 2,3-dichloro-5,6-dicyano-1,4-benzoquinone (DDQ, **9**, Scheme 1). This rapid oxidation resulted in precipitation of equimolar complexes **1a–c · DDQ**.<sup>28</sup>



**Scheme 1** Synthesis of (6-hydroxy-3-oxo-3*H*-xanthen-9-yl)methyl derivatives **1a–c**.

For a long time, we considered these products to be non-complexed (*i.e.* without DDQ) because DDQ complex **1a–c** · DDQ cannot be observed by  $^1\text{H}$  NMR as it does not contain any hydrogen atoms. Moreover, DDQ hydrolyses in solvents used for NMR analyses (DMSO,  $\text{D}_2\text{O}$ ) to a complex mixture of quinones which have very weak signals in  $^{13}\text{C}$  NMR. The complex **1a–c** · DDQ also dissociates after most commonly used mass spectrometry ionization techniques. Elemental analysis revealed the presence of nitrogen atoms in the sample and suggested equimolar complex **1a–c** · DDQ which was further characterized by direct inlet HRMS with mild ionization technique.

Xanthene derivatives **1a–c** (synthesized as complexes **1a–c** · DDQ) have strong absorption bands ( $\epsilon_{\max} \sim 4 \times 10^4 \text{ M}^{-1} \text{ cm}^{-1}$ ) at  $\lambda_{\max} = 519\text{--}528 \text{ nm}$  similar to fluorescein derivatives. In accordance with our expectations, all xanthene-based compounds were photoactive. The course of the irradiation of aqueous solution of **1a** followed by UV-vis spectrometry is shown in Fig. 2. The primary photoproduct has the absorption maximum at  $\sim 490 \text{ nm}$ . This species is formed from all derivatives (**1a–c**) and indicates that the leaving group was released. The shape and molar absorption coefficient indicate that the primary photoproduct has also xanthene chromophore. The quantum yields of the photodegradation are ranging from  $\sim 0.3\%$  for acetate **1b** to  $\sim 2\%$  for bromide and phosphate **1c** and **1a**. This corresponds to the  $\text{p}K_a$  of the conjugated acid of the leaving group (LGH). Higher quantum yield for strong acids indicates the heterolytic bond fission from the excited state.

The photoproduct was obtained in milligram amounts by preparative irradiation and was fully characterized. Since the xanthene-based PPG have properties analogous to coumarins, we anticipated also similar photochemical behavior.

Coumarins release the leaving group from the first excited singlet mainly by heterolytic bond fission and give the product of photo-solvolytic. To our surprise, we found that the photoproduct is not the

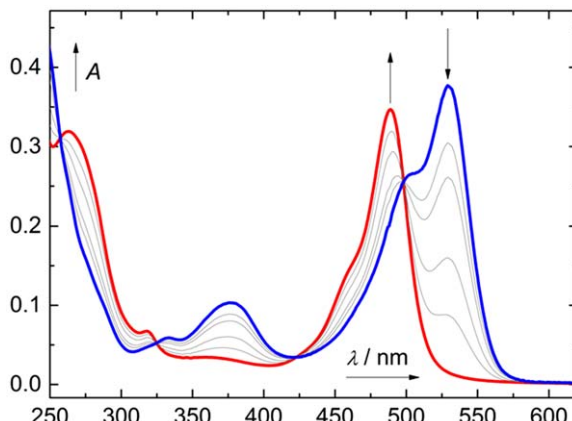


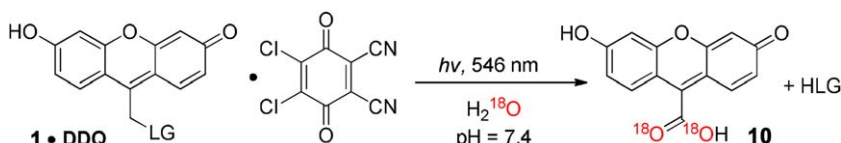
**Fig. 2** Irradiation of **1a** (first spectrum,  $\lambda_{\max} = 528 \text{ nm}$ , thick black line,  $c \sim 2 \times 10^{-5} \text{ M}$ ) at  $\lambda = 546 \text{ nm}$  in phosphate buffer ( $I = 0.1 \text{ M}$ ,  $\text{pH} = 7.0$ ) as monitored by absorption spectroscopy. The last spectrum ( $\lambda_{\max} = 489 \text{ nm}$ , thick grey line) was taken after 15 min of irradiation.

expected (6-hydroxy-3-oxo-3*H*-xanthen-9-yl)methanol, but 6-hydroxy-3-oxo-3*H*-xanthene-9-carboxylic acid **10** (Scheme 2).

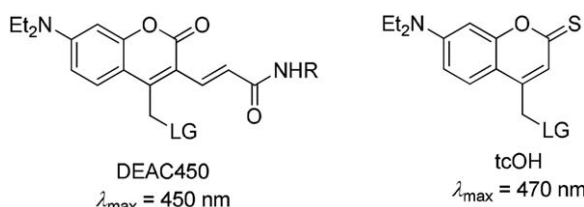
Since the presence/absence of oxygen dissolved in the reaction mixture had neither influence on the quantum yield nor the product distribution, the acid **10** is probably formed by rapid oxidation of the primary alcohol (solvolytic product; (6-hydroxy-3-oxo-3*H*-xanthen-9-yl)methanol) by DDQ present in the complex. The irradiation in an isotopically labeled aqueous buffer revealed that the oxygen atoms of the carboxylic functionality originate from the solvent (Scheme 2). A detailed time-resolved fluorescence study of **1c** revealed that the leaving group is released from the first excited singlet with a lifetime of 0.4 ns. This observation is analogous to the mechanism of photodeprotection of coumarinyl PPG.

The introduction of xanthen-9-ylmethyl PPG **1** in 2013 started a pursuit for PPGs based on dye chromophores. Commercial dyes have strong absorption of visible light but usually have been designed to be extremely stable towards photobleaching and other photoinduced reactions.<sup>20</sup> The first new photoremoveable protecting groups absorbing visible light were based on coumarins. A derivative of 7-diethylaminocoumarin-4-ylmethyl PPG, **DEAC450** (Scheme 3, left part), was prepared by Ellis-Davies *et al.* in 2013.<sup>21</sup> It has a strong absorption at 450 nm ( $\epsilon_{450} = 43\,000 \text{ M}^{-1} \text{ cm}^{-1}$ ) and was used to cage cAMP. The photodeprotection of cAMP occurs with exceptionally high quantum yield ( $\Phi = 0.78$ ). The substitution of the carbonyl oxygen of a lactone functionality to sulfur leads to 7-diethylamino-4-thiocoumarinylmethyl PPG (tcOH, Scheme 3, right part).<sup>22</sup> This derivative has even more red-shifted absorption ( $\lambda_{\max} = 470 \text{ nm}$ ) and has high molar absorption coefficient ( $\epsilon_{500} > 10\,000 \text{ M}^{-1} \text{ cm}^{-1}$ ) even at 500 nm. The quantum yield of the leaving group release is  $\Phi \sim 5 \times 10^{-3}$ .

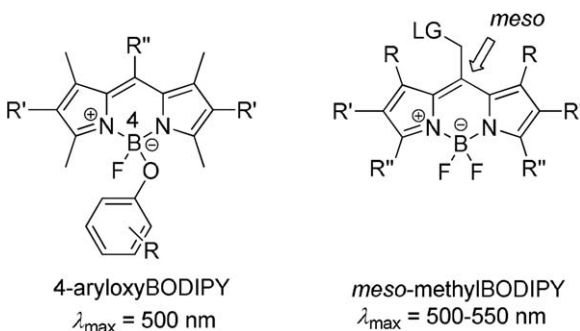
In 2014, Urano and co-workers designed a 4-aryloxyBODIPY-based PPG absorbing at 500 nm for protection of various electron-rich phenols<sup>23</sup> (Scheme 4, left part). The mechanism of the deprotection includes photoinduced electron transfer from the electron rich aryl to the BODIPY



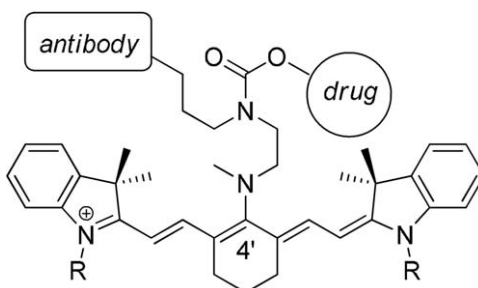
**Scheme 2** Photoinduced release of the leaving group from **1**-DDQ and formation of 6-hydroxy-3-oxo-3*H*-xanthene-9-carboxylic acid **10**. The incorporation of  $^{18}\text{O}$  from water is highlighted.



**Scheme 3** Visible-light-absorbing coumarinylmethyl PPGs.



**Scheme 4** BODIPY-based photoremoveable protecting groups.



**Scheme 5** Cyanine-based PPG absorbing near-IR light.

moiety which is concomitantly cleaved. Histamine was caged by this methodology with substituted phenol as a linker. Further studies by Winter<sup>24</sup> and Weinstain<sup>25</sup> used *meso*-methyl BODIPY PPGs (Scheme 4, right part). The absorption properties of these derivatives can be modulated by substitution and the absorption maximum reaches 550 nm. The mechanism of photodeprotection analogical to coumarinyl PPGs has been suggested by Winter. The photo- $S_N1$  reaction heterolytically cleaves the bond between the leaving group and the BODIPY-*meso* methyl group, and the subsequent nucleophilic attack of the solvent to the *meso*-methyl cation leads to the product of photosolvysis.

Recently, the group of Schnermann has introduced a cyanine-based PPG (Scheme 5) which is capable of cleavage in the near-IR region (690 nm).<sup>26</sup> The compound has been used as a photolabile linker for antibody-drug conjugates. The mechanism of the photodeprotection might be analogous to 4-aryloxyBODIPY derivatives. The excited cyanine core is reduced by photoinduced electron transfer from the amino group attached to the 4' position.

Photoremoveable protecting groups have been rapidly developed over last 50 years. From the early investigations of photochemistry of “classical” protecting groups by Barltrop<sup>9</sup> to the work of Schnermann<sup>26</sup> many features have been optimized. The irradiation wavelengths have moved from deep UV to NIR, internal filter effect of photoproducts has been reduced, quantum and chemical yields of deprotection have raised. Nevertheless, there are still several issues to be solved in this field, such

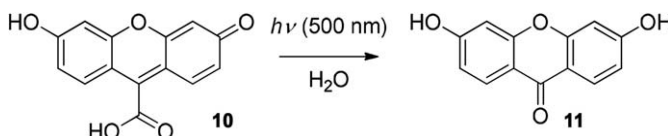
as unwanted singlet oxygen sensitization, phototoxicity, instability in presence of reactive oxygen species (ROS), low penetration through cell membranes, aggregation, DNA intercalation, and poor solubility.

### 3 Photoactivatable carbon monoxide-releasing molecules (photoCORMs): 1st generation

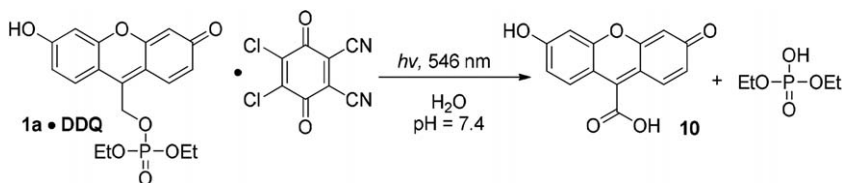
In our research of xanthene-based photoremovable protecting groups, we found that the product of photochemical degradation of xanthenylmethyl PPGs **1**, 6-hydroxy-3-oxo-3*H*-xanthene-9-carboxylic acid (**10**, Scheme 6), is also photochemically active.<sup>27</sup> Its photochemical degradation was approximately two orders of magnitude slower than the release of a leaving group from **1** and, therefore, we did not pay much attention to this process at first. Nevertheless, we analyzed the reaction mixture after exhaustive irradiation of **10** and found that the only product is 3,6-dihydroxy-9*H*-xanthen-9-one **11** (Scheme 6). The structure of the product invoked our interest in this reaction. The carboxylic group of **10** got cleaved and the carbon at the position C-9 is oxidized to ketone. Therefore, we wanted to reveal the mechanism of this transformation and find out possible applications of this process.

Firstly, we needed a reliable synthetic method for preparation of **10** in at least multi-milligram amounts. The first batches of **10** were prepared by irradiation of solutions of **1a · DDQ** in NMR tubes according to our previous research<sup>28</sup> (Scheme 7) and the isolated amounts of the target acid were in the range of 1–2 mg.

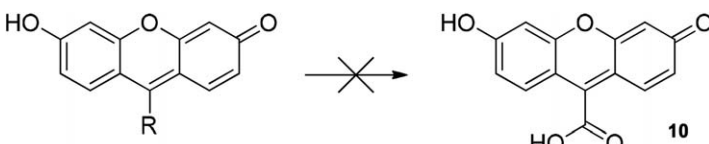
We decided to synthesize the acid **10** by an alternative chemical method. We tested the oxidation of 9-methyl xanthenes, hydrolysis and subsequent oxidation of **1a · DDQ** and **1b · DDQ**, acid- or base-catalyzed hydrolysis of 9-cyanoxanthene and acidic hydrolysis of -CX<sub>3</sub> derivative (X = F, Cl) (Scheme 8). Unfortunately, all attempts either did not yield any product and starting material was isolated, or led to xanthenone **11**.



**Scheme 6** Photodegradation of 6-hydroxy-3-oxo-3*H*-xanthene-9-carboxylic acid **10** to 3,6-dihydroxy-9*H*-xanthen-9-one **11**.



**Scheme 7** Photochemical synthesis of **10** from complex **1a · DDQ**.



R = -CH<sub>3</sub>, -CH<sub>2</sub>OAc,  
-CH<sub>2</sub>OP(=O)(OEt)<sub>2</sub>  
-CN, -CF<sub>3</sub>, -CCl<sub>3</sub>

**Scheme 8** Attempted syntheses of **10**.

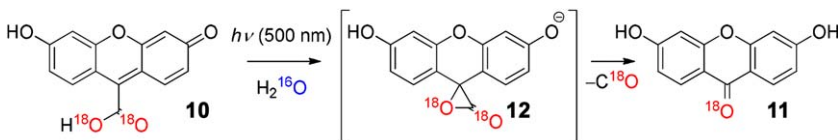
After a year of unsuccessful experiments, we decided to return to the photochemical preparation of the xanthene carboxylic acid **10**. We managed to upscale the synthesis by irradiation a solution of **1a·DDQ** in a large Petri-dish with a 400 W broad-band halogen lamp. With this method, we produced **10** in amounts of tens of milligrams (up to ~100 mg in one batch) and in high purity.

The xanthene carboxylic acid **10** can exist in four acid-base forms (dianion, anion, neutral and cation). The respective pK<sub>a</sub>'s of acid-base equilibria were found by spectrophotometric titration (pK<sub>a,1</sub> = 2.96; pK<sub>a,2</sub> = 5.08; pK<sub>a,3</sub> = 6.39). At physiological pH (7.4), >90% of dianion is present in the solution. The quantum yield of the photodegradation is pH dependent which indicates that different acid-base forms have different reactivity. At pH = 2.5 the acid precipitates and the quantum yield could not be determined. At pH = 4.5 (neutral form of **10** prevails) almost no photochemistry was observed. The highest quantum yield ( $\sim 4 \times 10^{-3}$ ) was measured at pH = 5.7 where the anion form of **10** dominates. The complex analysis of the quantum yields measured at different pH and the distribution of the respective acid-base forms of **10** revealed that the mono-anion is about one order of magnitude more reactive than the dianion (other forms are non-active).

The photodegradation of **10** to **11** involves a formal loss of one carbon atom in the molecule. The most common mechanism of the cleavage of carboxylic group is decarboxylation (loss of CO<sub>2</sub>).<sup>29</sup> We therefore suggested a two-step mechanism of photoinduced decarboxylation and subsequent photo-oxidation of the formed 6-hydroxy-3-oxo-3H-xanthene to **11**. The second part of this mechanism has been described before on similar substrates in presence of oxygen as an oxidant.<sup>30</sup>

Moreover, the thermal decomposition of **10** gives carbon dioxide which was proved by DSC/TG analysis with coupled IR detector.

The photoinduced decarboxylation/photo-oxidation mechanism was ruled out by the fact that the reaction quantum yield was independent on oxygen presence/absence in the reaction system (no oxidant present for possible photo-oxidation) and by isotope scrambling experiments. We prepared <sup>18</sup>O-labeled **10** according to our previously published procedure<sup>28</sup> (see Scheme 2). The irradiation of labeled acid in <sup>16</sup>O-based aqueous buffer did not lead in any incorporation of <sup>16</sup>O into the structure of the xanthone **11** (Scheme 9). Also the experiment with the non-labeled **10** in <sup>18</sup>O-based aqueous buffer did not show any isotope scrambling.



**Scheme 9** Mechanism of the CO release from isotopically labeled **10** in  $\text{H}_2^{16}\text{O}$ -based buffer with the depiction of the putative intermediate **12**.

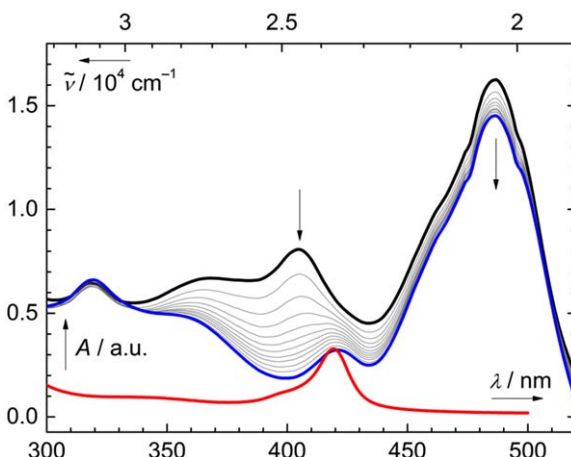


**Fig. 3** Absorption spectra measured following irradiation of **10** ( $c \sim 1.3 \times 10^{-4} \text{ M}$ ; the total irradiation time was 4.6 h) in the presence of MetHb ( $c \sim 2.3 \times 10^{-5} \text{ M}$ ) and  $\text{Na}_2\text{S}_2\text{O}_4$  ( $c = 2.5 \times 10^{-5} \text{ M}$ ) in 0.1 M aq phosphate buffer at  $\text{pH} = 7.4$  purged with  $\text{N}_2$  at  $503 \pm 15 \text{ nm}$ . The initial (top bold line) and final (centre bold line) spectra are highlighted. Pure COHb formed from Hb and CO dissolved in water (bottom bold line) is shown for comparison.

This suggests an intramolecular mechanism through an  $\alpha$ -lactone **12**.  $\alpha$ -Lactones are short-lived intermediates known to release CO by decarbonylation.<sup>31–33</sup> The expected product of the photodegradation of **10** was therefore carbon monoxide if the intramolecular mechanism is valid.

We attempted many tests to determine/exclude the presence of carbon monoxide in the reaction mixture after irradiation of **10**. The initial experiments with head-space mass spectrometry did not detect any CO. Also experiments with gas-phase IR were unsuccessful due to low concentrations of released CO. Finally, we tried to detect the released carbon monoxide by biomimetic trapping with hemoglobin (Hb).

Hemoglobin is known to form a strong complex with CO by creating carboxyhemoglobin (COHb). The characteristic change of absorption spectrum of Hb to COHb is used in physiology for determination of CO in blood.<sup>34</sup> We prepared the solution of Hb from commercially available methemoglobin (MetHb) isolated from bovine blood by reduction with sodium dithionite according to a known procedure.<sup>35</sup> Hemoglobin ( $\lambda_{\text{max}} = 405 \text{ nm}$ , Fig. 3) mixed with **10** was quantitatively transformed to COHb ( $\lambda_{\text{max}} = 419 \text{ nm}$ ) after irradiation at  $\sim 500 \text{ nm}$ .

This clearly indicates that carbon monoxide is released by photo-degradation of **10** to **11**.

After we have proven the photoinduced release of carbon monoxide from **10**, we looked for some applications of this process. Carbon monoxide is known to be toxic for humans at high concentrations but it was found recently that it has many beneficial effects. Since the delivery of carbon monoxide by direct inhalation to body is rather complex, a family of compounds called carbon monoxide releasing molecules (CORMs) has been developed. We suggested the xanthene carboxylic acid **10** as a novel metal-free CORM.

#### 4 Second generation of photoCORMs

After we introduced the 6-hydroxy-3-oxo-3*H*-xanthene-9-carboxylic acid **10** as the first metal-free CORM activatable by visible light, we decided to design a second generation of fully organic CORMs that could be easily synthetized and would absorb light of a wavelength in the tissue-transparent window (650–950 nm).<sup>36</sup> Both of these factors would help to establish this system in practical biological and medicinal research.

In order to rationally design an alternative chromophore with photo-reactivity similar to **10**, we searched for the system with frontier molecular orbitals with similar nodal properties and symmetry.<sup>37</sup> Using Hückel molecular orbital calculations (HMO), we screened the frontier molecular orbitals (MOs) of several well-known chromophores which have strong absorption in the visible region, and we identified that the boron-dipyrromethene (BODIPY) molecule has a similar antisymmetric highest occupied MO (HOMO) compared to that of **10** (Fig. 4).

HMO predicts an increase in electronic density on the C-9 (*meso*) position upon excitation for both systems. Therefore, we deduced that *meso*-carboxy BODIPY derivatives are promising photoCORM candidates. Moreover, BODIPY derivatives are well-known for their distinctive and easily tunable absorption and emission properties.<sup>38–40</sup>

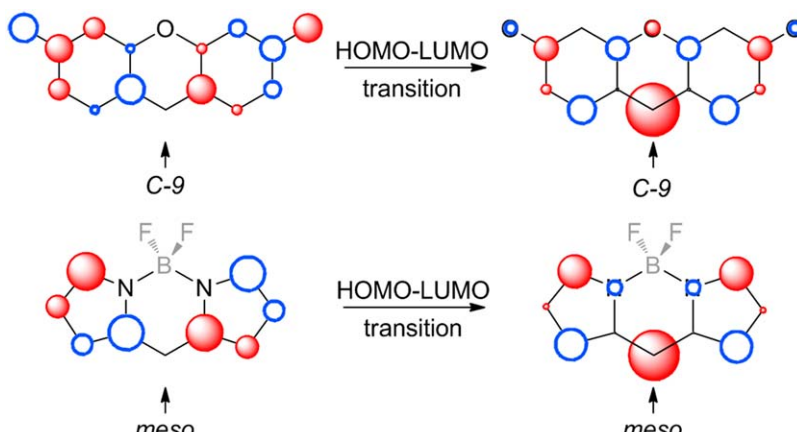
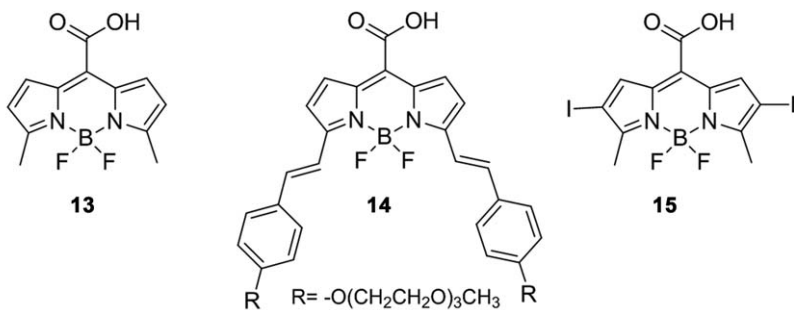


**Fig. 4** A comparison of the frontier MOs (left: HOMO, right: LUMO) of 6-hydroxy-3-oxo-3*H*-xanthene (top) and BODIPY (bottom) chromophores using the Hückel MO theory. The C-9 (*meso*) positions are indicated by an arrow. The  $\text{BF}_2$  group of BODIPY (in light grey) was not explicitly considered in the Hückel calculation.



**Scheme 10** Structures of synthesized BODIPY derivatives **13** to **15**.

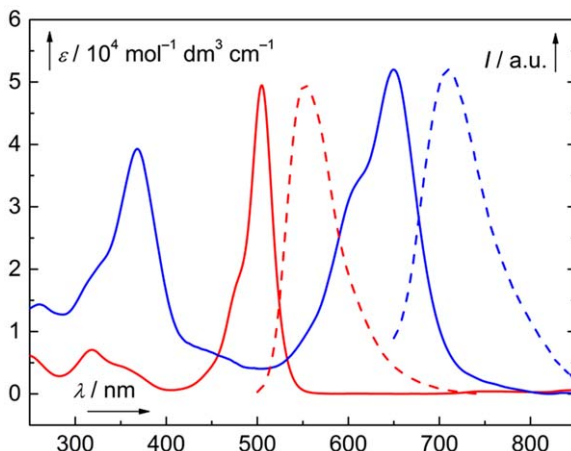


**Fig. 5** Absorption (solid lines) and normalized emission (dashed lines) spectra of **13** (grey,  $\lambda_{\text{max}} \sim 500$  nm) and **14** (black,  $\lambda_{\text{max}} \sim 370$  nm and  $\sim 660$  nm) ( $c = 1 \times 10^{-5}$  M; phosphate buffered saline pH = 7.4;  $I = 0.15$  M).

To test our hypothesis, we synthesized three model compounds **13** to **15** (Scheme 10). The compound **13** was prepared as a simple model structure by a simple two-step procedure. The condensation of benzyl chlorooxalate and 2-methylpyrrole<sup>41</sup> produces a benzyl ester of **13** and subsequent debenzylation by hydrogenolysis leads to the target compound in overall 82% yield. We further prepared the compound **14** which has extended chromophore by two styryl groups. This feature shifts the absorption maximum to the red part of the visible spectrum. The compound **14** was prepared from **13** by condensation with the corresponding PEG-substituted benzaldehyde in the presence of piperidine in glacial acetic acid and subsequent hydrogenation on Pd/C in 56% overall yield. The PEG substituents were used to increase the solubility in water. The heavy-atom substituted BODIPY analogue, compound **15** was synthesized by direct electrophilic iodination of **13** by ICl in 68% yield.

Absorption and emission spectra of aqueous solutions of **13** and **14** are shown in Fig. 5. The unsubstituted BODIPY acid **13** shows a major band with  $\lambda_{\text{max}} = 502$  nm and exhibits a bright fluorescence with a quantum yield  $\Phi_f$  of 67%. The absorption and emission resemble the

photophysical properties of xanthene-based CORM **10**. The quantum yield of fluorescence is higher than that of **10** ( $\Phi_f(10)$ ) is  $\sim 40\%$ ) which corresponds to a lower fraction of non-radiative decay processes for a BODIPY derivative. The compound **14** has the absorption maximum bathochromically shifted by  $\sim 150$  nm compared to that of **13** to  $\lambda_{max} = 652$  nm with a tail absorption up to  $\sim 750$  nm; Fig. 5. The presence of two styryl groups in **14** are probably responsible for its lower fluorescence quantum yield ( $\Phi_f = 12\%$ ) as compared to that of **13** due to enhanced radiationless decay of the singlet excited state.<sup>42,43</sup> The absorption properties of **15** are similar to **13**. The absorption maximum is bathochromically shifted by  $\sim 40$  nm to 540 nm and the fluorescence quantum yield dropped significantly to 2%. This was expected as the presence of two iodine atoms enhances the intersystem crossing which diminishes the fluorescence quantum yield.<sup>44</sup>

All three derivatives **13** to **15** are photoactive. The compound **13** underwent a complete decomposition upon irradiation at  $\sim 500$  nm with quantum yields of  $(2.7 \pm 0.4) \times 10^{-4}$  and  $(1.1 \pm 0.1) \times 10^{-4}$  in degassed and aerated buffered solutions (pH = 7.4), respectively. The benzyl ester of **13** was found to be stable upon irradiation.

This indicates that the free carboxylate is needed for efficient photodegradation of studied BODIPY derivatives. We found by head-space gas chromatographic analysis of irradiated solutions that CO is released almost quantitatively from **13** (87%). Only UV-light absorbing photo-products were formed in the solution upon exhaustive irradiation. 2-Methylpyrrole and 2*H*-pyrrole-4-carbaldehyde were found by HRMS analysis of exhaustively irradiated reaction mixture.

Irradiation of **14** in an aqueous solution (PBS, pH = 7.4) released CO not only upon excitation at the major absorption band maxima (368 and 652 nm) but also at the absorption tail in the near-infrared region (732 nm). The quantum yield of photorelease of CO was approx. one order of magnitude lower ( $\sim 1.2 \times 10^{-5}$ ) than that of **13** which is probably caused by higher fraction of non-radiative decay pathways induced by flexible PEG chains.

The influence of oxygen on the photolysis quantum yield of **13** ( $\Phi_{decomp}$  is lower by a factor of 2 in an aerated sample) suggested that its excited triplet state is involved in the CO release. The formation of a triplet state in **13** is apparently not efficient due to fluorescence ( $\Phi_f = 67\%$ ) and perhaps other radiationless processes, and this may also partially explain the rather low decomposition quantum yields.

Even though the quantum yield of photolysis of **15** is high ( $\sim 1 \times 10^{-2}$ ) compared to other derivatives, the total chemical yield of released CO is low ( $\sim 3\%$ ). This indicates that the excited triplet of **15** undergoes a concurrent photoreaction that does not lead to CO production.

To characterize the triplet state, we measured nanosecond transient spectroscopy of derivatives **13** and **15**. The triplet state of **13** has a very weak signal due to its low quantum efficiency of formation and sophisticated methods for data accumulation had to be used to measure its transient spectrum. The triplet state of **13** possesses absorption maxima at 430 and 640 nm and has a lifetime of  $\sim (5 \pm 1)$   $\mu$ s in an aerated solution.

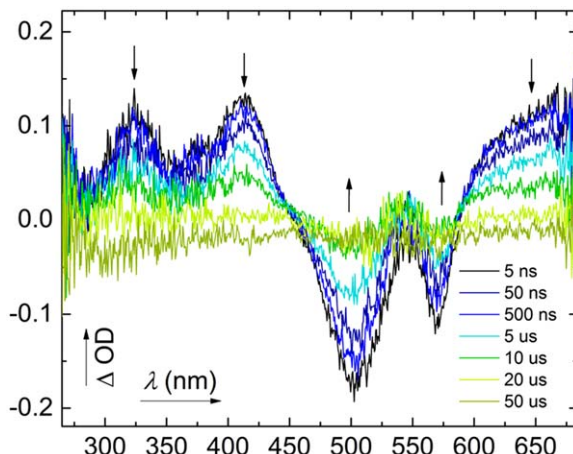
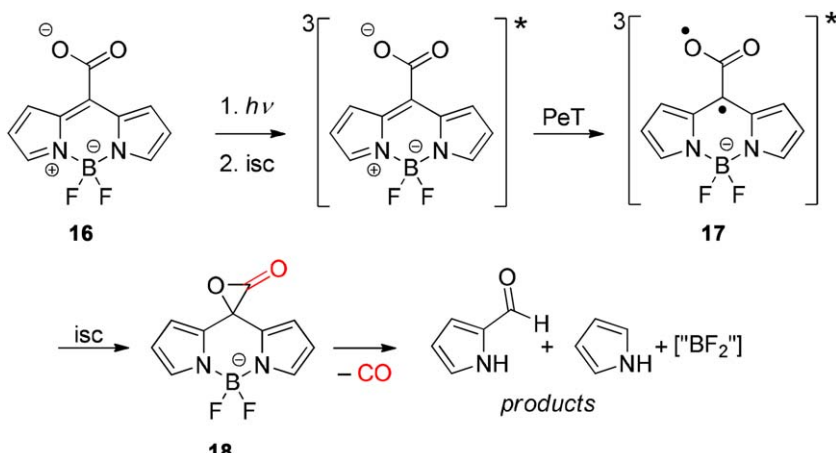


**Fig. 6** The transient absorption spectrum of **15** ( $c \sim 5.0 \times 10^{-5}$  M; phosphate buffered saline; pH = 7.4; non-degassed); excited by a 532 nm laser pulse measured after 5 ns–50  $\mu$ s after excitation.

The compound **15** has much higher population of triplet (which corresponds to the diminished fluorescence quantum yield discussed above). The transient triplet-triplet absorption spectrum of **15** possesses three absorption maxima at 325, 415 and 660 nm (Fig. 6) which exhibit the same decay kinetics. Triplet-state absorption bands in the region of 410–450 nm have already been reported for analogous brominated BODIPY derivatives.<sup>44</sup>

The final evidence that a triplet state is involved in the mechanism of CO release was provided by irradiation of **13** in a degassed aqueous solution containing CsCl (1 M aqueous solution; an analogous NaCl-containing sample was used as a reference) as a heavy-atom effect mediator.<sup>45</sup> The quantum yield of photodegradation and CO production increased by a factor of 1.6 in the presence of  $\text{Cs}^+$  ions due to enhancement of the intersystem crossing, whereas the fluorescence quantum yield decreased from 67% to 53%.

Based on our findings, we proposed the mechanism of photolysis of BODIPY-based CORMs (Scheme 11). The model chromophore **16** (the methyl groups of **13** were omitted due to limited number of atoms suitable for sophisticated quantum chemical calculations) undergoes an inter system crossing to the triplet state upon excitation. Our DFT calculations suggest that a photoinduced intramolecular electron transfer (PeT) takes place between the carboxylate and the BODIPY system in the triplet excited state to form a triplet diradical **17**. The thermodynamics of the electron transfer has been calculated from the ground state redox potentials of BODIPY reduction and carboxylate oxidation determined by cyclic voltammetry and from the triplet energy of excited BODIPYs estimated from its phosphorescence spectra.<sup>46</sup> The diradical **17** closes to the  $\alpha$ -lactone **18** and subsequently releases carbon monoxide. The unstable primary photoproduct with hydroxyl in the *meso*-position is hydrolyzed to a mixture of products.



**Scheme 11** Proposed mechanism of photoinduced release of carbon monoxide from a BODIPY-based CORM.

We tested the toxicity of **13** and **14** and their photoproducts in *in vitro* experiments on hepatoblastoma HepG2 and/or neuroblastoma SH-SY5Y cell lines.

No toxicity was found up to the concentrations of  $100 \mu\text{mol l}^{-1}$ . Encouraged by these results, we tested the photoinduced release of CO *in vitro* in samples of blood and *in vivo* with a nude SKH1 mouse strain. We observed a significant rise of the COHb concentration in blood samples as well as in blood and tissue (hepatic and kidney tissue) of live animals upon application of **14** and irradiation with polychromatic white light. No rise has been observed in the control samples and groups of animals (no CORM added and/or no irradiation).

We managed to improve our xanthene-based CORM **10** and introduced a novel structural type of CORMs based on *meso*-substituted BODIPY.<sup>47</sup> The synthesis of these derivatives is simple and high-yielding and they can be activated by visible-to-NIR (up to 730 nm) light. We investigated the ability of **13** and **14** to efficiently release CO in a fully controllable way, and demonstrated their performance in both *in vitro* and *in vivo* experimental settings. We performed a detailed mechanistic study of the photodegradation of derivatives **13** to **15**. Based on our steady-state and transient absorption spectroscopy experiments and quantum chemical calculations, we proposed a mechanism of the CO release. The decarbonylation occurs through photoinduced electron transfer from the triplet state of BODIPY and subsequent formation of the  $\alpha$ -lactone **18**.

## 5 Summary

We managed to develop a novel class of fully organic photoremoveable protecting groups and carbon monoxide-releasing compounds activatable by visible light.

These compounds were rationally designed, carefully synthetized and used in biological applications. In collaboration with other research

groups we are currently further developing and investigating new PPGs and photoCORMs which are tailor-made for specific applications.

## References

- 1 J. W. Verhoeven, *Pure Appl. Chem.*, 1996, **68**, 2223–2286.
- 2 M. J. Maisels and A. F. McDonagh, *N. Engl. J. Med.*, 2008, **358**, 920–928.
- 3 L. Li, *Opt. Lasers Eng.*, 2000, **34**, 231–253.
- 4 R. C. Kuhad and A. Singh, *Biotechnology for Environmental Management and Resource Recovery*, Springer, New Delhi, 2013.
- 5 Not Everyone Knows This, <http://donaitkin.com/not-everyone-knows-this/>, (accessed June 2017).
- 6 M. E. Weeks, *J. Chem. Educ.*, 1933, **10**, 302.
- 7 G. S. H. David, H. Volman Douglas and C. Neckers, *Advances in Photochemistry.*, Wiley-Interscience, New York, 1971.
- 8 G. Ciamician and P. Silber, *Berichte Dtsch. Chem. Ges.*, 1902, **35**, 1992–2000.
- 9 J. A. Barltrop and P. Schofield, *Tetrahedron Lett.*, 1962, **3**, 697–699.
- 10 P. G. Conrad, R. S. Givens, J. F. W. Weber and K. Kandler, *Org. Lett.*, 2000, **2**, 1545–1547.
- 11 P. Klan, T. Solomek, C. G. Bochet, A. Blanc, R. Givens, M. Rubina, V. Popik, A. Kostikov and J. Wirz, *Chem. Rev.*, 2013, **113**, 119–191.
- 12 L. Zayat, M. G. Noval, J. Campi, C. I. Calero, D. J. Calvo and R. Etchenique, *ChemBioChem*, 2007, **8**, 2035–2038.
- 13 E. M. Rial Verde, *Front. Neural Circuits*, 2008, **2**, 2.
- 14 O. Filevich and R. Etchenique, *Photochem. Photobiol. Sci.*, 2013, **12**, 1565.
- 15 J. Shi, X. Zhang and D. C. Neckers, *J. Org. Chem.*, 1992, **57**, 4418–4421.
- 16 H. E. Zimmerman and V. R. Sandel, *J. Am. Chem. Soc.*, 1963, **85**, 915–922.
- 17 A. Alberola, C. Andrés, A. G. Ortega, R. Pedrosa and M. Vicente, *J. Heterocycl. Chem.*, 1986, **23**, 1781–1783.
- 18 G. Höfle, W. Steglich and H. Vorbrüggen, *Angew. Chem., Int. Ed. Engl.*, 1978, **17**, 569–583.
- 19 H. Ohno, R. Wakayama, S. Maeda, H. Iwasaki, M. Okumura, C. Iwata, H. Mikamiyama and T. Tanaka, *J. Org. Chem.*, 2003, **68**, 5909–5916.
- 20 G. S. Egerton and A. G. Morgan, *J. Soc. Dyers Colour.*, 2008, **86**, 242–249.
- 21 J. P. Olson, M. R. Banghart, B. L. Sabatini and G. C. R. Ellis-Davies, *J. Am. Chem. Soc.*, 2013, **135**, 15948–15954.
- 22 L. Fournier, C. Gauron, L. Xu, I. Aujard, T. Le Saux, N. Gagey-Eilstein, S. Maurin, S. Dubruille, J.-B. Baudin, D. Bensimon, M. Volovitch, S. Vriz and L. Jullien, *ACS Chem. Biol.*, 2013, **8**, 1528–1536.
- 23 N. Umeda, H. Takahashi, M. Kamiya, T. Ueno, T. Komatsu, T. Terai, K. Hanaoka, T. Nagano and Y. Urano, *ACS Chem. Biol.*, 2014, **9**, 2242–2246.
- 24 P. P. Goswami, A. Syed, C. L. Beck, T. R. Albright, K. M. Mahoney, R. Unash, E. A. Smith and A. H. Winter, *J. Am. Chem. Soc.*, 2015, **137**, 3783–3786.
- 25 N. Rubinstein, P. Liu, E. W. Miller and R. Weinstain, *Chem. Commun.*, 2015, **51**, 6369–6372.
- 26 R. R. Nani, A. P. Gorka, T. Nagaya, H. Kobayashi and M. J. Schnermann, *Angew. Chem., Int. Ed.*, 2015, **54**, 13635–13638.
- 27 L. A. P. Antony, T. Slanina, P. Šebej, T. Solomek and P. Klán, *Org. Lett.*, 2013, **15**, 4552–4555.
- 28 P. Šebej, J. Wintner, P. Müller, T. Slanina, J. Al Anshori, L. A. P. Antony, P. Klán and J. Wirz, *J. Org. Chem.*, 2013, **78**, 1833–1843.

- 29 L. J. Goossen, F. Manjolinho, B. A. Khan and N. Rodríguez, *J. Org. Chem.*, 2009, **74**, 2620–2623.
- 30 S. Hassoon and D. C. Neckers, *J. Phys. Chem.*, 1995, **99**, 9416–9424.
- 31 G. L'Abbé, *Angew. Chem., Int. Ed. Engl.*, 1980, **19**, 276–289.
- 32 P. L. Coe, A. Sellars, J. C. Tatlow, G. Whittaker and H. C. Fielding, *J. Chem. Soc., Chem. Commun.*, 1982, 362.
- 33 W. Adam, J.-C. Liu and O. Rodriguez, *J. Org. Chem.*, 1973, **38**, 2269–2270.
- 34 B. Widdop, *Ann. Clin. Biochem.*, 2002, **39**, 378–391.
- 35 F. L. Rodkey, T. A. Hill, L. L. Pitts and R. F. Robertson, *Clin. Chem.*, 1979, **25**, 1388–1393.
- 36 K. Konig, *J. Microsc.*, 2000, **200**, 83–104.
- 37 Similar nodal properties of frontier MOs is a necessary but not sufficient condition for predicting the same type of a photoreaction of two, seemingly unrelated chromophores.
- 38 N. Boens, V. Leen and W. Dehaen, *Chem. Soc. Rev.*, 2012, **41**, 1130–1172.
- 39 A. Bessette and G. S. Hanan, *Chem. Soc. Rev.*, 2014, **43**, 3342–3405.
- 40 H. Lu, J. Mack, Y. Yang and Z. Shen, *Chem. Soc. Rev.*, 2014, **43**, 4778.
- 41 M. M. C. Lo and G. C. Fu, *J. Am. Chem. Soc.*, 2002, **124**, 4572–4573.
- 42 M. J. Ortiz, I. Garcia-Moreno, A. R. Agarrabeitia, G. Duran-Sampedro, A. Costela, R. Sastre, F. L. Arbeloa, J. B. Prieto and I. L. Arbeloa, *Phys. Chem. Chem. Phys.*, 2010, **12**, 7804–7811.
- 43 A. Costela, I. Garcia-Moreno, M. Pintado-Sierra, F. Amat-Guerri, M. Liras, R. Sastre, F. L. Arbeloa, J. B. Prieto and I. L. Arbeloa, *J. Photochem. Photobiol., A*, 2008, **198**, 192–199.
- 44 X. F. Zhang and X. D. Yang, *J. Phys. Chem. B*, 2013, **117**, 5533–5539.
- 45 F. Saito, S. Tobita and H. Shizuka, *J. Chem. Soc., Faraday Trans.*, 1996, **92**, 4177–4185.
- 46 X. F. Zhang, X. D. Yang, K. Niu and H. Geng, *J. Photochem. Photobiol., A*, 2014, **285**, 16–20.
- 47 E. Palao, T. Slanina, L. Muchová, T. Šolomek, L. Vítek and P. Klán, *J. Am. Chem. Soc.*, 2016, **138**, 126–133.

---

# Photocatalytic applications of conjugated microporous polymers

Jingzhi Lu and Jian Zhang\*

DOI: 10.1039/9781788010696-00191

Conjugated microporous polymers (CMPs) represent an emerging new class of porous materials that display high stability, low toxicity, and strong visible-light activity. These unique characteristics of CMPs enable their wide potential uses as a new generation of heterogeneous photocatalysts for both laboratory and scale-up applications. Here we review the most recent developments of CMPs-based photocatalytic systems. We discuss the synthetic control of the composition, structure, optoelectronic properties of CMPs that relate to their photocatalytic activities toward both organic and inorganic transformations, including artificial photosynthesis.

## 1 Introduction

Solar energy has been long investigated as a green and sustainable source to produce value-added fine chemicals as well clean energy fuels.<sup>1–3</sup> Inorganic semiconductors and transition metal complexes are two classes of most commonly used photocatalysts. Visible light photocatalysis will certainly continue to grow in both academic and industrial settings, with an increasing effort focusing on replacing the non-recyclable, precious-metal-based homogeneous catalysts with heterogeneous metal-free materials without compromising the catalytic efficiency and selectivity.<sup>4</sup> Organic conjugated polymers provide an intriguing candidate as metal-free photocatalyst;<sup>5</sup> however, their high tunability and diverse synthesis modularity are significantly hampered by their limited catalytic activity and stability.<sup>6–8</sup> Polymeric graphitic carbon nitride ( $\text{g-C}_3\text{N}_4$ ) exhibit improved stability;<sup>9</sup> however, their inadequate band-gap tunability remains a challenge for photocatalytic reactions that require a wider range of redox potentials.<sup>10</sup> Recently, another type of organic polymers, conjugated microporous polymers (CMPs), has received a great deal of attention since Cooper *et al.* reported their high porosity and use for gas adsorption in 2007.<sup>11</sup> Despite their amorphous structures, CMPs exhibit large surface area<sup>12</sup> and high thermal and physicochemical stability due to strong covalent bonds such as C–C and C–N and three-dimensional network structures, and they are ideal for gas capture and storage,<sup>13</sup> sensing, and energy storage.<sup>14–17</sup> CMPs can be easily recycled due to low solubility and have been used as heterogeneous catalysts<sup>18–20</sup> or catalyst supports.<sup>21–23</sup> In particular, the extended  $\pi$ -conjugation network enables the chemical tunability of their optoelectronic properties,<sup>24–26</sup> which can be utilized in photocatalytic applications. This review will discuss the most recent developments of CMPs in photocatalytic applications. We focus mostly on CMPs of which the photoactivities are originated from the extended

---

Department of Chemistry, University of Nebraska-Lincoln, Lincoln, Nebraska 68588, USA. E-mail: jzhang3@unl.edu

$\pi$ -conjugation throughout the entire polymeric structure. Therefore, exciton generated by introducing transition metals (Ru or Ir)<sup>27</sup> or organic dyes<sup>28–37</sup> are excluded from the discussion despite of their important applications in photocatalysis.

## 2 Photocatalytic applications of CMPs

### 2.1 Singlet Oxygen Generation

Early photocatalytic application of CMPs started with the recognition of the capability of certain CMPs for photosensitization. This is based on the rationalization that the combination of an electron donor and acceptor would lead to an effective exciton localization with a slow charge recombination, which can facilitate the intersystem crossing to the triplet state as well as the possible subsequent energy transfer to generate singlet oxygen ( ${}^1\text{O}_2$ ).<sup>38</sup>

In 2013, Vilela and coworkers synthesized a series of CMPs using the Sonogashira cross-coupling polycondensation between 4,7-dibromobenzo[*c*]-[1,2,5]thiadiazole (**BT**) and 1,3,5-triethynylbenzene (Fig. 1a).<sup>39</sup> A templating agent,  $\text{SiO}_2$  NPs, was used during the synthesis to further enhanced the porosity of resulted polymers up to 2.4 times. The non-fluorescent properties of the CMPs suggested a possible efficient intersystem crossing process. Indeed, **CMP\_60** (60 mg  $\text{mL}^{-1}$   $\text{SiO}_2$  used in

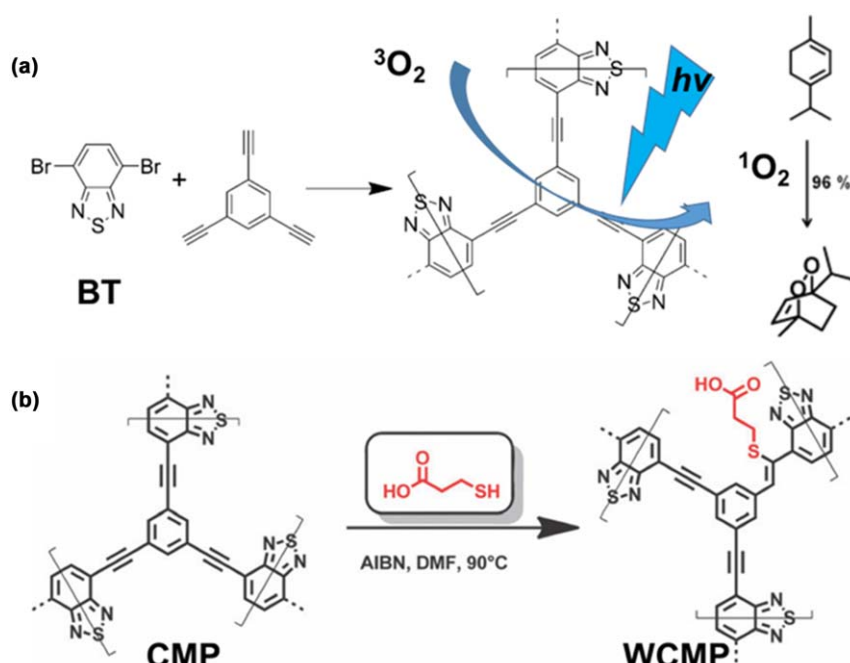


**Fig. 1** (a) Synthesis of conjugated microporous polymer CMP and its photocatalytic conversion of  $\alpha$ -terpinene to ascaridole. Adapted with permission from ref. 39, K. Zhang, D. Kopetzki, P. H. Seeberger, M. Antonietti and Filipe Vilela, *Angewandte Chemie, International Edition*, John Wiley and Sons. Copyright © 2013 WILEY-VCH Verlag GmbH & Co. KGaA, Weinheim. (b) Postsynthetic modification of CMP via thiol-yne chemistry. Adapted from ref. 40 with permission from The Royal Society of Chemistry.

the synthesis) exhibits an enhanced dispersity and thus efficiency to generate  ${}^1\text{O}_2$ , as indicated by the fastest rate of the conversion of  $\alpha$ -terpinene to ascaridole under visible light irradiation ( $>420\text{ nm}$ ). However, such efficiency is still about one order of magnitude lower than the well-known homogeneous photosensitizer tetraphenylporphyrin (TPP). To increase the water compatibility, a subsequent modification of the CMP was carried out *via* thiol-yne chemistry by reacting with 3-mercaptopropionic acid (MPA) and azobis(2-methyl-propionitrile) (AIBN) (Fig. 1b).<sup>40</sup> The resulting polymer **WCMPs** can indeed be used in aqueous environment and a 90% yield of the photo conversion of furoic acid to 5-hydroxy-2(*H*)-furanone was realized. However, complete recover of the photocatalyst was not successful due to a partial decomposition.

Vilela and coworkers further prepared three fluorene-based CMPs using the HIPE (high internal phase emulsions) polymerization approach: **B-FL**<sub>3</sub>, **B-BT-FL**<sub>2</sub> and **B-BT**<sub>2</sub>-**FL**, where the electron acceptor BT was incorporated in the latter two polymers (Fig. 2a).<sup>41</sup> The essential role of electron acceptor is striking: for example, for the oxidation of  $\alpha$ -terpinene, a conversion of 50% was obtained after 6 h reaction when **B-FL**<sub>3</sub> was used, whereas complete reaction was realized using **B-BT-FL**<sub>2</sub> and **B-BT**<sub>2</sub>-**FL** after 60 and 30 min, respectively. Impressively, **B-BT**<sub>2</sub>-**FL**

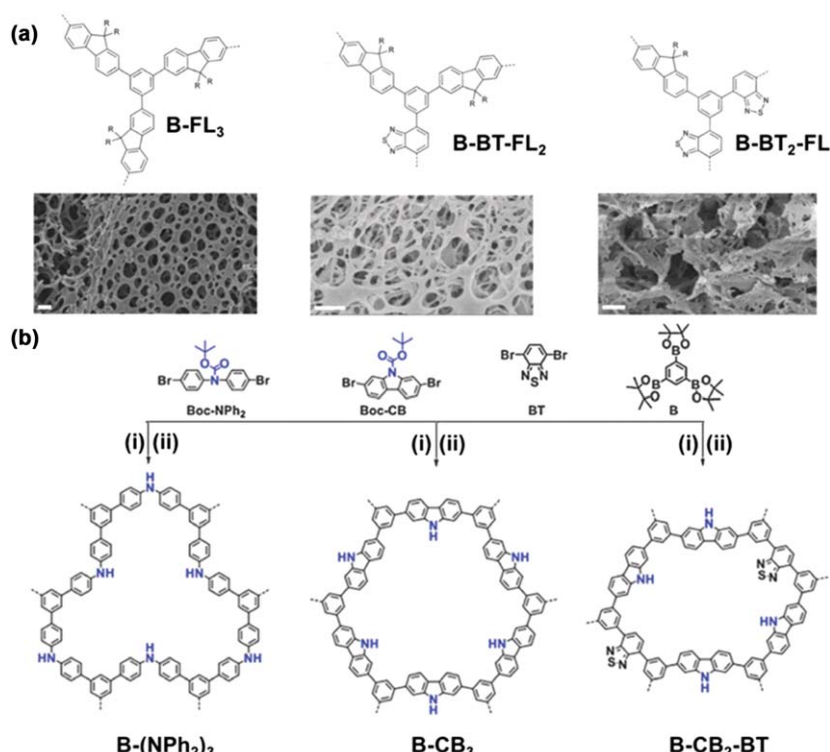


**Fig. 2** (a) Idealized structures and SEM images (scale bar = 1  $\mu\text{m}$ ) of **B-FL**<sub>3</sub>, **B-BT-FL**<sub>2</sub> and **B-BT**<sub>2</sub>-**FL**. (b) Idealized structures and synthesis of **B-(NPh**<sub>2</sub>)<sub>3</sub>, **B-CB**<sub>3</sub>, and **B-CB**<sub>2</sub>-**BT** *via* (i) Suzuki coupling and (ii) deprotection at 250 °C for 12 h. Adapted from ref. 41 and 42 with Permission from The Royal Society of Chemistry.

can be reused for ten times with no significant decrease of the reaction yield, demonstrating an excellent photostability. Similar HIPE strategy was employed by K. Zhang and coworkers for incorporating diphenylamine, carbazole, and carbazole/BT in **B-(NPh<sub>2</sub>)<sub>3</sub>**, **B-CB<sub>3</sub>**, and **B-CB<sub>2</sub>-BT**, respectively (Fig. 2b).<sup>42</sup> Again, it was determined that the electronic structure, rather than the surface area, dictates the overall photocatalytic efficiency. With the combination of electron donor and acceptor, **B-CB<sub>2</sub>-BT** exhibits the highest activity in the photo oxidation of organic sulfides to sulfoxides under visible light, which presumably proceeds *via* a singlet oxygen process.

## 2.2 Polymerization

Photopolymerization is an advantageous strategy to prepare polymers that have industrial applications in adhesives, coatings, and dental fillings, as well as many bioengineering materials for bone and tissue.<sup>43</sup> Many traditional photoinitiators only absorb light in the UV range and are based on small molecules,<sup>44</sup> it is of interest to develop heterogeneous photoinitiators that absorbs visible light.

K. Zhang and coworkers used a Suzuki coupling reaction between 1,3,5-benzenetriboronic acid tris(pinacol) ester (**B**) with *tert*-butylcarbonate dibromocarbazole (**Boc-CB**) and dibromobenzoxadiazole (**BO**) and prepared the porous polymer **B-(Boc-CB)<sub>2</sub>-BO** *via* a HIPE process (Fig. 3a).<sup>45</sup> The monolithic HIPE polymer has an optical gap of 2.16 eV and further used as a photoinitiator in the free radical photopolymerization of methyl methacrylate (MMA) (Fig. 3b). The polymerization reaction was conducted in the presence of 25 mg of **B-(Boc-CB)<sub>2</sub>-BO** and co-initiator Et<sub>3</sub>N (30 mg) in 50 wt% of MMA in THF under the irradiation from a CFL (23 W). The conversion can reach 82% with the average molar mass of the product of 34 300 gmol<sup>-1</sup>. Three recycled use of the polymer resulted in an insignificant decay of the catalytic efficiency, suggesting the high stability of the polymer photoinitiator.

Yagci *et al.* reported the use of thioxanthone-based CMP, TX-CMP, in the visible light induced free radical and cationic polymerizations (Fig. 4a).<sup>46</sup> Thioxanthone itself is an efficient Type-II photoinitiator

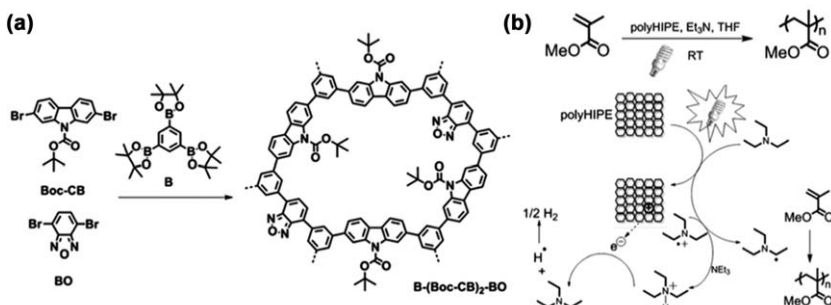


**Fig. 3** (a) Synthesis route of **B-(Boc-CB)<sub>2</sub>-BO**. (b) Visible light initialized free radical polymerization using **B-(Boc-CB)<sub>2</sub>-BO** as a photoinitiator and proposed mechanism. Adapted from ref. 45 with permissions from The Royal Society of Chemistry.

(polymerization *via* hydrogen abstraction), which however only absorbs UV light. Upon polymerization, the resulting **TX-CMP** exhibits a broad and strong visible absorbance peak, which enables its capability to be an effective photoinitiator even in the sunlight for both free radical and cationic polymerization. In the free radical polymerization (Fig. 4b), photoexcited **TX-CMP** abstracts a hydrogen atom from the amine-based co-initiator (*e.g.* triethylamine) or reduces diphenyliodonium hexafluorophosphate to initialize the polymerization of MMA. Such reaction can be repeated for three times using the same batch of **TX-CMP**, indicating its outstanding stability. In the cationic polymerization (Fig. 4c), the corporative function of photoexcited **TX-CMP** and the iodo-nium salt oxidizes an electron donor (*e.g.* amine or THF) to afford a cation which subsequently initializes the polymerization of cyclohexene oxide (CHO). Importantly, compared to TX, **TX-CMP** exhibits an enhanced initiation efficiency in terms of both conversion and molecular weight of the polymer product.

### 2.3 Organic transformations

Son and coworkers prepared a microporous organic network that is composed of benzodifurans (**BDF-MON**) using a tandem synthetic strategy.<sup>47</sup> Following a Sonogashira coupling between 1,3,5-triethynylbenzene and 2,5-diiodo-1,4-hydroquinone, an intramolecular cyclization proceeded *in situ*, which afford the final **BDF-MON** as the product. Under visible irradiation, **BDF-MON** can mediate the transfer of an electron from 1,4-bis(dimethylamino)benzene to oxygen to form the blue colored species. Therefore, it was tested in the photocatalytic oxidation of benzylamines. This is an important reaction in organic chemistry since imines are commonly used as precursors in industries. A high reaction yield of 96% for the oxidation of benzylamine was obtained under a blue LED irradiation in the presence of 8 mol% photocatalyst. **BDF-MON** can be recovered for recycled use and maintained the catalytic activity. The reaction mechanism was proposed to be a photoredox process which involves the photoinduced generation of the O<sub>2</sub><sup>•-</sup> radical and the benzylamine radical cation *via* single electron transfer. The subsequent formation of benzaldehyde and its reaction with benzylamine lead to the imine product. This mechanism is consistent with short fluorescence lifetime of **BDF-MON** and the its high LUMO energy, which makes the reduction of O<sub>2</sub> favorable. Moreover, the influence of the functional groups of the substrate was not significant, demonstrating a wide substrate scope (Fig. 5(a)).

The same reaction was studied by Son and coworkers using micro-porous triphenylamine-anthraquinone networks (**MTANs**).<sup>48</sup> Both non-hollow and hollow versions of **MTANs** were prepared, and the latter was synthesized using SiO<sub>2</sub> NPs as the template. Interestingly, no significant surface areas and pore size distribution was observed. When used as the photocatalyst for oxidative cross-coupling of benzylamine, hollow **MTAN** shows 99% conversion after 24 h of reaction time with only 1.7 mol% photocatalyst, much more efficient than **BDF-MON**. The enhanced

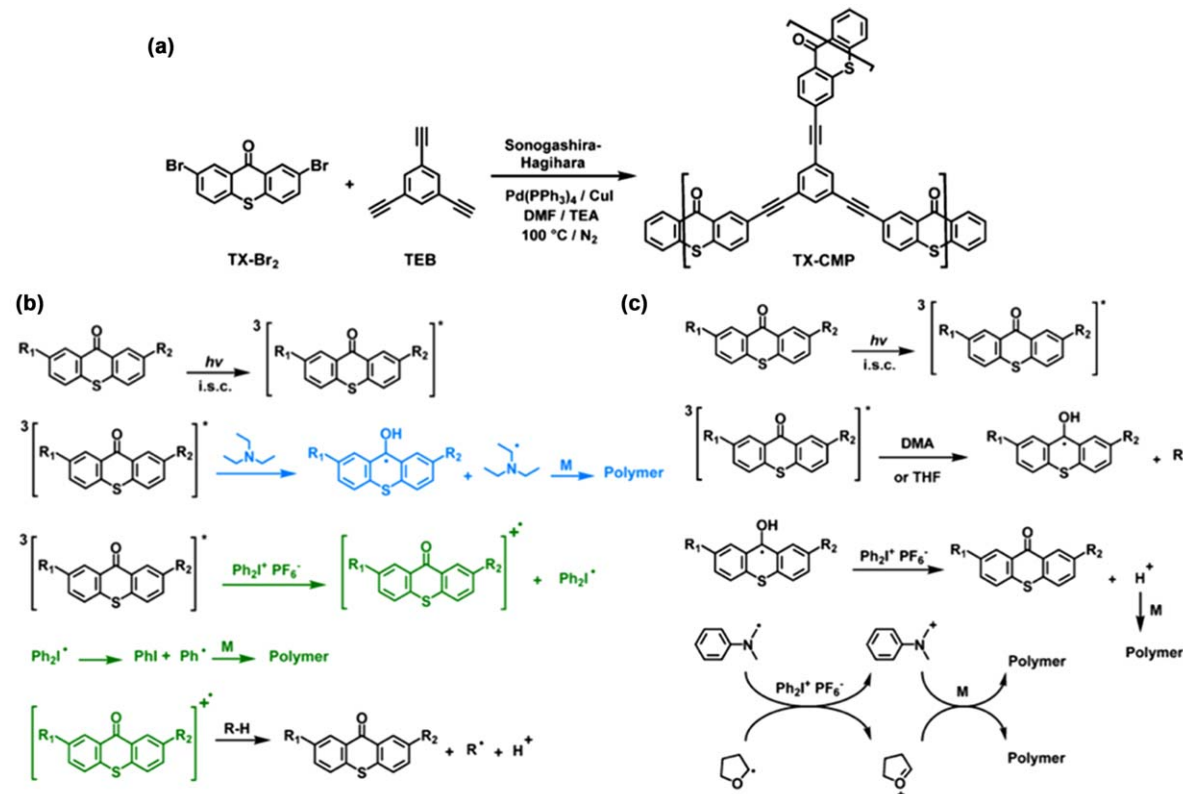


**Fig. 4** (a) Synthesis of TX-CMP. Proposed initialization mechanism of (b) free radical and (c) cationic polymerization reactions.<sup>46</sup> Adapted with permissions from S. Dadashi-Silab, H. Bildirir, R. Dawson, A. Thomas and Y. Yagci, *Macromolecules*, 2014, 47, 4607. Copyright (2014) American Chemical Society.

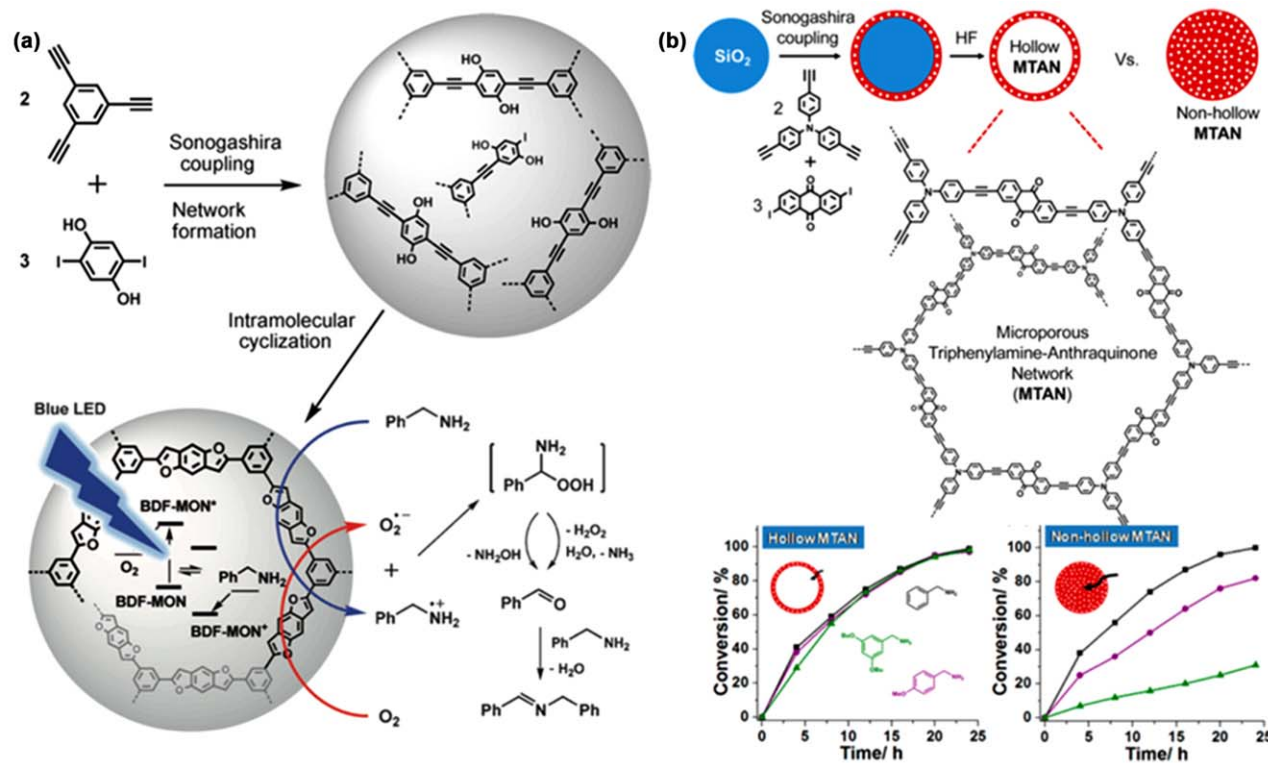


**Fig. 5** (a) Strategy of the synthesis of BDF-MON and the proposed mechanism of oxidative amine coupling. Adapted with permission from ref. 47, N. Kang, J. H. Park, K. C. Ko, J. Chun, E. Kim, H.-W. Shin, S. M. Lee, H. J. Kim, T. K. Ahn, J. Y. Lee and S. U. Son, *Angewandte Chemie, International Edition*, John Wiley and Sons. Copyright © 2013 WILEY-VCH Verlag GmbH & Co. KGaA, Weinheim. (b) Synthesis of MTAN and reaction kinetics of oxidative amine coupling.<sup>48</sup> Adapted with permission from J. H. Ko, N. Kang, N. Park, H.-W. Shin, S. Kang, S. M. Lee, H. J. Kim, T. K. Ahn and S. U. Son, *ACS Macro Lett.*, 2015, 4, 669. Copyright (2015) American Chemical Society.

activity of **MTAN** can be attributed to the better visible light absorption. However, the reaction was determined to proceed more likely through the singlet oxygen pathway. More interestingly, the hollow **MTAN** showed similar activities towards different amines, the nonhollow **MTAN**, however, exhibits a clear variation in the catalytic activities, which can be explained by the difference of the size of the substrate (Fig. 5(b)).

Wang *et al.* also studied the oxidative coupling reaction of benzylamine using two series of closely related CMPs. In one study, benzoxadiazole (BO) was utilized to connect to a phenyl unit on 1,3,5-, 1,2,4-, and 1,2,4,5-positions *via* a triple bond, forming **B-BO-1,3,5**, **B-BO-1,2,4**, and **B-BO-1,2,4,5**, respectively.<sup>49</sup> Among the three, **B-BO-1,3,5** exhibits the largest energy gap, and its oxidative (+1.55 V) and reductive (-1.19 V) potentials are capable to oxidize benzylamine ( $E_{\text{ox}} = +1.08$  V) and to reduce molecular oxygen (-0.86 V). The latter was supported by EPR spin trap experiment where 5,5-dimethyl-1-pyrroline-N-oxide (DMPO) was used to detect superoxide radicals. Interesting, positive result was also observed when 2,2,6,6-tetramethyl-piperidinyloxy (TEMPO) was used as the trapping agent, indicating that singlet oxygen can also be generated *via* photoexcitation of **B-BO-1,3,5**. Therefore, it was proposed that both superoxide and singlet oxygen are possible reactive species. This was further confirmed using holescavengers (*e.g.* KI), superoxide scavenger (*e.g.* benzoquinone), and singlet oxygen scavenger (*e.g.* sodium azide) to the reaction mixture: a retarded reaction was observed in all cases (Fig. 6(a)). In another study, benzoxadiazole (BO), benzothiadiazole (BT), and benzoselenadiazole (BS) were used as the building blocks for polymer **B-BO**, **B-BT**, and **B-BS**, respectively, with finely tuned redox potentials.<sup>50</sup> It was shown that the sulfur-containing **B-BT** has the largest energy gap, longest-lived electron hole pairs, and the best redox potential for the oxidative coupling reaction of benzylamine under visible light irradiation. A similar reaction mechanism was proposed in this study in which both superoxide and singlet oxygen are reactive oxidizing agents, generated *via* electron transfer and energy transfer from the photocatalyst **B-BT**, respectively (Fig. 6(b)).

From an industrial application point of view, post separation of the heterogeneous catalyst is still a costly process. Therefore, it is ideal to use the continuous flow synthesis in the fixed-bed systems. In order to further demonstrate the potential practical application of CMPs in process scale synthesis, Huang *et al.* recently synthesized **B-BT** as a coating to glass fiber and used it in a fixed-bed photoreactor (Fig. 7).<sup>51</sup> The experimental setup involves 200 mg of glass fibers consisting of 6.4 mg **B-BT** coating packed into a glass column with the diameter of 0.35 cm and the length of 7 cm and under a constant flow rate of 0.5 ml min<sup>-1</sup>. **B-BT** showed excellent photocatalytic activities toward the net reductive dehalogenation of  $\alpha$ -bromoacetophenone (Fig. 7*i*, 91–95% yields) and the redox neutral enantioselective  $\alpha$ -alkylation of aldehydes (Fig. 7*j*, 78–96% yields), for which the favorable redox potentials of **B-BT** are responsible. Impressively, the fixed-bed photoreaction exhibits a dramatic increase of the reaction rate (100% conversion with 6.4 mg photocatalyst in 5 h) compared to the monolithic form of **B-BT** (90.3% conversion with 100 mg

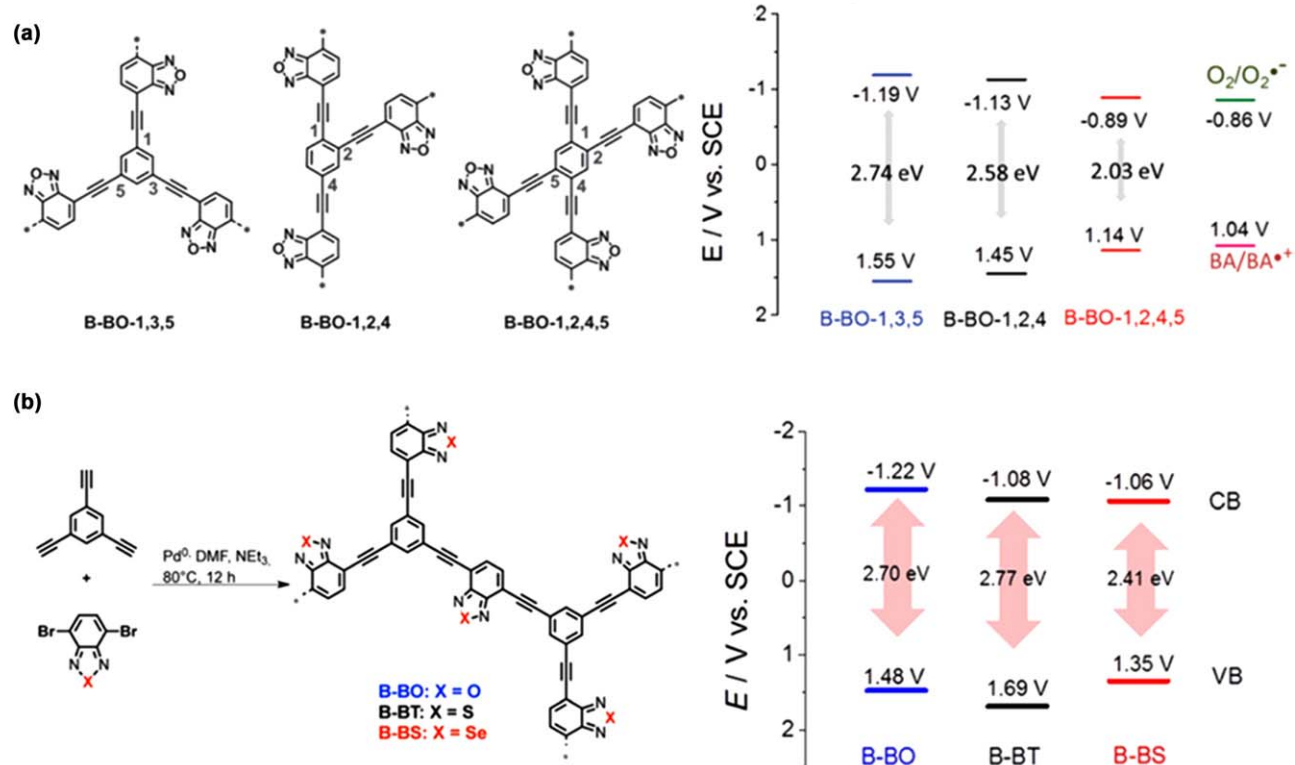


**Fig. 6** (a) Structure and optical band gaps of (a) B-BO-1,3,5, B-BO-1,2,4, and B-BO-1,2,4,5 and (b) B-BO, B-BT, and B-BS. Adapted with permission from ref. 49, Z. J. Wang, S. Ghasimi, K. Landfester and K. A. I. Zhang, *Advanced Materials* and ref. 50, Z. J. Wang, K. Garth, S. Ghasimi, K. Landfester and K. A. I. Zhang, *ChemSusChem*; John Wiley and Sons © 2015 WILEY-VCH Verlag GmbH & Co. KGaA, Weinheim.

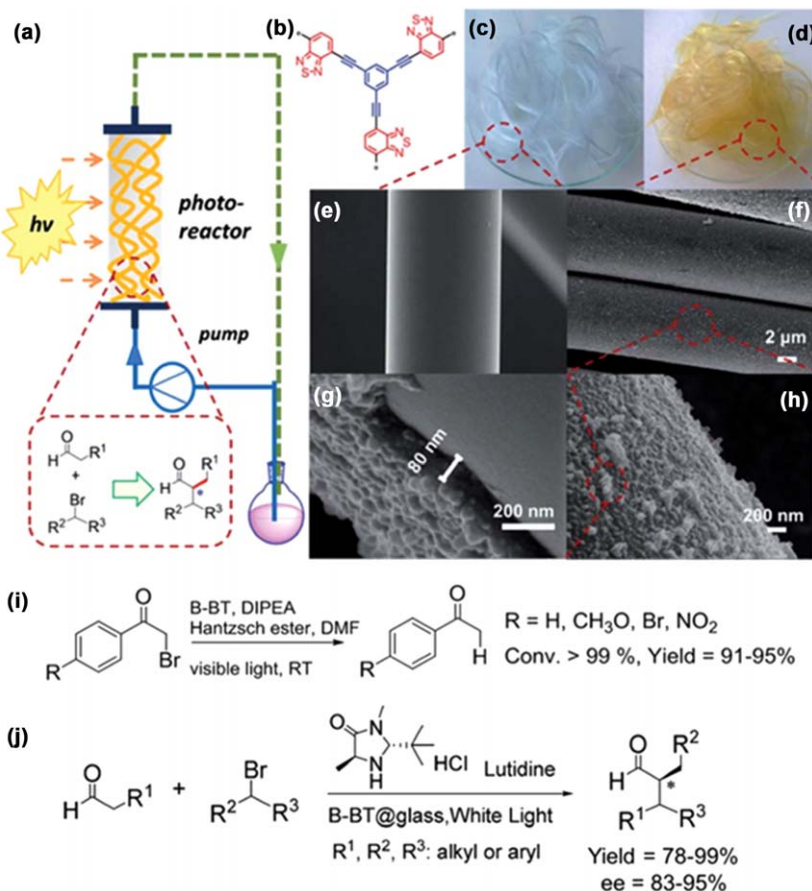


**Fig. 7** (a) Schematic setup of a fixed-bed photoreactor using B-BT-coated glass fibers. (b) Structure of B-BT. (c) Photography of glass fibers and (d) B-BT-coated glass fibers. (e) SEM images of glass fibers and (f–h) B-BT-coated glass fibers. (i and j) Reductive dehalogenation of  $\alpha$ -bromoacetophenone and redox neutral enantioselective  $\alpha$ -alkylation of aldehydes. Adapted from ref. 51 with permission from The Royal Society of Chemistry.

photocatalyst in 24 h). This is attributed to the much higher light absorption efficiency due to the nanoscale thickness of the photocatalyst on the glass fiber. Interestingly, the mechanic and chemical stability of the photoreactors were very high: no apparent decrease of the reaction efficiency after five additional reaction cycles.

Copolymerization strategy was also recently utilized by Wang *et al.* for engineering the bandgap of CMPs (Fig. 8). In one study, a Sonogashira coupling between 1,3,5-triethylbenzene with a mixture of FL (di-hexyl-dibromofluorene) and BBT (dibromobenzo[1,2-*c*;4,5-*c'*]bis[1,2,5]thia-diazole) at different molar ratios, and two polymers, namely, **B**<sub>2</sub>-FL<sub>2</sub>-BBT and **B**<sub>2</sub>-FL<sub>3</sub>, were prepared and tested for dehalogenation of  $\alpha$ -bromoacetophenones.<sup>52</sup> The incorporation of BBT decreases the optical gap of **B**<sub>2</sub>-FL<sub>2</sub>-BBT from 2.40 eV in **B**<sub>2</sub>-FL<sub>3</sub> to 1.5 eV, which however significantly increased the catalytic activity from 19% to >99 yield in 4 h. Later, a similar approach was used to generate another series CMPs for the photo-mediated

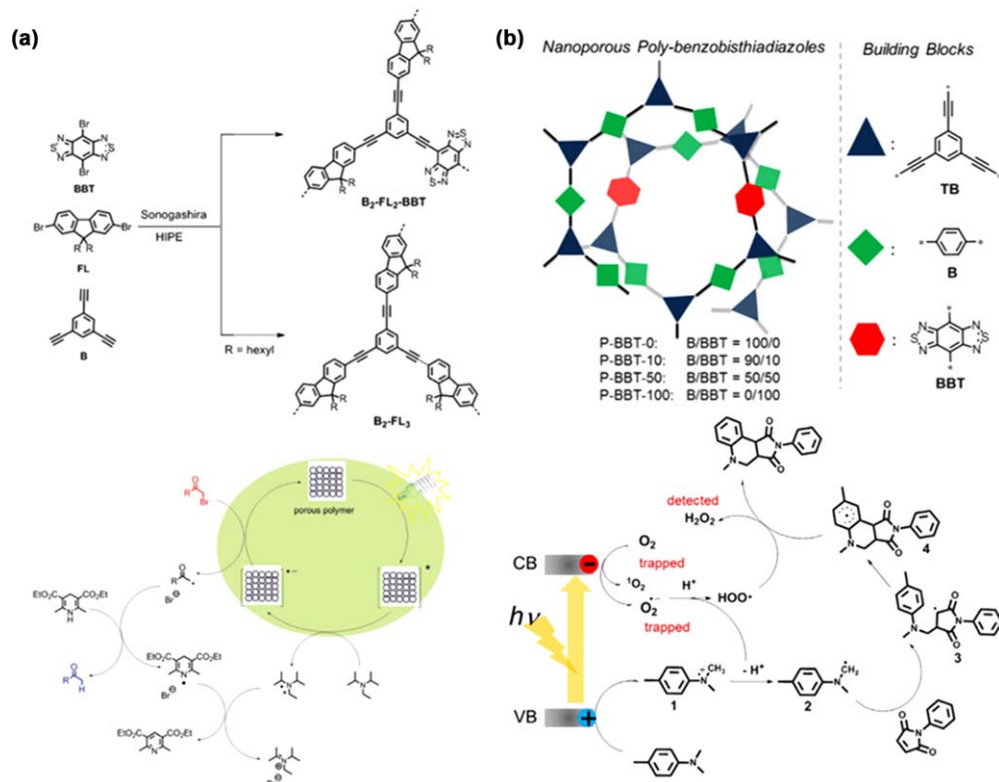


**Fig. 8** (a) Synthesis of  $\mathbf{B}_2\text{-FL}_2\text{-BBT}$  and  $\mathbf{B}_2\text{-FL}_3$  and the proposed mechanism of reductive dehalogenation of  $\alpha$ -bromoacetophenone. Adapted from ref. 52 with permission from The Royal Society of Chemistry. (b) Synthesis of P-BBT-0, P-BBT-10, P-BBT-50 and P-BBT-100 and reaction mechanism of oxidative cyclization reaction of  $N,N$ -dimethylaniline with  $N$ -phenylmaleimide. Adapted with permission from ref. 53, Z. J. Wang, S. Ghasimi, K. Landfester and K. A. I. Zhang, *Advanced Synthesis & Catalysis*, John Wiley and Sons. © 2016 WILEY-VCH Verlag GmbH & Co. KGaA, Weinheim.

synthesis of 1,2,3,4-tetrahydroquinoline.<sup>53</sup> Again, a Sonogashira coupling between 1,3,5-triethynylbenzene with a mixture of BT (1,4-dibromobenzene) and BBT at different molar ratios, and four polymers, namely, **P-BBT-0**, **P-BBT-10**, **P-BBT-50** and **P-BBT-100** were prepared. As the component of BBT increases, the band gap decreases, with **P-BBT-0** showing the largest gap of 3.13 V. However, the photocatalytic activities of **P-BBT-10** was determined to be the best among the four polymers, evaluated using an oxidative cyclization reaction of *N,N*-dimethylaniline with *N*-phenylmaleimide, which was attributed to its appropriate redox potentials and better visible light absorbance. The mechanistic study assisted by scavenging experiments also concluded that both superoxide and singlet oxygen are possibly generated during the reaction and act as the oxidant for *N,N*-dimethylaniline.

Photoactive COFs have also been tested as the photocatalysts for organic transformations. Recently, Wu and coworkers reported the use of a hydrozone-linked COF, **TFB-COF**, as the photocatalyst toward the cross-dehydrogenative coupling reaction between tetrahydroisoquinolines (THIQ) and various nucleophiles.<sup>54</sup> **TFB-COF** was synthesized using an acid-catalyzed condensation of 2,5-dimethoxyterephthalohydrazide (DMTH) with 1,3,5-triformyl-benzene (TFB) under solvothermal conditions (Fig. 9). The resulted COF material exhibits a good crystallinity and a high BET surface area of  $1501\text{ m}^2\text{ g}^{-1}$ , a large pore volume of  $0.88\text{ cm}^3\text{ g}^{-1}$ . Importantly, the large meso-sized pores (2.2 nm) are ideal for conducting organic catalysis. **TFB-COF** has a large band gap of 2.8 eV, showed excellent activities in the photoinduced dehydrogenative coupling of THIQ with nitromethane (70–87% yield), acetone (80% yield), and acetophenone (82% yield). Although the crystallinity of the COF decreased after the reactions, it can still be recycled for at least three times without loss of catalytic activity.

Carbazole is a useful building block for synthesizing carbazole-based CMPs, which was dubbed as **Cz-POFs** (carbazolic porous organic frameworks). **Cz-POFs** can be readily prepared by oxidative polymerization of carbazole-based monomers using cheap, green oxidants such as  $\text{FeCl}_3$ .<sup>55</sup> Recent investigation by J. Zhang and coworkers has shown that monomer **Cz-1** with its four carbazole moieties can support up to eight cross-linking connections and the resulted **Cz-POF-1** exhibits a remarkable Brunauer–Emmett–Teller (BET) specific surface area ( $\text{SA}_{\text{BET}}$ ) ( $2065\text{ m}^2\text{ g}^{-1}$ ) (Fig. 10a).<sup>56</sup> Importantly, 72% of the pore volume is contributed by mesopores (pore width  $>2\text{ nm}$ ), an ideal feature for organic reactions involving large-sized substrates or products. More importantly, **Cz-POFs** can be suitable for heterogeneous photoredox catalysis (Fig. 10b). For example, **Cz-POF-1** has an optical gap of 2.91 eV and a high reduction potential that is capable for the reduction of several common substrates in organic synthesis, including phenacyl bromide ( $E_{1/2}^{\text{red}} = -0.49\text{ V}^{57}$ ), diethyl bromomalonate, or molecular oxygen ( $E_{1/2}^{\text{red}} = -0.92\text{ V}^{58}$ ). Thus, it was used in three prototypic organic transformations: net reductive dehalogenation of phenacyl bromide (reaction (1) in Fig. 10), net oxidative Mannich reaction (reaction (2) in Fig. 10), and redox neutral  $\alpha$ -alkylation of aldehydes (reaction (3) in Fig. 10). In each case, **Cz-POF-1** underwent

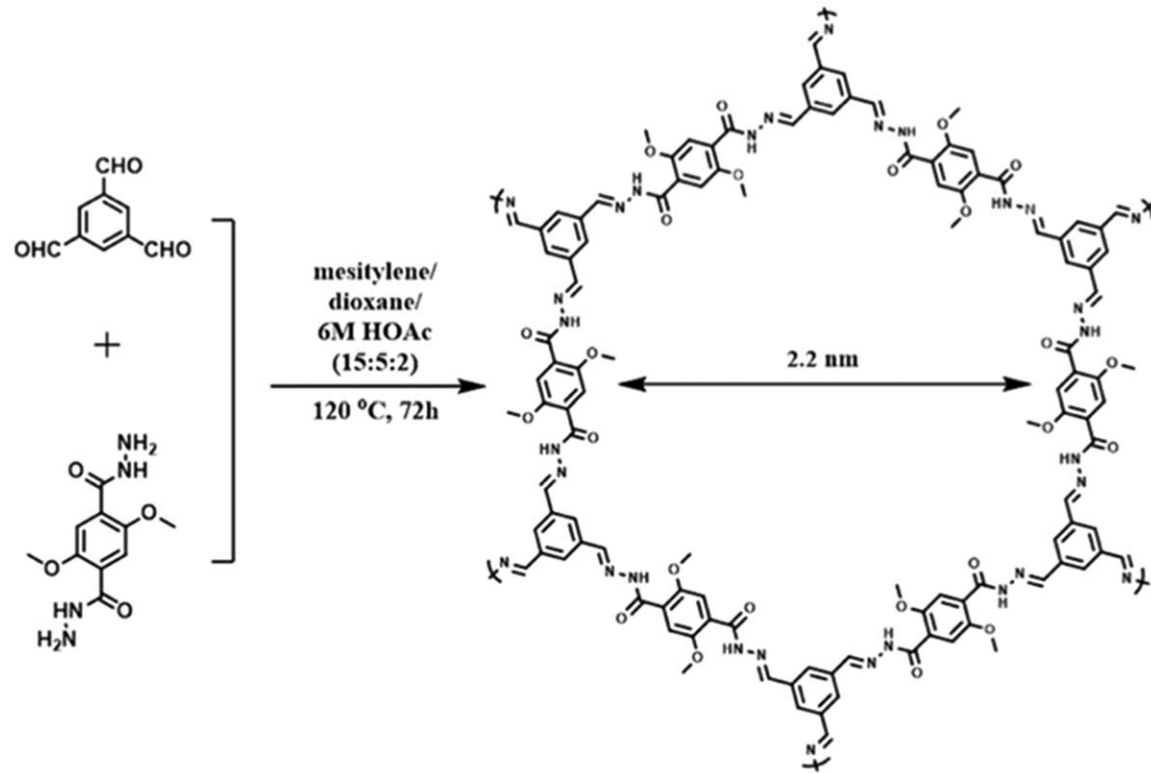


**Fig. 9** Synthesis of TFB-COF. Adapted with permission from ref. 54. W. Liu, Q. Su, P. Ju, B. Guo, H. Zhou, G. Li and Q. Wu, *ChemSusChem*, John Wiley and Sons, © 2017 Wiley-VCH Verlag GmbH & Co. KGaA, Weinheim.

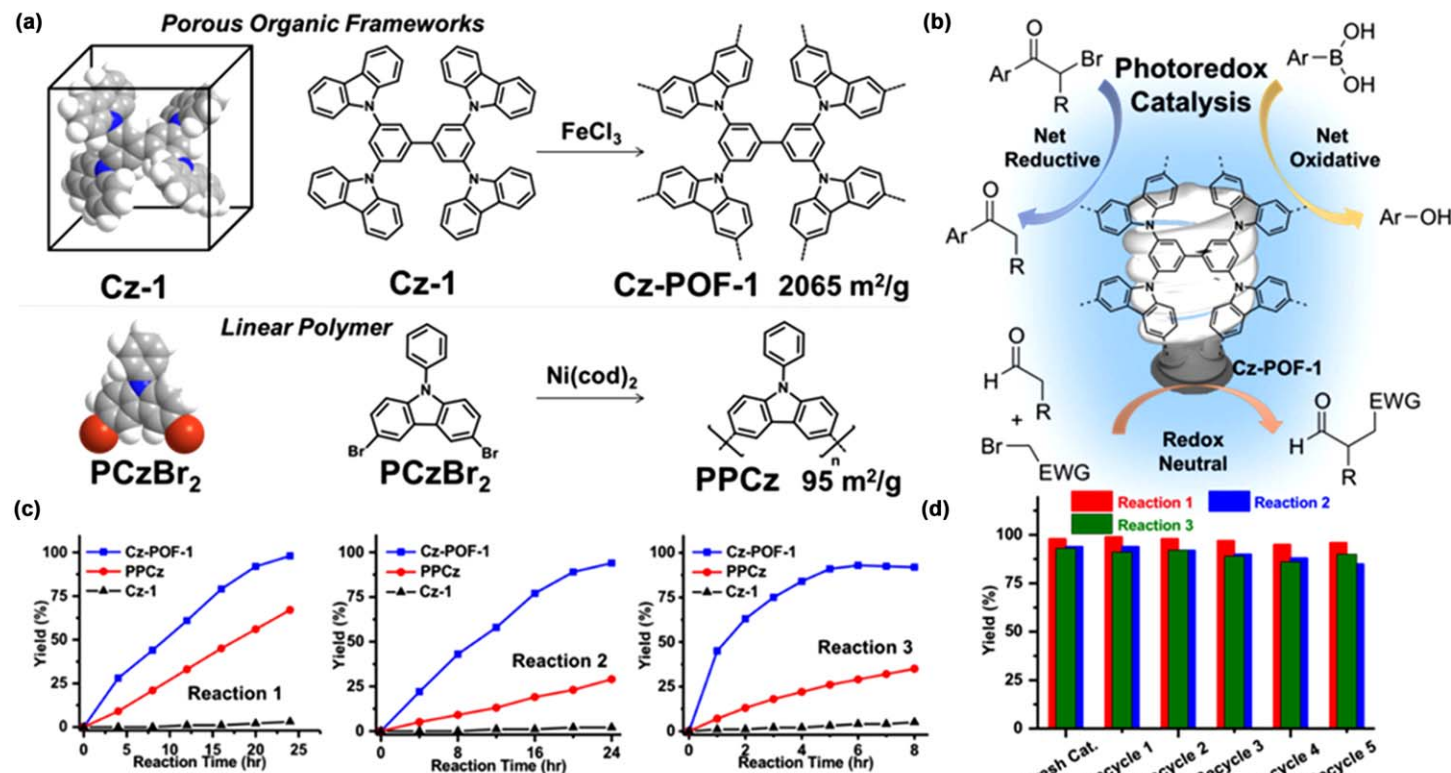


**Fig. 10** (a) Space-filling models of Cz-1 and  $\text{PCzBr}_2$  (3,6-dibromo-9-phenyl-9*H*-carbazole) and their polymerization (right) to form Cz-POF-1 and PPCz, respectively. (b) Schematic illustration of the three reactions for evaluating the photocatalytic activities of Cz-POF-1. (c) Comparison of rates of conversion using Cz-POF-1, PPCz, and Cz-1 as the photocatalyst. (d) Recyclability of Cz-POF-1 for three reactions.<sup>56</sup> Adapted from J. Luo, X. Zhang and J. Zhang, ACS Catal., 2015, 5, 2250. Copyright (2015) American Chemical Society.

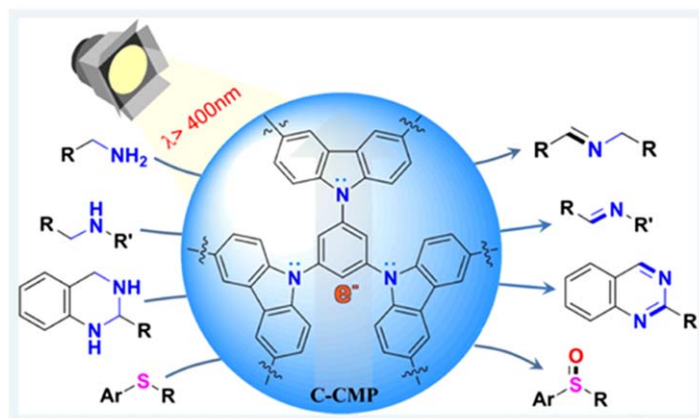


**Fig. 11** Schematic illustration of the three reactions for evaluating the photocatalytic activities of C-CMP.<sup>59</sup> Adapted from C. Su, R. Tandiana, B. Tian, A. Sengupta, W. Tang, J. Su and K. P. Loh, *ACS Catal.*, 2016, 3594. Copyright (2016) American Chemical Society.

efficient oxidative quenching pathway and exhibited remarkable photo-redox catalytic activities and a wide substrate scope.<sup>56</sup> Compared to its linear counterpart **PPCz** (a one dimensional polycarbazole) (Fig. 10a), **Cz-POF-1** exhibits much faster reaction kinetics in all three reactions (Fig. 10c). Besides the large portion of mesopores and excellent recyclability of **Cz-POF-1** (Fig. 10d), the insensitivity towards to oxygen and moisture in  $\alpha$ -alkylation of aldehydes is noteworthy. For instance, oxygen and moisture residue (0.5% water) in the aerated solvent significantly decreased the yield and selectivity for the reaction between heptaldehyde and diethyl bromomalonate when  $[\text{Ru}(\text{bpy})_3]^{2+}$  was used as the photocatalyst. However, such detrimental effect was insignificant when the reaction was catalyzed by **Cz-POF-1**, possibly due to the framework's hydrophobic pore environment.

More recently, Loh and coworkers reported another example of the application of Cz-POFs as photoredox catalysts in selective aerobic oxidations (Fig. 11).<sup>59</sup> Using **C-CMP** synthesized *via* the oxidative self-coupling of 1,3,5-tri(9-carbazolyl)-benzene (TCB),<sup>60</sup> three different organic transformations were tested with good to excellent performance: aerobic oxidative coupling of primary amines (94–98% yield), dehydrogenation of non-active secondary amines including pharmaceutically relevant nitrogen heterocycles (58–76% yield), and selective oxidation of sulfides (92–99% yield).

## 2.4 Water compatible photocatalytic applications

Increasing the dispersibility and compatibility of CMPs is necessary to expand their applications in economically and environmentally friendly reaction media, including water. Indeed, the use of organic solvents usually generates a large amount of liquid waste in both laboratory and industrial settings. In the absence of polar groups, the water wettability of most as synthesized CMPs are not ideal for their applications in aqueous environment. Ma *et al.* attempted to address

this issue by synthesizing CMP nanoparticles in an oil-in-water mini-emulsion.<sup>61</sup> Using Suzuki and Sonogashira coupling reactions, **B-FL<sub>3</sub>-a**, **B-BPh<sub>3</sub>-a**, **B-BT<sub>3</sub>-a** and **B-FL<sub>3</sub>-b**, **B-BPh<sub>3</sub>-b**, **B-BT<sub>3</sub>-b** that can be dispersed in organic solvents and water were synthesized (Fig. 12). As shown in the SEM images, nanosized CMP particles with different shapes including spheres, rods, and rings were obtained for these polymers. The NP CMPs were used to generate activated oxygen species for degradation of a water-soluble dye, rhodamine B (RhB). **B-BT<sub>3</sub>-b** exhibits the fastest degradation rate among the six polymers, which was attributed to its lowest optical band gap of 1.76 eV. About 80% of RhB have been degraded in 25 min. Interestingly, in comparison to its bulk form, **B-BT<sub>3</sub>-b** NPs showed higher photocatalytic efficiency. This is consistent with the expected larger accessibility of CMPs NPs. After five additional photodegradation, no decrease of reaction rate was observed, indicating the high stability and recyclability. Scavenging control experiments pointed that a combination of direct oxidation and indirect oxidation *via* singlet oxygen are operational in this reaction.

A post-synthetic modification strategy was employed to increase the water dispersibility and compatibility of CMPs.<sup>62</sup> Polymers **P-Az-1** and **P-Az-2** were synthesized by Sonogashira coupling of 1,4-dibromobenzene and 1,3-dibromoazulene with 1,3,5-triethynylbenzene, respectively. Since in the presence of an acidic environment, the azulene moiety can be protonated at the electron-rich cyclopentadiene ring and form a stable aromatic tropylum cation.<sup>63</sup> Thus, the protonated version of the two polymers, **P-Az-1h** and **P-Az-2h** were subsequently prepared, which exhibited much enhanced hydrophilicity and dispersibility in water. CV measurements were used to determine the CB and VB energy levels of the two polymers, and upon protonation, the VB energy decreases in both pairs. Due to their excellent water compatibility, **P-Az-1h** and **P-Az-2h** were employed as photocatalysts to reduce Cr<sup>IV</sup> to less toxic Cr<sup>III</sup>. However, the identity of the reducing agent was not clear although it was found that formic acid, which increases the reaction rate, can serve as extra electron donor,. Interestingly, adding Fe<sup>III</sup> or Cu<sup>II</sup> also significantly increases the photocatalytic efficiency of the reaction, demonstrating a cascade catalytic process (Fig. 13).

## 2.5 Hydrogen evolutions

Artificial photosynthesis, a process during which the energy of sunlight is stored in the product fuels such as hydrogens *via* photocatalytic reactions, has been considered as one of the most important approaches for the clean and sustainable energy source for the future. Most of the investigated inorganic semiconductors for photocatalytic hydrogen evolution reaction (HER) are based on metal oxides, (oxy)sulphides, and (oxy)nitrides.<sup>64</sup> Conjugated organic polymers have also been explored in the past, marked by the pioneering work of Yanagida and coworkers in 1985 on the use of linear poly(*p*-phenylene)s (**PPP**) as the photocatalyst for HER.<sup>5</sup> One advantage of organic polymers is that their electronic structure can be efficiently modified by tailoring the structure of the monomers. However, due to the low apparent quantum yield (0.006% for

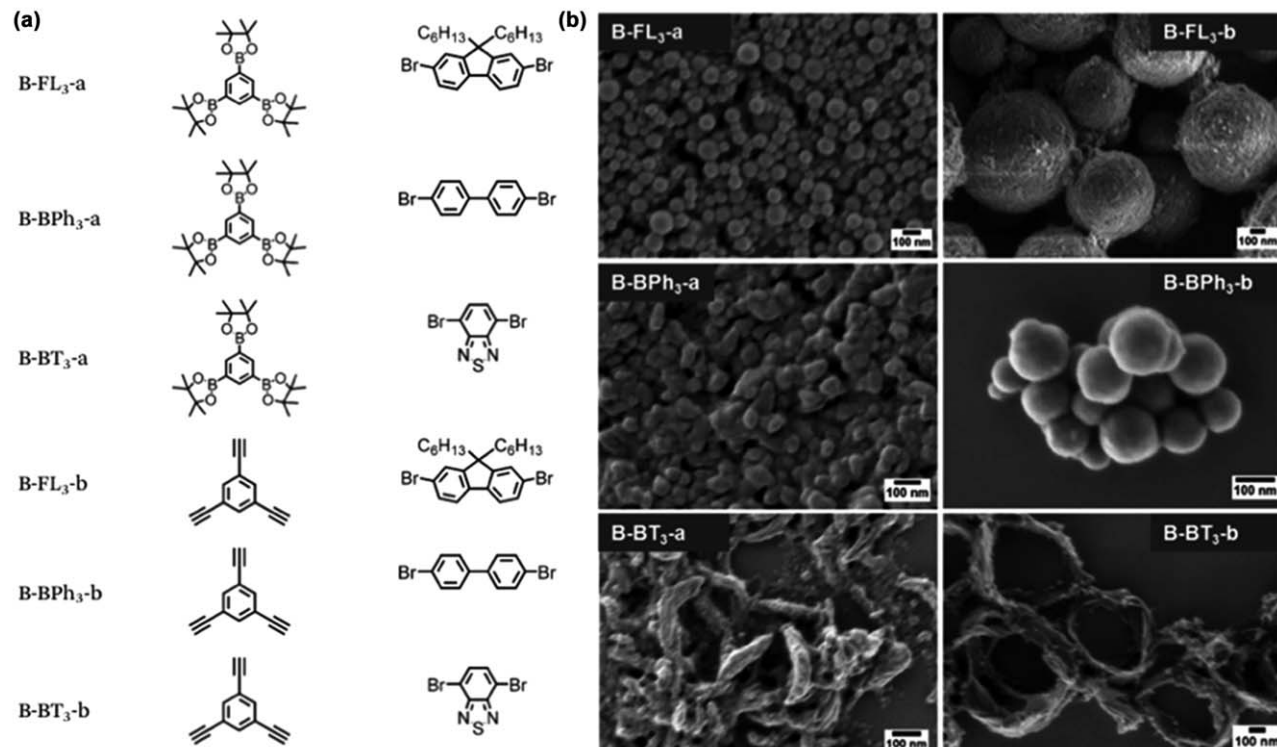


**Fig. 12** (a) Structure of monomers for synthesizing CMPs. (b) SEMs images of CMPs NPs. Adapted from ref. 61 with permission from The Royal Society of Chemistry.

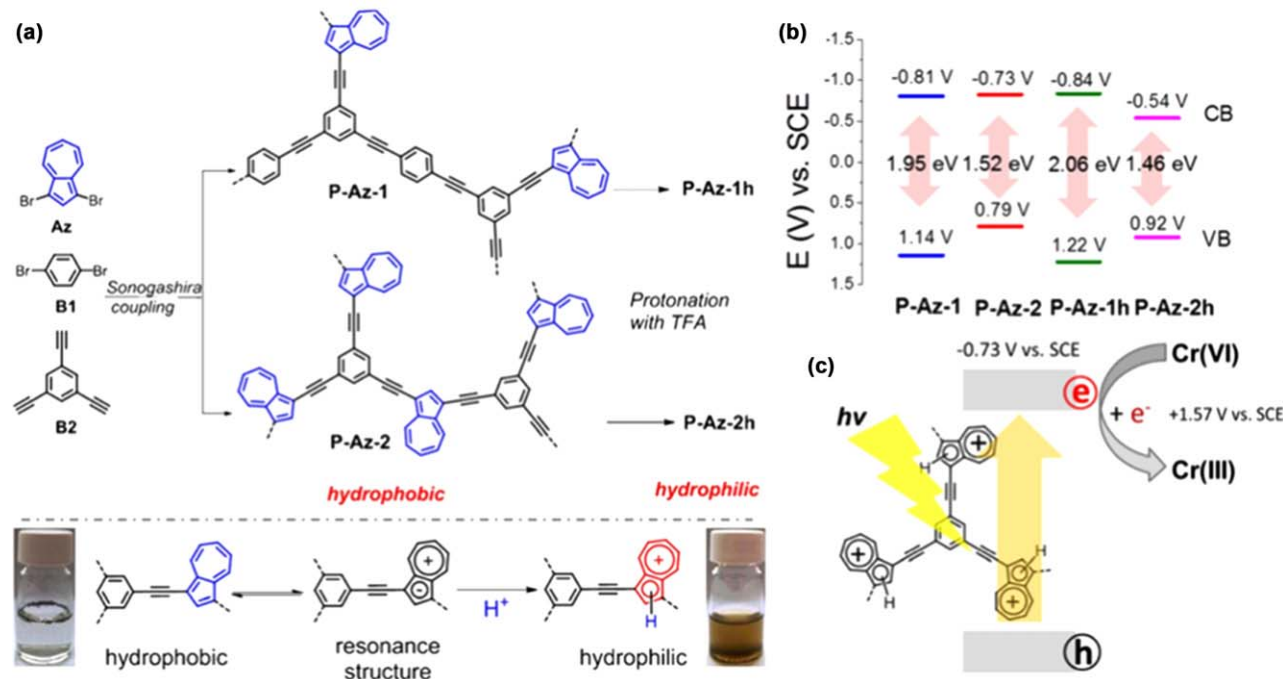


**Fig. 13** (a) Synthetic and postsynthetic modification polyazulene networks. (b) Positions of VB and CB of P-Az-1, P-Az-2, P-Az-1h, and P-Az-2h. (c) Proposed mechanism for the photocatalytic reduction of Cr<sup>IV</sup>. Adapted with permission from ref. 62, S. Ghasimi, K. Landfester and K. A. I. Zhang, ChemCatChem, John Wiley and Sons. © 2016 WILEY-VCH Verlag GmbH & Co. KGaA, Weinheim.

**PPP**) of these type of materials, this field of study did not make significant progress.

Müllen and coworkers reported the preparation of three-dimensional conjugated poly(azomethine) networks (**ANW1-4**) from a facile polycondensation between 1,3,5-tris(4-aminophenyl)-benzene and four different aromatic aldehydes: terephthalaldehyde, naphthalene-2,6-dicarbaldehyde, anthracene-2,6-di-carbaldehyde and anthracene-9,10-dicarbaldehyde.<sup>65</sup> All four **ANWs** were tested in the photocatalytic experiments in water where 3 wt% Pt was used as the co-catalyst and 10 vol% of triethanolamine as the electron donor. In general, the rate of hydrogen production depends on the size of the aldehyde. A maximum of  $7 \mu\text{mol H}_2 \text{ h}^{-1}$  (100 mg photocatalyst) was obtained for **ANW2**, which is significantly higher than **PPPs** ( $1\text{--}3 \mu\text{mol H}_2 \text{ h}^{-1}$ ).<sup>5</sup> Four consecutive experiments were performed on **ANW2** over 20 h, and remarkably no apparent deactivation was observed. Interestingly, despite their similar band gap, **ANW4** exhibits much lower activity compared to **ANW3**. The authors attributed this to the distortion of the network and the large deviation from planarity in **ANW4**, which prevents the efficient transport of charge carriers (Fig. 14).

Thomas *et al.* reported the synthesis of heptazine-based microporous polymer networks **HMP-1** and **HMP-2** using the reaction of cyameluric chloride with *p*-phenylenediamine and benzidine, respectively.<sup>66</sup> Again, the HER measurements were carried out using 3 wt% Pt as the co-catalyst and 10 vol% of triethanolamine as the electron donor. The **HMP-1** and **HMP-2** exhibit a good activity of 21 and  $18 \mu\text{mol H}_2 \text{ h}^{-1}$  (20 mg photocatalyst), respectively. Most activity was contributed by the UV excitation (300–420 nm). No deactivation of **HMP-1** was observed over a 20 h. In order to further tune the bandgap of HMPs, 4,4'-(benzo[*c*][1,2,5]thiadiazole-4,7-diyl)dianiline was used in the polymerization of **HMP-3**, which exhibits a band gap of 2.0–2.1 eV.<sup>67</sup> Indeed, an increase of the HER activity was observed:  $31\text{--}32 \mu\text{mol H}_2 \text{ h}^{-1}$  (20 mg photocatalyst) (Fig. 15).

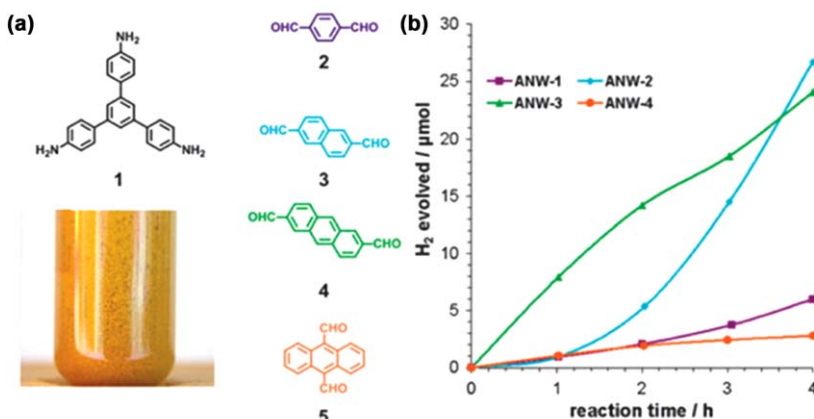


**Fig. 14** (a) Molecular structures of the building units for the ANWs. (b) Time course of  $\text{H}_2$  production through ANW networks. Adapted from ref. 65 with permission from The Royal Society of Chemistry.

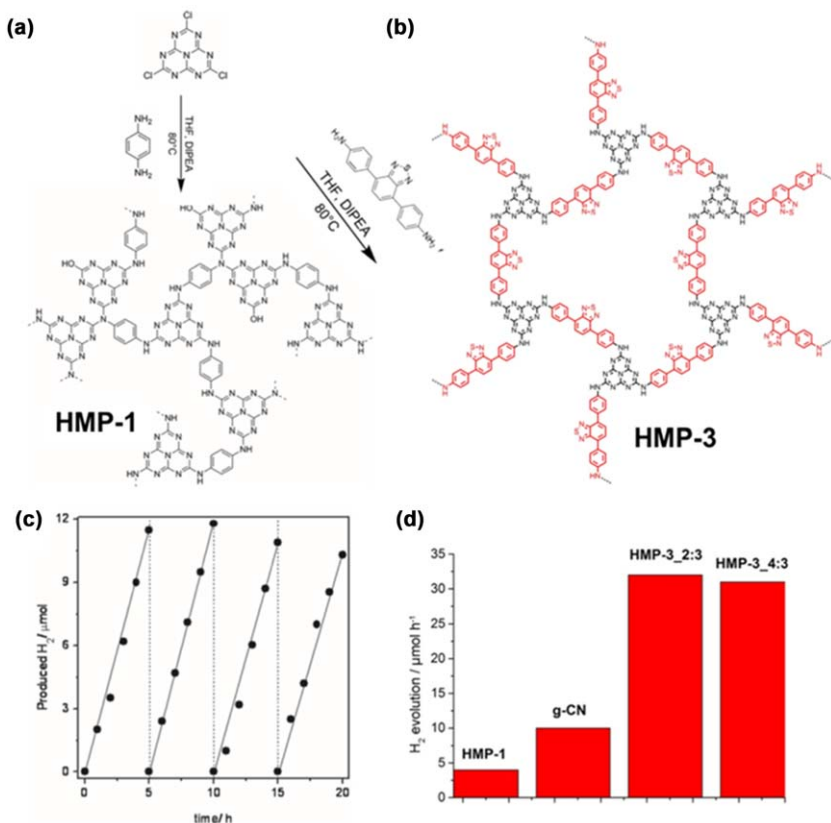


**Fig. 15** (a and b) Synthesis of HMP-1 and HMP-3. Adapted with permission from ref. 66, K. Kailasam, J. Schmidt, H. Bildirir, G. Zhang, S. Blechert, X. Wang and A. Thomas, *Macromolecular Rapid Communications*, John Wiley and Sons. Copyright © 2013 WILEY-VCH Verlag GmbH & Co. KGaA, Weinheim. (c) Hydrogen evolution over 20 h of HMP-1. Adapted with permission from ref. 67, K. Kailasam, M. B. Mesch, L. Möhlmann, M. Baar, S. Blechert, M. Schwarze, M. Schröder, R. Schomäcker, J. Senker and A. Thomas, *Energy Technology*, John Wiley and Sons, © 2016 WILEY-VCH Verlag GmbH & Co. KGaA, Weinheim. (d) Photocatalytic  $\text{H}_2$  generation of HMPs compared to bulk g-CN under similar conditions.

Son and coworkers used Knoevenagel condensation and prepared visible light harvesting microporous organic networks (**VH-MON**) with electronic push-pull skeletons.<sup>68</sup> A composite photocatalytic system **VH-MON/TiO<sub>2</sub>-Pt** was further fabricated. Although its surface area decreased from  $474 \text{ m}^2 \text{ g}^{-1}$  to  $237 \text{ m}^2 \text{ g}^{-1}$  due to the increase of the mass of **TiO<sub>2</sub>-Pt**, **VH-MON/TiO<sub>2</sub>-Pt** showed promising catalytic activity with 50 mmol hydrogen produced in the first 5 h. The stability was also excellent manifested by the consistent hydrogen production 47, 52, 46, and 45 mmol for the next four runs. The external quantum yield in the first run and the average value in the five runs were calculated to be 5.2% and 5.0%, respectively. The enhanced stability of system compared to eosin-Y/TiO<sub>2</sub>-Pt and N719/TiO<sub>2</sub>-Pt was attributed to the crosslinked nature of **VH-MON** (Fig. 16).

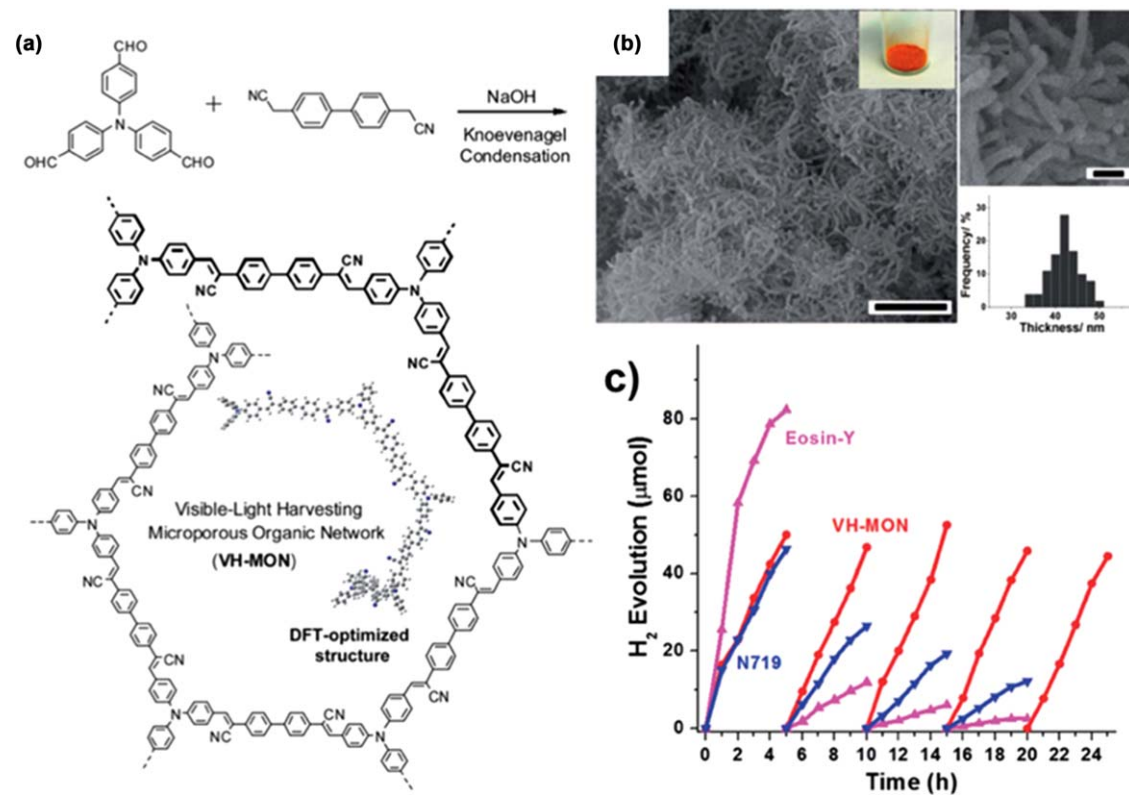


**Fig. 16** (a) Synthesis of VH-MON. (b) SEM images, photograph (inset), and thickness distribution diagram of VH-MON nanorods. Scale bars 1  $\mu\text{m}$  and 100 nm, respectively. (c) Photocatalytic  $\text{H}_2$  production from water using different catalysts. Adapted from ref. 68 with permission from The Royal Society of Chemistry.

CMPs with ordered structures, more commonly termed as COFs (covalent organic frameworks), were also tested for HER. Lotsch and coworkers synthesized a hydrozone-based COF (**TEPT-COF**) from the acetic acid catalyzed reversible condensation between 1,3,5-tris-(4-formyl-phenyl)triazine (**TEPT**) and 2,5-diethoxy-terephthalohydrazide (**DETH**). **TEPT-COF** is a crystalline network that is composed of co-facially stacked 2-D layers with a remarkably high surface area of  $1603\text{ m}^2\text{ g}^{-1}$ .<sup>69</sup> With a large band gap of 2.8 eV, **TEPT-COF** offers enough energy to drive HER. Indeed, with sodium ascorbate as sacrificial electron donor, a large, continuous, and stable hydrogen production of  $230\text{ }\mu\text{mol h}^{-1}\text{ g}^{-1}$ . Switching to the 10 vol% aqueous triethanolamine (**TEOA**) solution, the even higher hydrogen evolution rate of  $1970\text{ }\mu\text{mol h}^{-1}\text{ g}^{-1}$  was obtained. This is equivalent to an impressive quantum efficiency of 2.2%. It is noted that exfoliation of COFs during the decoration of Pt nanoparticles and photocatalysis did not destroy the connectivity, thus the photoactivity is retained (Fig. 17(a)).

Lotsch and coworkers further investigated a series of 2-dazine-linked **N<sub>x</sub>-COFs** ( $x = 0\text{--}3$ ), which were synthesized between the condensation of hydrazine with different triphenylarylaldehydes with the central aryl ring containing 0–3 nitrogen atoms as the building blocks to systematically study the effect of change of the chemical and structural variation of the precursors on the optoelectronic properties as well as their HER performance.<sup>70</sup> Although *in situ* generated Pt nanoparticles and TEOA are still necessary for the HER process, interestingly, it is observed that as the number of nitrogen atoms in the triphenylarylaldehyde increases from 0 to 3, the amount of hydrogen produced also increased from 23, 90, 438, to  $1703\text{ }\mu\text{mol h}^{-1}\text{ g}^{-1}$ . FTIR and solid state NMR show no significant change of the structure of **N<sub>x</sub>-COFs** after the photocatalysis. It is argued that the smallest dihedral angle and better crystallinity of **N<sub>3</sub>-COF** among the series facilitate the exciton migration with the 2-D COF layers as well as along the stacks, which leads to a better photocatalytic activity (Fig. 17(b)).

Yu and coworkers recently reported the synthesis of a large family (20) of porous conjugated polymers (PCPs) using Pd-catalyzed Suzuki polycondensation reaction.<sup>71</sup> The boronic pinacolester based chromophore precursors include both strong electron donors and acceptors, and the arylbromide are contributed by weak donor biphenyl (bph) and weak acceptor bipyridyl (bpy) at various ratios. The overall activity follows the trend as **PCP4** > **PCP2** > **PCP3** > **PCP1**, somewhat similar to the extent of conjugation (Fig. 18(a)). Interestingly, the photocatalytic activity greatly increases as the ratio of bpy/bph increases. For example, **PCP4e** exhibited the best performance ( $33.0\text{ }\mu\text{mol h}^{-1}$ , 1 mg photocatalyst), five times more than **PCP4a**. This was explained by the possible interaction of bpy with water molecule *via* H-bonding which can increase the local concentration. However, when only visible light ( $\lambda > 400\text{ nm}$ ) was used as the light source, the hydrogen production significantly decreased (**PCP4e**,  $6.7\text{ }\mu\text{mol h}^{-1}$ ). Although the photocatalytic reaction was conducted in the absence of noble metal co-catalysts, the authors demonstrated that the trace amount of Pd resulted from the polymerization reaction may still play a significant role in the photocatalytic activity of PCPs due to the

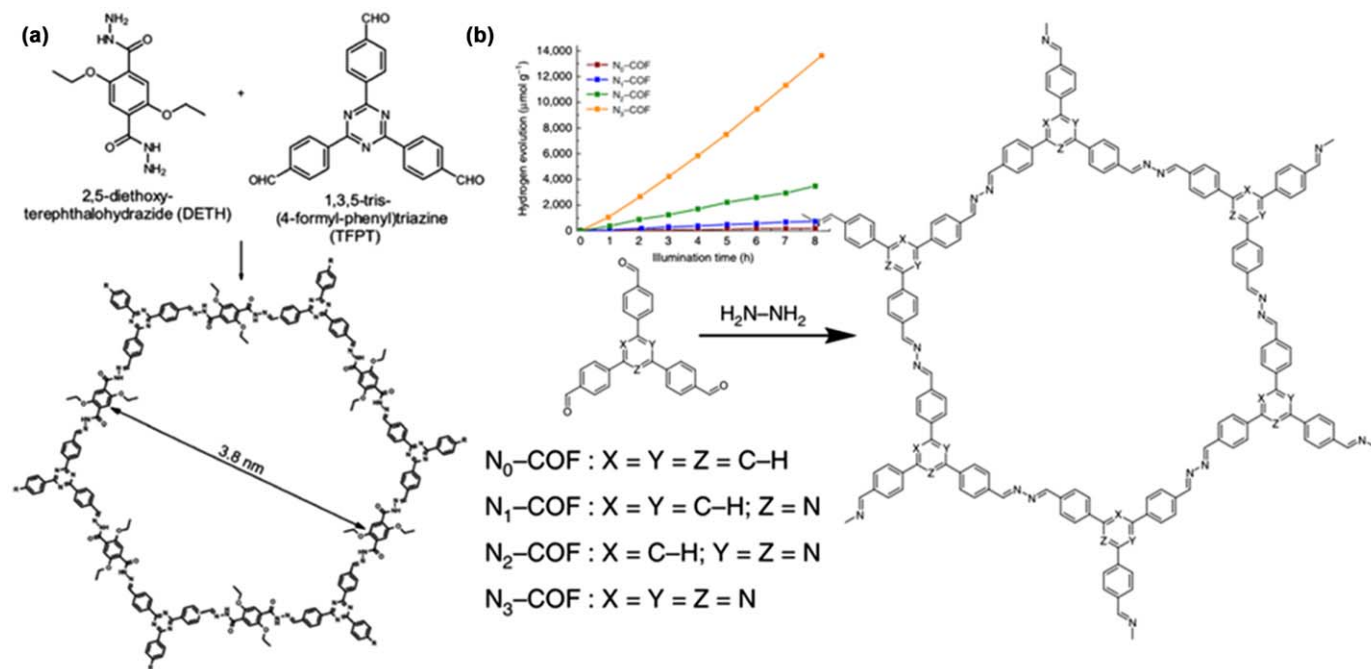


**Fig. 17** Synthesis scheme for (a) TFPT-COF (adapted from ref. 69 with permission from The Royal Society of Chemistry) and (b)  $N_x\text{-COFs}$  ( $x = 0-3$ ) (adapted from ref. 70, V. S. Vyas, F. Haase, L. Stegbauer, G. Savasci, F. Podjaski, C. Ochsenfeld and B. V. Lotsch, DOI:10.1038/ncomms9508. © 2015 Macmillan Publishers Limited. All rights reserved. Reproduced under creative commons license (<https://creativecommons.org/licenses/by/4.0/>)).

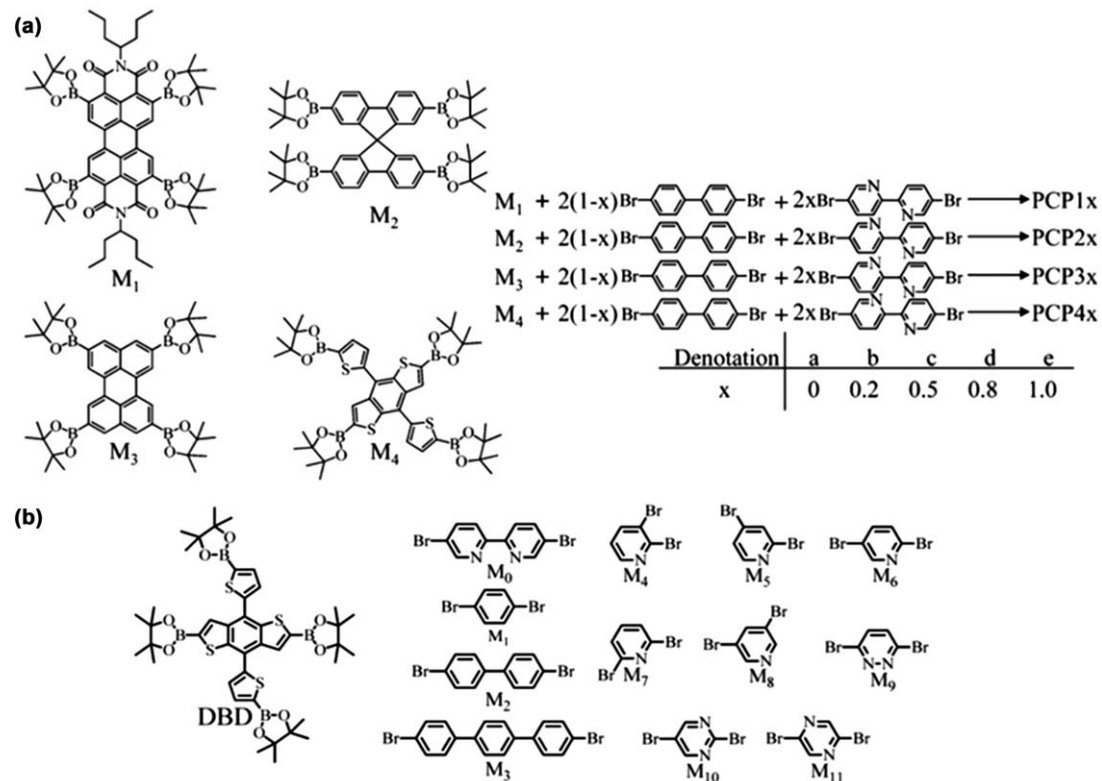


**Fig. 18** Synthesis scheme for (a) PCP1x-4x ( $x = 0, 0.2, 0.5, 0.8, 1.0$ ) (Adapted with permission from L. Li, Z. Cai, Q. Wu, W. Y. Lo, N. Zhang, L. X. Chen and L. Yu, *J. Am. Chem. Soc.*, 2016, **138**, 7681. Copyright (2016) American Chemical Society)<sup>71</sup> and (b) PCP1-12 (Adapted with permission from (L. W. Li, W. Y. Lo, Z. X. Cai, N. Zhang and L. P. Yu, *Macromolecules*, 2016, **49**, 6903). Copyright (2016) American Chemical Society).<sup>72</sup>

observation of correlation between the H<sub>2</sub> production and Pd residue in PCPs. In a related work, they further investigated the importance of the “internal polarization” induced by the bipyridyl comonomer.<sup>72</sup> Twelve different aryldibromides consisting of monodentate ligand monomers and ligand-free acceptor monomers were used for constructing the corresponding PCPs. Indeed, full donor based **PCP1–3** gave rise to a low activity (1.9–10.1 μmol h<sup>-1</sup>, 12 mg photocatalyst). The incorporation of *ortho*-substituted (**PCP4**) or *meta*-substituted (**PCP-5,-7,-8**) pyridines into PCPs either twisted the structures or break the conjugation of the backbone, which resulted in a detrimental of the charge transport and photocatalytic activity. On the other hand, stronger acceptor diazine based **PCP11** and **PCP12** show good activity (~107 μmol h<sup>-1</sup>) (Fig. 18(b)).

Cooper and coworkers used the statistical copolymerization and synthesized a series of CMPs using the cross coupling between 1,4-benzene diboronic acid and/or 1,3,6,8-tetraboronic pinacol ester of pyrene and/or 1,2,4,5-tetrabromobenzene and/or 1,3,6,8-tetrabromopyrene.<sup>73</sup> The significance of this work is that a wide range of absorption/emission spectra and optical gaps were obtained *via* changing the molar ratio of the monomers for the resulted fifteen CMPs (**CP-CMP1-15**) for the first time. More importantly, the photocatalytic HER from water in the presence of electron donor were all performed in the absence of noble metal co-catalysts. Among all the CP-CMPs, **CP-CMP10** (optical gap 2.33 eV) exhibits the highest HER rate (17.4 μmol h<sup>-1</sup>, 100 mg photocatalyst) (Fig. 19(a)). Remarkably, such rate almost retained when switched to visible light excitation (>420 nm). Interestingly, other CMPs with either higher or lower gaps all show an inferior catalytic activity. Using TD-DFT calculations,<sup>74–76</sup> two possible explanations were given. First, for polymers beyond **CP-CMP10**, the dark, nonradiative electron – hole recombination becomes more significant due to the large percentage of pyrene component in the copolymer, which loses the electrons *via* charge recombination. Second, the kinetic energy barrier between the electron transfer between the polymer and proton increases as the pyrene content increases. As for the dominant catalytic effect of the Pd residue, this remained inside CMPs (*e.g.* 0.42 wt% in **CP-CMP-10**) and a further mechanism was ruled out *via* several controlled experiments. In a following work, Cooper *et al.* further studied the effect of the monomer linker length on the photocatalytic performance of the resulting CMPs.<sup>77</sup> Among the six different CMPs investigated, **SP-CMP** and **ESP-CMP** exhibit the highest HER performance (~28 μmol h<sup>-1</sup>, 25 mg photocatalyst, >295 nm) although the correlation with surface area is poor. However, it is clear that meta-linkages in **M-CMP** and **ME-CMP** are detrimental to the light absorption and photocatalytic performance due to the poor conjugation compared to *para*-linkages (Fig. 19(b)).

Wang and coworkers recently reported the synthesis of a series of conjugated polybenzothiadizoles using BT with either benzene-1,2,4- and 1,3,5-phenyltriboronic acid tris(pinacol) ester or 1,2,4,5-phenyltetraboronic acid tetrakis(pinacol) ester as a comonomer.<sup>78</sup> In addition, another comonomer, benzene-1,4-diboronic acid bis(pinacol) ester was introduced

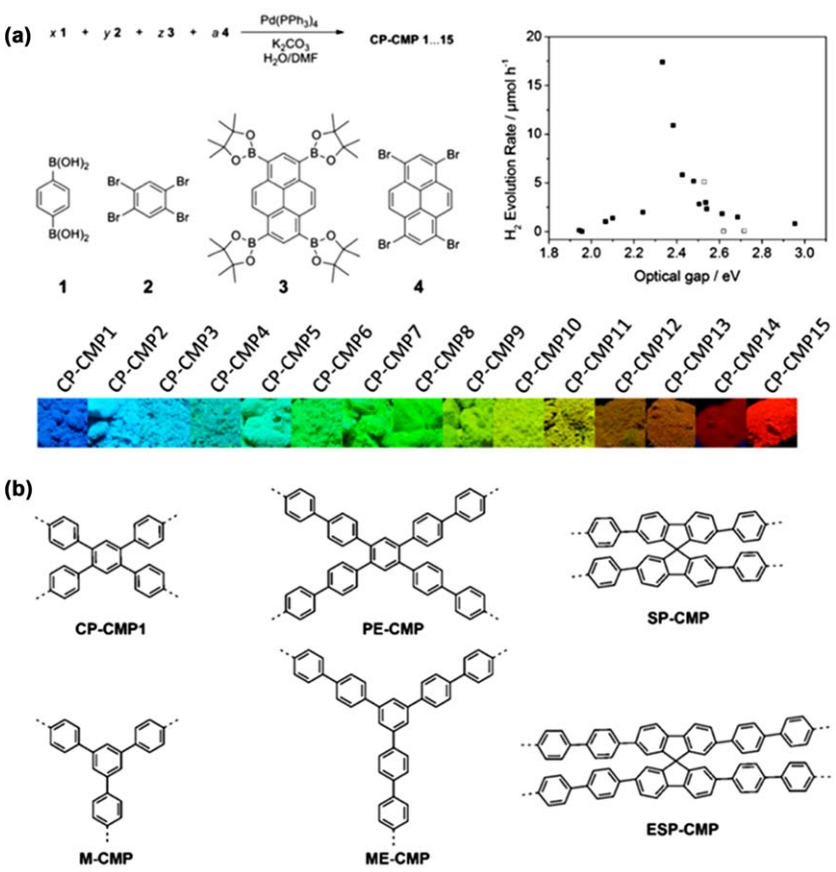


**Fig. 19** (a) Synthesis of conjugated copolymer photocatalysts CO-CMP1-15 and their photographs. Rate of photocatalytic hydrogen production correlated with the optical gap in the polymers. Adapted from R. S. Sprick, J. X. Jiang, B. Bonillo, S. Ren, T. Ratvijitvech, P. Guiglion, M. A. Zwijnenburg, D. J. Adams and A. I. Cooper, *J. Am. Chem. Soc.*, 2015, **137**, 3265.<sup>73</sup> Published under Creative Commons CC-BY licence. (b) Molecular structures of CP-CMP-1, PE-CMP, SP-CMP, M-CMP, ME-CMP, and ESP-CMP. Adapted from ref. 77 – Published by The Royal Society of Chemistry.

to further fine-tune the 3-D network skeleton. It is observed that as the 3D character of B-BTs increases, the optical gap also increase (*e.g.* from 2.25 eV in **B-BT-1,2,4** to 2.42 eV in **B-BT-1,3,5**), which can be attributed to the more disruptive conjugation. In the presence of 3 wt% Pt and TEOA as the electron donor, **B-BT-1,3,5** showed a moderate HER rate of  $20 \mu\text{mol h}^{-1}$ , 50 mg photocatalyst. Surprisingly, as the content of co-monomer (benzene-1,4-diboronic acid bis(pinocyclic ester) increases, the photocatalytic activity significant increases, with the highest being the linear polymer, **B-BT-1,4** ( $116 \mu\text{mol h}^{-1}$ ). Apparently, it can be deduced from this study that, although the 3-D structure is useful for an enhanced surface area, it might not contribute positively to a high light-induced charge-transfer, charge-separation, and electron-transfer ability (Fig. 20).

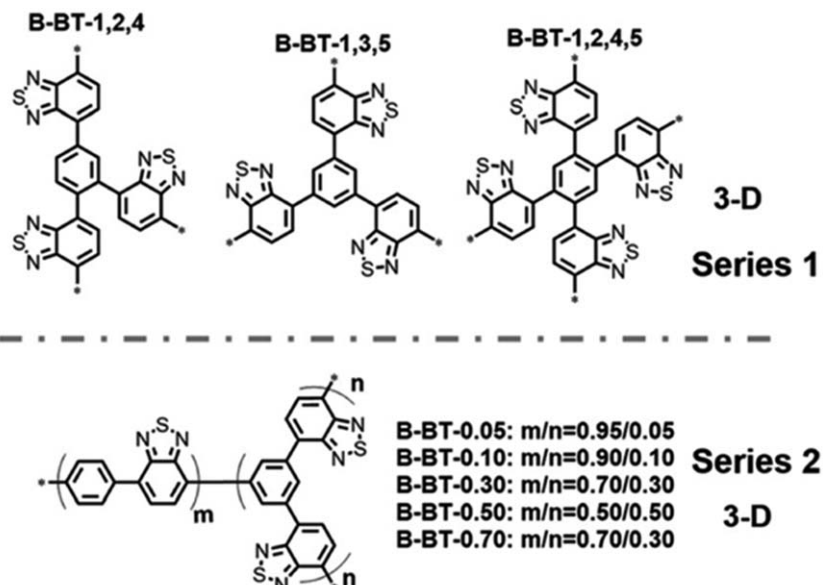


**Fig. 20** Structures of two classes of polybenzothiadiazoles with different molecular designs. Adapted with permission from ref. 78, C. Yang, B. C. Ma, L. Zhang, S. Lin, S. Ghasimi, K. Landfester, K. A. Zhang and X. Wang, *Angewandte Chemie, International Edition*, John Wiley and Sons. © 2016 WILEY-VCH Verlag GmbH & Co. KGaA, Weinheim.

### 3 Conclusions and outlook

In the past six years, the fast development of CMPs in photocatalytic applications has firmly established their unique role in heterogeneous photocatalysis. Besides the excellent stability and recyclability, CMPs have also demonstrated their potential capability in device integration, manifested by the forms of films, monoliths, and dispersible nanoparticles. These create massive opportunities in many other light harvesting applications. At the same time, there still exist several important fundamental questions that call for further detailed investigations. First, there is a need to establish a well-accepted experimental protocol for reporting the efficiencies of catalytic reactions. Ideally, quantum yield should be incorporated as the universal measure. Second, more detailed photophysical characterization involving ultrafast spectroscopy should be utilized to assist the understanding the fundamental photophysics of CMPs, especially for copolymers. Indeed, the generation, transport, and recombination of excitons are essential for the ultimate chemical reactions. Third, applications of CMPs should be quickly moved to the photochemical production of important clean organic fuels. Although some works have been done on hydrogen evolution reactions, other more challenging reactions should also be tested including CO<sub>2</sub> reduction and even water oxidation reactions. Overall, the positive impact of further research on CMPs for sustainable chemistry is highly significant.

## References

- 1 G. Ciamician, *Science*, 1912, **36**, 385.
- 2 T. Bach and J. P. Hehn, *Angew. Chem., Int. Ed.*, 2011, **50**, 1000.
- 3 N. Hoffmann, *Chem. Rev.*, 2008, **108**, 1052.
- 4 D. M. Schultz and T. P. Yoon, *Science*, 2014, **343**, 1239176.
- 5 S. Yanagida, A. Kabumoto, K. Mizumoto, C. Pac and K. Yoshino, *J. Chem. Soc., Chem. Commun.*, 1985, 474.
- 6 T. Shibata, A. Kabumoto, T. Shiragami, O. Ishitani, C. Pac and S. Yanagida, *J. Phys. Chem.*, 1990, **94**, 2068.
- 7 S. Matsuoka, K. Yamamoto, T. Ogata, M. Kusaba, N. Nakashima, E. Fujita and S. Yanagida, *J. Am. Chem. Soc.*, 1993, **115**, 601.
- 8 D. L. Jiang, C. K. Choi, K. Honda, W. S. Li, T. Yuzawa and T. Aida, *J. Am. Chem. Soc.*, 2004, **126**, 12084.
- 9 X. Wang, K. Maeda, A. Thomas, K. Takanabe, G. Xin, J. M. Carlsson, K. Domen and M. Antonietti, *Nat. Mater.*, 2009, **8**, 76.
- 10 Y. Wang, X. Wang and M. Antonietti, *Angew. Chem., Int. Ed.*, 2012, **51**, 68.
- 11 J. X. Jiang, F. Su, A. Trewn, C. D. Wood, N. L. Campbell, H. Niu, C. Dickinson, A. Y. Ganin, M. J. Rosseinsky, Y. Z. Khimyak and A. I. Cooper, *Angew. Chem., Int. Ed.*, 2007, **46**, 8574.
- 12 D. Yuan, W. Lu, D. Zhao and H. C. Zhou, *Adv. Mater.*, 2011, **23**, 3723.
- 13 B. Li, Y. Zhang, R. Krishna, K. Yao, Y. Han, Z. Wu, D. Ma, Z. Shi, T. Pham, B. Space, J. Liu, P. K. Thallapally, J. Liu, M. Chrzanowski and S. Ma, *J. Am. Chem. Soc.*, 2014, **136**, 8654.
- 14 D. Wu, F. Xu, B. Sun, R. Fu, H. He and K. Matyjaszewski, *Chem. Rev.*, 2012, **112**, 3959.
- 15 M. Rueping, C. Vila and T. Bootwicha, *ACS Catal.*, 2013, **3**, 1676.
- 16 X. Zou, H. Ren and G. Zhu, *Chem. Commun.*, 2013, **49**, 3925.
- 17 Y. Jin, Y. Zhu and W. Zhang, *CrystEngComm.*, 2013, **15**, 1484.
- 18 X. Du, Y. Sun, B. Tan, Q. Teng, X. Yao, C. Su and W. Wang, *Chem. Commun.*, 2010, **46**, 970.
- 19 A. M. Shultz, O. K. Farha, J. T. Hupp and S. T. Nguyen, *Chem. Sci.*, 2011, **2**, 686.
- 20 P. Kaur, J. T. Hupp and S. T. Nguyen, *ACS Catal.*, 2011, **1**, 819.
- 21 R. Palkovits, M. Antonietti, P. Kuhn, A. Thomas and F. Schüth, *Angew. Chem., Int. Ed.*, 2009, **48**, 6909.
- 22 C. E. Chan-Thaw, A. Villa, P. Katekomol, D. Su, A. Thomas and L. Prati, *Nano Lett.*, 2010, **10**, 537.
- 23 Q. Sun, Z. Dai, X. Meng, L. Wang and F.-S. Xiao, *ACS Catal.*, 2015, 4556.
- 24 J. Weber and A. Thomas, *J. Am. Chem. Soc.*, 2008, **130**, 6334.
- 25 L. Chen, Y. Honsho, S. Seki and D. Jiang, *J. Am. Chem. Soc.*, 2010, **132**, 6742.
- 26 J.-X. Jiang, A. Trewn, D. J. Adams and A. I. Cooper, *Chem. Sci.*, 2011, **2**, 1777.
- 27 J.-L. Wang, C. Wang, K. E. deKrafft and W. Lin, *ACS Catal.*, 2012, **2**, 417.
- 28 J.-X. Jiang, Y. Li, X. Wu, J. Xiao, D. J. Adams and A. I. Cooper, *Macromolecules*, 2013, **46**, 8779.
- 29 S. Bandyopadhyay, A. G. Anil, A. James and A. Patra, *ACS Appl. Mater. Interfaces*, 2016, **8**, 27669.
- 30 J. Hynek, J. Rathouský, J. Demel and K. Lang, *RSC Adv.*, 2016, **6**, 44279.
- 31 X. Ding and B. H. Han, *Angew. Chem., Int. Ed.*, 2015, **54**, 6536.
- 32 M. Liras, M. Iglesias and F. Sánchez, *Macromolecules*, 2016, **49**, 1666.
- 33 K. C. Park, J. Cho and C. Y. Lee, *RSC Adv.*, 2016, **6**, 75478.
- 34 J. M. Tobin, J. Liu, H. Hayes, M. Demleitner, D. Ellis, V. Arrighi, Z. Xu and F. Vilela, *Polym. Chem.*, 2016, **7**, 6662.

- 35 C.-A. Wang, Y.-W. Li, X.-L. Cheng, J.-P. Zhang and Y.-F. Han, *RSC Adv.*, 2017, **7**, 408.
- 36 B. Kiskan, M. Antonietti and J. Weber, *Macromolecules*, 2012, **45**, 1356.
- 37 Z. Xiao, Y. Zhou, X. Xin, Q. Zhang, L. Zhang, R. Wang and D. Sun, *Macromol. Chem. Phys.*, 2016, **217**, 599.
- 38 C. Schweitzer and R. Schmidt, *Chem. Rev.*, 2003, **103**, 1685.
- 39 K. Zhang, D. Kopetzki, P. H. Seeberger, M. Antonietti and F. Vilela, *Angew. Chem., Int. Ed.*, 2013, **52**, 1432.
- 40 H. Urakami, K. Zhang and F. Vilela, *Chem. Commun.*, 2013, **49**, 2353.
- 41 K. Zhang, Z. Vobecka, K. Tauer, M. Antonietti and F. Vilela, *Chem. Commun.*, 2013, **49**, 11158.
- 42 Z. J. Wang, S. Ghasimi, K. Landfester and K. A. Zhang, *Chem. Commun.*, 2014, **50**, 8177.
- 43 Y. Yagci, S. Jockusch and N. J. Turro, *Macromolecules*, 2010, **43**, 6245.
- 44 J. Lalevée, M.-A. Tehfe, F. Dumur, D. Gigmes, N. Blanchard, F. Morlet-Savary and J. P. Fouassier, *ACS Macro Lett.*, 2012, **1**, 286.
- 45 Z. J. Wang, K. Landfester and K. A. I. Zhang, *Polym. Chem.*, 2014, **5**, 3559.
- 46 S. Dadashi-Silab, H. Bildirir, R. Dawson, A. Thomas and Y. Yagci, *Macromolecules*, 2014, **47**, 4607.
- 47 N. Kang, J. H. Park, K. C. Ko, J. Chun, E. Kim, H. W. Shin, S. M. Lee, H. J. Kim, T. K. Ahn, J. Y. Lee and S. U. Son, *Angew. Chem., Int. Ed.*, 2013, **52**, 6228.
- 48 J. H. Ko, N. Kang, N. Park, H.-W. Shin, S. Kang, S. M. Lee, H. J. Kim, T. K. Ahn and S. U. Son, *ACS Macro Lett.*, 2015, **4**, 669.
- 49 Z. J. Wang, S. Ghasimi, K. Landfester and K. A. Zhang, *Adv. Mater.*, 2015, **27**, 6265.
- 50 Z. J. Wang, K. Garth, S. Ghasimi, K. Landfester and K. A. Zhang, *ChemSusChem.*, 2015, **8**, 3459.
- 51 W. Huang, B. C. Ma, D. Wang, Z. J. Wang, R. Li, L. Wang, K. Landfester and K. A. I. Zhang, *J. Mater. Chem. A*, 2017, **5**, 3792.
- 52 Z. J. Wang, S. Ghasimi, K. Landfester and K. A. I. Zhang, *J. Mater. Chem. A*, 2014, **2**, 18720.
- 53 Z. J. Wang, S. Ghasimi, K. Landfester and K. A. I. Zhang, *Adv. Synth. Catal.*, 2016, **358**, 2576.
- 54 W. Liu, Q. Su, P. Ju, B. Guo, H. Zhou, G. Li and Q. Wu, *ChemSusChem.*, 2017, **10**, 664.
- 55 X. Zhang, J. Z. Lu and J. Zhang, *Chem. Mater.*, 2014, **26**, 4023.
- 56 J. Luo, X. Zhang and J. Zhang, *ACS Catal.*, 2015, **5**, 2250.
- 57 D. D. Tanner and H. K. Singh, *J. Org. Chem.*, 1986, **51**, 5182.
- 58 D. Vasudevan and H. Wendt, *J. Electroanal. Chem.*, 1995, **392**, 69.
- 59 C. Su, R. Tandiana, B. Tian, A. Sengupta, W. Tang, J. Su and K. P. Loh, *ACS Catal.*, 2016, 3594.
- 60 Q. Chen, M. Luo, P. Hammershoj, D. Zhou, Y. Han, B. W. Laursen, C. G. Yan and B. H. Han, *J. Am. Chem. Soc.*, 2012, **134**, 6084.
- 61 B. C. Ma, S. Ghasimi, K. Landfester, F. Vilela and K. A. I. Zhang, *J. Mater. Chem. A*, 2015, **3**, 16064.
- 62 S. Ghasimi, K. Landfester and K. A. I. Zhang, *ChemCatChem*, 2016, **8**, 694.
- 63 E. Amir, R. J. Amir, L. M. Campos and C. J. Hawker, *J. Am. Chem. Soc.*, 2011, **133**, 10046.
- 64 F. E. Osterloh, *Chem. Mater.*, 2008, **20**, 35.
- 65 M. G. Schwab, M. Hamburger, X. Feng, J. Shu, H. W. Spiess, X. Wang, M. Antonietti and K. Müllen, *Chem. Commun.*, 2010, **46**, 8932.
- 66 K. Kailasam, J. Schmidt, H. Bildirir, G. Zhang, S. Blechert, X. Wang and A. Thomas, *Macromol. Rapid Commun.*, 2013, **34**, 1008.

- 67 K. Kailasam, M. B. Mesch, L. Möhlmann, M. Baar, S. Blechert, M. Schwarze, M. Schröder, R. Schomäcker, J. Senker and A. Thomas, *Energy Technol.*, 2016, **4**, 744.
- 68 J. H. Park, K. C. Ko, N. Park, H.-W. Shin, E. Kim, N. Kang, J. Hong Ko, S. M. Lee, H. J. Kim, T. K. Ahn, J. Y. Lee and S. U. Son, *J. Mater. Chem., A*, 2014, **2**, 7656.
- 69 L. Stegbauer, K. Schwinghammer and B. V. Lotsch, *Chem. Sci.*, 2014, **5**, 2789.
- 70 V. S. Vyas, F. Haase, L. Stegbauer, G. Savasci, F. Podjaski, C. Ochsenfeld and B. V. Lotsch, *Nat. Commun.*, 2015, **6**, 8508.
- 71 L. Li, Z. Cai, Q. Wu, W. Y. Lo, N. Zhang, L. X. Chen and L. Yu, *J. Am. Chem. Soc.*, 2016, **138**, 7681.
- 72 L. W. Li, W. Y. Lo, Z. X. Cai, N. Zhang and L. P. Yu, *Macromolecules*, 2016, **49**, 6903.
- 73 R. S. Sprick, J. X. Jiang, B. Bonillo, S. Ren, T. Ratvijitvech, P. Guiglion, M. A. Zwijnenburg, D. J. Adams and A. I. Cooper, *J. Am. Chem. Soc.*, 2015, **137**, 3265.
- 74 P. Guiglion, C. Butchosa and M. A. Zwijnenburg, *J. Mater. Chem., A*, 2014, **2**, 11996.
- 75 P. Guiglion, C. Butchosa and M. A. Zwijnenburg, *Macromol. Chem. Phys.*, 2016, **217**, 344.
- 76 P. Guiglion, A. Monti and M. A. Zwijnenburg, *J. Phys. Chem. C*, 2017, **121**, 1498.
- 77 R. S. Sprick, B. Bonillo, M. Sachs, R. Clowes, J. R. Durrant, D. J. Adams and A. I. Cooper, *Chem. Commun.*, 2016, **52**, 10008.
- 78 C. Yang, B. C. Ma, L. Zhang, S. Lin, S. Ghasimi, K. Landfester, K. A. Zhang and X. Wang, *Angew. Chem., Int. Ed.*, 2016, **55**, 9202.